Crosstalk between the MMB complex and YAP in transcriptional regulation of cell cycle genes

Interaktion zwischen dem MMB-Komplex und YAP bei der transkriptionellen Regulation von Zellzyklusgenen

Dissertation
for a doctoral degree
at the Graduate School of Life Sciences,
Julius-Maximilians-Universität Würzburg,
Section Biomedicine

submitted by

Grit Pattschull

from
Kyritz, Germany

Würzburg, 2018

Submitted on: ……

office stamp

Members of the *Promotionskomitee*:

Chairperson: **Prof. Dr. Manfred Gessler**

Primary Supervisor: **Prof. Dr. Stefan Gaubatz**

Supervisor (Second): **Prof. Dr. Almut Schulze**

Supervisor (Third): **Prof. Dr. Alexander Buchberger**

Date of Public Defence: ……

Date of Receipt of Certificates: ……

Substantial parts of this thesis were published in the following article:

Iltzsche F.*, Simon K.*, Stopp S.*, **Pattschull G.***, Francke S., Wolter P., Hauser S., Murphy DJ., Garcia P., Rosenwald A., and Gaubatz S. (2016): **An important role for Myb-MuvB and its target gene KIF23 in a mouse model of lung adenocarcinoma.** *Oncogene* **36**, 110–121; https://doi.org/10.1038/onc.2016.181
(Iltzsche et al. 2017)

* These authors contributed equally to this work.

SUMMARY

The Myb-MuvB (MMB) multiprotein complex is a master regulator of cell cycle-dependent gene expression. Target genes of MMB are expressed at elevated levels in several different cancer types and are included in the chromosomal instability (CIN) signature of lung, brain, and breast tumors.

This doctoral thesis showed that the complete loss of the MMB core subunit LIN9 leads to strong proliferation defects and nuclear abnormalities in primary lung adenocarcinoma cells. Transcriptome profiling and genome-wide DNA-binding analyses of MMB in lung adenocarcinoma cells revealed that MMB drives the expression of genes linked to cell cycle progression, mitosis, and chromosome segregation by direct binding to promoters of these genes. Unexpectedly, a previously unknown overlap between MMB-dependent genes and several signatures of YAP-regulated genes was identified. YAP is a transcriptional co-activator acting downstream of the Hippo signaling pathway, which is deregulated in many tumor types. Here, MMB and YAP were found to physically interact and co-regulate a set of mitotic and cytokinetic target genes, which are important in cancer. Furthermore, the activation of mitotic genes and the induction of entry into mitosis by YAP were strongly dependent on MMB. By ChIP-seq and 4C-seq, the genome-wide binding of MMB upon YAP overexpression was analyzed and long-range chromatin interaction sites of selected MMB target gene promoters were identified. Strikingly, YAP strongly promoted chromatin-association of B-MYB through binding to distal enhancer elements that interact with MMB-regulated promoters through chromatin looping.

Together, the findings of this thesis provide a so far unknown molecular mechanism by which YAP and MMB cooperate to regulate mitotic gene expression and suggest a link between two cancer-relevant signaling pathways.

ZUSAMMENFASSUNG

Der Myb-MuvB (MMB) Multiproteinkomplex spielt eine wichtige Rolle in der Expression Zellzyklus abhängiger Gene, welche erhöhte Expressionsraten in verschiedenen Krebsarten aufweisen und Teil der sogenannten chromosomalen Instabilitätssignatur (CIN) von Lungen-, Gehirn- und Brusttumoren sind.

In dieser Arbeit konnte gezeigt werden, dass die Deletion von LIN9, einer zentralen Untereinheit des MMB-Komplexes, in primären Lungenkarzinomzellen der Maus zu starken Proliferationsdefekten und Anomalitäten des Zellkerns führt. Analysen des gesamten Transkriptoms mit Hilfe von RNA-Seq ergaben, dass der MMB-Komplex die Expression einer Gruppe von Genen reguliert, die mit dem Voranschreiten des Zellzyklus, der Mitose und der Trennung der Chromosomen in Verbindung stehen. Die Regulation dieser Gene erfolgt durch direkte Bindung des MMB-Komplexes an die dazugehörigen Promotoren, wie die Analyse der genomweiten DNA-Bindung des MMB-Komplexes durch ChIP-Seq erkennbar werden ließ. Weiterhin wurde in dieser Arbeit eine neuartige Interaktion zwischen MMB und YAP, einem transkriptionellen Co-Aktivator und Effektorprotein des Hippo-Signalweges, gefunden. Die Dysregulation von Hippo/YAP ist an der Entstehung verschiedener Tumorentitäten beteiligt. Die Ergebnisse dieser Arbeit zeigen, dass YAP mit Untereinheiten von MMB interagiert und dass beide Signalwege ein überlappendes Set von Zielgenen, die für die Entstehung von Tumoren relevant sind, regulieren. Es konnte außerdem nachgewiesen werden, dass YAP den MMB-Komplex benötigt, um die Expression mitotischer Gene zu aktivieren und dass der durch YAP induzierte Eintritt in die Mitose vom MMB-Komplex abhängig ist.

In einem weiteren Teil der Arbeit wurden mittels ChIP-Seq und 4C-Seq Chromatin-Interaktionen von Promotoren der MMB-Zielgene mit weiter entfernt liegenden Bereichen des Genoms identifiziert. Hierbei konnte festgestellt werden, dass YAP die Bindung der MMB-Untereinheit B-MYB an die Promotoren der MMB-Zielgene verstärkt, indem es an weiter entfernte *Enhancer* bindet. Diese von YAP gebundenen *Enhancer* interagieren über Schleifenbildung des Chromatins mit den Promotoren MMB-regulierter Gene. Zusammengefasst konnten die Ergebnisse dieser Arbeit einen bisher unbekannten molekularen Mechanismus für die gemeinsame Regulation von Genen durch den MMB-Komplex und YAP enthüllen und somit einen Zusammenhang zwischen zwei krebsrelevanten Signalwegen aufdecken.

TABLE OF CONTENTS

1 Introduction

1.1 The mammalian cell cycle

1.1.1 Phases and checkpoints of the eukaryotic cell cycle

For the replication of the genomic DNA and the distribution of the replicated DNA among the two newly formed dividing daughter cells, a eukaryotic cell passes through the synthesis (S) and mitosis (M) phases of the cell cycle. These two phases are separated by the two gap phases G1 (before the S phase) and G2 (before the M phase), which allow cells to grow and to prepare for the entrance into the S or M phase (**Figure 1**). The M phase, which consists of the four sub-phases prophase, metaphase, anaphase, and telophase, is followed by cytokinesis, in which the two daughter cells separated by a plasma membrane are formed. As the G1, S, and G2 phases together display the section between two mitosis phases, they are often referred to collectively as the interphase. In the presence of anti-mitogenic signals or in the absence of mitogenic signals a cell will exit the cell cycle to enter a non-dividing, quiescent state referred to as G0 phase (Malumbres and Barbacid 2001; Harashima et al. 2013; Weinberg 2014).

Several checkpoints within the cell cycle exist to ensure that a cell will not progress into the next cell cycle phase before all steps of the current phase are completed properly. In general, there are three major checkpoints. The first, the G1/S checkpoint or the restriction point (see section **1.1.4**), occurs in mid to late G1 and represents a point of no return after which cells do no longer respond to extracellular signals. At this point, entry into S-phase is blocked upon the presence of inhibitory signals or withdrawal of growth stimulatory factors (Blagosklonny and Pardee 2000-2013; Morgan 2007). The second, the G2/M checkpoint, ensures that a cell will not enter mitosis until the DNA replication is completed or if the DNA is damaged. The third, the mitotic spindle or spindle assembly checkpoint (SAC), controls metaphase-to-anaphase transition during mitosis and ensures that all sister-chromatids are attached correctly to the mitotic spindle in a bi-oriented manner (Morgan 2007; Barnum and O'Connell 2014).

1.1.2 Cell cycle control by cyclins, CDKs, and CKIs

The progression of the cell cycle is controlled by a class of serine/threonine kinases named cyclin-dependent kinases (CDKs). These kinases are regulated by binding of activating (cyclins) or inhibiting (CDK inhibitors, CKIs) partners as well as by phosphorylation at certain residues. As the name suggests, CDKs are bound by a class of proteins known as cyclins, which form their regulatory subunits and stimulate their catalytic activity. Throughout the cell cycle, several cyclin-CDK complexes consisting of different types of cyclins and CDKs are formed. Whereas the concentration of CDK proteins remains largely constant during the cell cycle, the levels of cyclins fluctuate during the distinct phases of the cell cycle, thereby regulating the activity of the different cyclin-CDK complexes.

From the onset of the G1 phase to the restriction/R point (see section **1.1.4**), D-type cyclins (D1-3) bind to and activate CDK4 and CDK6, which in turn activate the expression of E-type cyclins (E1 and E2). After the R point in late G1 phase, cyclin E1 and E2 bind to and activate CDK2, which will allow entry into S phase. Progression of S phase is promoted by exchanging the E-type cyclins with the A-type cyclins (A1 and A2) as the binding partners of CDK2. From mid S to late G2 phase, A-type cyclins are bound to CDK1, also known as CDC2, until they are replaced by B-type cyclins (B1 and B2) at the end of G2 phase. The cyclin B-CDK1 complex is finally active from late G2 until the end of M phase and regulates entry into and successful progression through mitosis (**Figure 1**).

Apart from binding to their corresponding cyclins, CDKs need to be further phosphorylated by the CDK-activating kinase (CAK, also known as CDK7-cyclin-H complex) to become fully activated. In addition to this activating phosphorylation, there are also known inhibitory phosphorylations mainly affecting the mitotic CDK1 kinase, which is inhibited by WEE1 or MYT1 phosphorylation and activated by CDC25A, -B, and -C dephosphorylation (Malumbres and Barbacid 2001; Morgan 2007; Weinberg 2014). Another mechanism of CDK regulation is the inhibition of CDK activity by CDK inhibitors (CKIs). There are two types of CKIs: the inhibitors of CDK4/6 (INK4) and the CDK-interacting protein/CDK inhibitory protein (Cip/Kip) family. The INK4 family comprises four members namely $p16^{INK4A}$, $p15^{INK4B}$, $p18^{INK4C}$, and $p19^{INK4D}$, which bind to CDK4 and CDK6 to inhibit their association with D-type cyclins during early and mid G1 phase. In contrast, the Cip/Kip family members $p21^{Cip1}$, $p27^{Kip1}$, and $p57^{Kip2}$ form heterotrimeric complexes by binding to all other cyclin-CDK complexes active from late G1 to M phase, thereby preventing cell cycle progression. However, $p21^{Cip1}$ and $p27^{Kip1}$ can also promote cell-cycle entry by stimulating the assembly of cyclin D-CDK4/6 complexes.

The expression of CKIs is influenced by both intra- and extracellular signals. Whereas transforming growth factor-ß (TGF-ß) is known to induce the expression of $p15^{INK4B}$ and weakly of $p21^{Cip1}$, mitogens lead to the cytoplasmic retention and thus inhibition of $p21^{Cip1}$ and $p27^{Kip1}$ through protein kinase B (AKT/PKB) signaling. DNA damage and subsequent stabilization of the tumor suppressor p53 increase the level of $p21^{Cip1}$, which in turn inhibits cyclin-CDK complexes resulting in cell cycle arrest (Harper et al. 1993; Polyak et al. 1994; Roussel 1999; Sherr and Roberts 1999; Weinberg 2014; The UniProt Consortium 2017).

1.1.3 The RB-E2F regulatory network

There are two major groups of proteins, which regulate cell cycle entry and G1/S transition. The first group is known as the pocket protein family and consists of the retinoblastoma protein (pRB) and its paralogs p107 and p130. The second group consists of transcription factors known as adenovirus early gene 2 binding factors (E2Fs) (Frolov and Dyson 2004; Iaquinta and Lees 2007; Fischer and Muller 2017).

The best described pocket protein is pRB, the protein product of the retinoblastoma tumor susceptibility gene (*RB1*). The *RB1* gene was first identified as a gene whose germ-line mutations cause a malignant childhood tumor of the retina called retinoblastoma. Later on, oncoproteins expressed by small DNA viruses suggested that pRB and its paralogs p107 and p130 play a role in controlling cell proliferation. Specifically, viral oncoproteins such as the adenovirus E1A, SV40 large T antigen, or the human papillomavirus E7 can bind to and inactivate pRB, p107, and p130. This results in activation of E2F target genes and induction of cell proliferation even in the absence of growth factor stimulation (Classon and Dyson 2001; Bracken et al. 2004).

Although all three pocket proteins associate with E2F transcription factors, several differences have been revealed. Regarding the amino acid sequence, one can say that p107 and p130 are more related to one another than either of them is to pRB. Whereas p107 is expressed at low levels in differentiated cells and increases in proliferating cells, p130 is highly expressed in quiescent and differentiated cells and its level decreases rapidly when cells enter the cell cycle. In contrast, pRB is expressed equally in quiescent, non-proliferating and proliferating cells. Another essential difference is the interaction with specific E2F transcription factors (Classon and Dyson 2001). Before going into detail, it is necessary to get to know the different members of the E2F family. There are eight E2F genes encoding in total nine E2F proteins, which are classified into activator and repressor E2Fs according to their effect on transcription.

E2F1, E2F2, and E2F3a are considered as activator E2Fs, whereas E2F3b and E2F4-8 mainly act as transcriptional repressors. The transcriptional activity of E2F1-5 is regulated through binding to members of the pocket protein family. In contrast, E2F6-8 lack domains for interacting with pocket proteins. In order to bind to DNA, E2F1-6 form heterodimers with their dimerization partners DP1 and DP2. As E2F7 and E2F8 contain a second DNA binding domain, they are able to bind DNA independently from DP proteins (Bracken et al. 2004; Iaquinta and Lees 2007).

To come back to the difference between p107/p130 and pRB regarding their binding behavior to certain E2Fs, p107 and p130 bind specifically to the repressor E2Fs, E2F4 and E2F5, whereas the activator E2Fs, E2F1, E2F2, and E2F3a, are exclusively bound by pRB (Frolov and Dyson 2004; Iaquinta and Lees 2007).

1.1.4 Cell cycle entry and the restriction point

In G0/G1 phase, the quiescent, non-proliferating state of the cell cycle, E2F4 and E2F5 bound to p107 and p130 repress E2F-responsive genes to keep the cell in a G0/G1 arrest and prevent expression of genes required for S phase entry. In this state, activator E2Fs are expressed at very low levels, as their respective genes are repressed by E2F4 and E2F5. The remaining low levels of activator E2Fs are bound to promoters of their target genes but are prevented from activating gene expression through the binding of pRB. There are several ways how pRB blocks transcription of genes when bound to E2F targets. Besides direct binding and blocking of the E2F transactivation domain, pRB also prevents the assembly of pre-initiation complexes and recruits enzymes such as histone deacetylases (HDACs) that modify the structure of the chromatin to a repressive conformation (Frolov and Dyson 2004; Iaquinta and Lees 2007; Morgan 2007).

To enter into the cell cycle, a cell can respond to extracellular mitogens or intracellular growth-regulating signals only in a certain window of the cell cycle, which ranges from the beginning to almost the end of G1. The point at which cells need to decide whether they want to stay in G1, exit the cell cycle into G0, or progress into S, G2, and M phases is referred to as the restriction or R point. In response to extracellular signals in early G1, several signaling pathways such as the RAS/RAF/MAPK pathway induce the expression of D cyclins, which subsequently bind to and activate CDK4/6. The cyclin D-CDK4/6-complex in turn weakly phosphorylates the pocket proteins pRB, p107, and p130 (Malumbres and Barbacid 2001; Barbacid et al. 2005; Weinberg 2014). Subsequently, E2F1-3a are partially released from their repression by pRB and as a consequence, genes important for G1/S transition such as E-type cyclins are expressed.

E-type cyclins bind to and activate CDK2, which further phosphorylates pRB, p107, and p130, leading to their complete release from binding to E2Fs (**Figure 1**). In contrast to the activator E2Fs, E2F4 and E2F5 lack a nuclear localization signal and, without the binding of p107 and p130, can no longer enter the nucleus (Barbacid et al. 2005; Sun et al. 2007). Activator E2Fs, now released from pRB-mediated inhibition, activate the expression of genes important for G1/S transition and DNA synthesis such as cyclin E1/E2, cyclin A1/A2, dihydrofolate reductase, and Myb-related protein B/Myb-like protein 2 (B-MYB/MYBL2) (Johnson and Walker 1999; Bracken et al. 2004; Barbacid et al. 2005; The UniProt Consortium 2017).

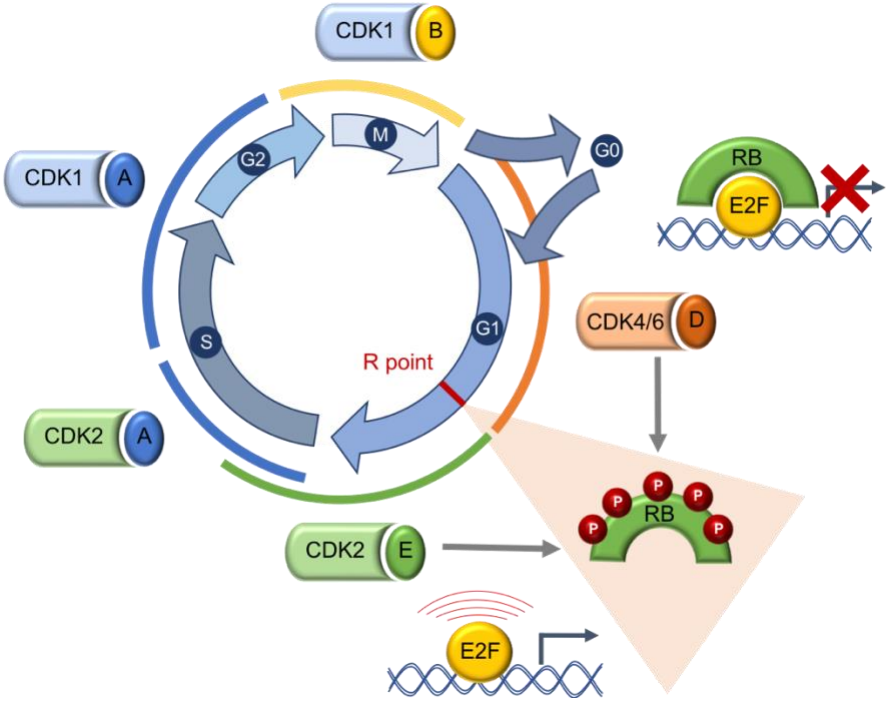

Figure 1: The mammalian cell cycle.
The mammalian cell cycle is subdivided into four major phases G1, S (synthesis; replication of DNA), G2, and M (mitosis; separation and distribution of replicated DNA among two daughter cells) phase. G1, S, and G2 are collectively called the interphase. Cells that exit the cell cycle enter a quiescent, non-proliferating state, the G0 phase. Progression through the cell cycle is controlled by complexes of different types of cyclins bound to certain CDKs. In G1, cyclin D-CDK4/6 hypophosphorylates the retinoblastoma protein pRB. When passing through the restriction “R” point, hyperphosphorylation of pRB by cyclin E-CDK2 leads to the release of E2F from its repressive binding by pRB and subsequent transcription of cell cycle genes. Adapted from Weinberg (2014) .

1.2 The DREAM and MMB complexes

1.2.1 The discovery of the DREAM and MMB complexes

The aforementioned pocket proteins p107/p130, the transcription factors E2F4/5, and their heterodimeric partners DP1/2 repress transcription in G0/G1 as part of the DP, RB-like, E2F and multi-vulval class B (MuvB) (DREAM) complex (Fischer and Muller 2017). The DREAM complex contains a core of proteins commonly known as the MuvB core. MuvB is composed of five evolutionary conserved proteins, which are homologous to proteins that were first discovered by the laboratory of Robert Horvitz in *Caenorhabditis elegans*. Genes encoding these proteins were named synthetic mulit-vulva class B (synMuvB) genes. Together with synMuvA and C genes, synMuvB genes belong to a group of genes in which synthetic loss-of-function mutations resulted in worms with a multi-vulva phenotype (synMuv). The synMuvB genes encode for LIN-35, EFL-1/-2, and DPL-1, the homologs of pRB, E2F, and DP1, but also for genes with at that time unknown functions: *lin-9*, *lin-37*, *lin-52*, *lin-53,* and *lin-54* (Sadasivam and DeCaprio 2013).

More than ten years later, the Botchan laboratory identified that in *Drosophila melanogaster* proteins encoded by homologs of the synMuvB genes are together with the protein Myb part of a five-subunit complex with important functions in DNA replication (Beall et al. 2002). Later on, the same laboratory found that the *Drosophila* Myb and MuvB proteins are part of a larger complex together with dLin52, RBF1, RBF2, E2F2, and DP (the fly homologs of human LIN52, pRB, E2F4/E2F5, and DP1/2) named the Myb-MuvB complex (Lewis et al. 2004; Sadasivam and DeCaprio 2013). At the same time, the Brehm and Dyson laboratories purified a *Drosophila* complex in which several Myb-interacting proteins (Mips) encoded by homologs of the synMuvB genes interact with RBF1, RBF2, DP, E2F2, and Myb. Thus, the complex was named the *Drosophila* RBF, E2F, and Mip (dREAM) complex (Korenjak et al. 2004). Two years after the discovery of the fly MMB and dREAM complexes, the same laboratory that initially identified the synMuvB genes purified a similar complex from *C. elegans* called the DP, Rb and MuvB (DRM) complex. In addition to the proteins encoded by the aforementioned synMuvB genes with so far unknown functions, this complex contained the worm RB, E2F, and DP homologs LIN-35, EFL-1, and DPL-1. In contrast to the fly MuvB complex, the DRM complex did not contain any Myb, which can be attributed to the absence of a related *Myb* gene in *C. elegans* as discovered later on (Harrison et al. 2006; Davidson et al. 2013).

Before a homologous complex in human cells was identified, the laboratory of Stefan Gaubatz initially isolated and characterized LIN9, the human homolog of the *C. elegans* LIN-9 synMuv and the *D. melanogaster* Mip130 proteins (Gagrica et al. 2004), as an pRB-interacting protein. Follow-up experiments indicated that human LIN9 also interacts with p130 and E2F4 in quiescent cells and that this interaction gets lost once the cell enters into S phase. During S/G2 phase LIN9 was found to bind to B-MYB independently of pocket proteins and to activate the expression of G2/M genes by binding to their promoters (Osterloh et al. 2007; Pilkinton et al. 2007). Later on, two mammalian homologous complexes consisting of the MuvB core with LIN9, LIN37, LIN52, LIN54, and RBBP4 were identified. The main difference to the fly complexes is that p107/p130, E2F4/5, and B-MYB are not permanent subunits but instead their interaction with MuvB dynamically changes throughout the cell cycle. Specifically, during G0/G1 phase, the MuvB core interacts with E2F4/5, DP1/2, and p107/p130 to form the DREAM (also known as LINC) complex, which represses G1/S and G2/M E2F target genes.
In late G1 phase, the repressive components dissociate from MuvB, which then binds to B-MYB in S phase to form the Myb-MuvB (MMB) complex (**Figure 2**). MMB activates the expression of G2/M genes required for mitosis and cytokinesis (Litovchick et al. 2007; Schmit et al. 2007; Fischer and Muller 2017).

1.2.2 The DREAM complex: repression of cell cycle genes

In G0 and early G1 phase of the cell cycle, the transcription of cell cycle-dependent genes is repressed by RB-E2F and DREAM complexes. On the one hand, E2F1-3 together with DP bind to E2F promoter sites (5'-TTTSSCGC-3'; with S being G or C) but are repressed from activating those genes through binding of pRB (see sections **1.1.3** and **1.1.4**). On the other hand, the DREAM complex represses E2F genes by binding to E2F promoter sites through the DNA binding domains of E2F/DP (Sadasivam and DeCaprio 2013; Fischer and Muller 2017). Binding of DREAM to E2F promoter sites can be supported through a weak interaction of the MuvB core protein LIN54 with cell cycle genes homology region (CHR)-like elements (CLE: CTTGAA, CTTGAC, or TCTGAA) located close to E2F binding sites (Muller et al. 2017). LIN54 contains two cysteine-rich (CXC) domains separated by a spacer. The CXC domains function as a DNA-binding domain (DBD) enabling LIN54 to bind to DNA in a sequence-specific manner (Schmit et al. 2009). As the promoters of G2/M genes such as *CDC20*, *CENPF*, and *AURKA* generally lack E2F consensus binding sites, pRB-E2F1-3 cannot bind to these late cell cycle genes.

Instead, G2/M genes are repressed by DREAM through the binding of LIN54 to cell cycle gene homology regions (CHRs: TTTGAA, TTCGAA, or TTTAAA), which is supported by binding of E2F/DP to nearby cell cycle-dependent elements (CDEs: GGGCGG or TGGCGG) (Schmit et al. 2009; Muller et al. 2012; Fischer and Muller 2017; Muller et al. 2017). Recently, the Hippo pathway (see section **1.3**) was shown to be connected to the assembly of the DREAM complex and entry into quiescence: The downstream effector kinase large tumor suppressor 2 (LATS2) of the Hippo pathway phosphorylates and activates the dual specificity tyrosine-phosphorylation-regulated kinase 1A (DYRK1A). DYRK1A in turn specifically phosphorylates LIN52 on serine residue 28 (S28), which promotes the assembly of the repressor DREAM complex (Litovchick et al. 2011; Tschop et al. 2011).

The precise mechanisms how DREAM represses gene expression are still being debated. Crystal structure analyses of the laboratory of Seth Rubin showed that LIN52 of the MuvB core uses an LxCxExL sequence and the S28 phosphate to bind to the LxCxE binding cleft of p130 and p107. This restricts the capability of p130/p107 to interact with repressive chromatin modifiers in an LxCxE-dependent manner, suggesting that an LxCxE-independent recruitment of co-repressors by DREAM could contribute to gene repression (Guiley et al. 2015; Fischer and Muller 2017). Another possible mechanism of gene repression by DREAM might be connected to the enrichment of the histone variant H2A.Z in gene bodies of DREAM target genes. In *D. melanogaster*, the loss of *Myb* resulted in a binucleate phenotype due to transcriptional repression of cytokinesis genes by the dREAM complex. This *Myb*-null binucleate phenotype could be suppressed by reducing the expression of *His2Av* (*H2Av*), the *Drosophila* ortholog of H2A.Z. Thus, one mechanism of *Drosophila* dREAM to repress gene expression might be due to the recruitment of H2Av, which promotes the formation of heterochromatin (DeBruhl et al. 2013). In line with this, target genes of DREAM in *C. elegans* show high levels of HTZ-1/H2A.Z, which is associated with transcriptional repression. Loss of LIN-35, the pocket protein ortholog in *C. elegans*, caused a loss of HTZ-1/H2A.Z in gene bodies and an enhanced expression of DREAM target genes (Latorre et al. 2015).

One important factor that has been shown to favor the formation of DREAM is cell stress such as DNA damage, which leads to the stabilization of p53 and the subsequent activation of the cyclin-CDK inhibitor $p21^{Cip1}$. In proliferating cells, CDK-mediated phosphorylation leads to the dissociation of p130/p107 from MuvB and activation of B-MYB and forkhead box M1 (FOXM1) (see section **1.2.3**). However, through $p21^{Cip1}$ activation and subsequent CDK inhibition, p130 and p107 will change from a hyper- to a hypophosphorylated state and, as part of the DREAM complex, contribute to the downregulation of cell cycle genes.

In addition, CDK inhibition blocks B-MYB and FOXM1 activation, further shifting the balance from the activator MMB/FOXM1-MuvB to the repressor DREAM complex (Mannefeld et al. 2009; Quaas et al. 2012; Sadasivam and DeCaprio 2013; Fischer and Muller 2017). Conversely, oncoproteins from small DNA tumor viruses such as HPV E7 (Nor Rashid et al. 2011) or SV40 large T (Fine et al. 2012; Hauser et al. 2012) can bind to p107 and p130, which disrupts DREAM complex formation and subsequently, induces an upregulation of cell cycle genes (Fischer and Muller 2017). Mechanistically, HPV E7 was shown to use an LxCxExL motif to bind the LxCxE cleft of p130, which prevents the interaction of p130 with LIN52 and DREAM assembly (Guiley et al. 2015).

1.2.3 The MMB complex: activation of cell cycle genes

Once a cell receives growth stimulatory signals, cyclin D-CDK4/6 and cyclin E-CDK2 complexes phosphorylate the pocket proteins in mid- and late G1 phase leading to the release of pRB-inhibited activator E2Fs and the dissociation of p130/p107 from E2F4/5-DP1/2 and MuvB of the DREAM complex (**Figure 2**). Recent findings of the laboratory of Seth Rubin suggest that CDK-mediated phosphorylation of p130/p107 not only interferes with the E2F4/5 interaction but also inhibits direct binding of p130/p107 to LIN52 (Guiley et al. 2015; Fischer and Muller 2017). Dissociated p130/p107 is degraded and E2F4/5 are transported out of the nucleus. Released activator E2F1-3 together with DP1/2 bound to E2F promoter sites activate the expression of G1/S genes such as genes encoding for B-MYB, cyclin E, the activator E2F1-3 themselves but also repressor E2F7 and E2F8. With progression through S phase, activator E2Fs are released from binding to the DNA through cyclin A-CDK2-mediated phosphorylation. Finally, when DNA synthesis is completed at the end of the S phase, G1/S genes are repressed by the replacement of E2F1-3 with E2F7 and E2F8 (Fischer and Muller 2017).

During S phase, the transcription factor B-MYB binds to the MuvB core to form the activator MMB complex (Litovchick et al. 2007; Schmit et al. 2007). B-MYB itself is encoded by a gene whose expression is repressed by DREAM and pRB/E2F complexes in G0/G1 and activated by E2F1-3 transcription factors during G1/S transition. Moreover, for full transactivation activity, B-MYB is phosphorylated at multiple residues by cyclin E- and cyclin A-CDK2. Through LIN54, MMB binds to CHR elements in promoters of several late cell cycle genes whose products have important functions in mitosis and cytokinesis. One of these target genes of the MMB complex is the gene encoding for FOXM1, which is recruited by MMB to the promoters of late cell cycle genes during G2. FOXM1 itself receives full transcriptional activity through phosphorylation by cyclin A- and cyclin B-CDK complexes and later on by PLK1.

It appears that both B-MYB and FOXM1 cannot bind and activate G2/M genes independently from MuvB, because promoters of MMB target genes are not enriched for Myb and Forkhead binding sites. While ubiquitinated B-MYB is degraded by the proteasome, the remaining FOXM1-MuvB complex bound to CHR promoter elements fully activates G2/M genes in G2 (Johnson et al. 1999; Down et al. 2012; Sadasivam et al. 2012; Sadasivam and DeCaprio 2013; Fischer and Muller 2017). During mitosis, FOXM1 is ubiquitinated by the anaphase-promoting complex/cyclosome-cadherin 1 complex (APC/C^{CDH1}), leading to its proteasomal degradation (Park et al. 2008). At the end of mitosis, the pocket proteins pRB, p107, and p130 are dephosphorylated and reactivated by PP1 and PP2A phosphatases. Together with the phosphorylation of LIN52-S28 by DYRK1A, this enables the reassembly of DREAM and pRB-E2F complexes (Kolupaeva and Janssens 2013; Fischer and Muller 2017).

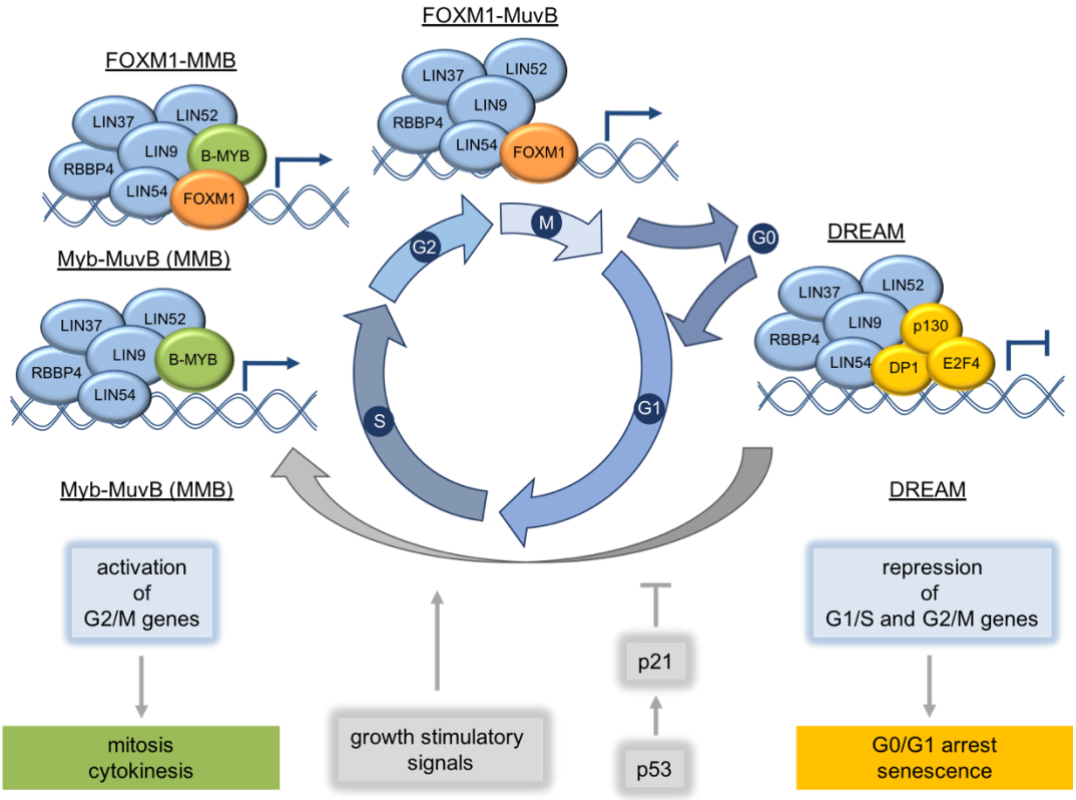

Figure 2: DREAM and MMB complexes regulate G1/S and G2/M gene expression.
The MuvB core consisting of LIN9, LIN37, LIN52, LIN54, and RBBP4 binds to p107/p130, E2F4/5, and DP1/2 to form the DREAM complex, which represses G1/S and G2/M gene expression in G0/G1 arrested, quiescent cells. In late G1 phase, p107/p130, E2F4/5, and DP1/2 dissociate from MuvB. During S phase, B-MYB binds to MuvB to form the MMB complex, which activates G2/M gene expression. In late G2 and M phase, MMB recruits FOXM1 to MuvB, which fully activates G2/M genes. Growth stimulatory signals leading to the entry into the cell cycle stimulate MMB formation. In contrast, DNA damage leads to p53 stabilization, which in turn induces expression of $p21^{Cip1}$. Inhibition of CDK2 and CDK1 complexes by $p21^{Cip1}$ results in reassembly of the repressor DREAM complex and cell cycle arrest. Adapted from Sadasivam and DeCaprio (2013); Fischer and Muller (2017).

1.2.4 The MMB complex *in vivo* and its role in cancer

The importance of DREAM and MMB for cell cycle-dependent gene regulation is supported by several *in vivo* studies. Loss of the DREAM/MMB core subunit LIN9 in mice resulted in embryonic lethality at the peri-implantation stage (Reichert et al. 2010). Furthermore, conditional knockout of *Lin9* in adult mice led to lethality within 7 days due to rapid loss of the intestinal epithelium. In line with this, conditional *Lin9* knockout mouse embryonic fibroblasts (MEFs) exhibit a decreased expression of mitotic genes, several mitotic defects, and premature senescence (Reichert et al. 2010). These *in vivo* findings together with data showing that LIN9 directly binds to several MMB and DREAM subunits such as FOXM1, LIN52, and RBBP4 suggest that LIN9 is a central structural component of both MMB and DREAM (Schmit et al. 2007; Wiseman et al. 2015). Similarly to *Lin9*, knockout of the transcription factors *B-myb* and *Foxm1b* in mice resulted in lethality during embryogenesis between E4.5 and E6.5 for *B-myb* and E18.5 for *FoxM1* (Tanaka et al. 1999; Krupczak-Hollis et al. 2004).

Interestingly, *LIN9*, *B-MYB*, *FOXM1,* and several MMB target genes such as Aurora kinase A (*AURKA*) and DNA topoisomerase 2α (*TOP2A*) are frequently expressed at elevated levels in human tumors (Sadasivam and DeCaprio 2013). *B-MYB* and MMB target genes such as *CCNB1* and *AURKA* are included in the Oncotype Dx (Genomic Health) clinical biomarker test. This test analyzes the expression of 16 cancer-related and five reference genes to quantify the likelihood of recurrence in node-negative, tamoxifen-treated breast cancer (Paik et al. 2004). Additionally, several direct mitotic targets of MMB including *CDC20* and *KIF20A* but also *B-MYB* and *FOXM1* themselves are part of the chromosomal instability 70 (CIN70) signature, which can be used as a predictor of clinical outcome for several cancer types such as breast and lung cancer. High expression of genes included in the CIN70 signature is associated with aneuploidy as a consequence of CIN and with a poor outcome in cancer patients (Carter et al. 2006). In addition, *LIN9* and MMB targets (e.g., *NUSAP1* and *PRC1*) are part of the MammaPrint (Agendia) profile, which includes 70 genes whose expression is associated with tumor progression and is used as a diagnostic tool to predict breast cancer metastasis (Tian et al. 2010).

The high expression of genes encoding for MMB subunits and target genes and its correlation with survival of cancer patients suggest a role of MMB in tumorigenesis. This hypothesis is supported by recent data from our laboratory showing that Cre-mediated deletion of *Lin9* and *B-Myb* in a non-small cell lung cancer (NSCLC) mouse model driven by oncogenic K-RAS and loss of p53 resulted in reduced tumor formation (Iltzsche et al. 2017).

Furthermore, RNA interference-mediated knockdown of the MMB target genes *Kif23* and *Prc1* in the same mouse model significantly impaired the development of lung tumors (Iltzsche et al. 2017; Hanselmann et al. 2018). In summary, these results represent the first milestone on the way to better understand the role of MMB in tumorigenesis.

1.3 The Hippo pathway

1.3.1 An overview about the Hippo signaling cascade

Another important pathway that regulates cell proliferation by controlling cell cycle gene expression and that is often altered in human cancers is the highly conserved Hippo pathway (Ehmer and Sage 2016). This pathway was first discovered in *Drosophila melanogaster* through screens for genes that generally restrict cell growth and whose mutations lead to tissue overgrowth (Kango-Singh et al. 2002; Tapon et al. 2002; Harvey et al. 2003; Wu et al. 2003).

Hippo signaling is involved in several physiological processes such as organ size control, cell differentiation, and tissue homeostasis. The core of the Hippo pathway consists of the two kinases mammalian STE20-like kinases 1/2 (MST1/2) and LATS1/2, in *Drosophila* Hippo (Hpo) and Warts (Wts) kinases, and the two adaptors/activators salvador homolog 1/45 kDa WW domain protein (SAV1/WW45) and Mps one binder (MOB) kinase activator-like 1B/1A (MOB1A/B), in *Drosophila* Sav and Mats. In response to upstream signals, MST1/2 are activated and together with SAV1/WW45 they phosphorylate and activate LATS1/2 kinases and MOB1A/B (**Figure 3**). LATS1/2 together with MOB1A/B phosphorylate the downstream effectors Yes-associated protein (YAP) and transcriptional co-activator with PDZ-binding motif (TAZ), the mammalian homologs of *Drosophila* Yorkie (Yki). Phosphorylation by LATS kinases results in 14-3-3-mediated cytoplasmic retention and ubiquitination-dependent proteasomal degradation of YAP/TAZ. Thus, active Hippo pathway signaling inhibits the function of YAP/TAZ through its nuclear exclusion and degradation. However, when Hippo signaling is inactive, unphosphorylated YAP/TAZ translocate into the nucleus and activate gene expression (Yu et al. 2015; Ehmer and Sage 2016; Meng et al. 2016; The UniProt Consortium 2017).

Due to differential splicing, there are two isoforms of YAP, called YAP1 and YAP2. Both isoforms contain an N-terminal proline-rich domain, a TEAD binding region, one (YAP1) or two (YAP2) WW domains, an SH3-binding motif, a coiled-coil domain, a transcription activation domain, and a C-terminal PDZ-binding motif.

TAZ is 50% identical with the sequence of YAP and has a very similar topology but it lacks the proline-rich domain, a second WW domain, and the SH3-binding motif. Although YAP/TAZ have a transactivation domain, they lack a DNA-binding domain and thus need to associate with several transcription factors to bind to DNA (Zhao et al. 2010; Guo and Zhao 2013). The primary binding partners of YAP/TAZ are the TEA domain family members/transcriptional enhancer factors 1-4 (TEAD/TEF 1-4). Together with TEAD and other binding partners YAP/TAZ activate the expression of several genes, which mainly promote cell proliferation, inhibit apoptosis, or drive migration and invasion. Mechanisms by which YAP/TAZ/TEAD activate gene transcription include the recruitment of the switch/sucrose non-fermenting (SWI/SNF) chromatin remodeling complex or the nuclear receptor co-activator 6 (NCOA6) methyltransferase complex (Kadoch and Crabtree 2015; Ehmer and Sage 2016; Meng et al. 2016; The UniProt Consortium 2017).

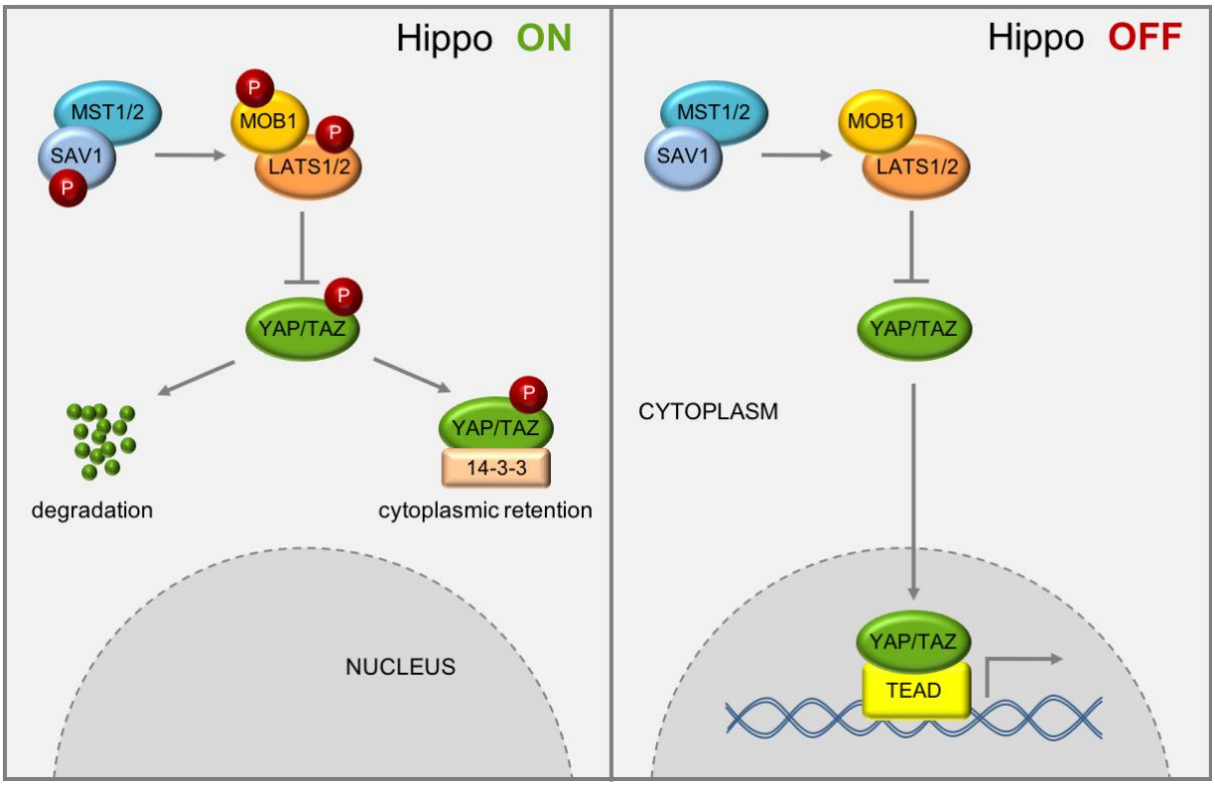

Figure 3: The mammalian Hippo signaling cascade.
When Hippo signaling is on (**left**), the upstream kinases MST1/2 are active and phosphorylate their binding partner SAV1, the kinases LATS1/2, and MOB1. LATS1/2 together with MOB1 phosphorylate the Hippo downstream effectors YAP and its paralog TAZ. This results in 14-3-3 protein-mediated cytoplasmic retention or ubiquitin-mediated proteasomal degradation of YAP and TAZ. When Hippo signaling is off (**right**), unphosphorylated YAP and TAZ translocate into the nucleus and together with members of the TEAD family, their main transcriptional binding partners, they induce the expression of pro-proliferative genes. Adapted from Yu et al. (2015) and Ehmer and Sage (2016).

1.3.2 Regulation of Hippo signaling and YAP/TAZ activity

Generally speaking, YAP/TAZ activity can be regulated either directly by LATS1/2 (canonical signaling) or independently of LATS1/2 (non-canonical signaling) (Low et al. 2014). The regulation of YAP/TAZ through both canonical or non-canonical signaling can be triggered by a plethora of extracellular signals or intracellular cell machineries such as soluble factors and their appropriate membrane receptors, cell mechanics and cytoskeleton status, the apical membrane protein Neurofibromin 2 (NF2; ortholog of *Drosophila* Merlin), interactions of YAP/TAZ with cell junction proteins, and Wnt signaling (Yu et al. 2015; Ehmer and Sage 2016).

1.3.2.1 Soluble factors and membrane receptors

Activation of G-protein-coupled receptors (GPCRs) linked to $G\alpha_{12/13}$ and $G\alpha_{11}$ through ligands such as serum-borne lysophosphatidic acid (LPA), sphingosine 1-phosphate (S1P), thrombin, angiotensin II, and estrogen can activate YAP/TAZ. In contrast, activation of GPCRs linked to $G\alpha_s$ by epinephrine and glucagon is associated with YAP/TAZ inhibition. Although the detailed mechanisms how GPCRs regulate YAP/TAZ remain elusive, the activation of Rho GTPases and subsequent inactivation of LATS1/2 by $G\alpha_{12/13}$- and $G\alpha_{11}$-coupled GPCRs seem to be involved (Yu et al. 2012; Yu et al. 2015). In addition to GPCRs, receptor tyrosine kinases (RTKs) such as the epidermal growth factor receptor (EGFR) have been shown to be important membrane receptors for YAP/TAZ regulation. Upon binding of EGF to EGFR, phosphoinositide-3-kinase (PI3K) and 3-phosphoinositide-dependent protein kinase 1 (PDK1) of the AKT/PKB pathway are activated. As TAZ degradation is induced by glycogen synthase kinase-3 (GSK3) phosphorylation, EGF-dependent activation of AKT/PKB signaling and subsequent GSK3 inhibition lead to enhanced levels of TAZ (Huang et al. 2012; Ehmer and Sage 2016; The UniProt Consortium 2017). In addition, it has been shown that in the absence of growth factors, PDK1 contributes to YAP inhibition by forming a complex with LATS, MST, and SAV. However, in the presence of growth factors, the PDK1 complex dissociates due to recruitment of PDK1 to the membrane and as a consequence, YAP can translocate into the nucleus (Fan et al. 2013).

1.3.2.2 The apical membrane protein NF2

A very important negative regulator of YAP/TAZ activity is the tumor suppressor NF2, the mammalian ortholog of *Drosophila* Merlin. In both mammals and flies, NF2 directly binds and recruits cytoplasmic LATS1/2 to the plasma membrane, which in turn promotes phosphorylation and activation of LATS1/2 by the MST1/2-SAV1 complex (Yin et al. 2013). Furthermore, NF2 can bind to and inactivate the E3 ubiquitin ligase CRL2-DCAF, which otherwise would inactivate LATS1/2 by ubiquitination and induce YAP/TAZ-dependent gene expression (Li et al. 2014).

1.3.2.3 Cell contact and mechanical stress

Several tight and adherens junction proteins such as members of the angiomotin (AMOT) family, protein tyrosine phosphatase non-receptor type 14 (PTPN14), and α-catenin inactivate YAP by recruiting it to cellular junctions (Yu et al. 2015). In line with this, cell-cell contacts were shown to modulate YAP/TAZ activity. High cell density in tissue culture and subsequent increased adherens and tight junctions activate LATS kinase activity. This in turn results in YAP/TAZ phosphorylation and cytoplasmic translocation, finally leading to growth inhibition. In sparse low-density cell cultures, LATS kinases are inactive and YAP/TAZ are localized in the nucleus leading to enhanced transcription of pro-proliferating genes. These findings suggest a critical role for the Hippo pathway and its effectors YAP/TAZ in cell contact inhibition. Because loss of cell contact inhibition has been shown to be a major hallmark of oncogenic transformation, dysregulation of the Hippo pathway might contribute to tumorigenesis by mediating proliferation of cancer cells (Zhao et al. 2007; Yu et al. 2015; Meng et al. 2016).

The laboratory of Stefano Piccolo could show that mechanical signals such as extracellular matrix (ECM) stiffness and cell geometry influence the activity of YAP/TAZ. When cells are grown on soft matrices or small islands, YAP/TAZ are mostly cytoplasmic. In contrast, in cells grown on stiff hydrogels or spread onto large islands, YAP/TAZ are active and mainly localized in the nucleus. Nuclear localization of YAP upon ECM stiffness seems to be independent of upstream LATS kinases and instead requires RhoA GTPase activation and tension of the actomyosin cytoskeleton (Dupont et al. 2011).

1.3.2.4 Wnt/ß-catenin and other signaling pathways

Binding of Wingless/Ints (Wnt) ligands to their membrane receptors leads to disassembly of the ß-catenin-destruction complex and thus stabilization of ß-catenin, which stimulates Wnt target gene expression. Without Wnt ligand, cytoplasmic YAP/TAZ are part of the ß-catenin destruction complex and recruit the E3 ubiquitin ligase ß-TrCP, which promotes phosphorylated ß-catenin degradation, thereby inhibiting Wnt signaling. In the presence of Wnt ligand, cytoplasmic YAP/TAZ are released from the ß-catenin destruction complex. As a consequence, recruitment of ß-TrCP for ß-catenin degradation is lost and both ß-catenin and YAP/TAZ translocate into the nucleus, leading to the transcription of ß-catenin and YAP/TAZ/TEAD target genes (Azzolin et al. 2014)

In addition to the regulation of YAP/TAZ by canonical Wnt signaling, binding of some Wnt ligands to the GPCR-like Frizzled receptor has been shown to activate YAP/TAZ independently of ß-catenin by $G\alpha_{12/13}$-Rho-LATS1/2 signaling. Additional findings support a model in which YAP/TAZ antagonize canonical Wnt/ß-catenin signaling by inducing the expression of Wnt inhibitors (Park et al. 2015).

1.3.2.5 Energy and oxidative stress

Energy stress induced by glucose deprivation and subsequent activation of AMP-activated protein kinase (AMPK) can inhibit YAP/TAZ activity in two ways. On the one hand, AMPK phosphorylates and thereby stabilizes AMOTL1, which in turn promotes phosphorylation and inactivation of YAP/TAZ by LATS1/2 kinases (DeRan et al. 2014). On the other hand, YAP, which can induce glucose metabolism by upregulating the expression of glucose-transporter 3 (GLUT3), is directly phosphorylated by energy stress induced AMPK. This phosphorylation disrupts the interaction between YAP and TEAD and inhibits YAP-dependent gene transcription (Mo et al. 2015; Wang et al. 2015).

Besides energy stress, the Hippo pathway has an important role in oxidative stress response. MST1 is activated upon exposure to hydrogen peroxide and induces cell death in primary mammalian neurons (Lehtinen et al. 2006). Moreover, it was shown that in the heart, YAP forms a complex with FOXO1 to induce antioxidant gene expression, thereby preventing reactive oxygen species (ROS) accumulation and promoting cardiomyocyte survival. Upon ischemia/reperfusion, activated LATS2 kinase results in YAP inhibition and subsequent suppression of antioxidant gene expression followed by ROS accumulation and cell death (Shao et al. 2014a). Other data show that in response to hypoxia, the hypoxia-inducible factor 1 (HIF-1) stimulates not only the expression of TAZ but also the expression of the E3 ubiquitin ligases seven in absentia homolog 1 and 2 (SIAH1/2), which promote ubiquitin-mediated degradation of LATS2 and thus activation of YAP/TAZ (Xiang et al. 2014; Ma et al. 2015; The UniProt Consortium 2017).

1.3.3 Cell Cycle regulation by YAP/TAZ

Several studies have shown that YAP/TAZ/TEAD regulate the expression of pro-proliferative genes and are essential for cell cycle entry and G1/S transition. A large proportion of genes regulated by YAP are known E2F-target genes. Importantly, YAP target genes are enriched for E2F binding sites, which supports the hypothesis that E2F cooperates with YAP and TEAD to regulate gene expression (Ehmer et al. 2014; Kapoor et al. 2014; Hiemer et al. 2015; Shen and Stanger 2015). Although some data indicate co-binding of YAP along with E2F at promoters of target genes, more recent data suggest that YAP regulates gene expression mainly by binding to distal enhancers (Kapoor et al. 2014; Galli et al. 2015; Stein et al. 2015; Zanconato et al. 2015). In addition to inhibiting YAP/TAZ-degradation and thus preventing gene expression, active LATS1/2 kinases can inhibit the expression of G1/S and G2/M genes by stimulating the assembly of the repressor DREAM complex (chapter **1.2.2**) (Litovchick et al. 2011; Tschop et al. 2011).
Besides inducing S-phase entry, YAP/TAZ also seem to be involved in the regulation of G2/M phase, since several mitotic and cytokinetic genes have been shown to be activated by YAP/TAZ (Bai et al. 2012; Tremblay et al. 2014; Lange et al. 2015). Hitherto, the detailed mechanisms by which YAP/TAZ regulate G1/S and G2/M gene expression still remain elusive but might involve interaction of YAP/TAZ with other cell cycle regulating transcriptional complexes (Ehmer et al. 2014; Ehmer and Sage 2016).

1.3.4 Keeping the balance – physiological role of the Hippo pathway

The Hippo pathway is of great importance for the control of embryonic development and tissue homeostasis (Ehmer and Sage 2016). Whereas YAP-null mice die at embryonic day E8.5 with several developmental defects, TAZ-null mice are viable but have a higher risk of suffering from kidney or pulmonary diseases (Hossain et al. 2007; Tian et al. 2007; Makita et al. 2008). The key physiological functions of YAP/TAZ include organ size control, the maintenance of tissue-specific stem cells, tissue regeneration, wound healing, and control of differentiation (Ehmer and Sage 2016). The best-known physiological function of the Hippo pathway is, however, regulating organ size (Yu et al. 2015). Mutations of the Hippo kinases or their upstream regulators as well as transgenic expression of *Yki* have been shown to result in overgrowth of several organs in *Drosophila*. Similarly, liver-specific transgenic expression of *Yap* or knockout of *Mst1/2*, *Sav1*, or *Nf2* in mice led to liver enlargement. In line with this, deletion of *Sav1*, *Mst1/2*, or *Lats1/2* induced an increase in the size of mouse embryonic hearts, further indicating the important role of YAP for organ size control (Yu et al. 2015).

Stem and progenitor cells of multiple tissues have an increased activity of YAP/TAZ whose key functions regarding stem and progenitor cells involve cell cycle regulation and the interaction with other stem cell-relevant signaling pathways such as the Hedgehog (Hh), Wnt, or Notch signaling pathway. Conversely, together with specific binding partners, such as the Runt-related transcription factor 2 (RUNX2) or the Krueppel-like factor 4 (KLF4), YAP/TAZ can also induce lineage-specific differentiation. Moreover, it has been shown that upon damage, YAP is required for the regeneration of multiple tissues such as the liver, intestine, and the heart (Yu et al. 2015; Ehmer and Sage 2016; The UniProt Consortium 2017). In addition, YAP/TAZ seem to be required for wound healing as indicated by delayed wound closure and reduced expression of TGF-ß1 upon downregulation of YAP/TAZ at mouse skin wound sites (Lee et al. 2014). Overall, the main function of the Hippo pathway is keeping the balance between the induction of physiological proliferation and prevention of pathological uncontrolled cell divisions that can cause cancer (Ehmer and Sage 2016).

1.3.5 Role of YAP/TAZ in cancer

Besides the physiological role, the pathological role of YAP/TAZ is no less important. In many cancers, high levels of nuclear YAP/TAZ can be found due to dysfunctional Hippo signaling. This can be caused either directly through mutations in Hippo pathway genes or indirectly through alterations in other signaling pathways that interact with Hippo signaling. With the exception of both inherited and somatically acquired mutations found in the tumor suppressor *NF2*, mutations in other components of the Hippo pathway are quite rare (Harvey et al. 2013; Ehmer and Sage 2016). However, some human and murine cancers such as head and neck, pancreatic, breast, and liver cancer were found to have amplified and overexpressed *YAP* (Overholtzer et al. 2006; Zender et al. 2006; Kapoor et al. 2014; The Cancer Genome Atlas Network 2015). Mutations in the upstream Hippo kinases *MST1/2* and *LATS1/2* are uncommon, instead hypermethylation of *MST1/2* and *LATS1/2* promoters, which is associated with reduced expression of these genes, could be observed amongst others in soft tissue sarcomas and breast cancer (Takahashi et al. 2005; Seidel et al. 2007).

In addition to alterations directly affecting Hippo pathway genes, somatic mutations in genes of other signaling pathways that interact with the Hippo pathway such as the Wnt, Notch, or Hh pathway have been shown to cause YAP and TAZ hyperactivation in several cancers, e.g., in gastrointestinal tract, colorectal, or non-small-cell lung cancers (Harvey et al. 2013).

Accordingly, activating Hippo signaling or inhibiting YAP/TAZ to prevent uncontrolled proliferation and tumor development represent promising approaches to treat tumors with increased YAP/TAZ activity (Ehmer and Sage 2016).

1.4 Aim of this thesis

Elevated levels of B-MYB, FOXM1, and some MMB target genes can be observed in several human cancers and are associated with a poor prognosis. These findings strongly suggest a role of MMB in tumorigenesis (Sadasivam and DeCaprio 2013). Even though a lot of research regarding the MMB complex has been done at the biochemical level, the specific function of MMB in tumor cells has not been investigated up to now. In order to consider MMB as a therapeutic target for the treatment of cancer, however, it is absolutely essential to gain a deeper insight into the role and the specific mechanisms of MMB-regulated gene expression in cancer cells.

The aim of this thesis was to better understand how MMB regulates cell cycle-dependent gene expression in cancer cells using genome-wide expression and binding analyses of *Lin9*-deleted primary murine lung adenocarcinoma-derived cells.

2 Materials and Methods

2.1 Materials

2.1.1 Chemical stocks and reagents

Unless otherwise stated, chemicals were purchased from AppliChem, Invitrogen, Merck, Roth, and Sigma Aldrich.

Table 1: Chemical stocks and reagents

Chemical	Stock concentration
Acetic acid (CH_3COOH)	N/A
Agarose	N/A
Ammonium persulfate (APS)	10% in ddH_2O
AMPure XP Beads (Beckman Coulter)	N/A
Bovine serum albumin (BSA)	N/A
Bromophenol blue	4 mg/ml in ddH_2O
Crystal violet	1% in ddH_2O
Diethyl pyrocarbonate (DEPC)	ready-to-use
Dimethyl sulfoxide (DMSO)	ready-to-use
Dithiothreitol (DTT)	1 M in ddH_2O
dNTPs	2 mM in ddH_2O
Eosin Y solution 0.5% in water (Roth)	dilute 5-fold to 0.1% in ddH_2O, add 1-2 drops CH_3COOH
Ethanol	N/A
Ethidium bromide	ready-to-use (10 mg/ml)
Formaldehyde, 37%	N/A
Glycine	1 M in dH_2O
Glycogen (Roche)	ready-to-use (20 mg/ml)
Hemalum solution acid acc. to Mayer (Roth)	ready-to-use
Hoechst 33258	10 mg/ml in ddH_2O
Isopropanol	N/A
Ketamine/Ketavet (Pfizer)	ready-to-use (100 mg/ml)
Luminol	250 mM in DMSO
NP-40	ready-to-use
p-Coumaric acid	90 mM in DMSO
peqGOLD TriFast (Trizol; Peqlab)	ready-to-use
Phenylmethylsulfonyl fluoride (PMSF)	100 mM in isopropanol
Polyethylene glycol (PEG) 6000	50% in ddH_2O (sterilized by autoclaving for cell culture use)
Ponceau S solution	0.1% Ponceau S in 5% CH_3COOH
Protease inhibitor cocktail (PIC; Sigma)	ready-to-use

Chemical	Stock concentration
Protein G Dynabeads (Thermo Fisher)	ready-to-use
Proteinase K	10 mg/ml in 50 mM Tris pH 8.0, 1 mM $CaCl_2$
ProtoGel (30%; Acrylamide) (National Diagnostics)	ready-to-use
PSP	3% paraformaldehyde, 2% sucrose in ddH_2O
Random primer (Roche)	500 µg/ml in ddH_2O
RNase A	10 mg/ml in 10 mM Tris pH 7.4, 150 mM NaCl
Shandon Immu-Mount (Thermo Fisher)	ready-to-use
Sodium dodecyl sulfate (SDS)	20% in ddH_2O
ß-Glycerolphosphate	1 M in ddH_2O
SYBR Green (Sigma)	1:10 in DMSO for storage
Triton X-100	ready-to-use
Tween-20	ready-to-use
Xylazine (CP-Pharma)	ready-to-use (2%)

2.1.2 Antibiotics

Table 2: Antibiotics used for the selection of bacteria and mammalian cells

Antibiotic	Stock concentration	Final concentration	Application
Ampicillin	100 mg/ml	100 µg/ml	Selection of transformed DH5α bacteria
Puromycin	10 mg/ml	1 µg/ml	Maintenance of KP and KPL cells stably transduced with retroviral $CreER^{T2}$ recombinase
		2.5 µg/ml	Added to KP and KPL cells seeded for the treatment with 4-hydroxytamoxifen (4-OHT)

2.1.3 Enzymes

Table 3: Enzymes and corresponding buffer

Enyzme	Company
5x RT reaction buffer (for Reverse Transcriptase)	Thermo Fisher
EcoRI [10 U/µl]	Thermo Fisher
HaeIII [10 U/µl]	NEB
HindIII [10 U/µl]	Thermo Fisher
HisTaq16 DNA Polymerase [5 U/µl]	provided by AG Gessler
NlaIII [10 U/µl]	NEB
Phusion Hot Start II DNA Polymerase [2 U/µl]	Thermo Fisher
RevertAid Reverse Transcriptase (RT) [200 U/µl]	Thermo Fisher
RiboLock RNase Inhibitor (RI) [40 U/µl]	Thermo Fisher
SYBR Select Master Mix	Thermo Fisher
T4 DNA Ligase	NEB

2.1.4 Kits and Protein/DNA markers

Table 4: Kits used for molecular biology and next-generation sequencing

Name	Company
(DNF-474) High Sensitivity NGS Fragment Analysis Kit (1bp – 6,000bp)	Advanced Analytical Technologies
Duolink In Situ Detection Reagents Red	Sigma-Aldrich
Experion DNA 1K Analysis Kit	Bio-Rad
Experion RNA StdSens Analysis Kit	Bio-Rad
NEBNext Multiplex Oligos for Illumina (Dual Index Primers Set 1)	NEB
NEBNext Poly(A) mRNA Magnetic Isolation Module	NEB
NEBNext Ultra II DNA library Prep Kit for Illumina	NEB
NEBNext Ultra RNA Library Prep Kit for Illumina	NEB
NucleoSpin Tissue XS Kit	Macherey-Nagel
PureLink™ HiPure Plasmid Filter Midi- or Maxiprep Kits	Thermo Fisher
QIAquick PCR Purification Kit	Qiagen
Quant-iT PicoGreen dsDNA Assay Kit	Thermo Fisher
RNase-Free DNase Set	Qiagen
RNeasy Mini Kit	Qiagen

Table 5: Protein and DNA markers

Marker	Company
DNA Ladder 100 bp	Thermo Fisher
GeneRuler 1 kb DNA Ladder	Thermo Fisher
PageRuler Prestained Protein Ladder, 10 to 180 kDa	Thermo Fisher

2.1.5 Buffers and solutions

2.1.5.1 General buffers

Table 6: General buffers

Buffer	Ingredients	Storage temperature
0.5 M EDTA, pH 8.0	0.5 M EDTA in ddH_2O adjust pH to 8.0 with NaOH pellets	RT
10x PBS	1.37 M NaCl 26.8 mM KCl 101.4 mM Na_2HPO_4 17.5 mM KH_2PO_4 adjust pH to 7.4 with HCl	RT
1x PBS	dilute 10x PBS 1:10 in ddH_2O, autoclaved	RT
10x TE	100 mM Tris-HCl, pH 7.5 10 mM EDTA (pH 8.0)	RT
1x TE	dilute 10x TE 1:10 in ddH_2O, autoclaved	RT

2.1.5.2 Buffers for mammalian cell culture

Table 7: Buffers used for mammalian cell culture

Buffer	Ingredients	Storage temperature
1x PBS	see **2.1.5.1**, autoclaved	RT
50% Polyethylene glycol (PEG) 6000	in ddH_2O, autoclaved	4 °C
4 M NaCl	in ddH_2O, autoclaved	4 °C
50 mM Tris-HCl pH 7.4	in ddH_2O, autoclaved	4 °C
PSP (3% paraformaldehyde, 2% sucrose in PBS)	15 g paraformaldehyde 10 g sucrose ad 500 ml 1x PBS	-20 °C
2x HBS (pH 7.05)	see **Table 27**, sterile filtered	4 °C
2.5 M $CaCl_2$	see **Table 27,** sterile filtered	4 °C
0.1 % Crystal violet staining solution	1% Crystal violet dissolved in ddH_2O is diluted 1:10 in 20% Ethanol	RT
10% Acetic acid (CH_3COOH)	100% Acetic acid (CH_3COOH) is diluted 1:10 in ddH_2O	RT

2.1.5.3 Buffers for molecular biology

Table 8: Buffers used for molecular biology

Buffer	Ingredients	Storage temperature
LB medium	see **2.1.13**	RT
Base buffer	25 mM NaOH 0.2 mM EDTA, pH 8.0 adjust pH to 12.0 with NaOH	RT
Neutralization buffer	40 mM Tris-HCl, pH 5.0	RT
Tail buffer	100 mM Tris-HCl pH 8.5 5 mM EDTA 0.2% SDS 200 mM NaCl	RT
6 M NaCl	in ddH_2O	RT
10x ReproFast buffer	100 mM $(NH_4)_2SO_4$ 200 mM Tris-HCl, pH 8.8 100 mM KCl 20 mM $MgSO_4$ 1% BSA 1% Triton X-100 sterile filtered	-20°C

Buffer	Ingredients	Storage temperature
50x TAE	242 g Tris base 57.1 ml CH_3COOH 100 ml 0.5 M EDTA, pH 8.0 ad 1 l ddH_2O	RT
1x TAE	dilute 50x TAE 1:50 in VE H_2O	RT
5x Loading buffer	15% Ficoll 0.05% Bromophenol blue 0.05% Xylene cyanol 0.05 M EDTA	4 °C
DEPC water	1 ml DEPC is added per 1000 ml of ddH_2O to a final concentration of 0.1%, stirred until completely dissolved, and autoclaved	RT

2.1.5.4 Buffers for protein biochemistry

Table 9: Buffers used for whole cell lysates and nuclear extracts

Buffer	Ingredients	Storage temperature
TNN buffer, pH 7.5	50 mM TrisHCl, pH 7.5 120 mM NaCl 5 mM EDTA 0.5% NP-40 10 mM $Na_4P_2O_7$ 2 mM Na_3VO_4 100 mM NaF adjust pH with 37% HCl to 7.5	4 °C
Bradford solution	50 mg Coomassie Brilliant Blue G250 23.75 ml Ethanol 50 ml 85% (v/v) H_3PO_4 ad 500 ml ddH_2O filter twice	4 °C
Buffer A (for nuclear extracts)	10 mM HEPES, pH 7.4 10 mM NaCl 3 mM $MgCl_2$	4 °C
Nuclei lysis buffer (for nuclear extracts)	20 mM HEPES, pH 7.4 400 mM NaCl 1.5 mM $MgCl_2$ 0.1 mM EDTA 15% Glycerol	4 °C
20 mM HEPES, pH 7.4	in ddH_2O	RT

Table 10: Buffers used for SDS-PAGE and immunoblotting

Buffer	Ingredients	Storage temperature
0.5 M Tris, pH 6.8	0.5 M Tris base in ddH_2O adjust pH with 37% HCl to 6.8	RT
1.5 M Tris, pH 8.8	1.5 M Tris base in ddH_2O adjust pH with 37% HCl to 8.8	RT
10x SDS running buffer	144 g Glycine 30 g Tris 10 g SDS ad 1 l ddH_2O	RT
1x SDS running buffer	dilute 10X SDS running buffer 1:10 in ddH_2O	RT
3x ESB	300 mM Tris-HCl pH 6.8 15 mM EDTA 150 mM DTT 12% (w/v) SDS 15% (w/v) Glycerol 0.03% Bromophenol blue	- 20°C
5x Blotting buffer	75 g Tris 282.25 g Glycine ad 5 l ddH_2O, autoclaved	RT
1x Blotting buffer	dilute 5X Blotting buffer 1:10 in ddH_2O and add 150 ml Methanol per 1 l	4 °C
Ponceau S solution	0.1% Ponceau S 5% CH_3COOH	RT
20x TBS	1 M Tris-HCl 3 M NaCl adjust pH with 37% HCl to 7.4	RT
1x TBS	dilute 20x TBS 1:20 in ddH_2O	RT
TBS-T	1x TBS with 0.1% Tween 20	RT
Enhanced chemiluminescence solution (ECL)	10 ml 100 mM Tris-HCl pH 8.5 50 µl 250 mM Luminol 22 µl 90 mM p-Coumaric acid 3 µl 30% H_2O_2	RT

Table 11: Buffers used for Proximity Ligation Assay (PLA)

Buffer	Ingredients	Storage temperature
Wash buffer A	10 mM Tris-HCl, pH 7.4 150 mM NaCl 0.05% Tween 20	4 °C
Wash buffer B	200 mM Tris-HCl, pH 7.5 100 mM NaCl	4 °C

Table 12: Buffers used for ChIP and 4C-seq

Buffer	Ingredients	Storage temperature
Lysis buffer I	5 mM PIPES, pH 8.0 85 mM KCl 0.5% NP-40	4 °C
Lysis buffer II (RIPA buffer)	50 mM HEPES, pH 7.9 140 mM NaCl 1 mM EDTA 1% Triton X-100 0.1% $C_{24}H_{39}NaO_4$ 0.1% SDS	4 °C
5 M NaCl	in ddH_2O	RT
3 M C_2H_3NaO2 (sodium acetate)	in ddH_2O	RT
Wash buffer I	20 mM Tris-HCl, pH 8.1 150 mM NaCl 2 mM EDTA 0.1% SDS 1% Triton X-100	4 °C
Wash buffer II	20 mM Tris-HCl, pH 8.1 500 mM NaCl 2 mM EDTA 0.1% SDS 1% Triton X-100	4 °C
Wash buffer III	10 mM Tris-HCl, pH 8.1 250 mM LiCl 1 mM EDTA 1% NP-40 1% $C_{24}H_{39}NaO_4$	4 °C
Elution Buffer (freshly prepared)	1% SDS 0.1 M $NaHCO_3$	RT
Lysis buffer for 4C-seq	50 mM Tris-HCl, pH 7.5 150 mM NaCl 5 mM EDTA 0.5% NP-40 1% Triton-X 100	4 °C
2 M C_2H_3NaO2 for 4C-seq (sodium acetate)	in ddH_2O	RT
1x PK buffer for 4C-seq	10 mM Tris-HCl, pH 8.0 5 mM EDTA, pH 8.0 0.5% SDS	RT

Table 13: Buffers used for histology

Buffer	Ingredients	Storage temperature
4% Paraformaldehyde (PFA)	40 g PFA + 100 ml 10x PBS (DEPC) + 3.5 ml 2 M NaOH (DEPC) warm up to approx. 68 °C; adjust pH with 1 M HCl to 7.0; ad 1 l DEPC-H_2O	-20°C
0.1% Eosin Y solution	dilute 0.5% Eosin Y solution (Roth) in ddH2O to 0.1% and add 1-2 drops CH_3COOH	RT (dark)
1% DAB	0.1 g DAB dissolved in 10 ml ddH_2O, acidified with 200 µl 10 M HCl	-20°C
DAB staining solution (freshly prepared)	4.5 ml Tris, pH 7.5 250 µl 1% DAB 250 µl 0.3% H_2O_2	for immediate use

2.1.6 Antibodies

Table 14: Primary antibodies

Name	Internal no.	Origin	Application and dilution	Company	Catalog number
α-TUBULIN (B-5-1-2)	295	mouse monoclonal	IF 1:150	Santa Cruz	sc-23948
ß-ACTIN (C4)	196	mouse monoclonal	WB 1:5000	Santa Cruz	sc-47778
B-MYB (N-19)	79	rabbit polyclonal	IP 2 µg ChIP-qPCR 3 µg ChIP-seq 9 µg	Santa Cruz	sc-724
B-MYB phospho T487 (EPR2204Y)	233	rabbit monoclonal	PLA 1:100 IHC 1:400	Abcam	ab76009
B-MYB (LX015.1)	149	mouse monoclonal	WB 1:3 – 1:5	gift from Watson lab (Hybridoma)	Tavner et al. (2007)
CYCLIN A (BF683)	39	mouse monoclonal	WB 1:500	Santa Cruz	sc-239
CDC20 (p55 CDC; E-7)	197	mouse monoclonal	WB 1:500	Santa Cruz	sc-13162
FLAG (M2)	93	mouse monoclonal	IP 2.5 µg WB 1:5000	Sigma-Aldrich	F3165
HA (HA.11)	92	mouse monoclonal	WB 1:1000	Covance	MMS-101P
Histone H3K4me3	307	rabbit polyclonal	ChIP-seq 5 µg	Abcam	ab8580

Name	Internal no.	Origin	Application and dilution	Company	Catalog number
Histone H3K4me1	308	rabbit polyclonal	ChIP-seq 5 µg	Abcam	ab8895
Histone H3K27ac	309	rabbit polyclonal	ChIP-seq 5 µl	Merck Millipore	07-360
IgG	104	rabbit polyclonal	IP 2 µg ChIP-qPCR 3 µg ChIP-seq 9 µg	Sigma-Aldrich	I5006
LIN9	292	rabbit polyclonal	IP 1 µg WB 1:2000 PLA 1:150 ChIP-qPCR 3 µg ChIP-seq 9 µg	Biomol (Bethyl); from the lab of James A. DeCaprio	A300-BL2981; Litovchick et al. (2007)
phospho H3 (Ser10)	290	rabbit polyclonal	IF 1:100 – 1:200	Santa Cruz	sc-8656-R
TOP2A (Topo IIα; F-12)	224	mouse monoclonal	WB 1:1000	Santa Cruz	sc-365916
YAP (D8H1X)	299	rabbit monoclonal	IF 1:200	Cell Signaling	14074S
YAP	302	rabbit polyclonal	IP 2 µg ChIP-qPCR 3 µg ChIP-seq 9 µg	Novus Biologicals	NB110-58358
YAP	303	rabbit polyclonal	IHC 1:200 WB 1:1000	Cell Signaling	4912
YAP (63.7)	297	mouse monoclonal	WB 1:1000 PLA 1:200	Santa Cruz	sc-101199

Table 15: Secondary antibodies

Name	Application and dilution	Company	Catalog number
anti-mouse HRP conjugated	WB 1:5000	GE Healthcare	NXA931
anti-mouse IgG (H+L) Alexa Fluor 488	IF 1:500	Thermo Fisher	A-11029
anti-mouse IgG (H+L) Alexa Fluor 594	IF 1:500	Thermo Fisher	A-11032
anti-rabbit HRP conjugated	IHC 1:200	Thermo Fisher	656120
anti-rabbit IgG (H+L) Alexa Fluor 488	IF 1:500	Thermo Fisher	A-21206
anti-rabbit IgG (H+L) Alexa Fluor 594	IF 1:500	Thermo Fisher	A-11037
Duolink In Situ PLA Probe Anti-Mouse PLUS	PLA 1:5	Sigma-Aldrich	DUO92001
Duolink In Situ PLA Probe Anti-Rabbit MINUS	PLA 1:5	Sigma-Aldrich	DUO92005
HRP Protein A	WB 1:5000	BD Biosciences	610438
mouse TrueBlot ULTRA: Anti-Mouse IgG HRP	WB 1:1000	eBiosciences	18-881733

2.1.7 Plasmids

Table 16: Plasmids for transient expression and lentivirus production in mammalian cells

Name	Internal lab no.	Description
pBABE-H2B-GFP	746	GFP expression vector used to determine transfection efficiency and for co-transfection of KP and KPL cells in YAP rescue experiment
pBABE-Puro-CreER^{T2}	924	retroviral infection of KP and KPL cells
pcDNA3	212	empty vector used to transfect equal plasmid amounts
pcDNA4/TO-HA-BMYB	1159	transient expression of HA-tagged B-MYB
pCMV-2N3T	645	empty control vector (ev) for YAP rescue experiment in KP and KPL cells
pCMV-2xFlag-YAP	1504	transient expression of FLAG-tagged wild-type YAP
pCMV-2xFlag-YAP-5SA	1505	transient expression of FLAG-tagged constitutively active YAP5SA
pCMV-VSV-G	1348	lentiviral envelope plasmid
psPAX2	1386	lentiviral packaging plasmid
Ubc-shLuc-pgk-Cre	1558	Cre-expressing lentiviral construct for intratracheal infection of *K-Ras*$^{LSL-G12D/+}$; *p53*$^{fl/fl}$ mice

2.1.8 Primers

All primers for genotyping or qPCR were purchased from Metabion or Eurofins Genomics. 4C-seq primers were purchased from Sigma-Aldrich. Primers were dissolved in 1x TE to a stock concentration of 100 µM for long-term storage at – 20 °C. For setting up PCRs, primers were pre-diluted in ddH_2O to a concentration of 10 µM.

Table 17: Primers for genotyping of mice and murine cells

Gene	Internal no.	Sequence (5' to 3')	Directionality
K-Ras	SG2031	GTCTTTCCCCAGCACAGTGC	forward
	SG2032	CTCTTGCCTACGCCACCAGCTC	reverse
	SG2033	AGCTAGCCACCATGGCTTGAGTAAGTCTGCA	forward
Lin9	SG893	CCTGGCTGCCTAGCATTTAC	forward
	SG722	GCAAAAGCTGCAAGTCCTCT	reverse
p53	SG1556	GGTTAAACCCAGCTTGACCA	forward
	SG1557	GGAGGCAGAGACAGTTGGAG	reverse

Table 18: Primers for quantitative real-time PCR (qPCR) of murine cDNA

Gene	Internal no.	Sequence (5' to 3')	Directionality
Aspm	1026	GATGGAGGCCGAGAGAGG	forward
	1027	CAGCTTCCACTTTGGATAAGTATTTC	reverse
Axl	2397	TGCATGAAGGAATTTGACCA	forward
	2398	ATCTGAGTGGGCAGGAACAC	reverse
Birc5	961	CCCGATGACAACCCGATA	forward
	962	CATCTGCTTCTTGACAGTGAGG	reverse
Cdc20	2191	ACATCAAGGCGCTGTCAAG	forward
	2192	AATGTGCCGGTCACTGGT	reverse
Cenpf	1038	AGCAAGTCAAGCATTTGCAC	forward
	1039	GCTGCTTCACTGATGTGACC	reverse
Cyr61	2395	CAGCACCTCGAGAGAAGGAC	forward
	2396	GGTCAAGTGGAGAAGGGTGA	reverse
Ect2	2195	TGCTCTGCTTCACTGGATTC	forward
	2196	ATGATGAACCAACGTCACCA	reverse
Gas2l3	1034	GCAGCCTGCAATCCAAGT	forward
	1035	AGGGGACACCTGGGACTTA	reverse
Hmmr	1202	TCACGGAGTCTAAGGGAAAAAT	forward
	1203	TTCATCGATCTTTTCTTTCTCTATTG	reverse
Hprt	783	TCCTCCTCAGACCGCTTTT	forward
	784	CCTGGTTCATCATCGCTAATC	reverse
Lin9	785	TTGGGACTCACACCATTCCT	forward
	786	GAAGGCCGCTGTTTTTGTC	reverse
Mybl2	820	TTAAATGGACCCACGAGGAG	forward
	821	TTCCAGTCTTGCTGTCCAAA	reverse
Nusap1	1030	TCTAAACTTGGGAACAATAAAAGGA	forward
	1031	TGGATTCCATTTTCTTAAAACGA	reverse
Sdpr	2203	CTTCAAAGTGCTCATCTTCCAG	forward
	2204	CCTCCAGGGACTTGTTCTCA	reverse
Top2a	2193	CAAAAGAGTCATCCCCCAAG	forward
	2194	GGGGTACCCTCAACGTTTTC	reverse
Yap	2170	GAGGGACTCCGAATGCAG	forward
	2171	CGAGAGTGATAGGTGCCACTG	reverse

Table 19: Primers for qPCR of human cDNA

Gene	Internal no.	Sequence (5' to 3')	Directionality
ANLN	2275	GCGAGCTAGACAGCCACTTT	forward
	2276	TTTTTGATGGCGATGGTTTT	reverse
AURKA	2548	GCAGATTTTGGGTGGTCAGT	forward
	2549	TCCGACCTTCAATCATTTCA	reverse
BIRC5	568	GCCCAGTGTTTCTTCTGCTT	forward
	569	CCGGACGAATGCTTTTTATG	reverse
CCNA2	572	GGTACTGAAGTCCGGGAACC	forward
	573	GAAGATCCTTAAGGGGTGCAA	reverse
CDC20	2273	CTGTCTGAGTGCCGTGGAT	forward
	2274	TCCTTGTAATGGGGAGACCA	reverse
CENPF	1083	GAGTCCTCCAAACCAACAGC	forward
	1084	TCCGCTGAGCAACTTTGAC	reverse
CTGF	2295	CAAGGGCCTCTTCTGTGACT	forward
	2296	ACGTGCACTGGTACTTGCAG	reverse
ECT2	2269	GTGGTTCTGGGGAAGCATT	forward
	2270	AAGCATTGACACTGATTTCTTGAG	reverse
GAPDH	645	GCCCAATACGACCAAATCC	forward
	646	AGCCACATCGCTCAGACAC	reverse
GAS2L3	1058	GCTGTCGGCATGAAGAGC	forward
	1059	AATCGATGAGAACAACTACAAGGA	reverse
KIF23	1862	CCTAACGTCCCGCAGTCTT	forward
	1863	AGGTTTCCGGGGTGTCTTAG	reverse
LIN9	580	CCCCACCACGGTTACATTAT	forward
	581	CGGCGACTGTCCTAATAAAGG	reverse
LIN9	2572	CAAAGTTTTGCATAAAGTTCAACAGT	forward
	2573	CGTCTCATATCTGTTGGCTGAT	reverse
MYBL2	630	TCCACACTGCCCAAGTCTCT	forward
	631	AGCAAGCTGTTGTCTTCTTTGA	reverse
NUSAP1	1060	TTTTGAAGAACACAATTCCATGA	forward
	1061	GTCCTGACCCCTCCCTTATT	reverse
TBP	2297	CACGAACCACGGCACTGATT	forward
	2298	TTTTCTTGCTGCTGCCAGTCTGGAC	reverse
TOP2A	2421	TCTGGTCCTGAAGATGATGCT	forward
	2422	TTAGTTAACCATTCCTTTCGATCA	reverse
YAP	2277	GACATCTTCTGGTCAGAGATACTTCTT	forward
	2278	GGGGCTGTGACGTTCATC	reverse

Table 20: Primers for qPCR of human ChIP-DNA.

Name	Internal no.	Sequence (5' to 3')	Directionality
AMOTL2 promoter	2364	TGCCAGGAATGTGAGAGTTTC	forward
	2365	AGGAGGGAGCGGGAGAAG	reverse
AURKA promoter	2534	CGCACTTGCTCCCTAAGAAC	forward
	2535	TGGGACTGCCACAGGTCT	reverse
AURKA enhancer	2528	TTCAGCTCCCATGACACATC	forward
	2529	TTTCCCTGCACACAGACCTT	reverse
BIRC5 promoter	612	CCATTAACCGCCAGATTTGA	forward
	613	GCGGTGGTCCTTGAGAAAG	reverse
CDC20 promoter	2556	GGTTGCGACGGTTGGATTTT	forward
	2557	CTTTAACACGCCTGGCTTACG	reverse
CDC20 enhancer	2558	GGATCAGACCACACCCTCAA	forward
	2559	GCCCTCATTCCGTGCATACT	reverse
CENPF promoter	1091	GGCGTGGAGGTAAGTTTGG	forward
	1092	TGGAGCCCAGAGTCTAATTCA	reverse
CTGF promoter	2366	TGTGCCAGCTTTTTCAGACG	forward
	2367	TGAGCTGAATGGAGTCCTACACA	reverse
CYR61 promoter	2368	CACACACAAAGGTGCAATGGAG	forward
	2369	CCGGAGCCCGCCTTTTATAC	reverse
ECT2 promoter	2354	ACACACGCACAACCAATCAA	forward
	2355	CGCGTGATGTCAACCTCTTT	reverse
GAPDHS promoter	540	GGCAGCAAGAGTCACTCCA	forward
	541	TGTCTCTTGAAGCACACAGGTT	reverse
KIF23 promoter	1894	CCTAACGTCCCGCAGTCTT	forward
	1895	GCCTCGTACTCACGCTGAC	reverse
KIF23 enhancer 1	2592	TGCAGAACCCCTCAGTCTCA	forward
	2593	CCCAATTCCCCGCAACACA	reverse
KIF23 enhancer 3	2590	GCTTGGCATTTGGTCTTGGA	forward
	2591	CACACCACTCACGACTTCTGA	reverse
MYBL2 promoter	2600	CTGGGGTGTGTGTGTGTGTT	forward
	2601	CCCAGGACGCAGCATTTCC	reverse
MYBL2 enhancer	2602	GTGGCCTCGACCTCTTCAC	forward
	2603	TTGCTCCCTTCCCCAAATCC	reverse
TOP2A promoter	2342	GGTGCCTTTTGAAGCCTCTC	forward
	2343	TCCACCTATGAACGGCTGAG	reverse

Table 21: Primers for 4C-seq (*indicates a phosphorothioate bond)

Gene	Internal no.	Primer name	Sequence (5' to 3')	Sample
AURKA	2482	AURKA_P5_CGT	AATGATACGGCGACCACCGAGATCTACACTCTTTCCCTACACGACGCTCTTCCGATCTCGTAACAGCCCCTTGACGTCA*A	- doxy
	2483	AURKA_P5_ACA	AATGATACGGCGACCACCGAGATCTACACTCTTTCCCTACACGACGCTCTTCCGATCTACAAACAGCCCCTTGACGTCA*A	+ doxy
	2484	AURKA_P7	CAAGCAGAAGACGGCATACGAGATGTGACTGGAGTTCAGACGTGTGCTCCCGTCCCTGAGTGTCCTT*G	-/+ doxy
CDC20	2479	CDC20_P5_CGT	AATGATACGGCGACCACCGAGATCTACACTCTTTCCCTACACGACGCTCTTCCGATCTCGTTGAGGTTGAAAAGGGTGAATG*A	- doxy
	2480	CDC20_P5_ACA	AATGATACGGCGACCACCGAGATCTACACTCTTTCCCTACACGACGCTCTTCCGATCTACATGAGGTTGAAAAGGGTGAATG*A	+ doxy
	2481	CDC20_P7	CAAGCAGAAGACGGCATACGAGATGTGACTGGAGTTCAGACGTGTGCTCGGTGGCCCTGATTTTGTG*G	-/+ doxy
KIF23	2491	KIF23_P5_CGT	AATGATACGGCGACCACCGAGATCTACACTCTTTCCCTACACGACGCTCTTCCGATCTCGTGAGACTGAATGTTTGTTGAATG*A	- doxy
	2492	KIF23_P5_ACA	AATGATACGGCGACCACCGAGATCTACACTCTTTCCCTACACGACGCTCTTCCGATCTACAGAGACTGAATGTTTGTTGAATG*A	+ doxy
	2493	KIF23_P7	CAAGCAGAAGACGGCATACGAGATGTGACTGGAGTTCAGACGTGTGCTCACCACCACACCCAGCTAAT*T	-/+ doxy
MYBL2	2488	MYBL2_P5_CGT	AATGATACGGCGACCACCGAGATCTACACTCTTTCCCTACACGACGCTCTTCCGATCTCGTACCACAGAAGGAAGACTAACTC*A	- doxy
	2489	MYBL2_P5_ACA	AATGATACGGCGACCACCGAGATCTACACTCTTTCCCTACACGACGCTCTTCCGATCTACAACCACAGAAGGAAGACTAACTC*A	+ doxy
	2490	MYBL2_P7	CAAGCAGAAGACGGCATACGAGATGTGACTGGAGTTCAGACGTGTGCTCAATCAGTTCTCCCACCTCG*G	-/+ doxy

2.1.9 siRNAs

Non-targeting control siRNA and siRNAs specifically targeting murine *Yap/Taz*, human *Lin9* or human *Mybl2* were purchased from Dharmacon or Eurofins Genomics and dissolved in the appropriate buffer provided by the supplier to a stock concentration of 75 µM.

Table 22: siRNAs and their corresponding sequences

Target gene	Name	Species	Internal lab no.	Sequence (5' to 3')	Supplier
LIN9	si*LIN9*	human	S5	GGAAGAGAGAUCAGCAUUAUU	Dharmacon
MYBL2	si*MYBL2*	human	S6	GAAACGAGCCUGCCUUACAUU	Dharmacon
Non-targeting	siCtrl	/	S52	UGGUUUACAUGUCGACUAA	Dharmacon
Taz	si*Taz*	mouse	S69	CAGCCGAAUCUCGCAAUGA	Eurofins Genomics
Yap	si*Yap* #1	mouse	S67	CGGUUGAAACAACAGGAAU	Eurofins Genomics
Yap	si*Yap* #2	mouse	S68	GAAGCGCUGAGUUCCGAAA	Eurofins Genomics

2.1.10 Cell lines

Table 23: Human and mouse cell lines

Designation	Organism	Description	Reference
A549	*homo sapiens*	epithelial lung carcinoma cell line	ATCC® CCL-185™
HEK293TN	*homo sapiens*	human embryonic kidney cells with constitutive expression of SV40 large T antigen and neomycin resistance gene; used as a lentivirus producer cell line	SBI Cat.-no.: LV900A-1
HeLa	*homo sapiens*	epithelial cervical adenocarcinoma cell line; used for protein-protein interaction studies	ATCC® CCL-2™
KP1	*mus musculus*	primary cell line from a dissected lung adenocarcinoma from a *K-Ras*$^{LSL\text{-}G12D/+}$*; p53*$^{fl/fl}$*; Lin9*$^{+/+}$ mouse; stably transduced with the hormone-inducible CreER^{T2} recombinase	Iltzsche et al. (2017)

Designation	Organism	Description	Reference
KP2	*mus musculus*	primary cell line from a dissected lung adenocarcinoma from a *K-Ras$^{LSL-G12D/+}$; p53$^{fl/fl}$; Lin9$^{+/+}$* mouse; stably transduced with the hormone-inducible CreER^{T2} recombinase	Iltzsche et al. (2017)
KPL1	*mus musculus*	primary cell line from a dissected lung adenocarcinoma from a *K-Ras$^{LSL-G12D/+}$; p53$^{fl/fl}$; Lin9$^{fl/fl}$* mouse; stably transduced with the hormone-inducible CreER^{T2} recombinase	Iltzsche et al. (2017)
KPL2	*mus musculus*	primary cell line from a dissected lung adenocarcinoma from a *K-Ras$^{LSL-G12D/+}$; p53$^{fl/fl}$; Lin9$^{fl/fl}$* mouse; stably transduced with the hormone-inducible CreER^{T2} recombinase	Iltzsche et al. (2017)
MCF10A YAP5SA	*homo sapiens*	non-tumorigenic, epithelial cells from the mammary gland/breast stably transduced with pInducer21-Strep-YAP5SA	von Eyss et al. (2015)
NIH/3T3-pZ/EG	*mus musculus*	embryonic fibroblasts (NIH/3T3) stably transfected with the GFP-reporter plasmid pZ/EG; used for lentivirus titration	Novak et al. (2000) Iltzsche et al. (2017)
Plat-E	*homo sapiens*	retrovirus packaging cell line based on 293T cells	Morita et al. (2000)

2.1.11 Cell culture reagents, media, and additives

Table 24: Reagents used to culture mammalian cells

Reagent	Supplier
1x PBS	13.7 mM NaCl 0.3 mM KCl 0.64 mM Na_2HPO_4 0.15 mM KH_2PO_4 adjust pH to 7.4 with HCl
Cholera Toxin	Sigma-Aldrich
DMEM (1X) + GlutaMAX	Thermo Fisher
FBS	Thermo Fisher
Ham's F-12 Nut Mix (1X) + GlutaMAX	Thermo Fisher
Horse serum (donor herd)	Sigma-Aldrich
Human EGF	Sigma-Aldrich
Hydrocortisone	Sigma-Aldrich
Insulin solution human	Sigma-Aldrich
Penicillin-Streptomycin (10,000 U/ml)	Thermo Fisher

Reagent	Supplier
RPMI Medium 1640 (1X) + GlutaMAX	Thermo Fisher
Trypsin-EDTA (0.05%), phenol red	Thermo Fisher
Trypsin-EDTA (0.25%), phenol red	Thermo Fisher

Table 25: Composition of media

Media	Cell line	Composition
DMEM	KP, KPL, HEK293TN, NIH/3T3-pZ/EG, HeLa	DMEM 10% FBS 1% pen-strep
MCF10A medium	MCF10A YAP5SA	DMEM/F-12 (1:1) 5% horse serum 1% pen-strep 20 ng/ml hEGF 100 ng/ml cholera toxin 10 µg/ml insulin 500 ng/ml hydrocortisone
RPMI	A549	RPMI 10% FBS 1% pen-strep

Table 26: Reagents used for the treatment of mammalian cells

Reagent	Dissolved in	Stock concentration	Final concentration	Supplier
4- Hydroxytamoxifen (4-OHT)	100% Ethanol	25 µM	10 nM	Sigma-Aldrich
Verteporfin	DMSO	2 mg/ml (2.78 mM)	7.5 µM	Sigma-Aldrich
Doxycycline (hyclate) (dox)	ddH_2O	1 mg/ml	0.5 µg/ml	Sigma-Aldrich
Nocodazole	DMSO	1 mg/ml	50 ng/ml	Sigma-Aldrich
Polybrene	ddH_2O	4 mg/ml	8 µg/ml	Sigma-Aldrich

2.1.12 Transfection reagents

Table 27: Reagents used for transfections

Transfection reagent	Supplier/composition
2.5 M CaCl2	sterile filtered
2x HBS (HEPES buffered saline)	8.2 g NaCl 5.95 g HEPES, free acid 0.105 g Na_2PO4 add ddH2O to a final volume of 500 ml adjust pH with 5 M NaOH to 7.05 sterile filtered
Lipofectamine 2000	Thermo Fisher
Lipofectamine RNAiMAX	Thermo Fisher
Opti-MEM (1X) + GlutaMAX	Thermo Fisher

2.1.13 Bacterial strains and media

Bacterial strain:	DH5α	genotype: F– Φ80lacZΔM15 Δ(lacZYA-argF) U169 recA1 endA1 hsdR17 (rK–, mK+) phoA supE44 λ– thi-1 gyrA96 relA1 (source: Thermo Fisher)
Media:	Luria Bertani (LB) agar	40 g powder in 1 l ddH_2O, autoclaved
	Luria Bertani (LB) medium	25 g powder in 1 l ddH_2O, autoclaved

2.1.14 Mouse strains

All mouse strains were maintained on a C57BL/6 background. *Kras*^{tm4Tyj} (*K-Ras*$^{LSL-G12D/+}$) mice were crossed with *Trp53*^{tm1Brn} (*p53*$^{fl/fl}$) to get *K-Ras*$^{LSL-G12D/+}$; *p53*$^{fl/fl}$ mice (Marino et al. 2000; Jackson et al. 2001).

2.1.15 Devices

Table 28: Devices and their suppliers

Device	Supplier
Agarose gel electrophoresis system	Peqlab
Cytomics FC 500 flow cytometer	Beckman Coulter
DynaMag-2 Magnet	Thermo Fisher
DynaMag-96 Side Magnet	Thermo Fisher
Electrophoresis Power Supply E835	Consort
Experion Automated Electrophoresis Station	Bio-Rad
Fragment Analyzer Automated CE System	Advanced Analytical
Hyrax M 40	Carl Zeiss
Infinite M200 plate reader	Tecan
Leica DFC350 FX digital camera	Leica Microsystems
Leica DMI 6000B inverted microscope	Leica Microsystems
Lumen 200 fluorescence light source	Prior
Microm EC 350 modular paraffin embedding center	Thermo Fisher
Min-PROTEAN 3 Cell System	Bio-Rad
Mini Trans-Blot Cell System	Bio-Rad
Multiskan Ascent plate reader	Labsystems
Mx3000P qPCR System	Stratagene
NanoDrop 2000 spectral photometer	Peqlab
NextSeq 500	Illumina
Nikon Eclipse TS100	Nikon
PowerPac HC High Current Power Supply	Bio-Rad
Sonifier W-250 D	Branson
T1 Thermocycler	Biometra
Ultrospec 2100 pro spectrophotometer	Amersham Biosciences

2.1.16 Software

Table 29: Software and supplier/reference

Software	Supplier/Reference
BEDTools v2.26.0	Quinlan and Hall (2010)
Bowtie v1.1.2	Langmead et al. (2009)
Bowtie v2.3.2	Langmead and Salzberg (2012)
CASAVA	Illumina
CXP Acquisition and Analysis (Cytomics FC 500)	Beckman Coulter
DAVID v6.8	Huang da et al. (2009)
EdgeR	Robinson et al. (2010)
FASTQ Generation Software v1.0.0	Illumina
Fiji	Schindelin et al. (2012)
GSEA (Broad Institute)	Subramanian et al. (2005)
Integrative Genomics Viewer (IGV)	Ramirez et al. (2016)
KM-plotter	Gyorffy et al. (2013) http://kmplot.com/analysis/
Leica Application Suite (LAS) 3.7	Leica Microsystems
MACS v.2.1.1	Zhang et al. (2008)
Oncomine	Rhodes et al. (2004) www.oncomine.org
Prism 7.0c	GraphPad Software, Inc
R environment	https://www.r-project.org
ROSE	Loven et al. (2013); Whyte et al. (2013)
SICER v1.1	Xu et al. (2014)
Tecan i-control	Tecan
TopHat v2.1.0	Kim et al. (2013)
Venn diagram webtool	http://bioinformatics.psb.ugent.be/webtools/Venn/
w4CSeq	Cai et al. (2016) https://github.com/WGLab/w4CSeq

2.2 Methods

2.2.1 Mammalian cell culture

2.2.1.1 Cell lines and culturing conditions

Cells used in this thesis were cultured at 37 °C and 95% humidity with 5% CO_2. All cell lines except for MCF10A YAP5SA and A549 cells were maintained in GIBCO® Dulbecco's Modified Eagle Medium (DMEM) supplemented with 10% (v/v) fetal bovine serum (FBS) and 1% (v/v) penicillin-streptomycin (pen-strep). KP1, KP2, KPL1, and KPL2 cells were cultured in the presence of 1 µg/ml puromycin, since they were stably transduced with a Cre-expressing retroviral vector encoding a puromycin resistance gene. A549 cells were maintained in GIBCO® Roswell Park Memorial Institute (RPMI) 1640 medium with 10% FBS and 1% pen-strep. MCF10A YAP5SA cells were cultured in a 1:1 mixture of Ham's F-12 Nutrient Mix and DMEM supplemented with 5% horse serum, 1% pen-strep, 20 ng/ml human EGF, 100 ng/ml cholera toxin, 10 µg/ml insulin, and 500 ng/ml hydrocortisone.

2.2.1.2 Passaging and seeding cells

Cells were subcultured every two to three days by washing once with 1x PBS followed by a 5-15 min incubation with 0.05% (HEK293TN, NIH/3T3-pZ/EG, HeLa, Plat-E, A549 and MCF10A YAP5SA cells) or 0.25% (KP1, KP2, KPL1, and KPL2 cells) Trypsin/EDTA at 37 °C. Subsequently, detached cells were resuspended in medium and seeded onto a new cell culture dish or plate according to demand or individual growth rate. **Table 30** shows the seeding densities for subconfluent and confluent cultures of MCF10A YAP5SA cells used for isolation of RNA, generation of whole cell lysates for Western Blot, and chromatin immunoprecipitation (ChIP).

Table 30: MCF10A YAP5SA cell numbers for subconfluent and confluent cultures

Application	MCF10A YAP5SA cell number	
	subconfluent/low density	confluent/high density
RNA isolation	145,000 cells/6 cm dish	735,000 cells/6 cm dish
Whole cell lysates (proteins)	$1x10^6$ cells/15 cm dish	$5x10^6$ cells/15 cm dish
ChIP	$1x10^6$ cells/15 cm dish	$5x10^6$ cells/15 cm dish

2.2.1.3 Freezing cells

Trypsinized cells were resuspended in fresh culture medium, transferred into a 15 ml falcon tube and centrifuged for 5 min at 300 x g and room temperature (RT). After discarding the supernatant, the cell pellet was dissolved in freezing medium (for KP1, KP2, KPL1, KPL2, HEK293TN, NIH/3T3, Plat-E, and HeLa cells: 50% DMEM, 40% FBS, 10% DMSO; for MCF10A YAP5SA cells: 25% F-12, 25% DMEM, 40% horse serum, 10% DMSO; for A549 cells: 50% RPMI, 40% FBS, 10% DMSO). Aliquots of 1 ml were transferred into cryotubes, which were placed at -80 °C for short-term and transferred into liquid nitrogen for long-term storage.

2.2.1.4 Thawing cells

Cells were quickly thawed in a 37 °C water bath, immediately transferred to a 15 ml falcon tube filled with 9 ml of fresh pre-warmed culture medium and centrifuged for 5 min at 300 x g and RT. The supernatant was removed, the cell pellet resuspended in 10 ml of the appropriate cell culture medium (**2.2.1.1**) and transferred onto a 10 cm cell culture dish.

2.2.1.5 Counting cells

In order to seed an appropriate cell number, cells were trypsinized and resuspended in medium as described in **2.2.1.2**. For counting, 10 µl of the cell suspension were filled into a Neubauer chamber. Cells within all four quadrants of the grid were counted under a light microscope. Cells touching the upper and left limits of the grid were counted, whereas cells touching the lower and right limits were not included. The average number of cells of all four quadrants was multiplied with the factor 10,000 to calculate the number of cells per milliliter.

2.2.1.6 Treatment of cells with reagents

With the exception of puromycin and 4-OHT treatment for growth curves, all substances were added in fresh medium one day after seeding.

4-OHT	KP and KPL cells were seeded in 2.5 µg/ml puromycin. The next day, to induce the hormone-inducible $CreER^{T2}$ recombinase and subsequent deletion of *Lin9*, the medium was replaced by fresh medium containing 2.5 µg/ml puromycin and 10 nM 4-OHT. Cells were incubated with 4-OHT for the time indicated.
Verteporfin	To disrupt the interaction between YAP and TEAD, A549 cells were treated with 7.5 µM verteporfin for 24 h.

Doxycycline	To induce the expression of constitutively active YAP5SA, MCF10A YAP5SA cells were treated with 0.5 µg/ml doxycycline (dox) for the time indicated.
Nocodazole	Treatment with 50 ng/ml nocodazole for 24 h was used to arrest serum-starved MCF10A YAP5SA cells in G2/M phase of the cell cycle.

2.2.1.7 Plasmid transfection using Lipofectamine 2000

For transient overexpression of wild-type YAP (YAPwt) or constitutively active YAP5SA in *Lin9* deleted KP and KPL cells followed by immunofluorescence, 18,750 KP or KPL cells per well were seeded with 2.5 µg/ml puromycin on coverslips in a 6-well plate. 24 h later, *Lin9* deletion was induced by treating cells with 10 nM 4-OHT. Another 20 h later and 4 h before transfection, cells were fed with fresh antibiotic-free (w/o pen-strep and w/o puromycin) DMEM (10% FBS) containing 10 nM 4-OHT. Cells were transfected with 2.5 µg plasmid DNA in total (2.0 µg empty/ YAPwt/ YAP5SA plasmids + 0.5 µg GFP plasmid) using Lipofectamine 2000 according to the following scheme:

Table 31: Lipofectamine 2000 transfection setup for overexpressing YAP (6-well plate)

For 2 wells	
A = DNA mix	350 µl Opti-MEM containing + 5.6 µg empty vector (#645), YAPwt (#1504) or YAP5SA (#1505) + 1.4 µg GFP vector (#746)
B = Lipo mix	288 µl Opti-MEM + 12 µl Lipofectamine 2000

Mixture B (Lipo mix) was incubated for 5 min at RT before 300 µl of A (DNA mix) were added to B (Lipo mix). The transfection solution was mixed by pipetting up and down carefully and incubated for 20 min at RT. 250 µl/well of DNA-Lipo mix was added dropwise to the cells. The next day, medium was aspirated and replaced by complete DMEM supplemented with 2.5 µg/ml puromycin and 10 nM 4-OHT. Cell were harvested for immunofluorescence two days after transfection.

2.2.1.8 Plasmid transfection using calcium phosphate

For calcium phosphate transfection of cells seeded onto 10 or 15 cm cell culture dishes, plasmid DNA was added to 50 µl (10 cm dish) or 125 µl (15 cm dish) 2.5 M $CaCl_2$ in a 1.5 ml tube and filled up with sterile ddH_2O to 500 µl (10 cm) or 1250 µl (15 cm). A pipette aid and a Pasteur pipette were used to bubble 500 µl (10 cm) or 1250 µl (15 cm) of 2x HBS solution (pH 7.05) in a 15 ml falcon. While continuously bubbling, the DNA/$CaCl_2$ mixture was added dropwise to the 2x HBS solution by using a P1000 pipette. The transfection mixture was directly added to the cells by dropping slowly into the medium trying to evenly cover the whole plate. To assess transfection efficiency, a separate 10 or 15 cm cell culture dish was transfected with a GFP encoding vector (pBABE-H2B-GFP; #746).

2.2.1.9 siRNA transfection with Lipofectamine RNAiMAX reagent

Cells seeded one day before were transfected with each siRNA (**Table 22**) at a final concentration of 30 nM in antibiotic-free medium (2 ml/6 cm dish or 22.5 µl/per well of 18-well ibidi slide for KPL2 cells; 3 ml/6 cm dish or 1.5 ml/6-well for MCF10A YAP5SA cells) as indicated below.

Table 32: siRNA transfection set-up for knockdown of murine *Yap/Taz* in KPL2 cells on a 6 cm cell culture dish (for RNA isolation)

For one 6 cm cell culture dish	siCtrl	si*Yap/Taz*
A = siRNA mix	496.4 µl Opti-MEM + 3.6 µl siCtrl (S52) (90 nM)	496.4 µl Opti-MEM + 1.2 µl si*Yap* #1 (S67) (30 nM) + 1.2 µl si*Yap* #2 (S68) (30 nM) + 1.2 µl si*Taz* (S69) (30 nM)
B = Lipo mix	488.75 µl Opti-MEM + 11.25 µl RNAiMAX	488.75 µl Opti-MEM + 11.25 µl RNAiMAX

Table 33: siRNA transfection set-up for knockdown of human *LIN9* and *MYBL2* in MCF10A YAP5SA cells on a 6 cm cell culture dish (for RNA isolation)

For one 6 cm cell culture dish	siCtrl	si*LIN9*	si*MYBL2*
A = siRNA mix	498.4 µl Opti-MEM + 1.6 µl siCtrl (S52) (30 nM)	498.4 µl Opti-MEM + 1.6 µl si*LIN9* (S5) (30 nM)	498.4 µl Opti-MEM + 1.6 µl si*MYBL2* (S6) (30 nM)
B = Lipo mix	495 µl Opti-MEM + 5 µl RNAiMAX	495 µl Opti-MEM + 5 µl RNAiMAX	495 µl Opti-MEM + 5 µl RNAiMAX

Table 34: siRNA transfection set-up for knockdown of human *LIN9* and *MYBL2* in MCF10A YAP5SA cells on a 6-well plate (for pH3 immunofluorescence and RNA isolation)

For 2 wells	siCtrl	si*LIN9*	si*MYBL2*
A = siRNA mix	598 µl Opti-MEM + 1.92 µl siCtrl (S52) (30 nM)	598 µl Opti-MEM + 1.92 µl si*LIN9* (S5) (30 nM)	598 µl Opti-MEM + 1.92 µl si*MYBL2* (S6) (30 nM)
B = Lipo mix	594 µl Opti-MEM + 6 µl RNAiMAX	594 µl Opti-MEM + 6 µl RNAiMAX	594 µl Opti-MEM + 6 µl RNAiMAX

For transfecting cells seeded on 0.2 cm^2-wells in 18-well ibidi slides for proximity ligation assay (PLA), siRNAs were pre-diluted using RNase free water as follows:

1 µl siCtrl (S52) + 9 µl RNase free water

1 µl si*Yap* #1 (S67) +1 µl si*Yap* #1 (S68) +1 µl si*Taz* (S69) +27 µl RNase free water

Table 35: siRNA transfection set-up for knockdown of murine *Yap/Taz* in 18-well ibidi slides (for PLA)

For 5 wells	siCtrl	si*Yap/Taz*
A= siRNA Mix	20.34 µl Opti-MEM + 2.16 µl siCtrl (S52) (pre-diluted 1:10) (≙ 90 nM per 30 µl)	20.34 µl Opti-MEM + 2.16 µl si*Yap/Taz*-Mix (S67-69) (each pre-diluted 1:30) (≙ 30 nM of each siRNA per 30 µl)
B = Lipo Mix	21.825 µl Opti-MEM + 0.675 µl RNAiMAX	21.825 µl Opti-MEM +0.675 µl RNAiMAX

Lipo mix B was incubated for 5 min at RT before siRNA mix A was added to Lipo mix B. After carefully mixing by pipetting up and down, the siRNA/Lipo mix was incubated for 10-20 min at RT and finally 1 ml (per 6 cm dish), 500 µl (per 6-well) or 7.5 µl (per 18-well of ibidi slide) was added dropwise to the cells. The next day, medium was aspirated and fresh medium was added. Cells were harvested for RNA isolation, immunofluorescence or PLA, 2-3 days after transfection.

2.2.1.10 Retrovirus production and infection of KP and KPL cells

The retroviral packaging cell line Platinum-E (Plat-E) was used to produce retroviral vectors encoding Cre-recombinase (pBABE-Puro-CreER^{T2}; #924) for the infection of KP and KPL cells. Plat-E cells were seeded on 10 cm cell culture dishes one day before transfection. Approx. 2-3 h prior to transfection, cells were about 80% confluent and old medium was replaced by 8 ml fresh medium.

Plat-E cells were transfected with 30 µg DNA using calcium phosphate as described in **2.2.1.8**. The next morning, the medium was replaced by 8 ml of fresh medium. Another 24 h later and two days after transfection, the retroviral supernatant was harvested from Plat-E cells, filtered (0.45 µm pore size), diluted 1:1 with fresh DMEM and supplemented with 8 µg/ml polybrene. To infect KP and KPL cells seeded one day before infection (8×10^5 cells/10 cm dish) on 10 cm cell culture dishes, 6-7 ml of the retrovirus mixture was added to the cells. The next morning, cells were fed with fresh medium and 48 h after infection selection was started using 2.5 µg/ml puromycin.

2.2.1.11 Lentivirus production using HEK293TN cells

Lentivirus production, concentration (**2.2.1.12**), and titration (**2.2.1.13**) were carried out under Biosafety Level 2 (BSL-2) conditions. Human embryonic kidney 293TN (HEK293TN) cells were used as a lentiviral vector producer cell line and seeded onto 10 or 15 cm cell culture dishes (5×10^6 cells/ 10 cm dish; 1.35×10^7 cells/ 15 cm dish) 24 h before transfection. On the next day, approx. 2-3 h before transfection, medium was aspirated and 8 ml (10 cm) or 15 ml (15 cm) of antibiotic-free DMEM supplemented with 10% FBS was added. HEK293TN cells were transfected using calcium phosphate (**2.2.1.8**) with the following amounts of plasmid DNA:

9 µg (10 cm)	or	24 µg (15 cm)	lentiviral construct (e.g., Ubc-shLuc-pgk-Cre #1558)
6 µg (10 cm)	or	16 µg (15 cm)	psPAX2
3 µg (10 cm)	or	8 µg (15 cm)	pCMV-VSV-G

To assess transfection efficiency, a separate cell culture dish of HEK293TN cells was transfected solely with 18 µg (10 cm) or 48 µg (15 cm) GFP-encoding vector (pBABE-H2B-GFP; #746). The next morning, old medium was replaced by 8 ml (10 cm) or 15 ml (15 cm) fresh DMEM (10% FBS, 1% pen-strep). On the next day approx. 40 h after transfection, lentiviral supernatant was collected and stored at 4 °C and fresh medium was added to the dish. Another 20 h later (60 h after transfection), lentiviral supernatant was harvested for a second time and mixed with the 40-h supernatant stored at 4 °C. After centrifugation at 1000 rpm for 5 min (RT), the supernatant was filtered (0.45 µm) and either stored for a few days at 4 °C or directly concentrated using PEG-precipitation (see **2.2.1.12**).

2.2.1.12 Lentivirus concentration using PEG-precipitation

In order to concentrate the lentiviral supernatant of HEK293TN cells, polyethylene glycol 6000 (PEG 6000) precipitation was used as described by (Kutner et al. 2009). The following solutions were added per ml of collected virus supernatant in a 50 ml falcon tube:

50% PEG 6000	250.0 µl
4 M NaCl	106.4 µl
1x PBS	114.2 µl

The falcon tubes were inverted several times and incubated for 1.5 h at 4 °C while inverting every 20 to 30 min. The precipitation mixture was centrifuged for 30 min at 4500 rcf (RT) and the supernatant was aspirated completely. The precipitated virus pellet was resuspended either in 5.88 µl 50 mM Tris-HCl, pH 7.4 (for the use in cell culture) or in 4 µl PBS (for infection of mice) per ml of original HEK293TN supernatant by vigorously pipetting liquid up and down. Aliquots of 10-20 µl precipitated lentivirus were stored at -80 °C.

2.2.1.13 Lentivirus titration by flow cytometry

To determine the biological titer of Cre-expressing lentiviral vectors, a Cre-reporter cell line generated by stable transfection of NIH/3T3 cells with the GFP reporter plasmid pZ/EG was used (Novak et al. 2000; Iltzsche et al. 2017). NIH/3T3-pZ/EG cells, which express GFP upon Cre-mediated recombination, were seeded in 24-well plates (35,000 cells/well) 24 h prior to infection. Medium was changed with 1 ml/well of fresh DMEM (10% FBS; w/o pen-strep; with 8 µg/ml polybrene) 2-3 h before infection and cells out of 3 wells were counted to determine the average number of cells at the time of infection. NIH/3T3-pZ/EG cells were infected with 10 µl of the following serial dilutions of lentivirus with sample 1 being the negative control and containing no lentivirus:

Table 36: Serial dilution set-up for lentiviral vector titration

Sample	Dilution	Volume of lentivirus [µl]	Volume of medium [µl]
1	/	/	/
2	1:40	1 µl of concentrated lentivirus stock	39 µl
3	1:80	20 µl of sample 2 (1:40 dilution)	20 µl
4	1:160	20 µl of sample 3 (1:80 dilution)	20 µl
5	1:320	20 µl of sample 4 (1:160 dilution)	20 µl
6	1:640	20 µl of sample 5 (1:320 dilution)	20 µl

The next day, the medium was replaced by fresh DMEM (10% FBS, 1% pen-strep). Three to four days after infection, cells were washed twice with 1x PBS, trypsinized and resuspended in 500 µl medium. The number of GFP-positive cells was determined using a Cytomics FC 500 flow cytometer (Beckman Coulter). The virus titer was calculated in transducing units per ml (TU/ml) according to the following formula:

$$TU/ml = \frac{[(F/100) * N * D]}{V}$$

$F = percentage\ of\ GFP - positive\ cells$
$N = cell\ number\ at\ the\ time\ of\ infection$
$D = dilution\ factor$
$V = volume\ of\ virus\ used\ for\ infection\ (10\ \mu l = 0.01\ ml)$

2.2.1.14 Cell proliferation assay using crystal violet staining

KP and KPL cells were plated at a very low density (1,500 cells/6 cm dish; 750 cells/24-well) in the presence of 2.5 µg/ml puromycin and 10 nM 4-OHT. Every two to four days, cells were fed with fresh medium containing puromycin and 4-OHT. For generating growth curves, three wells of cells were seeded per condition.

Cells were harvested for crystal violet staining six hours (time point: 0 days), two, four, six, eight, and ten days after seeding. To do so, cells were washed once in 1x PBS, fixed with 3.7% formaldehyde (37% formaldehyde diluted 1:10 in ddH_2O) for 10 min at RT and rinsed two to three times with tap water. Air-dried plates were stained with 0.1% crystal violet staining solution (1% crystal violet dissolved in ddH_2O is diluted 1:10 in 20% ethanol) for 30 min at RT. Finally, stained plates were rinsed several times with tap water and air-dried.

For quantification, the crystal violet dye was extracted by adding 200 µl 10% acetic acid per well of a 24-well plate and shaking slowly for 30 min at RT. The absorbance at 590 nm of 100 µl extracted crystal violet dye was measured in a 96-well plate using a Multiskan Ascent microtiter plate reader (Labsystems). If the absorbance exceeded a value of 1.0, the dye was diluted 1:10 and measured again. The average absorbance values of three wells per condition were calculated and depicted in relation to the “0 days” values (harvested six hours after seeding) of the untreated or 4-OHT treated cells.

2.2.1.15 Immunofluorescence

For immunostaining, cells were seeded on coverslips in 6-well plates. All the following steps were conducted at RT. After cells were washed once in PBS, they were fixed in PSP (3% paraformaldehyde, 2% sucrose in PBS) for 10 min. Cells were then rinsed twice in PBS for a few seconds and once in PBS for 5 min. For permeabilization, cells were incubated for 5 min in PBS with 0.2% Triton X-100, rinsed once and washed for 5 min in PBS with 0.1% Tween 20 (PBS-T).

Blocking of unspecific binding sites was done by an incubation with 5% BSA in PBS-T for 1 h. Cells on coverslips were incubated with primary antibody diluted in 1% BSA in PBS-T in a humidified chamber for 1 h, followed by three washing steps in PBS-T for 5 min each. Incubation with Alexa Fluor® 488 (green) or 594 (red) secondary antibody and Hoechst 33258, both diluted 1:500 in 1% BSA in PBS-T for 30 min in a humidified chamber was followed by four washing steps with PBS-T for 5 min each. Coverslips were mounted on glass slides using ImmuMount, dried for at least 1 h in the dark and finally, sealed with colorless nail polish. Glass slides were stored at 4 °C in the dark before being analyzed using an inverted Leica DMI 6000B microscope equipped with a Prior Lumen 200 fluorescence light source and a Leica DFC350 FX digital camera. Leica Application Suite (LAS) 3.7 and Fiji (Schindelin et al. 2012) were used for the analysis.

2.2.2 Molecular biology

2.2.2.1 Transformation of chemically competent bacteria with plasmid DNA

For transformation of plasmid DNA, chemically competent DH5α *E.coli* bacteria were thawed on ice,1 µl of plasmid DNA was added to 50 µl of bacteria and mixed gently by flicking the tube. The DNA-bacteria mix was incubated for 10 min on ice and subsequent heat-shock transformation was performed by incubating tubes for 45 s at 42 °C. Directly afterwards, samples were placed on ice for 3 min and 400 µl of pre-warmed LB medium without any antibiotics was added. Samples were incubated for 30-60 min in a thermomixer at 37 °C while shaking at 600 rpm. Bacteria were pelleted in a centrifuge for 1 min at full speed, resuspended in LB medium and spread onto pre-warmed LB agar plates containing the appropriate antibiotics. Plates were incubated overnight upside down at 37 °C.

2.2.2.2 Midi and Maxi preparation of plasmid DNA from bacteria

A single colony of transformed bacteria picked from an LB agar plate was transferred into 3 ml of LB medium supplemented with antibiotics and cultured at 37 °C for 6-8 h with vigorous shaking at 130 rpm. The starter culture was diluted 1:500 to 1:1000 in 100-150 ml (Midi preparation) or 250-300 ml (Maxi preparation) LB medium with antibiotics and grown overnight at 37 °C and 130 rpm until an absorbance of 1-1.5 of 600 nm was reached. Plasmid DNA was purified using the PureLink™ HiPure Plasmid Filter Midi- or Maxiprep Kits from Thermo Fisher according to the manufacturer's instructions and quantified with the NanoDrop 2000 spectral photometer (Peqlab).

2.2.2.3 Genomic DNA isolation of mouse tails

In order to genotype mice, mouse tails were lysed in 75 µl base buffer at 95 °C for 30 min. After samples were cooled down for 5 min at 4 °C, 75 µl of neutralization buffer was added. Samples were then mixed and centrifuged shortly. Samples were stored at 4°C and 1-3 µl of the supernatant were used for genotyping polymerase chain reactions (PCRs) (**2.2.2.5**).

2.2.2.4 Genomic DNA isolation of cells

To isolate genomic DNA (gDNA), cells were trypsinized (**2.2.1.2**), resuspended in medium and transferred to a 15 ml falcon tube. Samples were centrifuged for 5 min at 300 x g and the supernatant was discarded. After the pellet was resuspended in 1 ml PBS and transferred to a 1.5 ml tube, cells were centrifuged again for 5 min at 300 x g. Pelleted cells were resuspended in 300 µl tail buffer and 10 µl Proteinase K and incubated at 55 °C in a thermomixer while shaking at 600 rpm. After 6 hours of incubation, samples were vortexed for 20 s and incubated for 10 min at 95 °C to inactivate Proteinase K. Samples were allowed to cool down before 166.7 µl 6 M NaCl was added. Samples were then mixed, centrifuged for 10 min at full speed (4 °C) and the supernatant was transferred into a fresh tube containing 767 µl ice-cold 95% ethanol. Tubes were carefully mixed by inverting a few times and spun for 15 min at full speed (4 °C). The remaining solution was carefully aspirated and the gDNA pellet was washed once in 700 µl ice-cold 70% ethanol by a 5 min long centrifugation at 4 °C and full speed. The supernatant was removed and the air-dried pellet was resuspended in 30 µl TE buffer by incubating it for 45 min at 60 °C with gentle shaking. gDNA samples were stored at -20 °C and 1-3 µl were used for PCR (see below).

2.2.2.5 PCR of genomic DNA

For genotyping of mice and cells using isolated gDNA, PCR reactions with primers specific for murine *K-Ras*, *p53*, and *Lin9* were set up as stated below. PCR products were mixed with 5x loading buffer and analyzed on 1% (Lin9 PCRs) or 2% (K-Ras and p53 PCRs) (w/v) agarose gels (**2.2.2.6**).

K-Ras PCR mix

ddH_2O	13.7 µl
10x ReproFast buffer	2.5 µl
primer SG2031 [10 µM]	1.0 µl
primer SG2032 [10 µM]	1.0 µl
primer SG2033 [10 µM]	1.0 µl
dNTPs [2mM]	2.5 µl
HisTaq16 [5 U/µl]	0.3 µl
gDNA	3.0 µl
total volume	25.0 µl

PCR conditions

		Cycles
95 °C	2 min	1
95 °C	30 s	
61 °C	30 s	35
72 °C	45 s	
72 °C	10 min	1
10 °C	hold	

p53 PCR mix

ddH_2O	16.8 µl
10x ReproFast buffer	2.5 µl
primer SG1556 [10 µM]	1.0 µl
primer SG1557 [10 µM]	1.0 µl
dNTPs [2mM]	2.5 µl
HisTaq16 [5 U/µl]	0.2 µl
gDNA	1.0 µl
total volume	25.0 µl

PCR conditions

		Cycles
95 °C	5 min	1
95 °C	30 s	
56 °C	1 min	30
72 °C	1 min	
72 °C	3 min	1
10 °C	hold	

Lin9 PCR mix

ddH_2O	16.5 µl
10x ReproFast buffer	2.5 µl
primer SG893 [10 µM]	1.0 µl
primer SG722 [10 µM]	1.0 µl
dNTPs [2mM]	2.5 µl
HisTaq16 [5 U/µl]	0.5 µl
gDNA	1.0 µl
total volume	25.0 µl

PCR conditions

		Cycles
94 °C	2 min	1
94 °C	30 s	
58 °C	1 min	31
72 °C	1 min	
72 °C	4 min	1
10 °C	hold	

2.2.2.6 Agarose gel electrophoresis

PCR products were separated and analyzed using agarose gel electrophoresis. The appropriate amount of agarose was weighed in a 250-ml Erlenmeyer flask and boiled in 50 ml (small gel tray) or 120 ml (bigger gel tray) 1x TAE using a microwave until the agarose was completely dissolved. When the agarose solution was cooled down to approx. 50-60 °C, ethidium bromide was added to a final concentration of 0.2 to 0.5 µg/ml and the gel was mixed by swirling the flask gently. The agarose was poured into a gel tray with inserted well comb. After 20-30 min the gel was completely solidified and placed into the gel box, which was filled with 1x TAE to completely cover the agarose gel. Samples mixed with 5x loading buffer were loaded onto the gel alongside a 100 bp or 1 kb molecular weight ladder and the gel was run at 80 V (small gel tray) or 100 V (bigger gel tray) for 45 to 90 min. DNA bands were visualized using a UV transilluminator.

2.2.2.7 RNA isolation

Total RNA was isolated using the ready-to-use reagent peqGOLD TriFast (Peqlab), which contains phenol and guanidinium thiocyanate. Immediately after taking out of the incubator, cells were placed on ice and the medium was aspirated completely. Cells were lysed directly on the cell culture dish by adding 1 ml of peqGOLD TriFast and passing the solution several times over the cell culture dish and through a pipette. Lysed cells were transferred into a 1.5 ml tube and either frozen at -80 °C for a few days up to several weeks or incubated at RT for 5 min.

Then, 200 µl chloroform was added, samples were mixed by vortexing for approx. 15 s and incubated at RT for 2-3 min. After samples were centrifuged at 12,000 x g and 4 °C for 10 min, the mixture separated into three phases: the lower red, the interphase, and the upper colorless aqueous phase. Without taking anything from the inter- or lower phase, the upper aqueous phase was transferred to a new tube, 500 µl ice-cold isopropanol was added and mixed by inverting a few times. Samples were incubated at RT for 10 min before being vortexed shortly and spun down at 12,000 x g and 4 °C for 10 min again. As the resulting RNA pellet is quite loose, the supernatant was removed carefully using a P1000 pipette with a P10 tip on top of the P1000 tip. The pellet was then washed twice by adding 1 ml of ice-cold 75% ethanol and centrifuging at 7,000 x g and 4 °C for 5 min. Following removal of the supernatant, the RNA pellet was air-dried for 5-10 min and dissolved in 15-25 µl RNase-free or DEPC water. RNA concentration and purity were examined using the NanoDrop 2000 spectrophotometer. RNA was stored at -80 °C.

2.2.2.8 Reverse transcription of RNA into cDNA

For reverse transcription of RNA into cDNA, 0.5 µl random primer was added to 1.0 to 2.5 µg RNA and filled up with DEPC water to a final volume of 10 µl on ice. After RNA was denatured at 70 °C for 5 min, the following mixture containing RevertAid Reverse Transcriptase (RevertAid RT) and RiboLock RNase Inhibitor (RiboLock RI) was added while keeping the RNA mix at 4 °C:

5.0 µl	5x RT reaction buffer
2.75 µl	DEPC water
6.25 µl	dNTPs
0.5 µl	RevertAid RT
0.5 µl	RiboLock RI
15 µl	Total volume

The reaction was incubated at 37 °C for 60 min before being terminated at 70 °C for 15 min. cDNA was diluted 1:15 with ddH_2O and stored at -20 °C.

2.2.2.9 Quantitative real-time PCR (qPCR)

Quantitative real-time PCR (qPCR) was used for two applications: First, for analyzing the expression of a specific gene in a given sample relative to the expression of this gene in a reference sample after normalizing to the expression of a housekeeping gene (relative mRNA expression). For this approach cDNA reversely transcribed from RNA was used (**2.2.2.8**). Second, qPCR along with chromatin immunoprecipitation (ChIP) (**2.2.3.8**) was used to measure the enrichment of a certain DNA region of the genome upon protein-specific immunoprecipitation relative to the total amount of input DNA (% of input).

2.2.2.9.1 qPCR with cDNA

SYBR Green (Sigma Aldrich) diluted 1:10 in DMSO was stored at -20°C. For setting up a self-made master mix, the 1:10-diluted SYBR Green was further diluted 1:200 in ddH_2O (final dilution 1:2000). The self-made qPCR master mix was set up as follows and stored at -20 °C:

qPCR master mix	
dNTPs [2 mM]	3.50 µl
10x ReproFast	2.50 µl
SYBR Green [1:2000 in DMSO]	0.75 µl
ddH_2O	11.45 µl
Total volume	18.20 µl

For setting up a qPCR, the required amount of qPCR master mix was thawed and mixed with primers, HisTaq polymerase, and ddH_2O as stated below.

qPCR master mix	18.20 µl
primer forward [10 µM]	0.75 µl
primer reverse [10 µM]	0.75 µl
HisTaq16 [5 U/µl]	0.30 µl
Total volume	20.00 µl

20 µl of this mix were pipetted in triplicates into a 96-well plate before adding 5 µl of cDNA (diluted 1:15) (**2.2.2.8**) or ddH_2O as a no-template control (NTC) into each well. The plate was sealed using transparent adhesive foil, centrifuged shortly at 1000 x g for 1 min and the qPCR was run onto a Stratagene Mx3000P qPCR machine with the following thermal profile:

95 °C	2 min	1 cycle	initialization
95 °C	15 s		
60 °C	30 s	40 cycles	amplification
72 °C	30 s		
95 °C	15 s		
60 °C	15 s	1 cycle	melting curve
95 °C	15 s		

The relative expression of a gene in a given sample relative to the gene expression in a reference sample was calculated according to the comparative C_T method:

$$2^{-\Delta\Delta C_T}$$

$$\text{with } \Delta C_T = C_T\,(gene\ of\ interest) - C_T\,(housekeeping\ gene)$$

$$\text{and } \Delta\Delta C_T = \Delta C_T\,(sample) - \Delta C_T\,(reference)$$

The error of $\Delta\Delta C_T$ was calculated using the law of error propagation:

$$s = \sqrt{{s_1}^2 + {s_2}^2}$$

$$\text{with } s_1 = standard\ deviation\,(housekeeping\ gene)$$

$$\text{and } s_2 = standard\ deviation\,(gene\ of\ interest)$$

Finally, the error of $2^{-\Delta\Delta C_T}$ used for the error bars was determined using the error margin with $(2^{-\Delta\Delta C_T + s}) - (2^{-\Delta\Delta C_T})$.

2.2.2.9.2 qPCR with ChIP-DNA

The commercially available SYBR Select Master Mix (Thermo Fisher) was used for qPCR of DNA material from ChIP experiments (**2.2.3.8**) and set up as follows:

SYBR Select Master Mix	10.0 µl
ddH_2O	8.2 µl
primer forward [10 µM]	0.4 µl
primer reverse [10 µM]	0.4 µl
ChIP DNA	1.0 µl
Total volume per well	20.0 µl

A master mix containing everything except DNA was prepared and 19 µl were pipetted in triplicate into a 96-well plate. Next, 1 µl of ChIP-DNA or 1 µl of ddH_2O (NTC) per well was added. After the plate was sealed and centrifuged shortly, the experiment was run onto the Stratagene Mx3000P cycler with the following settings:

95 °C	15 min	1 cycle	initialization
95 °C 60 °C	30 s 1 min	40 cycles	amplification
95 °C 60 °C 95 °C	1 min 30 s 30 s	1 cycle	melting curve

The $\%\ of\ input$ was calculated with $2^{-\Delta C_T}$, where $\Delta C_T = C_T(ChIP\ sample) - C_T(input)$. First, the error was determined by calculating the error of ΔC_T according to the error propagation law with $s = \sqrt{{s_1}^2 + {s_2}^2}$, where $s_1 = standard\ deviation\ of\ input$ and $s_2 = standard\ deviation\ of\ ChIP\ sample$. Second, this was used to calculate the final error margin with $2^{-(\Delta C_T + s)} - \%\ of\ input$.

2.2.3 Protein biochemistry

2.2.3.1 Whole cell lysates

Cells were scraped off from plate on ice in ice-cold PBS, transferred to a falcon tube and centrifuged at 1,200 rpm and 4 °C for 5 min. Supernatant was aspirated and the cell pellet was resuspended in 1 ml PBS to be transferred to a 1.5 ml tube. Cells were spun down and resuspended in TNN lysis buffer with freshly added protease inhibitor cocktail (PIC) 1:1000, 1 mM PMSF, 1 mM DTT, and 10 mM ß-glycerophosphate.

Samples were incubated on ice for 20 min, briefly vortexed and centrifuged at 14,000 rpm and 4 °C for 10 min. The protein-containing supernatant was transferred to a fresh tube and the protein concentration was determined according to Bradford (**2.2.3.3**).
Protein lysates were either used for immunoprecipitation of transient, exogenous proteins (**2.2.3.5**) followed by Western Blot (**2.2.3.7**) or directly used for Western Blot. For the latter, samples were mixed with 0.5x volume of 3x electrophoresis sample buffer (ESB), boiled at 95 °C for 5 min and finally, either directly loaded on SDS gels or frozen at -20 °C for later use.

2.2.3.2 Nuclear extracts

For co-immunoprecipitation of endogenous proteins (**2.2.3.4.2**) from KPL2 cells, nuclear extracts were generated. For this purpose, cell culture dishes were placed on ice, scraped off in PBS and transferred to a falcon tube. Cells were centrifuged at 1200 rpm and 4 °C for 5 min and the resulting pellet was washed in 1 ml PBS once in a 1.5 ml tube by spinning at 4,000 rpm and 4 °C for 1 min. The supernatant was discarded and the pellet resuspended in five volumes of buffer A with freshly added PIC 1:100 by pipetting up and down 10 times. Cells were allowed to swell on ice for 20 min, before they were transferred to a glass Dounce homogenizer and homogenized with 20 tight but slow up-and-down strokes. Nuclei were collected by centrifuging 5 min at 2800 rpm, 4 °C. The supernatant containing the cytoplasmic proteins was removed and the nuclei pellet was resuspended in five volumes of nuclei lysis buffer with freshly added PIC 1:100 and 0.5 mM DTT. Samples were incubated on ice for 20 min and spun down for 10 min in a cooling centrifuge at full speed. The supernatant containing the nuclear extracts was transferred to a fresh tube. Proteins were quantified as described in **2.2.3.3** and either immediately used for immunoprecipitation of endogenous proteins (**2.2.3.4.2**) or for later use, shock frozen in liquid nitrogen and stored at -80 °C.

2.2.3.3 Protein quantification according to Bradford

The protein concentration was determined with the assay established by Bradford (Bradford 1976). 1 µl of whole cell lysates or nuclear extracts were mixed with 100 µl of 0.15 M NaCl in disposable semi-micro cuvettes. To generate a standard curve, 1 µl of a BSA dilution series was used for comparison. Finally, 1 ml of Bradford solution was added and the extinction at 595 nm was measured using a spectrophotometer. Measurements were made in duplicates and protein concentrations were calculated by dividing the average extinction by the slope of the standard curve.

2.2.3.4 Immunoprecipitation of endogenous proteins

2.2.3.4.1 Immunoprecipitation of endogenous LIN9

For immunoprecipitation (IP) of endogenous LIN9, 2.5 mg proteins in 500 µl TNN (with 1 mM DTT, 1 mM PMSF, and PIC 1:1000) were incubated with 1 µg of LIN9-antibody on the rotating wheel overnight at 4 °C. 2% of the protein amount used for the IP were heated in 3x ESB at 95 °C for 5 min and stored at -20 °C for later use as input material.

The next day, 30 µl of Protein G Dynabeads were added and incubated for 1.5 h at 4 °C while rotating. Tubes were placed in a magnetic rack (DynaMag-2 magnet, Thermo Fisher), the supernatant was discarded and beads were washed five times in 1 ml TNN (with 1 mM DTT, 1 mM PMSF, and PIC 1:1000), each time for being 5 min in the cold room on the rotating wheel. After the last step, samples were transferred to a fresh tube, the remaining fluid was removed and beads were boiled in 3x ESB for 5 min at 95 °C. Half of the supernatant containing the immunoprecipitated LIN9 was loaded together with half of the input (25 µg) on 8% SDS-gels and used for immunoblotting LIN9.

2.2.3.4.2 Co-immunoprecipitation of B-MYB and YAP

For immunoprecipitation (IP) of endogenous proteins, 2 mg of nuclear extracts were used per IP and brought to a volume of 500 µl with nuclei lysis buffer. The nuclear extracts were further diluted 1:1 with 20 mM HEPES, pH 7.4 to a final volume of 1 ml containing 0.5 mM DTT, 1 mM PMSF, 1:100 PIC, and 10 mM ß-glycerophosphate.

Per IP and for pre-clearing (calculate 5 µl per IP + additional 5 µl), 25 µl Protein G Dynabeads were added to a 1.5 ml tube. Beads were washed once for 5 min in 1 ml BSA in PBS (5 mg/ml) on a rotating wheel at 4 °C. The tubes were placed into a magnetic rack and the supernatant was removed. 1 ml BSA in PBS (5 mg/ml) and 2 µg antibody were added to the beads used for IP and incubated in the cold room on a rotating wheel for 1 h. In parallel, beads for pre-clearing were resuspended in BSA to reach the initial volume and 5 µl of beads were added to 2 mg nuclear extracts in a volume of 1 ml. Samples for pre-clearing were incubated in the cold room on a rotating wheel for 1 hour. Beads with antibodies were washed with 1 ml BSA three times for 3 min in the cold room and, after removal of the supernatant, pre-cleared lysates were added to the antibody-coupled beads. Samples were incubated in the cold room on the rotating wheel for 4 h. Beads were washed five times on the rotating wheel with 1 ml of a 1:1 mixture of nuclei lysis buffer and 20 mM HEPES, pH 7.4 (with freshly added PIC 1:1000). After the last wash step, beads in buffer were transferred into a fresh tube and placed into the magnetic rack. The supernatant was aspirated completely, beads were centrifuged shortly and placed back into the magnetic rack to remove the last remaining fluid using a P10 pipette.

Beads were heated in 25 µl 3x ESB at 95 °C for 10 min and the supernatant containing the denatured proteins was transferred to a fresh tube. In parallel, 6.25% (=125 µg) of the protein amount used for the IP was heated in 3x ESB at 95 °C for 10 min and loaded as input next to the IP samples on 10% SDS gels.

2.2.3.5 Immunoprecipitation of transient, exogenous proteins

For studying protein-protein interactions with co-immunoprecipitation (Co-IP) of transiently expressed exogenous tagged-proteins, HeLa cells seeded at a density of 1.5 x 10^6 cells per 10 cm cell culture dish were transfected with 15 µg plasmid DNA using calcium phosphate (**2.2.1.8**) according to the following scheme:

Table 37: Transfection set-up for Co-IP of HA-tagged B-MYB and FLAG-tagged YAP

	Plasmid #1			Plasmid #2		
Sample	Internal plasmid no.	Plasmid name	Plasmid amount	Internal plasmid no.	Plasmid name	Plasmid amount [µg]
1	1159	pcDNA4/TO-HA-BMYB	7.5 µg	1504	pCMV-2xFlag-YAP	7.5 µg
2	1159	pcDNA4/TO-HA-BMYB	7.5 µg	212	pcDNA3 (empty vector)	7.5 µg
3	746	pBABE-H2B -GFP	15 µg	/	/	/

Cells were harvested two days after transfection. Whole cell lysates were prepared (500 µl TNN/pellet) and protein concentration was determined as described in **2.2.3.3**. Per IP, 2.5 µg of FLAG-antibody (0.5 µl) was added to 2 mg protein in a volume of 500 µl and incubated overnight at 4 °C on a rotating wheel. The next day, 30 µl Protein G Dynabeads were added and incubated for 2 h on a rotating wheel in the cold room. Next, the tubes were placed in a magnetic rack and the supernatant was aspirated. Beads were washed by resuspending in 1 ml TNN (with freshly added 1 mM DTT, PIC 1:1000, 1 mM PMSF, and 10 mM ß-glycerophosphate) and by incubating on a rotating wheel in the cold room for 5 min. After five washing steps in total, beads were transferred into a fresh. The supernatant was removed completely and the beads were heated in 50 µl 3x ESB at 95 °C for 5 min. In parallel, 2% of the protein amount (=40 µg) used for the IP was heated in 3x ESB for 5 min and used as input material. After heating, tubes with beads were placed back into the magnetic rack, the supernatant was transferred to a fresh tube and both, input and IP, were stored at -20 °C until being used for SDS-PAGE and immunoblotting.

2.2.3.6 Proximity ligation assay (PLA)

Proximity ligation assay (PLA) was developed by Fredriksson and colleagues in 2002 (Fredriksson et al. 2002). Several years later, the company Olink Bioscience developed Duolink immunoassay based on *in situ* PLA to study protein-protein interactions, making PLA commercially available for the first time (Gullberg and Andersson 2010).

In PLA, cells fixed on microscopy slides are incubated with two primary antibodies specific for the proteins, which are analyzed for their interaction with each other, e.g., antibodies against YAP and B-MYB. These primary antibodies must be produced in two different host species – such as mouse and rabbit – and are recognized by two Duolink species-specific secondary antibodies, which are coupled to unique DNA strands. Only when secondary antibodies are in close proximity (< 40 nm), the attached DNA strands can interact and will be ligated to circle-forming DNA oligonucleotides. DNA circles are amplified by rolling-circle amplification using a polymerase and are detected using complementary fluorescence-labeled oligonucleotide probes. Single-molecule protein interactions result in distinct fluorescent spots, which can be visualized using a fluorescence microscope (Fredriksson et al. 2002; Soderberg et al. 2006; Gullberg and Andersson 2010).

For PLA, cells seeded in 18-well ibidi slides, were washed in PBS once and fixed for 10 min at RT in PSP. Fixed cells were washed two times shortly and one time for 3 min in PBS and then, permeabilized for 5 min at RT in PBS with 0.2% Triton X-100. Subsequently, cells were rinsed twice in PBS and blocked in PBS with 3% goat serum and 0.2% Tween 20 for 20 min at RT. The blocking solution was removed and cells were incubated with primary antibody diluted in PBS with 3% goat serum and 0.2% Tween 20 overnight at 4 °C in a humidified chamber. The primary antibody solution was discarded and slides were washed twice for 5 min in a 10 cm dish filled with PBS while slowly shaking. Cells were incubated with 20 µl/well of the PLA Probe Anti-Mouse PLUS and Anti-Rabbit MINUS diluted 1:5 in antibody diluent for 1 h at 37 °C in a humidified chamber. Slides were then washed two times for 5 min in wash buffer A, before being incubated for 30 min at 37 °C with ligase (1 U/µl) diluted 1:40 in ligation buffer. Slides were washed two times with wash buffer A for 2 min and incubated with polymerase (10 U/µl) diluted 1:80 in amplification buffer for 120 min at 37 °C in a humidified chamber in the dark. To visualize nuclei, cells were incubated with 20 µl Hoechst 33258 diluted 1:1000 in PBS for 5 min at RT, washed twice with 1x wash buffer B for 10 min on the shaker and one additional time with 0.01x wash buffer for 1 min. Wash buffer was removed completely, one droplet of ImmuMount was added per well and slides were immediately analyzed by fluorescence microscopy.

2.2.3.7 Western Blot

2.2.3.7.1 SDS polyacrylamide gel electrophoresis (SDS-PAGE)

Sodium dodecyl sulfate polyacrylamide gel electrophoresis (SDS-PAGE) was carried out using the Min-PROTEAN 3 Cell system from Bio-Rad according to the instruction manual. For casting SDS-gels, 8-15% separating gels were prepared as stated in **Table 38** and poured between a 1.5 mm spacer plate and a short plate, which were assembled in the casting frame and fixed in the casting stand. The separating gel was overlaid with water and allowed to polymerize completely. Water on top of the separating gel was removed, the stacking gel (

Table 39) was poured on top of the separating gel and a 10- or 15-well comb was inserted.

Table 38: Composition for 10 ml of 8-15% separating gel

	Acrylamide percentage			
Reagent	8%	10%	12%	15%
ddH_2O	4.6 ml	3.8 ml	3.2 ml	2.2 ml
1.5 M Tris pH 8.8	2.6 ml	2.6 ml	2.6 ml	2.6 ml
30% Acrylamide/ProtoGel	2.6 ml	3.4 ml	4.0 ml	5.0 ml
20% (w/v) SDS	50 µl	50 µl	50 µl	50 µl
10% (w/v) APS	50 µl	50 µl	50 µl	50 µl
TEMED	5 µl	5 µl	5 µl	5 µl

Table 39: Composition for 5 ml stacking gel

Reagent	Volume
ddH_2O	3.0 ml
0.5 M Tris pH 6.8	1.25 ml
30% Acrylamide/ProtoGel	0.67 ml
20% (w/v) SDS	25 µl
10% (w/v) APS	25 µl
TEMED	2.5 µl

The polymerized gel was placed into the electrode assembly with the short plate facing inwards, which was further assembled in the clamping frame. After putting everything into the mini tank, the inner chamber of the electrode assembly and the lower chamber of the mini tank were filled with 1x SDS-running buffer. The comb was removed, the wells rinsed with buffer and samples were loaded onto the gel. The lid was placed on the mini tank and connected to a power supply. Gels were run with constant amperage (35 mA per gel) for 1 to 2 h.

2.2.3.7.2 Immunoblotting

To transfer proteins from SDS gels onto Polyvinylidene fluoride (PVDF) membranes, the Mini-Trans Blot system from Bio-Rad was used. The PVDF membrane was incubated in 100% methanol for 30 s, then placed into ddH_2O for 2 min and finally equilibrated in 1x blotting buffer for 5 min. To prepare the membrane-gel-sandwich, the gel holder cassette was placed in a box filled with 1x blotting buffer with the transparent side down. The following pre-wetted layers were placed on the transparent side of the cassette in the same order as they are listed here: fiber pad, three sheets of filter paper, PVDF membrane, gel pre-equilibrated in blotting buffer, three sheets of filter paper, and a fiber pad. The cassette was closed and placed into the electrode module inserted in the buffer tank with the transparent cassette side to the red side and the black cassette side to the black side of the electrode module. A frozen cooling unit was placed in the buffer tank and the tank was filled with pre-cooled 1x blotting buffer. The lid was put on, connected to a power supply and the transfer was conducted at 250 mA per blotting tank for 90 min.

Successful transfer of proteins onto the PVDF membrane was verified by staining the membrane for a few minutes in Ponceau S solution and subsequent destaining with ddH_2O. To detect proteins of interest using specific antibodies, non-specific binding was first blocked by incubating the membrane in either 5% BSA or milk powder in TBS with 0.1% Tween 20 (TBS-T) for 1 hour at RT. The membrane was then incubated with the primary antibody diluted in blocking solution overnight at 4 °C. The next day, the membrane was washed three times for 5 min in TBS-T and incubated with the secondary HRP-conjugated antibody diluted in blocking solution for 1 h at RT.

For whole cell lysates, either HRP-coupled Protein A (specifically used to detect primary antibodies raised in rabbit) or HRP-coupled anti-mouse antibody was used. In case of immunoprecipitated tagged-proteins (**2.2.3.5**), anti-mouse TrueBlot ULTRA antibody was utilized to avoid immunoblotting of the denatured heavy and light chain of the antibody used for immunoprecipitation and thus specifically detect the non-reduced primary antibody used for immunoblotting. After three wash steps in TBS-T for 5 min, the membrane was incubated in freshly prepared enhanced chemiluminescence (ECL) solution for 1 min, packed in plastic wrap and exposed to X-ray films in a dark room.

2.2.3.8 Chromatin-immunoprecipitation (ChIP)

Cross-linking and cell lysis

Cells were plated in 15 cm cell culture dishes and treated as appropriate. On the day of harvest, dishes were placed on ice and proteins were cross-linked to DNA by adding 540 µl 37% formaldehyde dropwise to the medium (final concentration: 1%). Dishes were then gently rocked at RT for 10 min before 2.5 ml of 1 M glycine was added to a final concentration of 125 mM and incubated at RT for 5 min on a shaker. Cells were placed on ice and rinsed twice with 20 ml ice-cold PBS. Subsequently, cells were scraped off in 5-8 ml ice-cold PBS with freshly added PMSF (1:100) and PIC (1:1000) and scraped cells of several dishes were pooled in 50 ml falcon tubes. Cells were centrifuged at 1200 rpm and 4 °C for 8 min and the pellet was resuspended in Lysis buffer I (3 ml per 5 x 10^7 cells) containing freshly added PMSF (1:100) and PIC (1:1000). After an incubation of 20 min on ice, all lysed cells were pooled and aliquots of 3 ml containing 5 x 10^7 cells were spun down at 1200 rpm, 4 °C for 5 min. Supernatants were removed and pellets snap frozen in liquid nitrogen were stored at -80 °C.

Fragmentation of chromatin by sonication

For sonication, one cell pellet was thawed on ice, resuspended in 1.5 ml Lysis II buffer (with 1:1000 PIC and 1:100 PMSF) and incubated on ice for 10 min. To shear DNA, lysed nuclei were transferred to a 15 ml falcon tube from which the upper part was cut off at around 12.5 ml. Tubes were placed in a beaker filled with ice and water and sonication was performed for 15 min in total using a Branson Sonifier equipped with a microtip with the following settings: 25% amplitude, 10 s ON and 45 s OFF (duration: 82.5 min per sample/per 5 x 10^7 cells). After sonication, all samples were pooled, placed on ice in the cold room and 60 µl were taken off to check the size of the chromatin. To do so, the sample was centrifuged at max. speed for 15 min at 4 °C and 50 µl were transferred to a new 1.5 ml tube.

Determination of DNA concentration and analysis of successful fragmentation

To reverse cross-links, 2 µl 5 M NaCl and 1 µl RNase A (10 mg/ml) were added to the sample and incubated overnight in a thermomixer at 65 °C and 550 rpm. Samples were cooled down briefly to RT and incubated with 2 µl Proteinase K (10 mg/ml) at 45 °C for 2 h while shaking at 550 rpm. DNA was purified by adding 1 ml peqGOLD TriFast Trizol reagent and 200 µl chloroform. Samples were vortexed for 15 s and incubated at RT for 5 min. Centrifugation at 12,000 x g, 4 °C for 10 min separated the sample into three phases. The upper aqueous phase was discarded and DNA was precipitated by adding 1 ml ice-cold 100% ethanol and 50 µl 3 M sodium acetate to the lower and interphase.

Samples were inverted a few times and incubated at -80 °C for at least 30 min. Frozen samples were centrifuged at maximum speed and 4 °C for 10 min and the resulting DNA pellet was washed with 1 ml ice-cold 70% ethanol at max. speed, 4 °C for 5 min. Ethanol was removed completely and the DNA pellet was air-dried for approx. 5 min and resuspended in 50 µl 1x TE buffer. DNA concentration was measured using a NanoDrop2000. DNA fragment size was analyzed using agarose gel electrophoresis (**2.2.2.6**). 20 µl of DNA was mixed with 5x loading buffer and loaded on a 1.2% agarose gel. When the size of the fragmented DNA was between 150 and 300 bp, the sheared chromatin stored overnight in the cold room was transferred to 2 ml tubes and centrifuged at max. speed for 15 min. Supernatants of all samples were pooled and aliquots were snap frozen in liquid nitrogen and stored at -80 °C.

Immunoprecipitation

For immunoprecipitation, 30 µl (ChIP-qPCR) or 90 µl (ChIP-seq) Protein G Dynabeads were washed three times with 1 ml BSA-PBS (5 mg/ml) using the DynaMag-2 Magnet (Thermo Fisher). After the last wash step, BSA was removed and beads were resuspended in 1 ml fresh BSA-PBS. Per IP, 3 µg (ChIP-qPCR) or 9 µg (ChIP-seq) specific primary antibody or non-specific IgG (as a negative control) was added and incubated overnight on a rotating wheel in the cold room. Beads were washed with 1 ml BSA-PBS three times and resuspended in 30 µl or 90 µl BSA-PBS. Chromatin (see **Table** 40 for amounts) diluted in 500-1000 µl Lysis II buffer (PIC 1:1000, PMSF 1:100) was added to the antibody-coupled beads and incubated on a rotating wheel in the cold room for 6 h. For the input, 1% of chromatin used for the IP was transferred to a fresh tube and stored at 4 °C.

Table 40: Chromatin amounts used for ChIP-qPCR and ChIP-seq

Cell line	Chromatin amount used for:	
	ChIP-qPCR	ChIP-seq
KPL2 cells	80 µg (approx. 6.6 x 10^6 cells)	240 µg (approx. 2 x 10^7 cells)
MCF10A YAP5SA	100 µg (approx. 1.4 x 10^7 cells)	250 µg (approx. 3.5 x 10^7 cells)

Afterwards, beads were washed three times with Wash Buffer I (PIC 1:1000, PMSF 1:100), three times with Wash Buffer II (PIC 1:1000, PMSF 1:100) and another three times with Wash Buffer III (PIC 1:1000, PMSF 1:100) by incubating each time for 5 min on a rotating wheel in the cold room. After washing one more time with 1 ml 1x TE Buffer (PIC 1:1000, PMSF 1:100), beads in 1x TE Buffer were transferred to a fresh 1.5 ml tube and placed in the magnetic rack.

The supernatant was removed completely and proteins were eluted from beads by incubating two times with 250 µl freshly prepared Elution Buffer on a rotating wheel at RT for 15 min each time.

Reversal of cross-links and DNA purification

16 µl 5 M NaCl (final concentration: 160 mM) and 1 µl 10 mg/ml RNase A (final concentration: 20 µg/ml) were added to merged eluates (500 µl in total) and incubated first at 37 °C for one hour and then at 65 °C overnight with shaking at 550 rpm to revert the cross-links. The next day, 5.2 µl 0.5 M EDTA (final concentration: 5 mM) and 10.3 µl 10 mg/ml Proteinase K (final concentration: 200 µg/ml) were added and incubated at 45 °C for 2 h. DNA was purified using the QIAquick PCR Purification Kit (Qiagen) according to the manufacturer's instructions and eluted in 50 µl EB buffer provided with the kit. 1 µl of ChIP DNA was used in qPCR to analyze the enrichment of a certain DNA region relative to the DNA input amount (% of input) as stated in **2.2.2.9.2**.

2.2.4 Next-generation sequencing (NGS)

2.2.4.1 RNA-sequencing (RNA-seq)

For RNA-sequencing (RNA-seq), 25,000 KPL2 cells were seeded in triplicate on 6 cm cell culture dishes in DMEM with 2.5 µg/ml puromycin. One day later, medium was replaced by fresh medium containing 2.5 µg/ml puromycin and 10 nM 4-OHT. RNA was isolated 4 d after starting 4-OHT treatment using the RNeasy Mini Kit with on-column DNase I digestion from Qiagen as described in the manual. RNA quality was assessed using the Experion Automated Electrophoresis System (Bio-Rad) with the Experion RNA StdSend Analysis Kit as described by the manufacturer. RNA concentration was determined using a NanoDrop2000 photometer. 500 ng RNA were used to generate cDNA libraries with the NEBNext Ultra RNA Library Prep Kit for Illumina (NEB) together with the Poly (A) mRNA Magnetic Isolation Module (NEB) and the DynaMag-96 Side Magnet (Thermo Fisher). Adapter ligation was performed using the NEBNext adapters for Illumina and the USER enzyme provided with the NEBNext Multiplex Oligos for Illumina (Dual Index Primers Set 1; E7600) Kit. cDNA libraries were size-selected and purified using Agencourt AMPure XP Beads (Beckman Coulter). Finally, cDNA libraries were enriched by 12 cycles of PCR amplification using the i5/i7 Dual Index primers from the abovementioned kit and again purified using Agencourt AMpure XP Beads. The complete protocol is outlined in detail in the instruction manual of the NEBNext Ultra RNA Library Prep Kit for Illumina (NEB) (#E7530).

Library quality and concentration were assessed using the Experion Automated Electrophoresis system with the DNA 1K Analysis Kit (Bio-Rad). Libraries were pooled with each sample being present at an equimolar concentration (multiplexing) and were sequenced on the NextSeq 500 platform (Illumina).

2.2.4.2 ChIP-sequencing (ChIP-seq)

Chromatin immunoprecipitation was performed as described in chapter **2.2.3.8**.

Quantification of ChIP-DNA using PicoGreen

Purified ChIP-DNA (**2.2.3.8**) was quantified in duplicate using the Quant-iT PicoGreen dsDNA Assay Kit (Thermo Fisher). 20x TE was diluted to 1x TE in nuclease-free water. 1x PicoGreen was prepared from the 200x PicoGreen stock using 1x TE and protected from the light by covering with aluminum foil. For PicoGreen, 1750 µl for the standard curve, 250 µl per sample/blank (EB buffer only), and 500 µl as backup were calculated. For the standard curve, the lambda DNA (100 µg/ml) was diluted 1:50 with 1x TE to a final concentration of 2 ng/µl. The following standard curve was prepared in 1.5 ml tubes:

Table 41: Standard curve for PicoGreen measurement

Sample	Final concentration (ng/ml)	DNA		1x TE
Standard 7	10	5 µl	of 2 ng/µl lambda DNA	495 µl
Standard 6	4	220 µl	of Standard 7	330 µl
Standard 5	2	275 µl	of Standard 6	275 µl
Standard 4	1	275 µl	of Standard 5	275 µl
Standard 3	0.5	275 µl	of Standard 4	275 µl
Standard 2	0.1	100 µl	of Standard 3	400 µl
Standard 1	0	0 µl		500 µl

Input DNA was diluted 1:10 using EB buffer from the QIAquick PCR Purification Kit (Qiagen). 1 µl of diluted input DNA, undiluted ChIP DNA, and EB buffer (blank) was brought to a final volume of 250 µl with 1x TE and mixed with 250 µl 1x PicoGreen. 200 µl/well of each sample were pipetted in duplicate into a black 96-well plate with F-bottom (Greiner) and the fluorescence intensity was measured using the Tecan Infinite M200 plate reader and the Tecan i-control software with settings stated in **Table 42**. DNA concentrations were calculated using the standard curve.

Table 42:Settings for PicoGreen measurement using the Tecan Infinite M200

Mode	Fluorescence Top Reading
Excitation Wavelength	485 nm
Emission Wavelength	535 nm
Excitation Bandwidth	9 nm
Emission Bandwidth	20 nm
Gain	178 Optional (100%)
Number of Flashes	25
Integration Time	20 µs
Lag Time	0 µs
Settle Time	0 ms

DNA library prep for ChIP-DNA

Quantified ChIP-DNA was diluted in EB buffer (QIAquick Kit) to a volume of 50 µl. The NEBNext Ultra II DNA Library Prep Kit for Illumina (NEB) was used for generating DNA libraries. In doing so, purified DNA was end-repaired (generation of blunted ends), dA-tailed, ligated to Illumina adapters (single A 3' overhangs will enable adapter ligation with single T overhangs) and size selected using Agencourt AMPure XP Beads (150 bp). Adapter-ligated DNA was amplified by PCR with i5 and i7 Index Primers included in the NEBNext Multiplex Oligos for Illumina (Dual Index Primers Set 1; E7600) Kit. Finally, PCR amplified DNA libraries were purified using AMPure XP beads. All steps were performed as stated in the instruction manual from the NEB Kit (#E7645) with the following DNA amounts, adapter dilutions, and number of PCR cycles:

Table 43: DNA amount, adapter dilution, and number of PCR cycles for DNA library prep of ChIP DNA

Cell line	ChIP sample	DNA amount	Adapter dilution	Number of PCR cycles
KPL2	input (for LIN9 and YAP), diluted 1:10	2 ng	1:25	13
	LIN9	1 ng	1:25	14
	YAP	1 ng	1:25	14
	input (for histone modifications), diluted 1:10	10 ng	1:10	10
	H3K4me1	10 ng	1:10	10
	H3K4me3	10 ng	1:10	10
	H3K27ac	10 ng	1:10	10
MCF10A YAP5SA	input, diluted 1:10	1.5 ng	1:25	15
	LIN9	1.5 ng	1:25	15
	B-MYB	1.5 ng	1:25	15
	YAP	1.5 ng	1:25	15
	H3K4me1	1.5 ng	1:25	15
	H3K4me3	1.5 ng	1:25	15
	H3K27ac	1.5 ng	1:25	15

DNA library size and concentration were analyzed using the Experion Automated Electrophoresis system with the DNA 1K Analysis Kit (Bio-Rad) or the Fragment Analyzer Automated CE System with the DNF-474 High Sensitivity NGS Fragment Analysis Kit (1 bp – 6,000 bp) (Advanced Analytical) according to the manufacturer's instructions. Libraries were pooled to an equimolar ratio and subjected to Illumina NextSeq 500 sequencing.

2.2.4.3 Circular chromosome conformation capture sequencing (4C-seq)

Circular chromosome conformation capture followed by high-throughput sequencing (4C-seq) is based on the original chromosome conformation capture (3C) technology introduced by Dekker and colleagues in 2002 (Dekker et al. 2002). 3C and 3C-based methods allow to analyze the nuclear organization and conformation of the chromosome by identifying genome-wide interactions (Dekker et al. 2002; Stadhouders et al. 2013). In contrast to 3C, 4C-seq does not require prior knowledge of the interaction loci and can thus be used to identify all genomic sites interacting with a genomic site of choice (viewpoint) (Splinter et al. 2012; Stadhouders et al. 2013). With the help of 3C and 4C, distal enhancers, which can initiate transcription by getting in contact with promoters through chromatin looping, can be identified (Stadhouders et al. 2012).

Cell lysis and nuclei preparation

4C-seq was performed as described previously with some modifications (Stadhouders et al. 2013). MCF10A YAP5SA cells were seeded on 15 cm cell culture dishes and treated with 0.5 µg/ml doxycycline for 2 days. On the day of harvest, dishes were placed on ice and cells were washed once in 20 ml ice-cold PBS. For cross-linking, cells were incubated with 20 ml 1.5% formaldehyde in PBS for 10 min at RT while shaking slowly. 2.5 ml of 1 M glycin was added to a final concentration of 125 mM and incubated at RT for 5 min. Cells were washed once with ice-cold PBS and were scraped off in 3 ml ice-cold PBS containing PIC (1:1000). The cell suspension of all dishes was collected in a 50 ml falcon and cells were centrifuged at 1200 rpm and 4 °C for 5 min. Cells were lysed by resuspension in Lysis Buffer (3 ml per 15 cm dish) containing PIC (1:1000) by a freeze/thaw cycle (frozen at -20 °C for 1 h/thawing on ice for 1 h) and by passing 20 times through a 20G needle attached to a syringe. Nuclei were collected at 1200 rpm, 4 °C for 5 min, snap frozen in liquid nitrogen and stored at -80 °C.

3C library preparation: first digestion, ligation, de-cross-linking, and DNA purification

Thawed nuclei were washed in 500 µl 1.2x restriction buffer (EcoRI or R buffer, Thermo Fisher; see **Table 44** for combinations of restriction enzymes), resuspended in 500 µl 1.2x restriction buffer and incubated with 7.5 µl 20% SDS (final: 0.3% SDS) at 37 °C for 1 h while shaking at 900 rpm. 50 µl of 20% Triton X-100 (final: 2% Triton X-100) was added and incubated at 37 °C and 900 rpm for 1 h. 10 µl aliquots were taken from each sample as undigested controls and stored at -20 °C. To the remaining sample, 400 U of EcoRI or HindIII (Thermo Fisher) was added and incubated overnight at 37 °C while shaking at 900 rpm. The next day, 10 µl were taken as the digested control and stored at -20 °C. Samples were incubated with 40 µl of 20% SDS (final: 1.6% SDS) for 20 min at 65 °C, 900 rpm. Digested nuclei were transferred to 50 ml falcon tubes and 6.125 ml of 1.15x T4 ligation buffer (NEB) together with 375 µl of 20% Triton X-100 (final: 1% Triton X-100) were added. Samples were mixed, distributed to 1.5 ml tubes and incubated on a thermomixer at 37 °C and 450 rpm for 1 h. Samples were transferred back to a 50 ml falcon tube and incubated with 20 µl T4 ligase (400 U/µl, NEB) for 4 h at 16 °C in order to enable proximity ligation. To reverse cross-links, 30 µl of 10 mg/ml Proteinase K (300 µg in total) was added. Falcon tubes were mixed by inverting and the sample was distributed to 1.5 ml tubes and incubated overnight at 65 °C, 450 rpm. The next day, samples were pooled in a 50 ml falcon tube and incubated with 30 µl of 10 mg/ml RNase A in a 37 °C warm water bath for 30 min. DNA was purified using phenol-chloroform extraction and precipitated with ethanol as described in steps 25 to 32 by Stadhouders et al. (2013).

Determination of digestion and ligation efficiency

To determine digestion efficiency, DNA was purified from 10 µl undigested and digested control samples frozen at -20 °C as described in Box 2 of the Nature protocol written by Hagege et al. (2007). Samples were mixed with 500 µl 1x PK buffer and 2 µl of 10 mg/ml Proteinase K (20 µg in total) and incubated for 30 min at 65 °C. After equilibrating for a few minutes at 37 °C, 1 µl of 1 mg/ml RNase A (1 µg in total) was added and incubated for 2 h at 37 °C. Samples were mixed with 500 µl of phenol/chloroform/isoamyl alcohol (25:24:1) and centrifuged at 16,100 x g at RT for 5 min. The supernatant was transferred to a fresh 2 ml tube. 50 µl of 2 M sodium acetate, pH 5.6 was added before samples were mixed with 1.5 ml 100% ice-cold ethanol and 2 µl of 20 mg/ml glycogen and placed at -80 °C until frozen (about 1 h). Frozen samples were centrifuged at 16,100 x g at 4 °C for 20 min and the DNA pellet was washed with 500 µl 70% ice-cold ethanol at 16,1000 x g at RT for 4 min. The pellet was air-dried (about 10 min) and resuspended in 20 µl ddH_2O by incubating at 37 °C for 15 min. The complete 20 µl of digested and undigested control samples and 0.5 µl of the 3C library were analyzed on a 0.6% agarose gel.

4C-seq library preparation: second digestion, ligation and DNA purification

To estimate DNA concentration, 0.25 and 0.5 µl of the 3C library were run on a 2% agarose gel next to 250, 500, and 1000 ng of genomic DNA isolated from MCF10A YAP5SA cells using the NucleoSpin Tissue XS Kit (Macherey-Nagel). 50 µg of the 3C library were digested with 50 units of NlaIII or HaeIII (NEB) in CutSmart buffer in a final volume of 500 µl overnight at 37 °C. DNA was purified using phenol/chloroform and precipitated with ethanol as stated in steps 36 to 43 of the Stadhouders et al. (2013) protocol. Successful digestion was assessed by running 5 µl of the digested DNA alongside 0.5 µl of the ligated 3C library on a 1.5% agarose gel. Digested DNA was transferred to a 50 ml falcon tube, mixed with 1.4 ml of 10x T4 ligation buffer and 40 µl T4 DNA ligase (400 U/µl; NEB) and filled up with ddH_2O to 14 ml. Ligation mixture was kept overnight at 16 °C. The resulting 4C library was precipitated as described in steps 46 to 54 and purified using the QIAquick PCR Purification Kit (Qiagen) as described in the manual. As one column can only bind a maximum of 10 µg DNA, 5 spin columns were used for purification of the 4C library (50 µg in total). DNA was eluted using 30 µl 60 °C-pre-warmed EB Buffer per column. Eluates of all 5 columns were combined and DNA concentration was determined using the NanoDrop 2000.

4C-seq inverse PCR

To test primers for linearity and reproducibility, first, primers without P5/P7 Illumina adapters were used in a 50 µl PCR with increasing amounts of the 4C-seq library (25, 50, 75, 100, 150, 200 ng) and were analyzed on 1.5% agarose gels. When primers were tested successfully, 11 single PCR reactions each with 200 ng 4C DNA were set up per sample using primers containing the P5/P7 Illumina sequencing adapters (see below).

Inverse PCR mix

ddH_2O	35.2 µl
5x HF Buffer	10.0 µl
primer P5 [10 µM]	0.5 µl
primer P7 [10 µM]	0.5 µl
dNTPs [2mM]	2.5 µl
Phusion Hot Start II [2 U/µl]	0.3 µl
4C DNA [200 ng/µl]	1.0 µl
Total volume	50.0 µl

PCR conditions

		Cycles
98 °C	30 s	1
98 °C	10 s	
60 °C/ 64 °C	15 s	35
72 °C	1 min	
72 °C	5 min	1
4 °C	hold	

Table 44: Restriction enzymes, P5/P7 primers, and annealing temperatures for 4C-seq

Promoter	Restriction enzymes		Primers for - doxy		Primers for + doxy		Annealing temperature
	1st	2nd	P5	P7	P5	P7	
AURKA	HindIII	NlaIII	2482	2484	2483	2484	64 °C
CDC20	EcoRI	NlaIII	2479	2481	2480	2481	60 °C
KIF23	HindIII	HaeIII	2491	2493	2492	2493	60 °C
MYBL2	HindIII	NlaIII	2488	2490	2489	2490	60 °C

Purification of 4C libraries using Qiagen columns and AMPure beads

All 11 PCR reactions were pooled and a 25 µl aliquot was removed for agarose gel electrophoresis. The remaining solution of amplified 4C libraries was purified using two QIAquick PCR purification spin columns and eluted in 50 µl ddH_2O per column. Both 50 µl eluates were pooled and further cleaned up by adding 1.8x volume of Agencourt AMPure XP beads (Beckman Coulter). DNA was mixed with beads by pipette mixing for 10 times, incubated at RT for 5 min and placed in a DynaMag-2 magnet for 2-5 min until the solution was clear. While the tubes were placed in the magnetic rack, the cleared solution was aspirated, 750 µl 70% ethanol was added to the tube and incubated for 30 s. This step was repeated one more time. Ethanol was removed completely and, while in the magnetic rack, beads were air-dried with open lid for a maximum of 5 min. Tubes were taken out from the magnetic rack and beads were resuspended in 100 µl 0.1x TE buffer by pipetting up and down 10 times and incubated for 2 min before tubes were placed back in the magnetic rack. After 5 min, the eluate became clear and was transferred to a fresh tube. To verify successful removal of potential primer dimers, 5 µl of the purified 4C material was run on a 1.5% agarose gel alongside the 25 µl of unpurified 4C library that was removed in the beginning. The 4C libraries were sequenced on an Illumina NextSeq 500 sequencer.

2.2.5 Animal experiments

All animal experiments were carried out according to German law and were approved by an institutional committee (*Tierschutzkommission der Regierung von Unterfranken*). Mice were maintained on a C57BL/6 background. *K-Ras*$^{LSL\text{-}G12D/+}$ and conditional *p53*$^{fl/fl}$ mice have been described before (Marino et al. 2000; Jackson et al. 2001) and were obtained from the NCI Mouse Repository, Bethesda, MD, USA.

The *K-Ras*$^{LSL\text{-}G12D}$ allele of *K-Ras*$^{LSL\text{-}G12D/+}$ mice contains a missense mutation at codon 12 (G12D) resulting in decreased GTPase activity and thus constitutive K-RAS signaling. The expression of *K-Ras G12D* is under the control of a stop sequence, which prevents gene expression and is flanked by loxP sites, collectively referred to as the Lox-Stop-Lox (LSL) cassette (Lakso et al. 1992; Jackson et al. 2001).

This LSL cassette is inserted into intron 0 upstream of the transcription start site (TSS). As the LSL cassette prevents gene expression of *K-Ras* and *K-Ras* null mice are embryonic lethal, mice have to contain a wild-type *K-Ras* allele in addition to the *K-Ras*$^{LSL\text{-}G12D}$ allele. The *p53* allele of *p53*$^{fl/fl}$ mice encodes the wild-type *p53* but exons 2 to 10 are flanked by loxP sites (Johnson et al. 1997; Jackson et al. 2005).

2.2.5.1 Infection of mice with Cre-encoding lentivirus

To infect *K-Ras*$^{LSL\text{-}G12D/+}$*; p53*$^{fl/fl}$ mice with Cre-expressing lentiviral vectors by intratracheal intubation, 8-12-week-old male and female mice were anesthetized with Ketamine/Xylazine. For this purpose, 900 µl 0.9% NaCl were mixed with 75 µl Xylazine and 225 µl Ketamine/Ketavet and 175 µl of this mixture per 25 g of body weight was injected intraperitoneally into mice. Mice were then infected with PEG-precipitated and titrated (chapters **2.2.1.11**; **2.2.1.12**; **2.2.1.13**) Cre-expressing lentiviral vectors (Ubc-shLuc-pgk-Cre; per mouse: 1x10^6 TU dissolved in 60 µl PBS) by intratracheal intubation as described previously (DuPage et al. 2009). Preparation of lentivirus and infection of mice were performed in a Biosafety Level 2 (BSL-2) environment.

2.2.5.2 Preparation of lung paraffin sections

16 weeks after infection, mice were sacrificed by cervical dislocation and excised lungs were fixed in 4% paraformaldehyde in PBS overnight at 4 °C. Lungs were washed twice in PBS and once in 0.9% NaCl, each time for 10 min at RT on a rotating wheel. Subsequently, tissues were dehydrated and embedded in paraffin according to the following scheme:

50% ethanol	1 h (RT)
70% ethanol	1 h (RT) or storage at 4 °C for several days/weeks
80% ethanol	1 h (RT)
90% ethanol	1 h (RT)
95% ethanol	1 h (RT) or overnight at 4 °C
100% ethanol	2 times, each 1 h (RT)
100% ethanol/Xylene (1:1)	1 h (RT)
Xylene	2 times, each 1 h (RT)
Xylene mixed with Paraffin (1:1)	1 h at 60 °C
Paraffin	at least overnight at 60 °C, changed 2-3 times

Tissues were embedded using a Microm EC 350 modular paraffin embedding center (Thermo Fisher). Paraffin-embedded tissues were allowed to solidify at 4 °C and cut into 5 µm sections with a Hyrax M 40 rotary microtome. Sections were fixed to glass slides overnight at 42 °C and stored at 4 °C.

For H/E staining and immunohistochemistry, paraffin sections were allowed to reach RT for 10-20 min before being deparaffinized and rehydrated as stated below:

Xylene I	10 min
Xylene II	10 min
100% ethanol	3 min
95% ethanol	3 min
80% ethanol	3 min
70% ethanol	3 min
50% ethanol	3 min
Demineralized H_2O (VE-H_2O)	5 min

2.2.5.3 Hematoxylin and Eosin (H/E) staining

To visualize different tissue structures under the microscope, deparaffinized and rehydrated (**2.2.5.2**) lung sections were stained with Hematoxylin and Eosin (H/E). First, nuclei were stained in a blue to dark violet color using Hemalum solution acid according to Mayer (Roth) for 8 min. After rinsing in running tap water for at least 15 min, counterstaining of cytoplasm was performed in 0.1% Eosin Y solution supplemented with 1-2 drops of glacial acetic acid for 3 min. Sections were rinsed shortly in tap water and dehydrated in 95% ethanol (3 min), 100% ethanol (3 min), Xylene I (10 min), and Xylene II (10 min). Finally, sections were mounted with Roti-Histokitt.

2.2.5.4 Immunohistochemistry (IHC)

For staining of specific proteins in paraffin-embedded tissue, sections were first deparaffinized and rehydrated as described in **2.2.5.2**. Endogenous peroxidase activity was blocked by incubating sections for 10 min in 3% H_2O_2 in PBS followed by three washing steps in PBS for 5 min each. Antigen retrieval was performed in 10 mM sodium citrate buffer, pH 6.0 by boiling in a microwave for 6 min. Sections were cooled down to RT for 30-45 min and rinsed three times in PBS for 5 min. Slides were blocked with 3% BSA in PBS-T (PBS with 0.1% Tween 20) for 1 h and incubated with primary antibody diluted in blocking solution overnight at 4 °C in a humidified chamber. The next day, slides were washed three times in PBS-T for 2 min each and incubated with HRP-coupled secondary antibody (diluted in blocking solution) for 1-2 h at RT in a humidified chamber. Slides were washed three times in PBS-T for 2 min and antigens were visualized using 3,3'-diaminobenzidine tetrahydrochloride (DAB) staining solution, which was prepared freshly by mixing 4.5 ml Tris pH 7.5 with 250 µl 1% DAB (0.1 g DAB dissolved in 10 ml ddH2O, acidified with 200 µl 10 N HCl; stored in aliquots at -20 °C) and 250 µl 0.3% H_2O_2.

Slides were incubated with DAB for 10 min and afterwards, rinsed three times in ddH_2O for 2 min. Nuclei were counterstained with Hemalum solution acid according to Mayer (Roth) for 3 min followed by bluing under running tap water for at least 5 min. Sections were dehydrated in 70% ethanol (2 min) for two times, 95% ethanol (2 min), 100% ethanol (2 min) and in Xylene (5 min) for two times. Sections were air-dried shortly and mounted with Roti-Histokitt. Visualization was done using the Nikon Eclipse TS100 microscope.

2.2.6 Data acquisition and statistical analysis

2.2.6.1 RNA-seq analysis

Analyses of RNA-seq data were performed by Susanne Walz (Comprehensive Cancer Center Mainfranken, Core Unit Bioinformatics, Biocenter, University of Würzburg, Würzburg, Germany). Reads were mapped to *Mus musculus* reference genome mm10 or the *Homo sapiens* genome Hg19 using TopHat v2.1.0 (Kim et al. 2013) with Bowtie v2.3.2 (Langmead and Salzberg 2012) and randomly subsampled based on the sample with the smallest number of mapped reads. Weakly- and non-expressed genes were removed (mean read count over all samples < 1) and edgeR (Robinson et al. 2010) was used to identify differentially expressed genes. Gene set enrichment analysis (Broad Institute) was performed as described previously (Subramanian et al. 2005) with 1000 permutations, “Signal2Noise” metric of RNA-seq read counts per gene and a gene set size filter of 15-900. The “C2” gene set database from MSigDB was spiked with YAP signatures from MSigDB “C6” (“Cordenonsi: YAP conserved signature”) as well as “YAP/TAZ” (Zhang et al. 2009), “induced by YAP” (Zhao et al. 2008), “YAP” (Dupont et al. 2011), and “YAP signature” (Zanconato et al. 2015).

2.2.6.2 ChIP-seq analysis

Analyses of ChIP-seq data were performed by Susanne Walz. Base calling was performed with Illumina’s CASAVA software or FASTQ Generation software v1.0.0 and overall sequencing quality was tested using the FastQC script. For ChIP-sequencing, reads were mapped to the human (hg19) or murine (mm10) genome with Bowtie v1.1.2 (Langmead et al. 2009) with default parameters. Mapped reads were randomly subsampled to the sample with the smallest number of mapped reads and peak calling for transcription factors was performed with MACS v2.1.1 (Zhang et al. 2008) and corresponding input samples as controls with variable “–keep-dup” settings (3 for Yap/YAP, 5 for Lin9/LIN9/B-MYB) and q-value cut-off (5.0e-2 for Yap/Lin9, 1.0e-3 for LIN9/B-MYB, 1.0e-5 for YAP).

Enrichments for histone modifications were determined using SICER v1.1 (Xu et al. 2014) with a window size of 200 bp, gap size of 600 bp and a q-value cut-off of 1.0e-3. Enhancer were defined by having an enrichment for H3K4me1 overlapping with H3K27ac without H3K4me3 enrichment and being at least 1 kb away from annotated transcriptional start sites (TSS) of Ensembl genes (mouse: GRCm38.p6, human: GRCh37.p13). Open and active promoters were defined by having an enrichment for H3K4me3 overlapping with H3K27ac without H3K4me1 enrichment and being in a region of $\pm$ 1 kb around annotated transcriptional start sites of Ensembl genes. H3K27ac enrichments and read density were used to identify super-enhancers with the ROSE software (Loven et al. 2013; Whyte et al. 2013). For visualization, read density files in bedgraph format were generated using the genomeCoverageBed function from BEDTools v2.26.0 (Quinlan and Hall 2010) and the Integrative Genomics Viewer (Robinson et al. 2011). Heat maps and density profiles were generated using DeepTools (Ramirez et al. 2016) and a resolution between 10 and 100 bp as indicated. To correlate LIN9 binding with gene expression changes, reads were counted in a region +/- 1kb around TSSs of expressed genes with more reads in the LIN9 sample than in input controls (n=10,981). Genes were sorted based on log2FC (+ OHT vs - OHT), grouped into 18 equally-sized bins and the mean of all bins was plotted. *P*-values for Pearson's correlation coefficients were calculated with two-tailed *t*-tests.

B-MYB occupancy was analyzed in a region of -100 to +400 bp around TSS and the empirical cumulative distribution function was calculated using the R environment (https://www.r-project.org). For the analysis of promoter-enhancer interactions, published Hi-C data from IMR90 cells were used (Jin et al. 2013). Positions of "anchor" (TSS) and "target" (enhancer) regions were converted to hg19 coordinates and overlapping "target" regions with YAP (+ dox) peaks were identified. For each of these YAP-bound "targets" the corresponding "anchor" was analyzed whether it is overlapping with LIN9 (- dox) peaks, B-MYB is bound and how gene expression changes upon induction of YAP5SA. Functional analyses of gene groups were done with DAVID v6.8 (Huang da et al. 2009) using only gene ontology (GO) terms as database and functional clustering of enriched GO terms. In box plots, the median is indicated, borders of boxes show the upper and lower quartile and whiskers extend to 1.5 of the interquartile range.

2.2.6.3 4C-seq analysis

The analysis of 4C-seq data was performed by Björn von Eyss (Leibniz Institute on Aging, Fritz Lipmann Institute e.V., Jena, Germany). Reads were trimmed by removing the first 3 base pairs, which contain the sample-specific barcode. The publicly available software w4CSeq (https://github.com/WGLab/w4CSeq) was used with default settings to analyze 4C-seq data and to identify intra- and inter-chromosomal interactions. Distal regions with an adjusted *P*-value < 0.01 were considered to significantly interact with promoters of indicated genes (Cai et al. 2016).

2.2.6.4 Analysis of human lung cancer data sets

Analysis of human lung cancer data sets was performed by Stefan Gaubatz (Theodor Boveri Institute and Comprehensive Cancer Center Mainfranken, Biocenter University of Würzburg, Würzburg, Germany). Oncomine (www.oncomine.org) was used to analyze the expression of B-MYB and to correlate it with genes regulated by YAP in a lung cancer microarray data set (Garber et al. 2001). Correlation of survival with the expression of certain genes in human lung cancer samples was done using the KM-plotter (http://kmplot.com/analysis/) (Gyorffy et al. 2013).

2.2.6.5 Data availability

All ChIP- and RNA-sequencing data sets of this thesis have been deposited in NCBI's Gene Expression Omnibus (Edgar et al. 2002) and are accessible through GEO Series accession number GSE115787.
(https://www.ncbi.nlm.nih.gov/geo/query/acc.cgi?acc=GSE115787)

2.2.6.6 Statistical analysis

Unless indicated otherwise, data are presented as mean $\pm$ standard deviation (SD). Statistical tests were applied as indicated in the figure legends. In general, statistical significance for the difference between two experimental groups was determined by two-tailed Student's *t*-test (unpaired *t*-test) or for more than two groups by one-way analysis of variance (one-way ANOVA) with Tukey's post-test. To compare the means of two or more groups in response to two independent variables, the two-way ANOVA with Bonferroni's multiple comparison test was used. P values ≤ 0.05 were considered statistically significant. Asterisks are as follows:
$^{*}P \leq 0.05$; $^{**}P \leq 0.01$; $^{***}P \leq 0.001$; $^{****}P \leq 0.0001$. In case of $P > 0.05$ results are labeled with ns (not significant). Statistical analyses were performed using the GraphPad Prism 7.0c software (GraphPad Software, Inc., La Jolla, CA, USA).

3 Results

3.1 Lung adenocarcinoma-derived cells are sensitive to the loss of the MuvB core subunit LIN9

Using a well-characterized mouse model for non-small cell lung cancer (NSCLC) driven by oncogenic K-RAS and loss of p53, our laboratory could show recently that MMB is required for lung tumor formation *in vivo* (Jackson et al. 2005; Iltzsche et al. 2017). The loss of MMB by deleting *Lin9*, the gene encoding for the MuvB core subunit LIN9, resulted in significantly smaller and less advanced tumors compared to tumors of control mice harboring wild-type *Lin9* alleles (Iltzsche et al. 2017). Mice of this study contained a conditional activatable *K-Ras*$^{LSL\text{-}G12D}$ allele, conditional loss-of-function *p53* (*p53*$^{fl/fl}$) alleles and either wild-type (*Lin9*$^{+/+}$) or conditional loss-of-function (*Lin9*$^{fl/fl}$) alleles of *Lin9* (Iltzsche et al. 2017) (**Figure 4A**). Activation of oncogenic K-RAS G12D by removal of the stop sequence (ΔLSL) and loss of p53 and LIN9 by recombination of the loxP sites were induced by infection of mice with adenovirus-expressing Cre-recombinase (Ade-Cre). Lung tumors were dissected 13 weeks after tumor initiation and *Lin9* PCR of dissected lung tumors revealed the presence of a non-recombined (fl) next to the recombined (Δfl) allele of *Lin9*. To analyze the importance of MMB for the proliferation of lung cancer cells *in vitro*, primary cell lines from dissected lung adenocarcinomas from *K-Ras*$^{LSL\text{-}G12D/+}$*; p53*$^{fl/fl}$*; Lin9*$^{fl/fl}$ mice (KPL1 and KPL2) and from control *K-Ras*$^{LSL\text{-}G12D/+}$*; p53*$^{fl/fl}$*; Lin9*$^{+/+}$ mice harboring wild-type alleles of *Lin9* (KP1 and KP2) were established (Iltzsche et al. 2017).

In first experiments of this thesis, KP and KPL cells were stably transduced with retroviral hormone-inducible CreER^{T2} recombinase. In this system, the bacteriophage P1 Cre-recombinase is fused to a mutated ligand binding domain of the human estrogen receptor (ER). This mutation prevents binding of the natural ligand estradiol to the ER but instead allows that CreER^{T2} is efficiently activated by the synthetic ER antagonist 4-hydroxytamoxifen (4-OHT) leading to the dissociation of CreER^{T2} from heat shock proteins and its translocation into the nucleus (Feil et al. 1997; Fuhrmann-Benzakein et al. 2000). Treatment of KP and KPL cells with 10 nM 4-OHT for 3 days induced the recombination and deletion of the second remaining floxed allele of *Lin9* and the complete loss of LIN9 protein expression in KPL1 and KPL2 cells as determined by genomic *Lin9* PCR and immunoblotting of immunoprecipitated LIN9 (**Figure 4B and C**).

Importantly, 4-OHT treatment did not affect the wild-type *Lin9* allele status or LIN9 protein expression in KP1 and KP2 cells. As expected, genomic PCR of *K-Ras* alleles revealed the presence of one wild-type (wt) *K-Ras* and one recombined (ΔLSL) *K-Ras*^{G12D} allele in KP and KPL cells (**Figure 4D**).

In order to investigate whether the complete deletion of *Lin9* influences the growth and proliferation of KPL cells, KP control and KPL cells were seeded at low density and treated with 10 nM 4-OHT for up to 10 days. Cells were harvested and stained with crystal violet 6 h after seeding (represents control time point “0 days”) and 2, 4, 6, 8, and 10 days after starting treatment with 4-OHT. As shown in **Figure 4E and F**, Cre-induced *Lin9* deletion upon 4-OHT treatment strongly impaired the proliferation of KPL1 and KPL2 cells, whereas 4-OHT treatment did not affect the proliferation of control KP1 and KP2 cells harboring wild-type *Lin9* alleles.

Immunofluorescent staining of tubulin and counterstaining of nuclei with Hoechst in KPL cells treated with 10 nM 4-OHT for 3 or 6 days to induce *Lin9* deletion revealed several cellular abnormalities indicative of cytokinesis failure (**Figure 5A, C, D**). Almost 100% of KPL1 and KPL2 cells were mononucleated without 4-OHT treatment, whereas the number of mononucleated cells strongly decreased to approx. 60% upon treatment with 4-OHT for 3 days (**Figure 5C**). About 40% of KPL cells became either binucleated or mega-multilobed when treated with 10 nM 4-OHT for 3 days. The number of cells with nuclear abnormalities even increased to 63% (KPL1) and 54% (KPL2) when KPL cells were treated with 10 nM 4-OHT for 6 days in total. Importantly, these effects can be specifically assigned to the loss of *Lin9*, since the 4-OHT treatment of control KP cells did not alter the phenotype of KP cells, thereby excluding Cre-mediated unspecific effects (**Figure 5B-D**). Together, these findings confirm that the MuvB core subunit LIN9 is essential for the proliferation and proper progress through mitosis and cytokinesis of lung cancer cells.

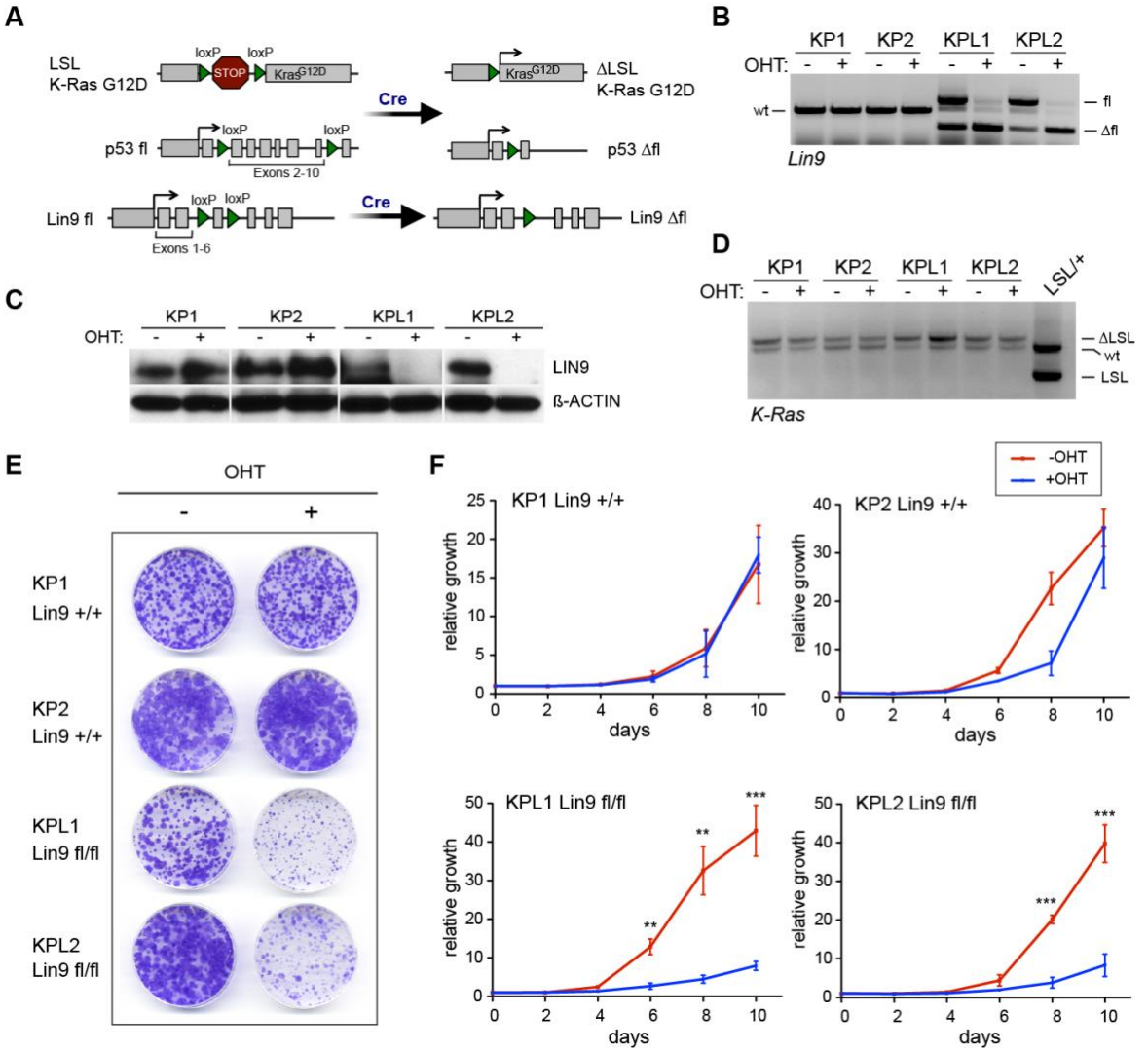

Figure 4: Proliferation defects in KPL cells upon the loss of LIN9.
(**A**) Scheme of the conditional activatable allele of oncogenic *LSL K-Ras G12D* and conditional loss-of-function alleles of *p53* (*p53fl*) and *Lin9* (*Lin9fl*). (**B-D**) KP cells (established from dissected lung tumors of *K-Ras*$^{LSL\text{-}G12D/+}$*; p53*$^{fl/fl}$*; Lin9*$^{+/+}$ mice) and KPL cells (from dissected lung tumors of *K-Ras*$^{LSL\text{-}G12D/+}$*; p53*$^{fl/fl}$*; Lin9*$^{fl/fl}$ mice) stably transfected with retroviral 4-OHT-inducible CreER^{T2} recombinase were left untreated or treated with 10 nM 4-OHT for 3 days. (**B**) Genomic PCR to verify the *Lin*9 allele status; wt, wild-type *Lin9* allele; fl, non-recombined *Lin9* allele; Δfl, recombined *Lin9* allele. (**C**) Analysis of LIN9 protein levels by immunoprecipitation (IP) followed by immunoblotting. 2% of the protein amount used for the IP was taken to determine ß-ACTIN levels as a loading control. (**D**) Genomic PCR of *K-Ras*. LSL, non-recombined *K-Ras*^{G12D} allele; ΔLSL, recombined *K-Ras*^{G12D} allele; wt, wild-type *K-Ras*^{G12D} allele. *K-Ras* PCR of genomic DNA isolated from the tail of a *K-Ras*$^{LSL\text{-}G12D/+}$ mouse was used as a control. (**E,F**) KP and KPL cells were seeded at low density and left untreated or treated with 10 nM 4-OHT for 10 days. Cells were fixed and stained with crystal violet. (**E**) One representative example. (**F**) Quantification of crystal violet staining. Means of three replicates are shown. Error bars represent SD. Statistics was done using the Student's t test, two-tailed; $^{**}P \leq 0.01$; $^{***}P \leq 0.001$

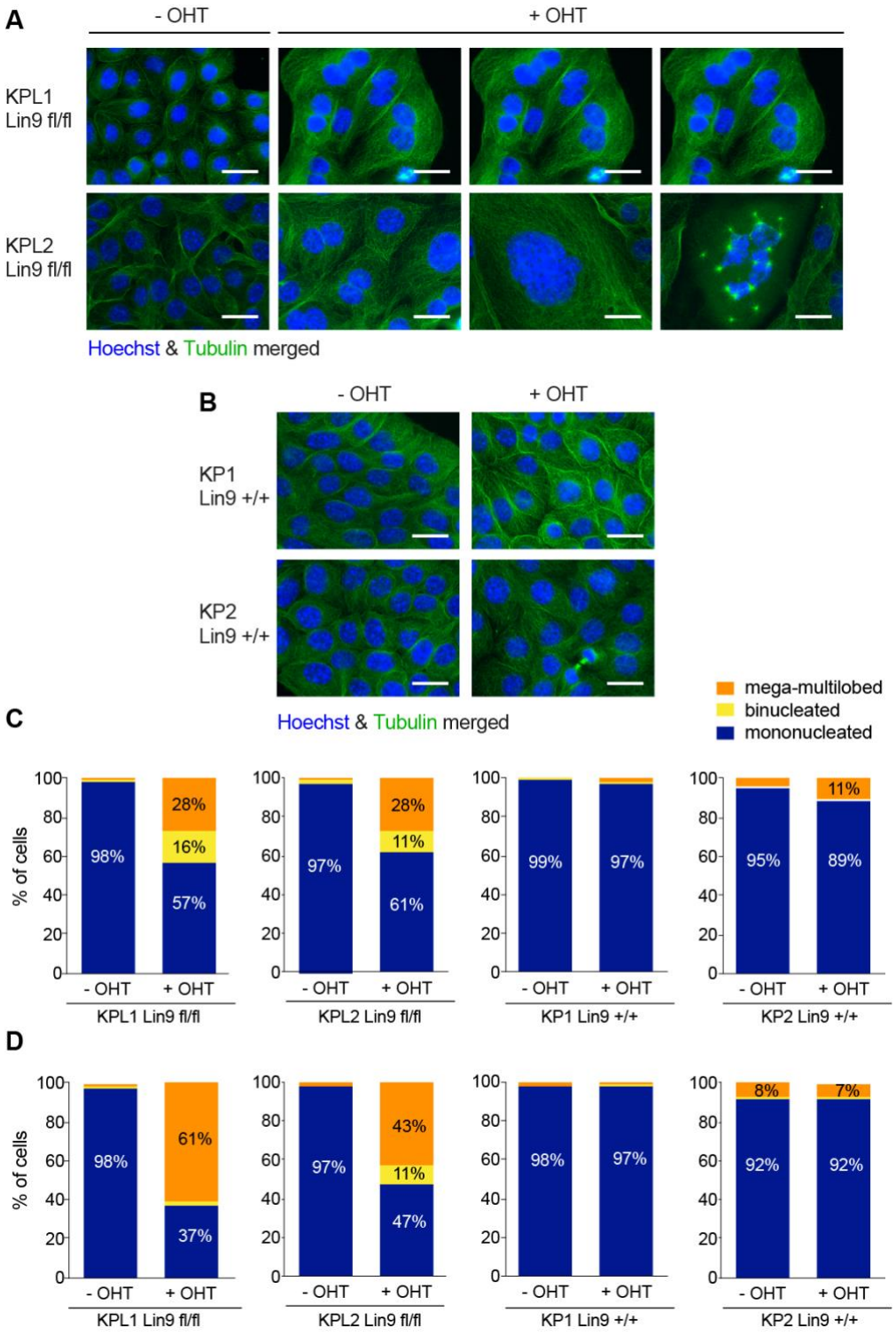

Figure 5: Loss of LIN9 in KPL cells results in several nuclear abnormalities.
(**A-D**) KPL and KP cells were treated with 10 nM 4-OHT for 3 days (**A-C**) or 6 days (**D**). Cells were fixed and stained with a Tubulin-specific antibody (green). Nuclei were counterstained with Hoechst 33548 (blue). (**A**) Representative examples of immunofluorescence stainings of KPL1 and KPL2 cells. Scale bars: 25 µm. (**B**) Representative examples of immunofluorescence stainings of control KP1 and KP2 cells. Scale bars: 25 µm. (**C-D**) Quantification of mitotic defects in KPL and KP cells treated with 10 nM 4-OHT for 3 days (**C**) or 6 days (**D**). Per condition, 500-800 cells were counted.

3.2 LIN9-dependent genes overlap with several signatures of YAP-regulated genes

To identify the MMB-dependent transcriptome in lung adenocarcinoma-derived cells and to analyze the cause of the *Lin9* deletion phenotype at the transcriptional level, RNA was isolated from KPL2 cells incubated with or without 10 nM 4-OHT for 4 days to delete *Lin9*. cDNA libraries were generated and subjected to next-generation sequencing. This revealed the identification of 795 genes, which were differentially expressed between control (-OHT) and *Lin9*-deleted (+OHT) cells (**Figure 6A**). Of these 795 genes, 323 genes were upregulated in *Lin9*-deleted cells, indicating that these genes are normally repressed by LIN9. However, with 472 genes, the majority of genes were downregulated upon *Lin9* deletion and thus identified as genes generally activated by LIN9.

To analyze which of these regulated genes are direct targets of MMB through promoter binding, genome-wide binding analyses were performed. KPL2 cells treated without or with 10 nM 4-OHT for 3 days were used for ChIP with a LIN9-specific antibody followed by next-generation sequencing (ChIP-seq). Intersecting RNA-seq with ChIP-seq data revealed that LIN9 occupancy at promoters significantly correlates with gene regulation as indicated by a Pearson's correlation coefficient *r* of -0.94 and a *P*-value smaller than 0.0001 (**Figure 6B**). To be more specific, LIN9 was enriched at promoters of genes whose expression was decreased upon 4-OHT-induced *Lin9* deletion, indicating that these genes are normally activated by LIN9. Furthermore, gene ontology (GO)-term analysis showed that the 1000 strongest LIN9-activated genes are mainly involved in cell cycle regulation and mitosis (**Figure 6C**). In contrast, the 1000 strongest LIN9-repressed genes have other functions not related to cell cycle or mitosis such as ion or transmembrane transport (**Figure 6D**). The strong downregulation of genes involved in mitosis and cytokinesis might explain the strong mitotic defects that have been observed as a result of *Lin9* deletion (**Figure 5**). Moreover, the much higher number of LIN9-activated (472) than -repressed genes (323) and the much stronger binding of LIN9 to the promoters of activated genes than to the promoters of repressed genes indicate that in KPL2 cells the MuvB core mainly exists as the activator MMB complex bound to B-MYB (**Figure 6A, 6B**).

For further analysis, Gene set enrichment analysis (GSEA) of differentially expressed genes between untreated and 4-OHT-treated *Lin9*-deleted KPL2 cells was performed with the C6 oncogenic gene sets from the Molecular Signatures Database (MSigDB) of the Broad Institute. C6 contains 189 gene sets of pathways, which are often dis-regulated in cancer (Subramanian et al. 2005; Liberzon et al. 2011).

Unexpectedly, this GSEA analysis revealed that LIN9-dependent genes are significantly enriched for an evolutionary conserved signature of genes regulated by the Hippo pathway effector YAP, which was described by Cordenonsi et al. (2011) (**Figure 7A, 7B**).

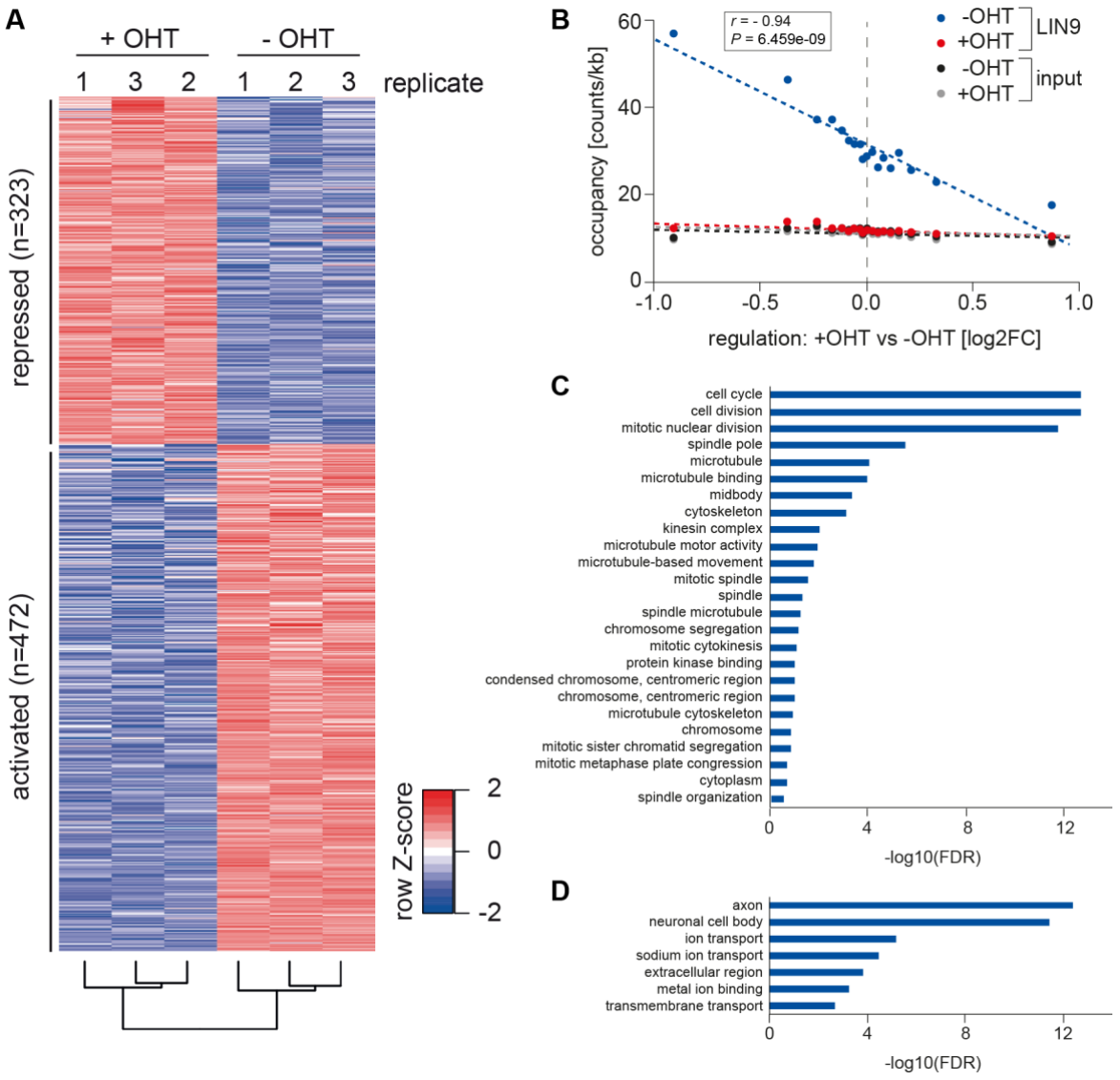

Figure 6: Mitosis- and cell cycle-related genes are directly regulated by MMB.
(**A**) RNA of three replicates was isolated from untreated KPL2 and KPL2 cells treated with 10 nM 4-OHT for 4 days and subjected to RNA-seq. Heat map documenting gene expression changes after 4-OHT-induced knockout of *Lin9*. Median-centered expression of significantly regulated genes (FDR q-value <0.01) was used for hierarchical clustering of samples. Blue represents low expression, red high expression. (**B**) KPL2 cells treated with 10 nM 4-OHT for 3 days were used for ChIP-seq to identify genome-wide LIN9 binding sites. Bin plot showing correlation of gene expression changes and LIN9-binding at transcriptional start sites (TSS) after 4-OHT-induced *Lin9*-deletion. 10,981 genes were sorted based on log2FC and binned in 18 equally-sized bins (600 genes per bin). Dashed lines show regressions using linear models with *r,* Pearson's correlation coefficient and the corresponding *P*-value determined using a two-tailed Student's *t*-Test. (**C**) Gene ontology analysis of 1000 strongest LIN9-activated genes. Enriched GO terms with a false discovery rate (FDR) <0.25 are shown. (**D**) Gene ontology analysis of 1000 strongest LIN9-repressed genes. Enriched GO terms with FDR<0.25 are shown.

Notably, out of 56 conserved YAP target genes, 17 (30%) genes were found to be also activated by LIN9 in KPL2 cells including several well-described MMB target genes such as *Cenpf, Cdc20*, and *Top2a* (**Figure 7B**). Further GSEA analyses with the C2 curated gene sets from MSigDB spiked with several previously published YAP-regulated gene sets showed the enrichment of several mitosis, G2/M, and cell cycle signatures as expected but also confirmed the overlap between LIN9-regulated and YAP-regulated genes (**Figure 7C, 7D**). Several well-characterized signatures of YAP-induced genes described by Zhao et al. (2008), Zhang et al. (2009), Cordenonsi et al. (2011), Dupont et al. (2011), and Zanconato et al. (2015) were significantly downregulated upon *Lin9*-deletion as indicated by the negative enrichment score (NES) (**Figure 7C, 7D**).

To validate the results obtained from RNA-seq, RNA was isolated from KPL2 cells treated with 10 nM 4-OHT for 4 days. qPCR experiments showed that the expression of multiple YAP target genes with known functions in cell cycle regulation and mitosis is dependent on LIN9 because their expression was significantly decreased when deleting *Lin9* (**Figure 8A**). Importantly, the expression of YAP target genes that do not have a direct function in mitosis such as *Axl* or *Cyr61* was not reduced by *Lin9* deletion.

RNA interference-mediated knockdown of *Yap* and *Taz* using specific siRNAs resulted in a strong reduction in protein levels of YAP and TAZ in KPL2 cells (**Figure 8B**). Expression analyses by qPCR confirmed that mitotic genes from the Cordenonsi signature are dependent on YAP and TAZ because their expression significantly decreased upon depletion of *Yap/Taz* (**Figure** 8**C**) (Cordenonsi et al. 2011). Additionally, the level of several genes that are not part of the Cordenonsi signature but are known direct MMB target genes such as *Aspm* or *Nusap1* also significantly dropped when *Yap/Taz* were depleted. Non-mitotic well-known YAP target genes such as *Axl* and *Cyr61* were also reduced upon Yap/Taz depletion (Zanconato et al. 2015).

To exclude that the regulation of common genes by YAP and MMB is restricted to murine cells, human A549 lung cancer cells were treated with the small molecule verteporfin, which disrupts the interaction between YAP and its DNA-binding partner TEAD, thereby inhibiting YAP-dependent gene expression (Liu-Chittenden et al. 2012; Zhang et al. 2015a). Verteporfin treatment significantly decreased the expression of the well-known YAP-target gene *CTGF* and of MMB target genes (e.g., *KIF23* and *NUSAP1*), indicating that the regulation of common genes by YAP and MMB is not species-specific and occurs in both, mouse and human (**Figure 8D**). Although *Lin9* expression was neither influenced by *Yap/Taz* depletion in KPL2 cells nor by verteporfin treatment of A549 cells, the expression of *Mybl2/MYBL2*, the gene encoding for B-MYB, was significantly reduced under both experimental conditions (**Figure 8C, 8D**).

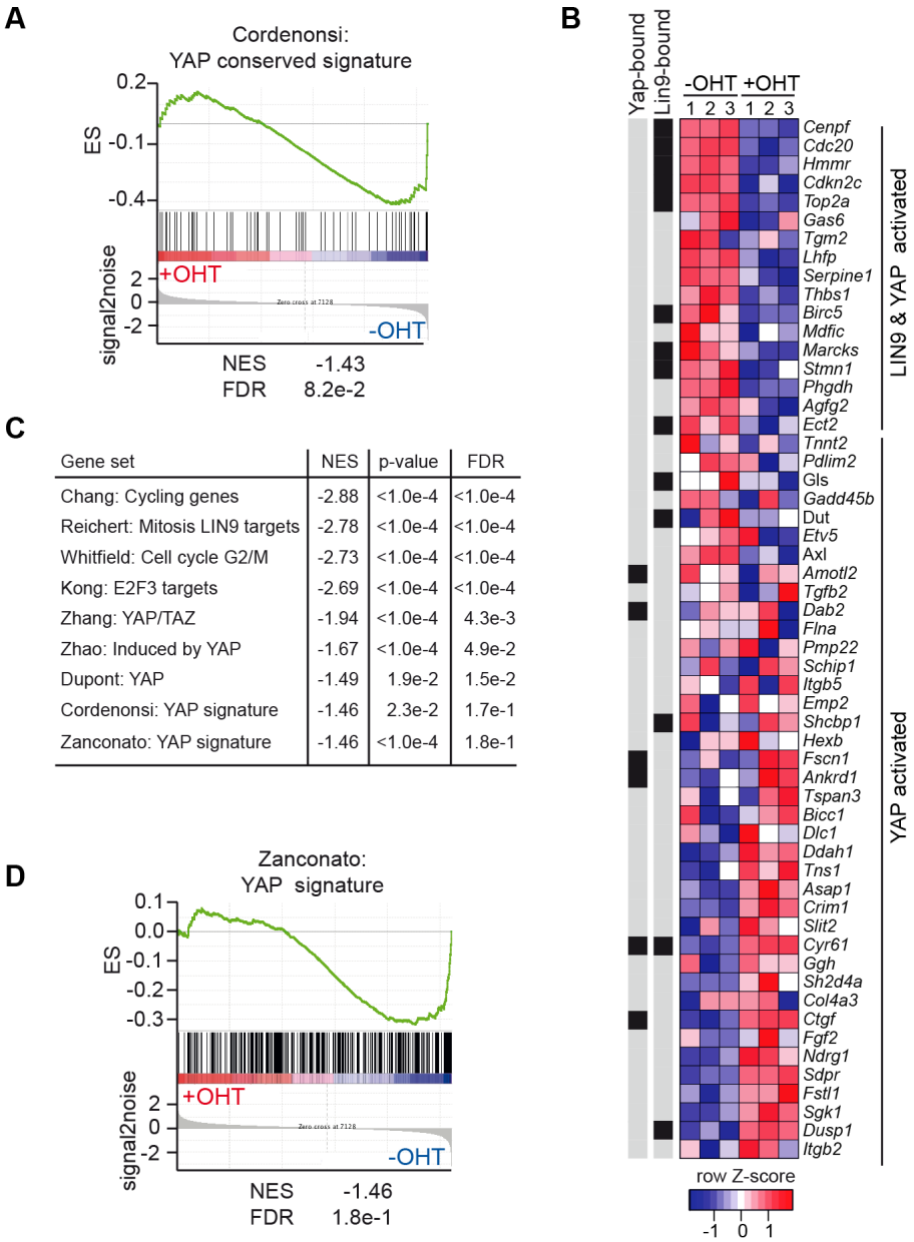

Figure 7: LIN9-dependent genes overlap with several YAP-regulated gene signatures.
(**A**) GSEA analysis of RNA-seq data from **Figure 6** was done using the C6 oncogenic gene sets from MSigDB. Enrichment plot of the YAP conserved signature described by Cordenonsi et al. (2011) is shown. NES, normalized enrichment score; FDR, false discovery rate. (**B**) Heat map showing the expression of YAP-conserved Cordenonsi signature genes in control (-OHT) and *Lin9*-deleted (+OHT) cells. Blue represents low and red represents high expression. Black boxes to the left of the gene list indicate binding of YAP or LIN9 in the promoter (-/+ 1 kb of TSS) of the corresponding gene as analyzed by ChIP-seq (see chapter **3.5**). (**C**) GSEA analysis was performed with the C2 curated gene sets from MSigDB spiked with several previously published YAP-regulated gene sets. Gene sets of YAP-induced genes are repressed upon 4-OHT-induced *Lin9*-deletion as indicated by the negative NES. (**D**) Enrichment plot from GSEA analyses shown in (**C**) of a YAP signature described by Zanconato et al. (2015). For detailed information about the GSEA method see Subramanian et al. (2005).

This decreased expression of *Mybl2* could contribute to the reduced expression of mitotic genes upon YAP inhibition and suggests that *Mybl2* itself could be a target gene of YAP. Collectively, these findings showed that YAP and MMB co-regulate a set of genes whose protein products fulfil important functions during mitosis and thus revealed a so far unknown overlap between the MMB complex and the Hippo pathway effector YAP.

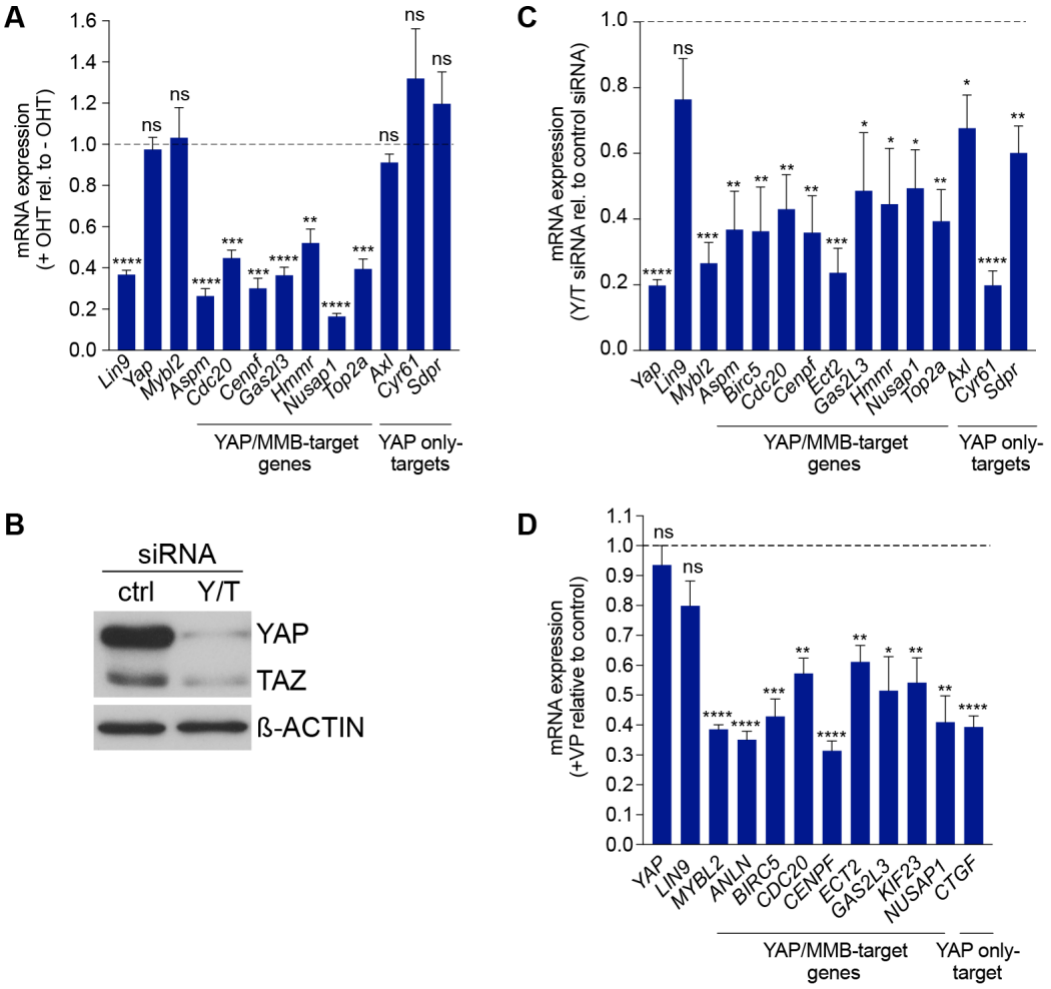

Figure 8: MMB and YAP regulate an overlapping set of genes with functions in mitosis.
(**A**) KPL2 cells were treated with 10 nM 4-OHT for 4 days. mRNA expression in 4-OHT treated *Lin9*-deleted cells relative to the mRNA expression in untreated control cells was analyzed by qPCR. (**B**) Protein lysates of KPL2 cells transfected with a control siRNA (siCtrl) or a mix of siRNAs directed at *Yap* and *Taz* (siY/T) were generated 3 days after siRNA transfection. Immunoblots of YAP/TAZ and ß-ACTIN as a loading control are shown. (**C**) KPL2 cells were transfected with siCtrl or siY/T and incubated for 2 days. qPCR was done to determine the mRNA expression of Y/T-depleted cells relative to mRNA expression of control siRNA-transfected cells. (**D**) Human lung cancer A549 cells were either treated with DMSO (control) or 7.5 µM verteporfin (VP) for 24 h. mRNA expression in VP-treated cells was analyzed relative to the expression in control DMSO-treated cells. *Hprt* (**A, C**) or *TBP* (**D**) expression was used for normalization. Means of three independent experiments, each measured in technical replicates, are depicted. Error bars represent standard error of the mean (SEM). Statistical significance was assessed using the Student's *t*-test, two-tailed. $^{*}P \leq 0.05$, $^{**}P \leq 0.01$; $^{***}P \leq 0.001$; $^{****}P \leq 0.0001$; ns, not significant, $P > 0.05$. (**A, C, D**) Experiments performed by Eva Rühl (B.Sc. student).

3.3 *Lin9* deletion does not alter protein levels and nuclear localization of YAP

In the canonical Hippo signaling, YAP activity and hence gene transcription of YAP-dependent genes is regulated by LATS1/2 kinases through affecting the protein stability and subcellular localization of YAP (Zhao et al. 2007; Yu et al. 2015). Thus, one possibility how LIN9 influences YAP-dependent gene expression might be by affecting the protein stability or subcellular localization of YAP e.g., by influencing the phosphorylation of YAP by upstream kinases.

However, immunoblotting of control and *Lin9*-deleted KPL2 cells showed no difference in YAP protein levels cells (**Figure 9A**). This is in line with the mRNA expression analysis in **Figure 8A** showing that *Lin9* deletion has no influence on *Yap* expression at mRNA level.

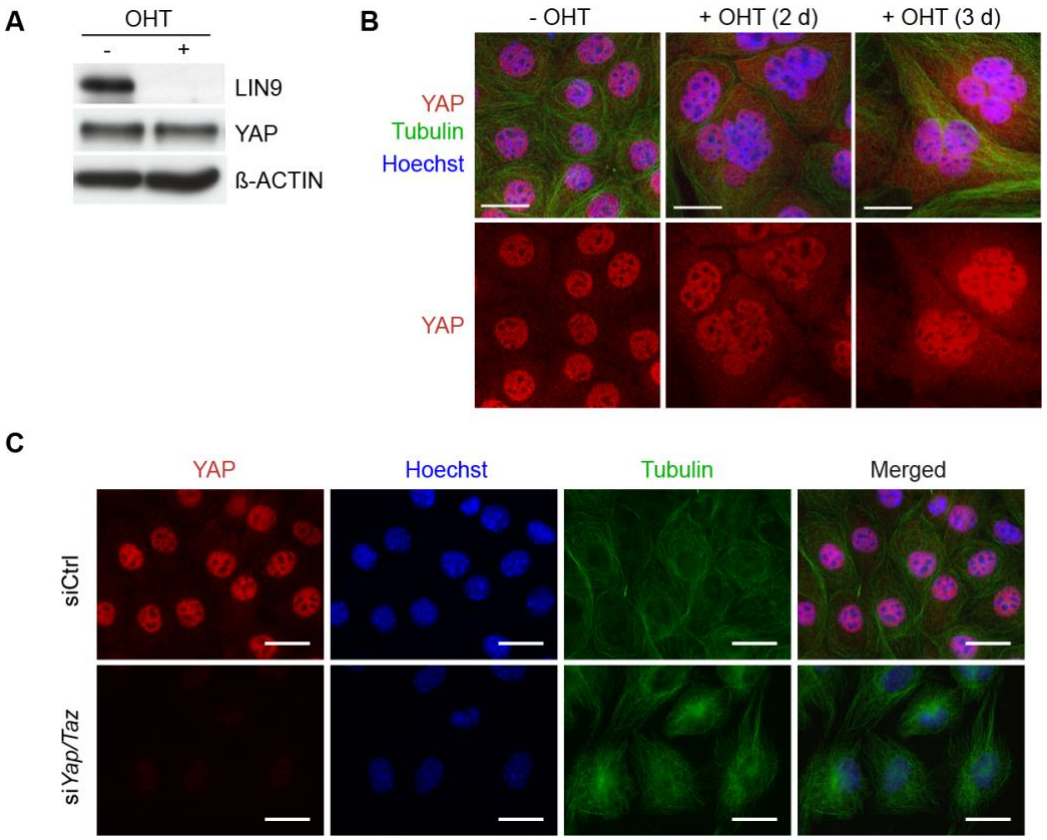

Figure 9: Protein levels and nuclear localization of YAP are not affected by *Lin9* deletion.
(**A**) KPL2 cells were treated with 10 nM 4-OHT for 3 days to induce Cre-mediated *Lin9* deletion. Whole cell lysates were used for immunoprecipitation followed by immunoblotting of LIN9. Input samples were used for immunoblotting of YAP and ß-ACTIN (loading control). (**B**) KPL2 cells were treated with 10 nM 4-OHT for 2 or 3 days. Cells were fixed and immunostained with anti-Tubulin (Green) and anti-YAP (red) antibodies. Nuclei were counterstained with Hoechst (blue). Scale bars: 25 µm. (**C**) Test for the specificity of the YAP antibody used in (**B**). KPL2 cells were transfected with control siRNA (siCtrl) or a mix of *Yap* and *Taz*-directed siRNAs (si*Yap/Taz*). Two days later, cells were fixed and stained with anti-Tubulin (green) and anti-YAP (red) antibodies. Nuclei were stained using Hoechst (blue). Scale bars: 25 µm. Cell seeding, transfection, and IF-staining (**B-C**) were performed by Ashley Curran.

Additionally, immunofluorescent staining of YAP revealed the presence of similar levels of nuclear-located YAP in both control and *Lin9*-deleted KPL2 cells (**Figure 9B**). Specificity of the YAP antibody was verified by the loss of immunofluorescent YAP staining in *Yap/Taz*-depleted cells (**Figure 9C**). Together these results confirm that the effects of *Lin9* deletion on YAP-dependent gene expression do not result from degradation or nuclear exclusion of YAP.

3.4 Overexpression of YAP can partially rescue the phenotype of *Lin9*-deleted cells

As both MMB and YAP regulate similar genes important for mitosis, the question arose whether YAP overexpression might be able to prevent *Lin9*-deleted KPL cells from developing mitotic defects and becoming nuclear abnormal.

To address this question, KP and KPL cells either untreated or treated with 10 nM 4-OHT for 24 h to delete *Lin9* were transfected with an empty control vector (ev), a FLAG-tagged wild-type YAP (YAPwt) or a FLAG-tagged constitutively active YAP5SA expressing construct. In the YAP5SA construct, five serine residues in the HXRXXS consensus motif for LATS1/2 phosphorylation are mutated to alanine. These mutations make YAP5SA resistant to the phosphorylation-mediated inhibition by LATS1/2 kinases and thus prevent the nuclear exclusion and degradation of YAP (Zhao et al. 2007).

Both YAPwt and YAP5SA were expressed in control and 4-OHT treated KPL2 cells at equal levels as verified by immunoblotting (**Figure 10C**). Immunofluorescent staining revealed an increase of mega-multilobed cells in empty vector transfected KPL1 and KPL2 cells from less than 2% in untreated cells to about 60-70% in 4-OHT-treated *Lin9*-deleted cells (**Figure 10A, 10B**). Notably, in KPL1 and KPL2 cells transfected with either YAPwt or YAP5SA the percentage of nuclear abnormal cells upon 4-OHT treatment was reduced by almost 50% on average when compared to empty vector transfected cells. Upon loss of *Lin9* only 24% of KPL1 cells remained mononucleated and 71% KPL1 cells became multi-megalobed. However, the expression of YAPwt or YAP5SA significantly increased the number of mononucleated *Lin9*-deleted cells to 51-56% and reduced the number of mega-multilobed cells to 37-42%. Conversely, neither the 4-OHT treatment nor the overexpression of YAP constructs changed the mononucleated phenotype of wild-type *Lin9* expressing KP1 and KP2 cells (**Figure 10B**). Importantly, YAP overexpression did not interfere with the Cre-mediated deletion of the second remaining *Lin9* allele in KPL2 cells (**Figure 10D**). Together, these findings indicate that YAP overexpression can partially rescue the *Lin9*-deletion phenotype.

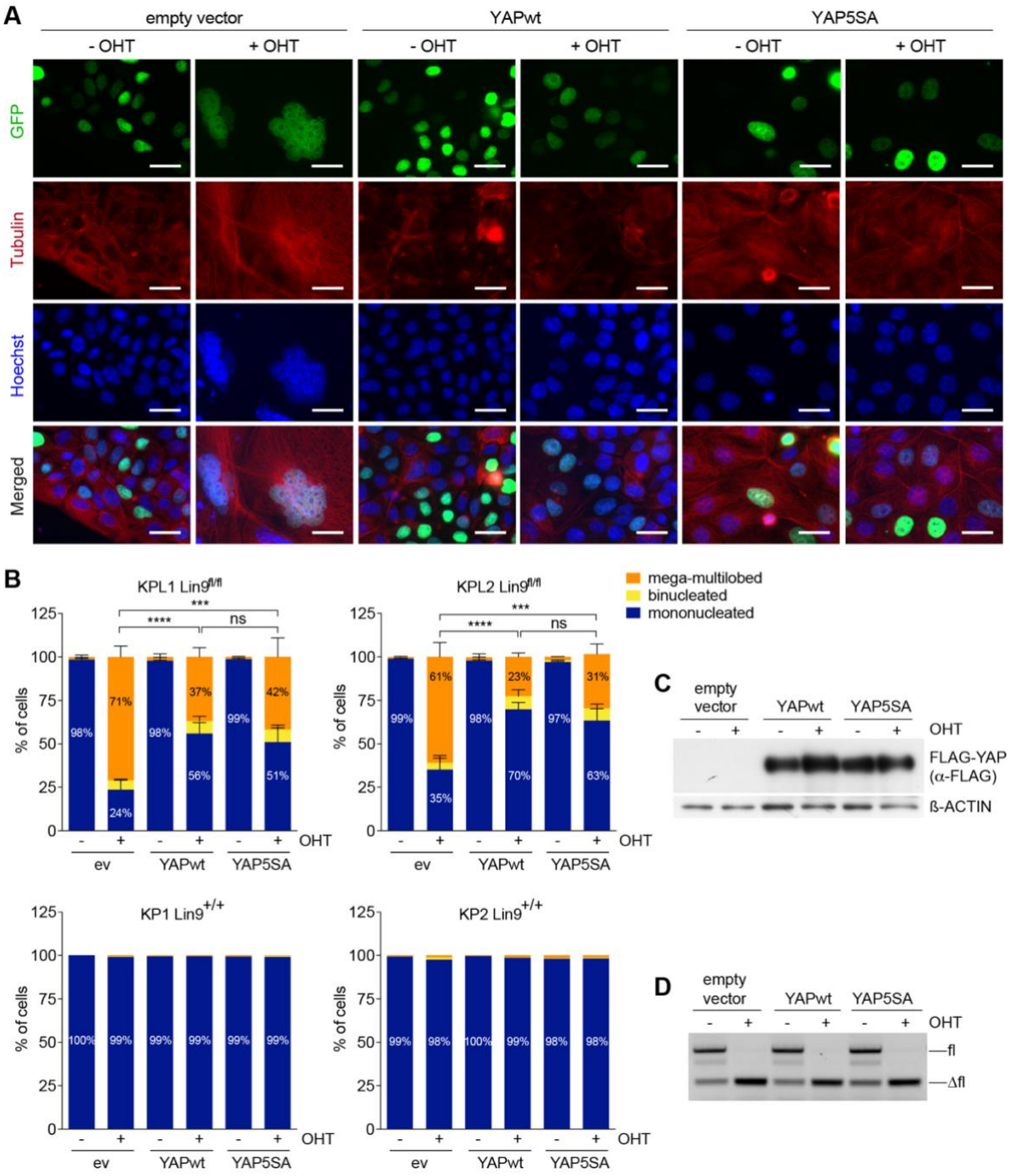

Figure 10: YAP can partially rescue the phenotype of LIN9 loss in KPL2 cells.
(**A-D**) KP and KPL cells untreated or treated with 10 nM 4-OHT for 24 h were transfected with an empty control vector (ev), FLAG-tagged wild-type YAP (YAPwt), or FLAG-tagged constitutively active YAP (YAP5SA) alongside with a GFP expression vector (green). 48 h after transfection, cells were harvested. (**A**) KP and KPL cells were fixed and immunostained using a Tubulin-specific antibody (red). Nuclei were counterstained using Hoechst (blue). Green: GFP. Scale bars: 25 µm. Representative microscopic images of KPL1 cells are shown. (**B**) Quantification of mono-, binucleated, and mega-multilobed cells described in (**A**). Bar diagram shows one experiment of KP1 and KP2 cells. Results of KPL1 and KPL2 cells are represented as the mean and SD of 3 independent experiments. Per experiment and per condition >500 GFP-positive cells were counted. Scale bars: 25 µm. Statistical significance ($^{***}P \leq 0.001$; $^{****}P \leq 0.0001$; ns, not significant, $P > 0.05$.) for differences in the amount of mononucleated cells was assessed by one-way ANOVA with Tukey's post-test. (**C**) Immunoblots of KPL2 cells using an anti-FLAG antibody to verify equal YAP expression levels. ß-ACTIN was used as a loading control. (**D**) Genomic DNA of KPL2 cells was isolated and used for PCR to show the 4-OHT-induced deletion of the remaining *Lin9* allele from fl to Δfl.

3.5 YAP-regulated genes are direct targets of MMB

To analyze whether LIN9 and YAP have overlapping binding sites and whether the loss of *Lin9* affects the genome-wide binding of YAP, control and 4-OHT-induced *Lin9*-deleted KPL2 lung adenocarcinoma-derived cells were used for ChIP-seq of YAP and LIN9. Moreover, in order to identify whether LIN9 and YAP peaks are located at promoter or enhancer sites, ChIP-seq was performed with antibodies specific for histone 3 (H3), lysine 4 (K4), mono- (me1) (H3K4me1) or trimethylation (me3) (H3K4me3) and H3, lysine 27 (K27), acetylation (H3K27ac).

Whereas promoters are located immediately upstream (at the 5' end) of the TSS, enhancers can be located upstream, downstream, or even within the target gene or another neighboring gene. Enhancers can be located only a few or even thousands of kilo base pairs (kb) away from the TSS of a gene and can activate gene expression over long distances by interacting with promoters via chromatin looping (Heintzman et al. 2007; Stadhouders et al. 2012; Calo and Wysocka 2013). Therefore, enhancers cannot be detected as easily as promoters by their distance to the TSS. Enhancers further differ from promoters in the methylation status of H3K4. Whereas promoters are known to have high levels of H3K4me3, enhancers are associated with high levels of H3K4me1 and low levels of H3K4me3. Further, H3K27 acetylation of both promoters and enhancers is linked to increased activity and H3K27ac is widely used to distinguish between active (high H3K27ac levels) and inactive/poised (low H3K27ac levels) enhancer elements (Creyghton et al. 2010; Calo and Wysocka 2013).

First, to identify the genome-wide distribution of LIN9 and YAP binding in KPL2 cells, the localization of all LIN9 (3780) and all YAP (1431) peaks was analyzed relative to the TSS of annotated genes (**Figure 11A**). This analysis revealed that YAP and LIN9 bind to different genomic sites. Only 27% of LIN9 binding sites were found in gene bodies or between genes (intergenic), whereas with 76% the majority of YAP peaks were located either intergenic or in gene bodies. With 72% of LIN9 peaks being located in promoters or immediately downstream of the TSS, LIN9 predominantly binds close to the transcription start sites (within $\pm$ 1 kb of the TSS).

To analyze the binding of YAP and LIN9 to promoter, enhancer, and super-enhancer sites, ChIP-seq of histone modifications in KPL2 cells was used to define those regions (**Figure 11B**). Promoters were defined by the presence of H3K4me3 within a distance of $\pm$ 1 kb to the TSS, the presence of H3K27ac, and the absence of H3K4me1. In contrast, enhancers were defined by the presence of H3K4me1 outside a distance of $\pm$ 1 kb to the TSS, the presence of H3K27ac, and the absence of H3K4me3.

Finally, to predict super-enhancers, a term which describes several enhancers in close genomic proximity to each other, the aforementioned enhancer definition together with the H3K27ac distribution and the Rank Ordering of Super-Enhancers (ROSE) algorithm developed by the laboratory of Richard A. Young were used (Hnisz et al. 2013; Whyte et al. 2013; Pott and Lieb 2015). Unlike LIN9 binding sites, which with more than 50% were mostly localized in promoter regions, only 11% of YAP binding sites were found directly in promoters. Instead, the majority of YAP peaks (approx. 30%) were located either in super-enhancer or enhancer regions (**Figure 11B**).

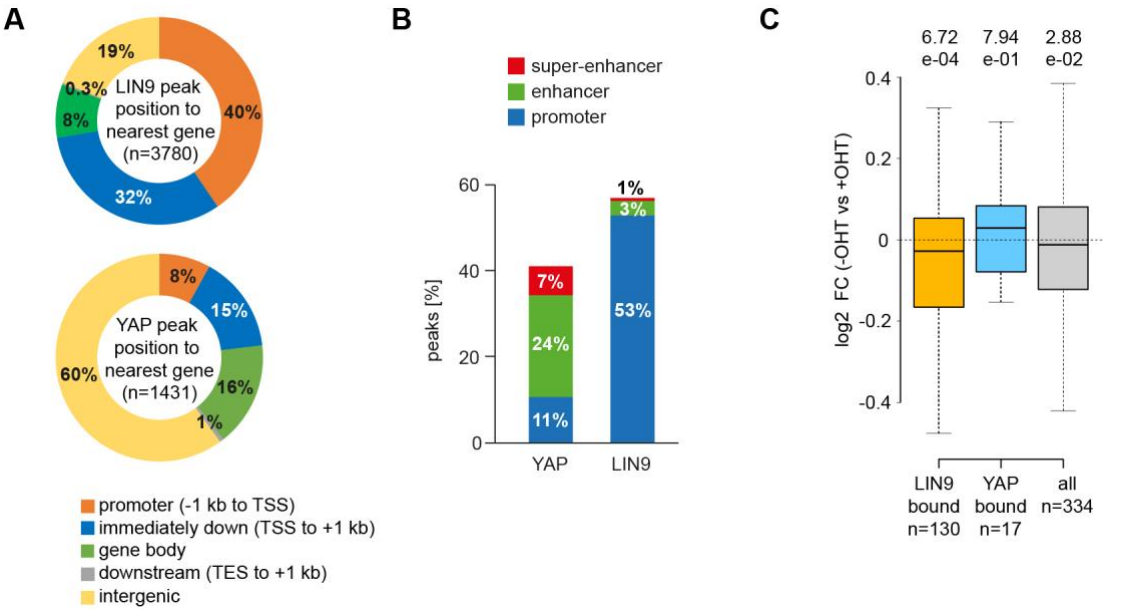

Figure 11: LIN9 promoter binding is needed for the regulation of YAP target genes.
(**A-C**) KPL2 cells treated without or with 10 nM 4-OHT for 3 days were used for ChIP-seq using LIN9- and YAP-specific antibodies. Histone modifications-specific antibodies against H3K4me1, H3K4me3, and H3K27ac were used to identify promoter and enhancer regions. (**A**) Localization of LIN9 (top) and YAP (bottom) peaks in KPL2 cells relative to the TSS of annotated genes. TSS, transcription start site; TES, transcription end site. (**B**) Percentage of YAP or LIN9 peaks overlapping with open/active promoters, enhancers, and super-enhancers defined by ChIP-seq of histone modifications. Promoters are defined by the presence of both H3K4me3 (within a distance of ± 1 kb to TSS) and H3K27ac and the absence of H3K4me1. Enhancers are defined by the presence of both H3K4me1 (outside a distance of ± 1 kb to TSS) and H3K27ac and the absence of H3K4me3. Super-enhancers are predicted by using the aforementioned enhancer definition, the H3K27ac distribution, and the algorithm ROSE developed by the laboratory of Richard A. Young (Loven et al. 2013; Whyte et al. 2013). (**C**) Box plot showing the log2 fold changes (FC) in expression of YAP target genes described by Zanconato et al. (2015) between control and 4-OHT-treated KPL2 cells separated into all genes, genes bound by LIN9, and genes bound by YAP in a distance of ± 2 kb to TSS. Of 379 genes from this signature, 334 were present in the RNA-seq analysis. *P*-values were calculated with a two-tailed one-sample Wilcoxon signed-rank test with μ=0. Outliers not shown.

In a next step, heat maps were generated in which the enrichment of histone modifications, LIN9, and YAP sorted from the strongest to the weakest signal was depicted. Peaks were centered ± 2 kb on the summits of all LIN9 (**Figure 12A**) or YAP peaks (**Figure 12B**) found in the control untreated (- OHT) sample and clustered in the two groups "promoter" or "no promoter" depending on whether they are located within ± 2 kb (promoter) or not within ± 2 kb (no promoter) of the TSS.

The overall genome-wide binding of LIN9 was strongly reduced when cells were treated with 4-OHT, indicating the complete loss of LIN9 protein expression and verifying the specificity of the LIN9 antibody (**Figure 12A**). In line with the results shown in **Figure 11A**, more than 75% of LIN9 peaks were found within ± 2 kb of the TSS with a strong enrichment of both H3K4me3 and H3K27ac, whereas less than 25% of LIN9 peaks were located in regions further away than 2 kb up- or downstream of the TSS (**Figure 12A**). In contrast, only slightly more than 25% of YAP peaks were located within ± 2 kb of the TSS and almost 75% of YAP peaks were located in regions further away than ± 2 kb of the TSS, which came along with high levels of H3K4me1 and H3K27ac indicative for enhancer regions (**Figure 12B**). The global binding pattern of YAP within the genome and the distribution of YAP binding sites seemed to be unaffected by the loss of LIN9. However, a reduced binding of YAP upon loss of LIN9 could be observed, as indicated in the read density profiles depicted above the heat maps (**Figure 12B**).

To analyze the binding of LIN9 and YAP to genes regulated by YAP, a list of YAP-regulated genes described by Zanconato et al. (2015) was compared with ChIP-seq data for YAP and LIN9 and RNA-seq data upon *Lin9* deletion in KPL2 cells from this study.

Of 379 genes included in the Zanconato signature, only 334 genes were found in the RNA-seq data of KPL2 cells since for some genes either the conversion from human to mouse failed or they were not or only weakly expressed in KPL2 cells. The overlap demonstrated that out of 334 genes, 130 genes were bound by LIN9 at the promoter and, strikingly, were significantly downregulated upon 4-OHT-induced *Lin9* deletion as analyzed by RNA-seq (**Figure 11C, orange box**). Only 17 of the 334 YAP-regulated genes showed direct binding of YAP to promoters. This indicates that YAP regulates the majority of genes without promoter binding and instead, most likely by binding to distal enhancers. In contrast to the LIN9-bound YAP-regulated genes, direct YAP target genes are not regulated by LIN9 as their expression was not significantly changed upon *Lin9* deletion (**Figure 11C, blue box**). Genes with promoters bound by YAP included previously identified YAP target genes such as *Ctgf*, *Cyr61*, and *Amotl2* (Zhao et al. 2008). A genome browser track of the *Amotl2* gene locus illustrating YAP promoter binding is shown in **Figure 13A**.

These findings were confirmed by comparing the binding data for LIN9 and YAP in KPL2 cells with YAP-regulated genes included in the Cordenonsi signature (**Figure 7B;** black boxes on the left side of the gene list) (Cordenonsi et al. 2011). Notably, 9 out of 56 YAP-regulated genes in the Cordenonsi signature are direct targets of LIN9 but have no YAP peak at the promoter, these include, inter alia, *Cdc20*, *Top2a*, and *Cenpf* (**Figure 7B** and **Figure 13B-D**).

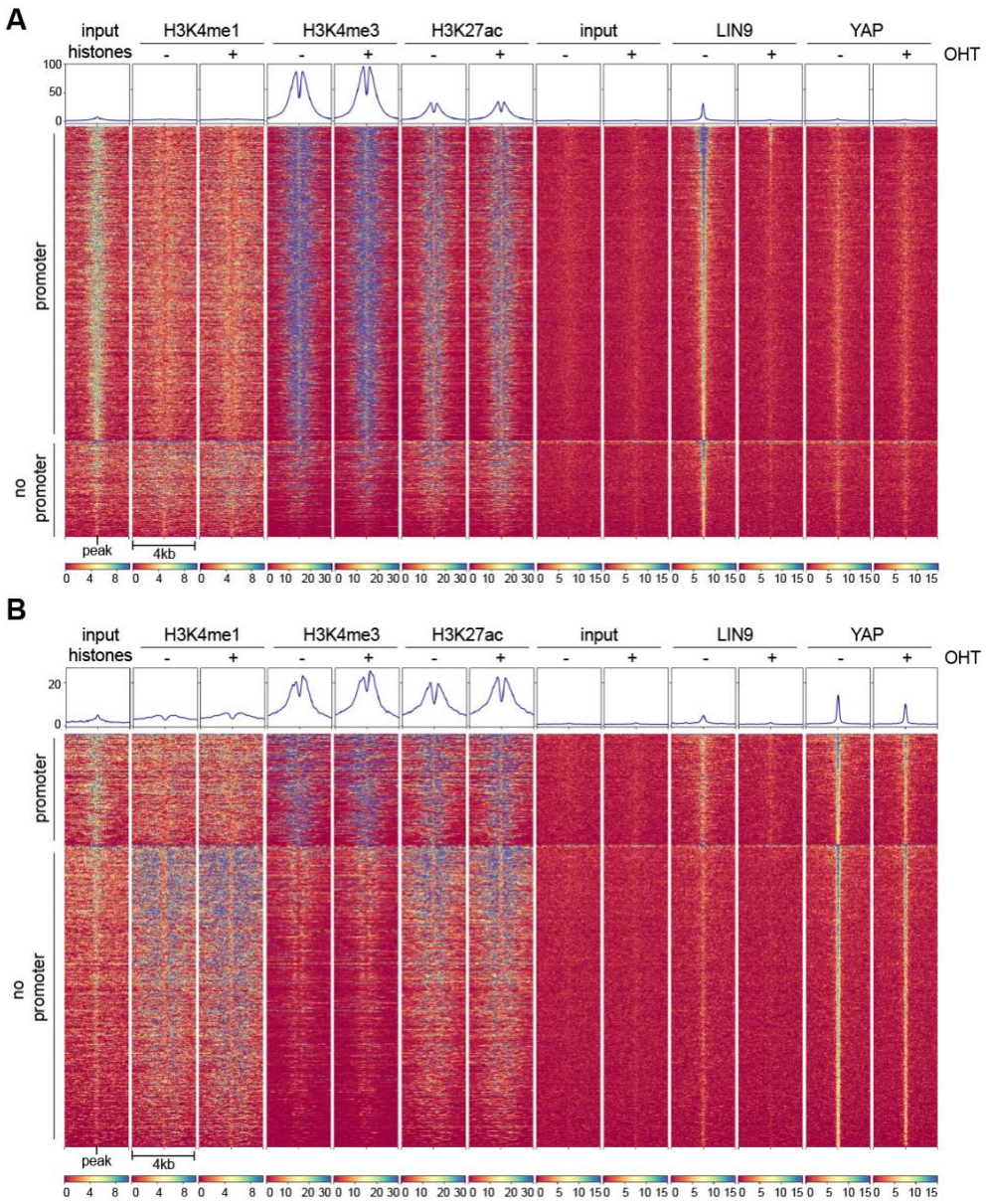

Figure 12: Little overlap between LIN9 and YAP chromatin binding in KPL2 cells.
(**A-B**) Untreated and 4-OHT-treated KPL2 cells were used for ChIP-seq as described in **Figure 11**. 1% of chromatin used for IP served as an input control. The merged and normalized input for ChIP-seq of the histone modifications H3K4me1, H3K4me3, and H3K27ac is shown on the left. Lane 8 and 9 represent inputs of untreated and 4-OHT-treated samples used for ChIP-seq of LIN9 and YAP. Heat maps show binding of the indicated proteins in promoter (within ± 2 kb of TSS) or no promoter (not within ± 2 kb of TSS) regions. Peaks are sorted from the strongest to the weakest signal in a window of ± 2 kb centered on the summit of all LIN9 (**A**) or YAP (**B**) peaks in the control sample (- OHT).

Collectively, ChIP-seq analysis revealed that LIN9 regulates gene expression directly through promoter binding, whereas YAP seems to regulate genes from a longer distance mainly by binding to intergenic- or gene body-located enhancers and super-enhancers. Furthermore, the comparison of YAP-regulated genes from previously published data with RNA-seq data upon *Lin9*-deletion and ChIP-seq data of YAP and LIN9 binding from this study demonstrated that only a few genes are directly regulated by YAP through promoter binding. Instead, the majority of YAP-regulated genes were directly bound by LIN9 at their promoters and their expression was dependent on LIN9.

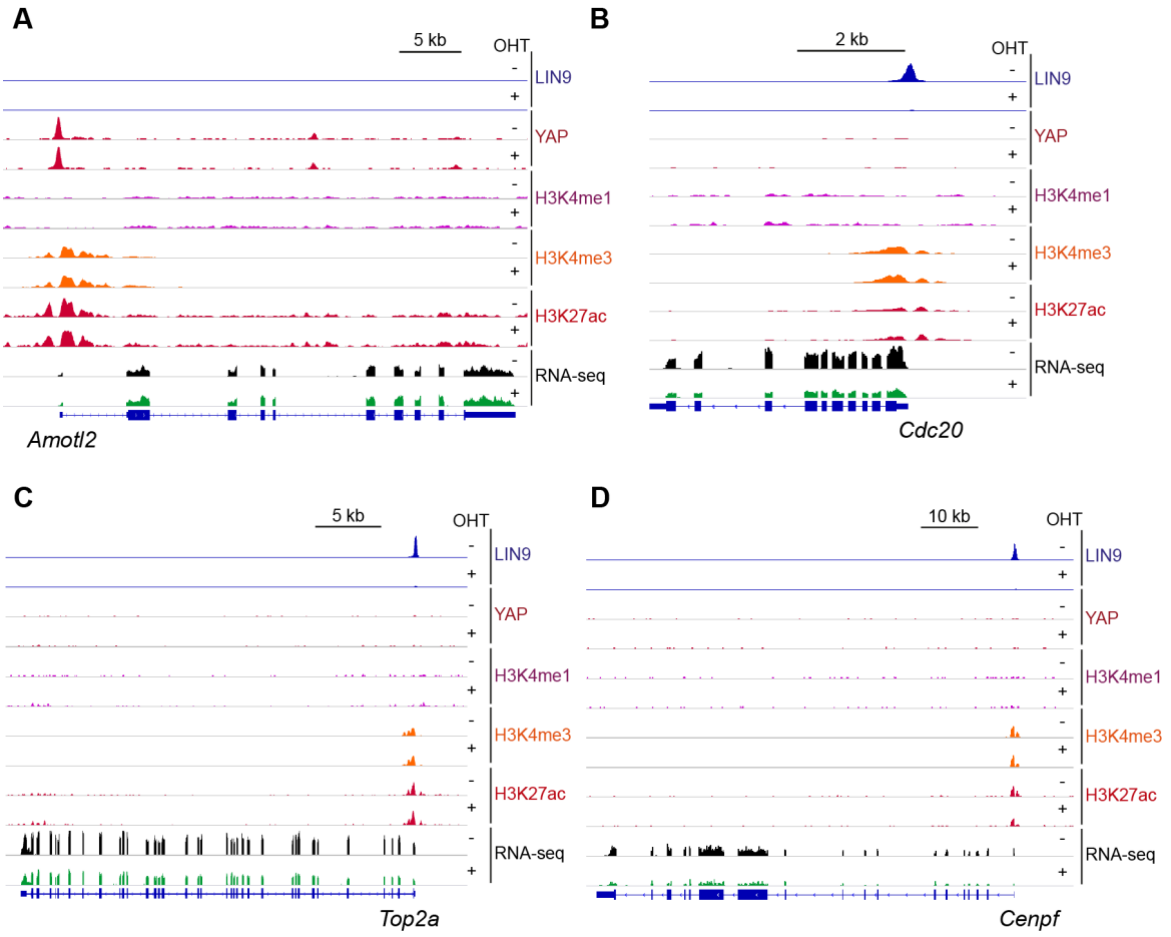

Figure 13: Genome browser tracks of murine *Amotl2*, *Cdc20*, *Top2a*, and *Cenpf* loci.
(**A-D**) Genome browser tracks of murine *Amotl2* (**A**), *Cdc20* (**B**), *Top2a* (**C**), and *Cenpf* (**D**) gene loci showing the binding of LIN9 and YAP as well as the enrichment of the histone modifications H3K4me1, H3K4me3, and H3K27ac as determined by ChIP-seq of untreated KPL2 cells or KPL2 cells treated with 10 nM 4-OHT to delete *Lin9*. Gene expression levels determined by RNA-seq are shown in black (- OHT) and green (+ OHT) below tracks of ChIP-seq data.

3.6 YAP activates the expression of mitotic MMB target genes in MCF10A cells

To analyze the mechanisms by which YAP and MMB co-regulate mitotic gene expression, untransformed human breast epithelial MCF10A cells stably expressing doxycycline (dox)-inducible constitutively active YAP5SA were used (von Eyss et al. 2015).

Treatment of MCF10A YAP5SA cells with 0.5 µg/ml doxycycline for 2 days strongly induced the protein expression of YAP as revealed by immunoblotting (**Figure 14A**). To see whether LIN9-activated genes overlap with YAP-activated genes in human MCF10A cells as it was seen before in murine KPL2 cells, RNA-seq data of MCF10A YAP5SA cells treated without or with doxycycline for 12 h (kindly provided by Björn von Eyss) and RNA-seq data of control and 4-OHT-treated *Lin9*-deleted KPL2 cells (see **3.2**) were compared. Of 1407 YAP-activated and 568 LIN9-activated genes, 89 genes were activated by both YAP and LIN9 (**Figure 14B**). In contrast, 1318 of the 1407 YAP-activated genes in MCF10A cells did not overlap with LIN9-activated genes in KPL2 cells such as *AMOTL2*, *CTGF*, and CYR61. The top 50 strongest YAP-activated genes of the 89 common YAP- and MMB-regulated genes included several well-described MMB target genes such as *AURKA*, *ANLN*, *KIF23*, and *CDC20* (**Figure 14C**). The activation of *ANLN*, *KIF23*, and *CDC20* gene expression by YAP could be validated in an independent experiment using qPCR (**Figure 14D**).

To analyze the genome-wide binding of YAP, LIN9, and B-MYB, ChIP-seq of untreated MCF10A YAP5SA cells or MCF10A YAP5SA cells treated with doxycycline for 2 days to induce YAP5SA expression was performed. Analysis of the number of called peaks revealed an increase of YAP peaks from 127 in untreated cells to 5630 in doxycycline-treated cells (**Figure 15A**). With an increase of B-MYB peaks to almost 120% and a decrease of LIN9 peaks to approx. 90% upon YAP induction, the number of LIN9 and B-MYB peaks between untreated and doxycycline-treated cells differed only slightly. Consistent with the binding analysis shown in KPL2 cells (**Figure 11**), the analysis of the localization of LIN9, YAP, and B-MYB peaks relative to the nearest TSS of annotated genes in YAP-induced MCF10A cells revealed distinct binding patterns for YAP and LIN9 (**Figure 15B**). Specifically, almost 90% of LIN9 bindings sites were located within a distance of $\pm$ 1 kb to the TSS, whereas with 85% the majority of YAP peaks were detected either in intergenic regions or in gene bodies. Unexpectedly, about 50% of all B-MYB peaks were detected in gene bodies or between genes. Only 40% of B-MYB peaks were detected around the TSS ($\pm$ 1 kb).

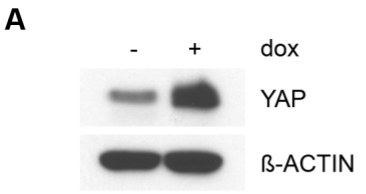

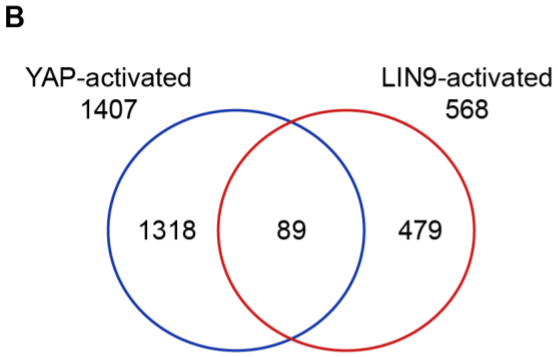

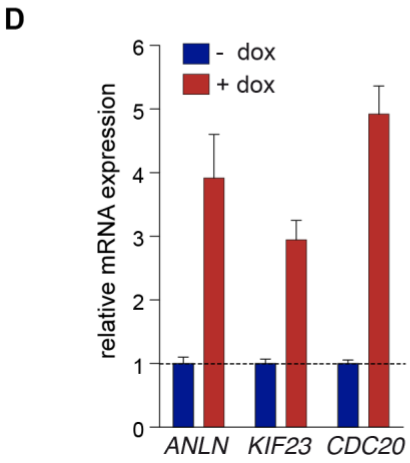

C

Gene	log2FC	FDR q-value
THBS1	3.66	5.1e-183
CCBE1	3.19	8.8e-051
DUSP5	2.09	1.5e-027
FAM84A	1.74	2.0e-002
BCAM	1.72	7.6e-008
MACF1	1.57	5.0e-005
TINAGL1	1.44	5.1e-028
CCND2	1.38	1.6e-032
SPC25	1.08	1.5e-003
PPARD	1.04	1.2e-008
CCDC85C	1.01	5.2e-008
KRT7	0.97	2.6e-043
CDC20	0.95	5.1e-025
HJURP	0.94	8.1e-007
ANLN	0.90	4.6e-026
RRM2	0.83	2.5e-019
UTP20	0.81	7.8e-005
PGP	0.80	1.0e-005
MARCKS	0.79	5.5e-006
TGFA	0.78	7.8e-007
HMGB3	0.76	1.4e-005
KNSTRN	0.73	2.5e-004
FAM84B	0.73	3.0e-005
STC2	0.71	3.9e-008
BUB1B	0.70	6.9e-008
UNG	0.69	4.4e-006
ASNS	0.69	2.4e-003
SERPINE1	0.67	9.8e-010
MCM5	0.64	1.4e-006
KIF23	0.64	2.9e-006
USP1	0.64	2.7e-006
CALM2	0.64	8.8e-011
ESPL1	0.64	2.8e-004
MESDC1	0.63	8.3e-004
MCM7	0.63	2.2e-012
MTHFD1L	0.63	1.2e-004
ARHGAP19	0.62	1.9e-003
DBF4	0.62	1.8e-002
XPOT	0.61	2.2e-009
NXN	0.60	9.7e-005
MTHFD2	0.59	8.3e-007
TRIP10	0.59	1.3e-004
PPRC1	0.55	7.9e-004
MCM6	0.54	5.2e-005
SLC3A2	0.53	4.0e-013
FUS	0.53	6.2e-007
UBE2S	0.53	3.2e-004
AURKA	0.52	1.5e-003
CKAP2L	0.51	7.0e-003
MSH6	0.51	8.8e-004

Figure 14: YAP-activated genes in MCF10A cells overlap with LIN9-activated genes in KPL2 cells.
(**A**) MCF10A cells stably expressing doxycycline (dox)-inducible YAP5SA either treated without or with 0.5 µg/ml dox for 2 days were used for immunoblotting of YAP. ß-ACTIN served as a loading control. (**B**) Overlap of YAP-activated and LIN9-activated genes. MCF10A YAP5SA cells control or dox-treated for 12 h to induce YAP5SA expression were subjected to RNA-seq (unpublished data by Björn von Eyss). KPL2 cells untreated or treated with 10 nM 4-OHT for 4 days to delete *Lin9* were used for RNA-seq (see **Figure 6**). 1407 YAP-activated genes in MCF10A YAP5SA with a positive log2FC and an FDR q-value < 0.025 were compared with 568 LIN9-activated genes with a negative log2FC and an FDR q-value < 0.025. 89 genes were activated by both YAP and LIN9. Log2FC, log2 fold change; FDR, false discovery rate (**C**) Top 50 strongest YAP-activated genes (sorted by log2FC) of the 89 genes shown in (**B**), which were also activated by LIN9 in KPL2 cells. (**D**) mRNA expression of the indicated genes of MCF10A YAP5SA cells treated with 0.5 µg/ml dox for 2 days relative to the mRNA expression of untreated cells. *GAPDH* expression was used for normalization. Mean and SD (error bars) of three technical replicates are shown.

ChIP-seq of the histone modifications H3K4me1, H3K4me3, and H3K27ac to identify open promoters and active enhancers or super-enhancers respectively revealed that only approx. 13% of all B-MYB peaks could be assigned to super-enhancer, enhancer or promoter sites (**Figure 15C**). The unusual high percentage of B-MYB peaks, which are not enriched for any of the three analyzed histone modifications, warrants further investigation in future studies. However, nearly all (10%) of the 13% of B-MYB peaks that could be assigned to either enhancer or promoter regions were located in active promoter regions with high H3K4me3 and H3K27ac levels (**Figure 15C**). This is consistent with the binding sites of LIN9, which were located in regions enriched for H3K4me3 and H3K27ac as indicative for open promoters. Similar to murine KPL2 cells, YAP binding sites in MCF10A cells were mainly located in super-enhancer (7%) or enhancer (31%) regions and only 2% of YAP peaks were localized at promoters (**Figure 15C**).

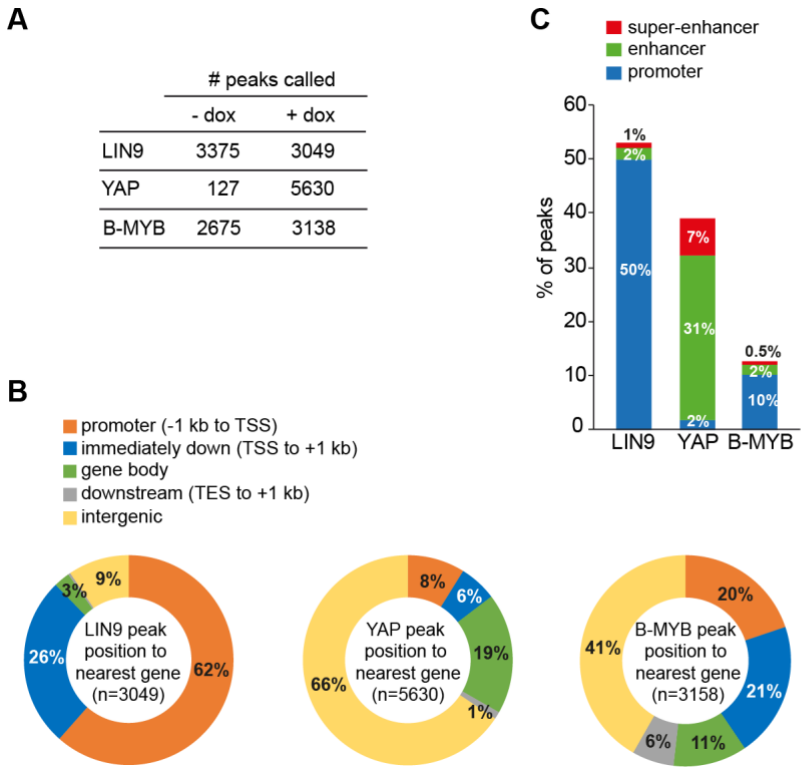

Figure 15: Genome-wide binding analyses of YAP and the MMB subunits LIN9 and B-MYB.
(**A-C**) MCF10A YAP5SA cells untreated or treated with 0.5 µg/ml dox for 2 days to induce YAP5SA expression were used for ChIP-seq using antibodies specific for YAP, LIN9, B-MYB, H3K4me1, H4K4me3, and H3K27ac. (**A**) Number of called LIN9, YAP, and B-MYB peaks in untreated and dox-treated MCF10A YAP5SA cells. (**B**) Localization of LIN9, YAP, and B-MYB peaks in dox-treated YAP-induced MCF10A YAP5SA cells relative to the TSS of annotated genes. TSS, transcription start site; TES, transcription end site. (**C**) Percentage of LIN9, YAP, and B-MYB peaks overlapping with open/active promoters, enhancers, and super-enhancers defined by ChIP-seq of the histone modifications H3K4me1, H3K4me3, and H3K27ac as described in **Figure 11B**.

The overlap of RNA- with ChIP-seq data revealed that YAP bound to the promoters of only 9% (94) of YAP-activated genes in MCF10A cells (**Figure 16A**). GO analysis showed that these direct YAP target genes are linked amongst others to cell adhesion, cell migration, metabolic processes, and wound healing (**Figure 16B**). In contrast, LIN9 bound to the promoters of almost 25% (245) of genes induced by YAP (**Figure 16A**). These LIN9-bound and YAP-activated genes included bona fide MMB target genes such as *AURKA*, *CCNA2*, and *CDC20*, which are connected to cell cycle regulation and mitosis (**Figure 16C**). Less than 2% of YAP-activated genes were bound by both LIN9 and YAP, including genes such as *THBS1* and *ACTN1* important for cell-to-cell/matrix interactions and cytoskeleton organization (Rebhan et al. 1997).

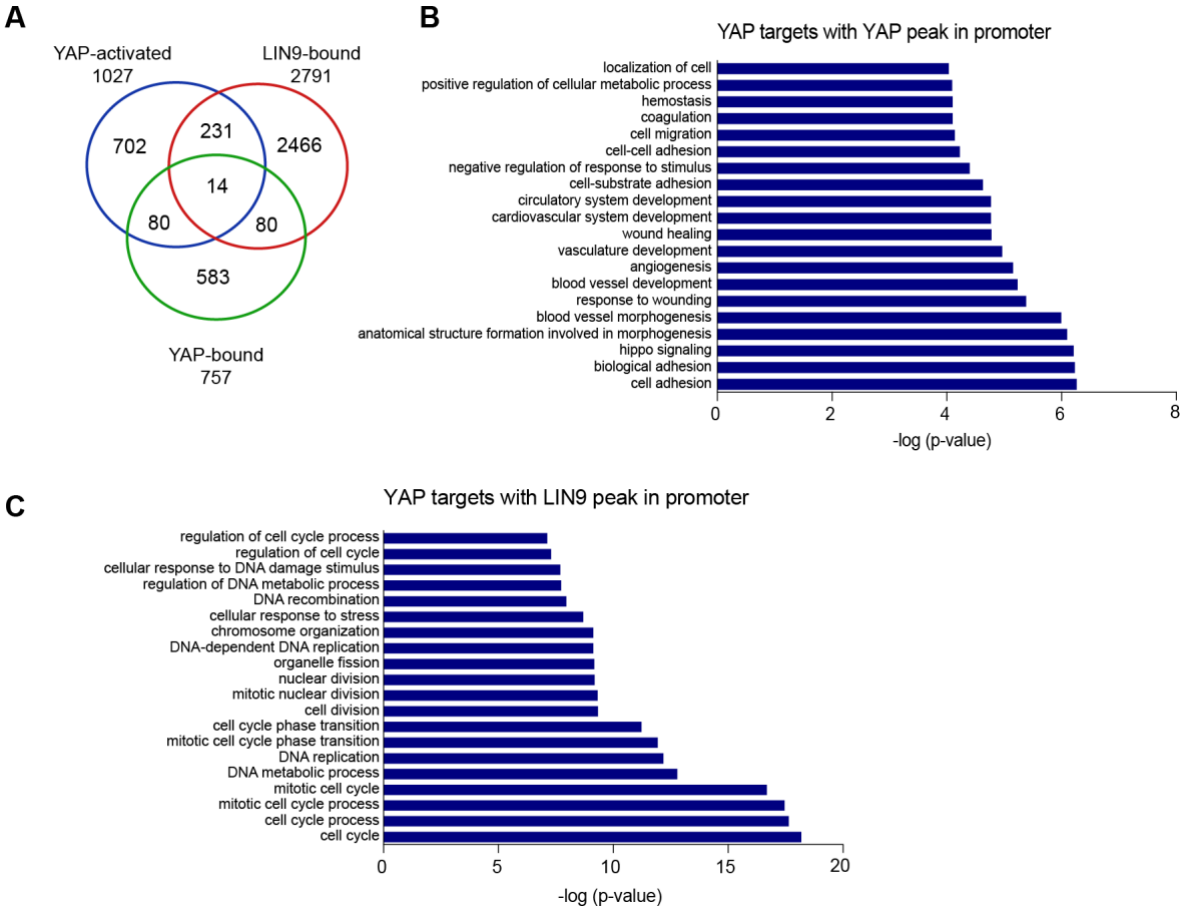

Figure 16: LIN9 binds to a large proportion of YAP-regulated genes in MCF10A cells.
(**A-C**) MCF10A YAP5SA cells untreated and treated with dox for 12 h (RNA-seq) or for 2 days (ChIP-seq) to induce YAP5SA expression were used for RNA- and ChIP-seq. (**A**) Venn diagram showing the overlap of 1027 genes that were activated by YAP (log2FC > 0.5, FDR q-value < 0.05) and bound by LIN9 and/or YAP at promoters (± 1 kb to TSS) upon YAP induction (+ dox) in MCF10A YAP5SA cells. (**B**) GO analysis of the 245 genes, which were induced by YAP5SA upon dox-treatment and had a LIN9 peak at their promoter (± 1 kb to TSS). The top 20 enriched GO terms according to the *P*-value are shown. (**C**) GO analysis of the 94 genes, which are induced by YAP5SA upon dox-treatment and have a YAP peak at their promoter (± 1 kb to TSS). The top 20 enriched GO terms according to the *P*-value are shown.

Together these results suggest that in human MCF10A cells, similar to mouse KPL2 cells, LIN9 regulates YAP-induced genes associated with cell cycle and mitosis directly by binding to their promoters, whereas binding of YAP to promoters of these genes could not be detected. Instead, YAP binding was localized mainly at enhancers, which suggests that enhancer-bound YAP induces the expression of mitotic genes by interacting with LIN9-bound promoters through chromatin looping.

3.7 YAP induction strongly enhances chromatin-binding of B-MYB to LIN9-bound loci

To specifically analyze the genome-wide binding strength of YAP and MMB in YAP-induced MCF10A YAP5SA cells, average read density profiles of LIN9, B-MYB, YAP, and the histone modifications H3K4me1, H3K4me3, and H3K27ac centered in a 4 kb window around the summit of all LIN9 (**Figure 17A**) or YAP (**Figure 17B**) peaks were generated. Histone modification density profiles at LIN9 binding sites revealed a strong enrichment of H3K4me3 and H3K27ac, indicating that these regions display active promoter sites (**Figure 17A**). The induction of YAP5SA upon treatment with doxycycline had only little effect on the binding of LIN9, but surprisingly, it strongly enhanced the overall binding of B-MYB to LIN9-bound loci. This enhanced binding of B-MYB at LIN9 binding sites upon YAP5SA induction came along with an enrichment of H3K27ac, suggesting an increased promoter activity. Although the previous analyses in MCF10A cells revealed little overlap between LIN9 and YAP binding, YAP5SA induction resulted in a small increase in YAP binding to LIN9-bound sites.

Furthermore, doxycycline treatment resulted in a strong enrichment of global YAP binding and in an increase of both H3K4me1 and H3K27ac at the center of all YAP peaks, indicative of an increase in enhancer activity (**Figure 17B**). The bimodal distribution of H3K4me1, H3K4me3, and H3K27ac around the summit of both YAP and LIN9 peaks indicates two nucleosomes flanking the binding sites of YAP and LIN9. Reduced nucleosome occupancy is a typical characteristic for chromatin regions bound by transcription factors since these compete with nucleosomes to get access to the DNA (Nie et al. 2013).

Similar to the observed YAP binding at LIN9-bound sites, LIN9 binding was detected at YAP-bound loci upon YAP5SA induction. The quite weak enrichment of YAP at LIN9-bound loci and of LIN9 at YAP-bound loci in YAP5SA-induced cells might display “shadow peaks”, which have been shown recently to be associated with long-range chromatin interactions mediated by long distant protein-protein interactions (Liang et al. 2014). The presence of these “shadow peaks” thus further supports the hypothesis that enhancer-bound YAP interacts with promoter-bound LIN9.

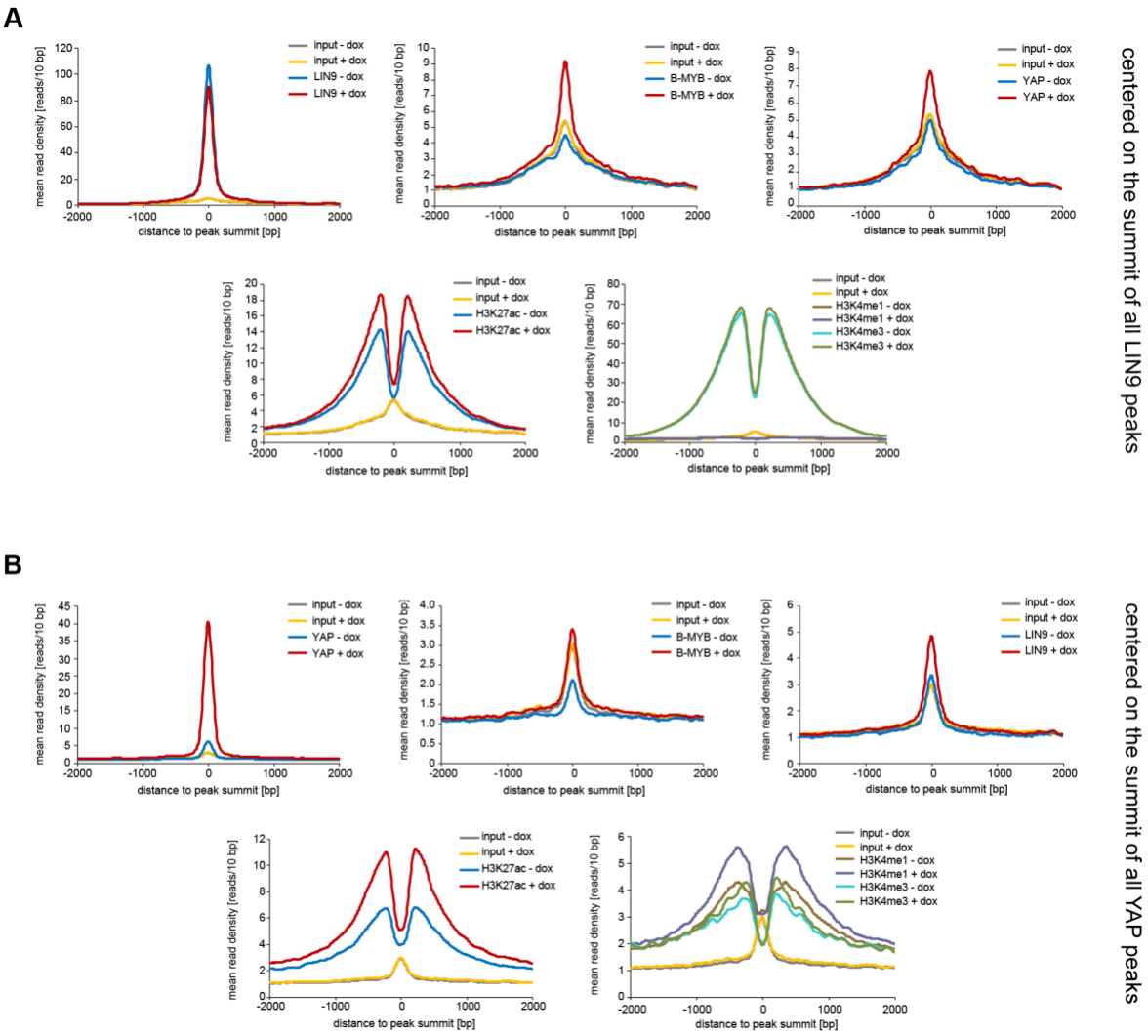

Figure 17: Increased overall B-MYB binding at LIN9-bound promoters upon YAP induction.
(**A-B**) Average profile of LIN9, B-MYB, YAP, H3K27ac, H3K4me1, and H3K4me3 tag density within a distance of ± 2 kb centered on the summit of all LIN9 (**A**) or YAP (**B**) peaks, as analyzed by ChIP-seq. Input -/+ dox served as a control. Mean read density is depicted with a resolution of 10 bp.

The most prominent model for long-distance interactions between promoters and enhancers is called the “looping” model because the chromatin has to form a loop to enable physical interactions between enhancers and promoters (Bulger and Groudine 2011). To link YAP-bound enhancers to their respective promoters in MCF10A YAP5SA cells, a previously published high-resolution map of chromatin interactions (Hi-C) in primary human fibroblasts IMR90 was used (Jin et al. 2013).

With this Hi-C map, 5,018 enhancers, which were bound by YAP in doxycycline-treated MCF10A YAP5SA cells, were assigned to 2,771 unique transcriptional start sites (**Figure 18A**). 504 of these 2,771 promoters that interact with YAP-bound enhancers were bound by LIN9, whereas 2,267 promoters were without a LIN9 peak. Notably, the expression of genes whose promoters were bound by LIN9 and could be assigned to a YAP-bound enhancer was significantly increased upon induction of YAP5SA in MCF10A cells (**Figure 18B**). In contrast, genes whose promoters interacted with YAP-bound enhancers but had no LIN9 binding at their TSS were not induced by YAP5SA (**Figure 18B**).

It was seen before that YAP5SA induction increases the overall binding of B-MYB (**Figure 17A**). The analysis using the Hi-C map further supported this observation since the induction of YAP5SA strongly enhanced binding of B-MYB to LIN9-bound loci linked to YAP-bound enhancers (**Figure 18C**). Notably, promoters linked to YAP-bound enhancers that were not bound by LIN9 did not show an enrichment of B-MYB binding upon YAP5SA induction. Increased chromatin-association of B-MYB was also observed at LIN9-bound promoters of YAP5SA-activated genes, which interacted with YAP-bound enhancers (**Figure 18D**).

Enhanced binding of B-MYB to selected MMB target gene promoters upon YAP5SA induction could be confirmed by ChIP-qPCR experiments (**Figure 19**). B-MYB was strongly enriched at promoters of *BIRC5*, *CENPF*, *TOP2A*, *ECT2*, and *KIF23* in YAP5SA-induced cells compared to control cells, whereas LIN9 binding to these promoters was only slightly increased. Conversely, no YAP could be detected at promoters of these genes, whereas YAP strongly bound to the promoters of the bona fide YAP targets *AMOTL2*, *CTGF*, and *CYR61* (**Figure 19**).

In summary, these results show that binding of LIN9 to the promoters of a certain subset of genes is important for their activation by YAP from distal enhancers. The strong enrichment of B-MYB-binding to these promoters upon YAP5SA induction suggests that YAP activates these genes from distal enhancers by stimulating the chromatin-association of B-MYB at LIN9-bound promoters.

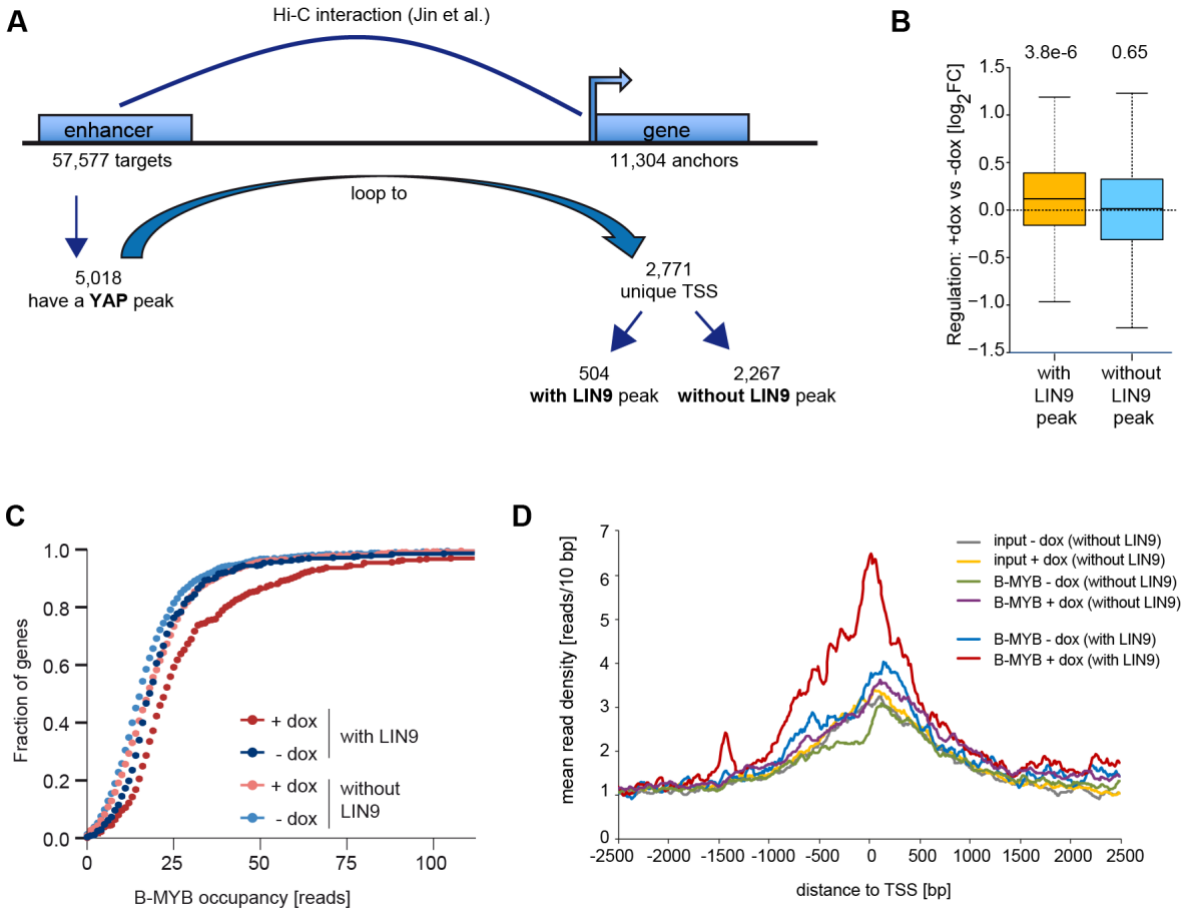

Figure 18: YAP promotes binding of B-MYB to LIN9-bound promoters that directly interact with YAP-bound enhancers.

(**A**) Scheme for the strategy to identify YAP-bound enhancers that interact with LIN9-bound promoters via chromatin looping. A high-resolution map of chromatin interactions (Hi-C) in primary human fibroblasts (IMR90) described by Jin et al. (2013) was used to filter enhancers, here described as "targets", for those containing a YAP-peak (5,018) in dox-treated MCF10A YAP5SA cells. These 5,018 YAP-bound enhancers interact via looping with 2,771 unique TSS ("anchors"), which were analyzed for the presence of a LIN9 peak in MCF10A cells. (**B**) Box plot depicting the changes in gene regulation in YAP5SA-induced MCF10A cells upon 12 h-long treatment with doxycycline as analyzed by RNA-seq (data provided by Björn von Eyss). Shown are all genes with (n=460) or without (n=1,950) LIN9 binding at promoters that were linked to YAP-bound enhancers as identified by ChIP-seq of LIN9 and YAP in MCF10A YAP5SA cells and Hi-C data from Jin et al. (2013) as described in (**A**). The *P*-value was calculated for the difference of the median to 0 using an unpaired two-tailed Wilcoxon rank-sum test. Outliers not shown. (**C**) Empirical cumulative distribution function (ECDF) showing the B-MYB occupancy at promoters linked to YAP-bound enhancers with (n=460) or without (n=1,950) LIN9 peak in untreated and dox-treated MCF10A YAP5SA cells. B-MYB reads were counted in a region of -100 bp to +400 bp relative to the TSS. Only genes that were included in RNA-seq data from (**B**) were used for this analysis. (**D**) Line plots showing the mean read density of B-MYB within a distance of ± 2.5 kb centered on the TSS of YAP5SA-activated genes with or without a LIN9 peak at the promoter (± 1 kb to TSS), which were linked to YAP-bound enhancers. The resolution is 10 bp.

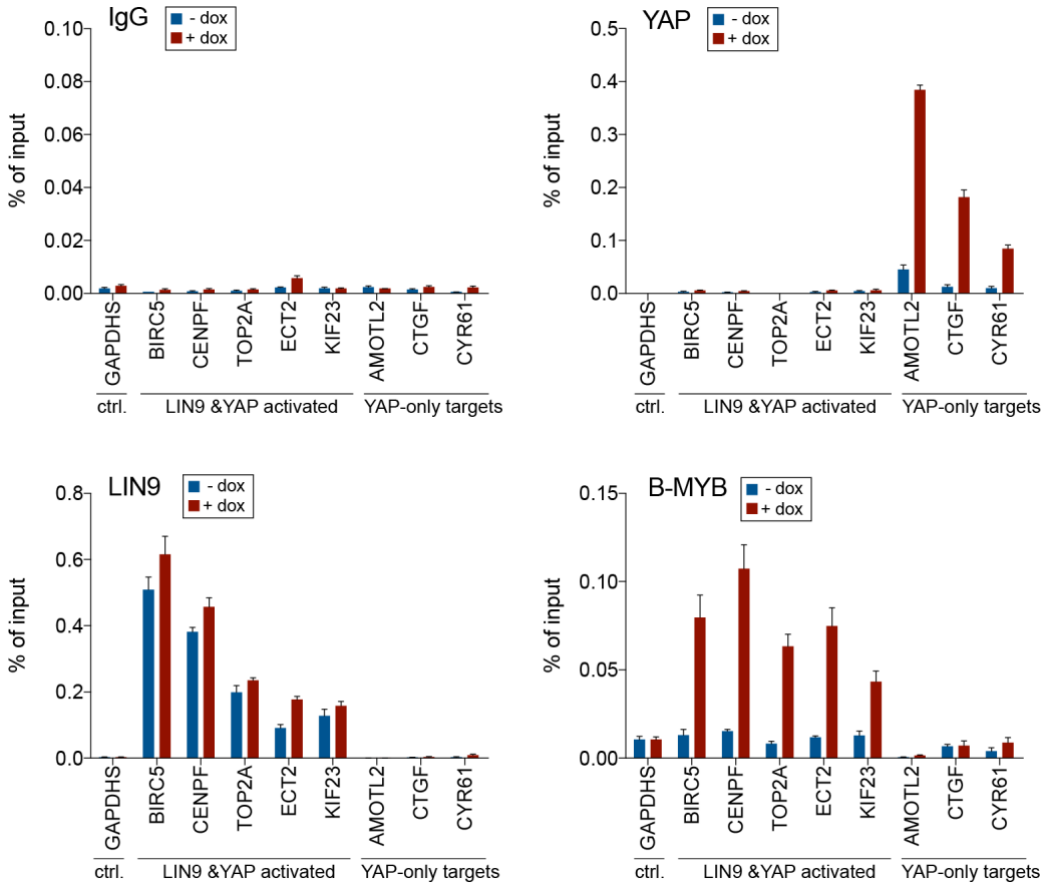

Figure 19: Enhanced binding of B-MYB to selected MMB target gene promoters upon YAP induction. Binding of YAP, LIN9, and B-MYB to the promoters of the indicated genes was analyzed by ChIP-qPCR. Chromatin was isolated from MCF10A YAP5SA cells treated without or with 0.5 µg/ml doxycycline (dox) for 2 days and used for immunoprecipitation with antibodies specific for YAP, LIN9, and B-MYB. Nonspecific IgG served as a control. 1% of chromatin amount used for the IP served as an input control. Immunoprecipitated chromatin and input chromatin were subjected to qPCR using primers specific for promoter regions of the indicated genes. GAPDHS promoter was analyzed as a control region. Enrichment was calculated as percent (%) of input. Error bars represent error margins calculated using the SD of three technical replicates from ChIP and input samples as described in **2.2.2.9.2**.

3.8 YAP interacts with promoters of MMB target genes from distal enhancers

It was shown that most of these long-range chromatin loops linking enhancers and promoters are conserved across cell types and species (Rao et al. 2014). Next, circular chromosome conformation capture with next-generation sequencing (4C-seq) of promoters of the three common MMB and YAP target genes *KIF23*, *AURKA*, and *CDC20* was performed to analyze whether they interact with YAP-bound enhancers (**Figure 20A-D**). Taking the promoters as viewpoints, four distal regions (E1-E4) interacting with the *KIF23* promoter could be identified using 4C-seq (**Figure 20A**).

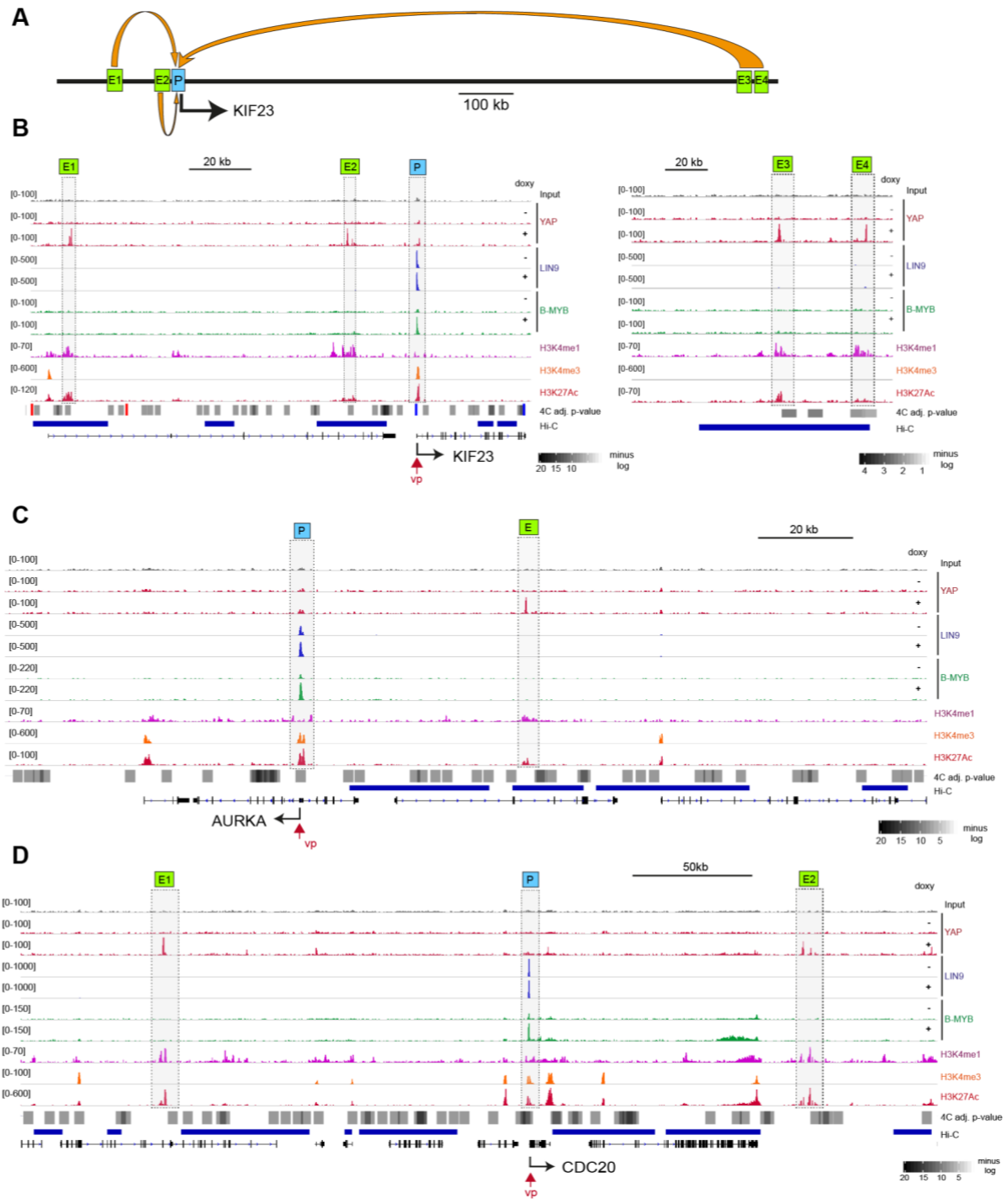

Figure 20: 4C-seq and ChIP-seq revealed interactions between B-MYB- and LIN9-bound promoters and YAP-bound enhancers in MCF10A cells.

(**A-D**) MCF10A YAP5SA untreated or treated with 0.5 µg/ml dox for 2 days were used for ChIP-seq and 4C-seq. (**A**) Scheme for long-range chromatin interactions between the human *KIF23* promoter (labelled as P) and distal enhancers (labelled as E1-E4) as identified by 4C-seq. (**B-D**) Genome browser tracks of the human *KIF23* (**B**), *AURKA* (**C**), and *CDC20* (**D**) gene loci illustrating the enrichment of YAP, LIN9, and B-MYB and of the histone modifications H3K4me1, H3K4me3, and H3K27ac as determined by ChIP-seq. The normalized and merged input is shown at the top as a control. YAP-bound enhancers interacting with LIN9- and B-MYB-bound promoters were identified using 4C-seq with the promoters as a viewpoint (vp). Adjusted *P*-values < 0.01 were used to identify distal regions that significantly interacted with promoters of the indicated genes and are shown as boxes in grey shades below browser tracks. For comparison, Hi-C data from Jin et al. (2013), which predict long-range chromatin interactions between promoters and enhancers, are shown as blue bars below adjusted *P*-values of 4C-seq.

As indicated by high levels of H3K4me1 and H3K27ac, these regions function as active enhancers located about 20 kb (E2) and 100 kb (E1) upstream or more than 1000 kb downstream (E3 and E4) of the *KIF23* promoter. Importantly, all of these four enhancers were bound by YAP (**Figure 20B**). For the *AURKA* gene, a YAP-bound enhancer about 50 kb upstream of the TSS was identified to interact with the promoter (**Figure 20C**). The promoter of *CDC20* interacted with two YAP-bound enhancers located approx. 150 kb upstream (E1) and 100 kb downstream (E2) of the TSS (**Figure 20D**). Binding of YAP to enhancers identified by 4C-seq was confirmed in later experiments using regular ChIP-qPCR (**Figure 22**).

Overall, these 4C-seq data support the results from the analysis of published Hi-C data described before and show that YAP binds to enhancers, which interact with MMB-bound promoters over a long distance via looping of the chromatin.

3.9 YAP induces the expression of B-MYB in confluent but not in subconfluent MCF10A cells

As it was seen before that inhibition of YAP in murine KPL2 (**Figure 8C**) and human A549 (**Figure 8D**) cells reduces the expression of the B-MYB encoding gene *MYBL2*, the following experiments aimed to answer the question whether YAP activates the expression of B-MYB and if so, whether this contributes to the enhanced chromatin binding of B-MYB upon YAP5SA induction.

Initially, the mRNA expression of *MYBL2* in MCF10A YAP5SA cells treated with doxycycline to induce YAP5SA for varying periods of time was analyzed by qPCR (**Figure** 21**A**). The most striking result to emerge from this analysis was that YAP5SA induced the expression of *MYBL2* depending on the cell confluency. Whereas YAP5SA strongly and significantly induced the *MYBL2* expression in confluent cultures, it had no significant effect on the *MYBL2* mRNA levels in subconfluent cultures. Unlike *MYBL2*, the MMB target gene *CDC20* was significantly induced in both subconfluent and confluent cultures (**Figure 21A**). Knockdown of *LIN9* and *MYBL2* mediated by RNA interference inhibited the induction of *CDC20* by YAP5SA in subconfluent MCF10A cells, indicating that YAP needs MMB to activate the expression of *CDC20* (**Figure 21B**). Consistent with the qPCR results, YAP5SA induced the B-MYB protein expression solely in confluent but not in subconfluent cells (**Figure 21C**). In contrast, the protein expression of the MMB targets CYCLIN A, CDC20, and TOP2A and also the mRNA expression of several other MMB targets were induced regardless of the cell confluency in both subconfluent and confluent cells (**Figure 21C, 21D**).

Strikingly, *LIN9* expression in confluent cells was not significantly changed, whereas in subconfluent cells the *LIN9* expression levels even slightly decreased upon YAP5SA induction (**Figure 21D**).

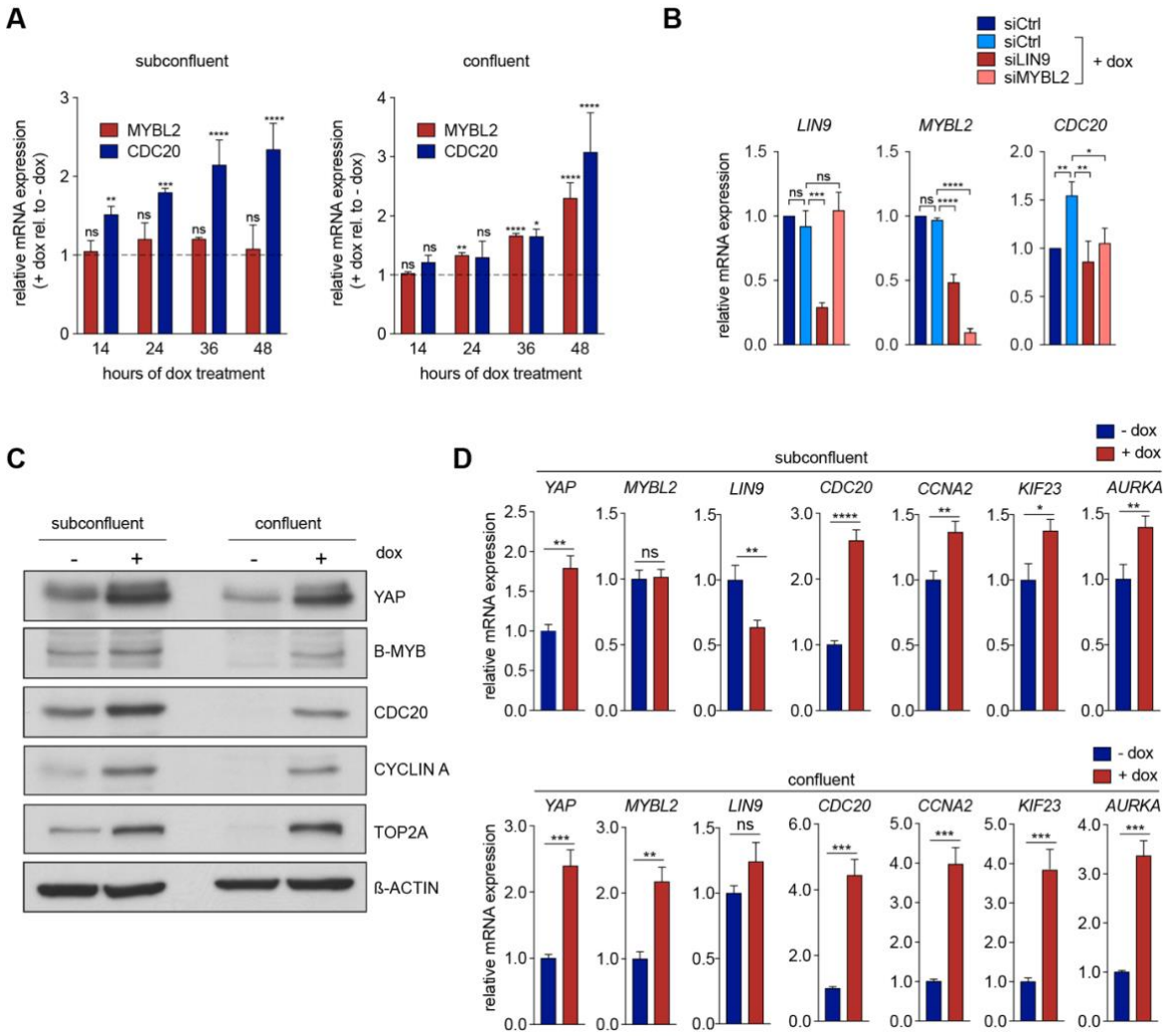

Figure 21: YAP induces the expression of B-MYB in confluent but not in subconfluent cultures.
(**A**) Subconfluent or confluent cultures of MCF10A YAP5SA cells were treated with 0.5 µg/ml doxycycline (dox) for the indicated hours. *MYBL2* and *CDC20* mRNA expression in dox-treated (+dox) cells was analyzed relative to the mRNA expression in untreated (-dox) cells at the 14 h time point. *GAPDH* expression was used for normalization. Mean and SD of three independent experiments, each performed as technical triplicate, are shown. Statistical significance was assessed using two-way ANOVA with Bonferroni's multiple comparison test. *P*-values ≤ 0.05 were considered statistically significant. (**B**) Subconfluent MCF10A YAP5SA cells were transfected with control siRNA (siCtrl) or siRNAs against *LIN9* (siLIN9) or *MYBL2* (siMYBL2). 24 h after siRNA transfection, YAP5SA expression was induced with 0.5 µg/ml dox for 24 h. RNA was isolated and the mRNA expression of the indicated genes was analyzed relative to the expression in siCtrl-transfected untreated (- dox) cells. Data are presented as the mean and SD of three independent experiments, each conducted in 3 technical replicates. Statistics was performed using one-way ANOVA with Tukey's post-test. (**C**) Western Blot analysis of the indicated proteins in subconfluent and confluent MCF10A YAP5SA cells treated with dox for 2 days. ß-ACTIN served as a loading control. (**D**) mRNA expression of the indicated genes in subconfluent and confluent MCF10A YAP5SA cells treated with doxycycline for 2 days relative to the mRNA expression in untreated cells as analyzed by qPCR. *GAPDH* was used for normalization. Mean and SD of 3 technical replicates are shown. Statistics was done using the Student's *t*-test, two-tailed. (**A-B,D**) Asterisks are as follows: $^{*}P \leq 0.05$, $^{**}P \leq 0.01$; $^{***}P \leq 0.001$; $^{****}P \leq 0.0001$; ns, not significant, $P > 0.05$.

Notably, the activation of the YAP/MMB target genes *AURKA*, *CDC20*, and *KIF23* upon YAP5SA induction was accompanied by enhanced binding of B-MYB and LIN9 to the promoters of these genes in both subconfluent and confluent cells as analyzed by ChIP-qPCR (**Figure 22, top**). Upon doxycycline treatment of subconfluent and confluent MCF10A YAP5SA cell cultures, YAP binding to the 4C-seq-identified enhancers of *AURKA*, *CDC20*, and *KIF23* and to the promoter of the well-known YAP target gene *AMOTL2* was strongly induced (**Figure 22, middle and bottom**).

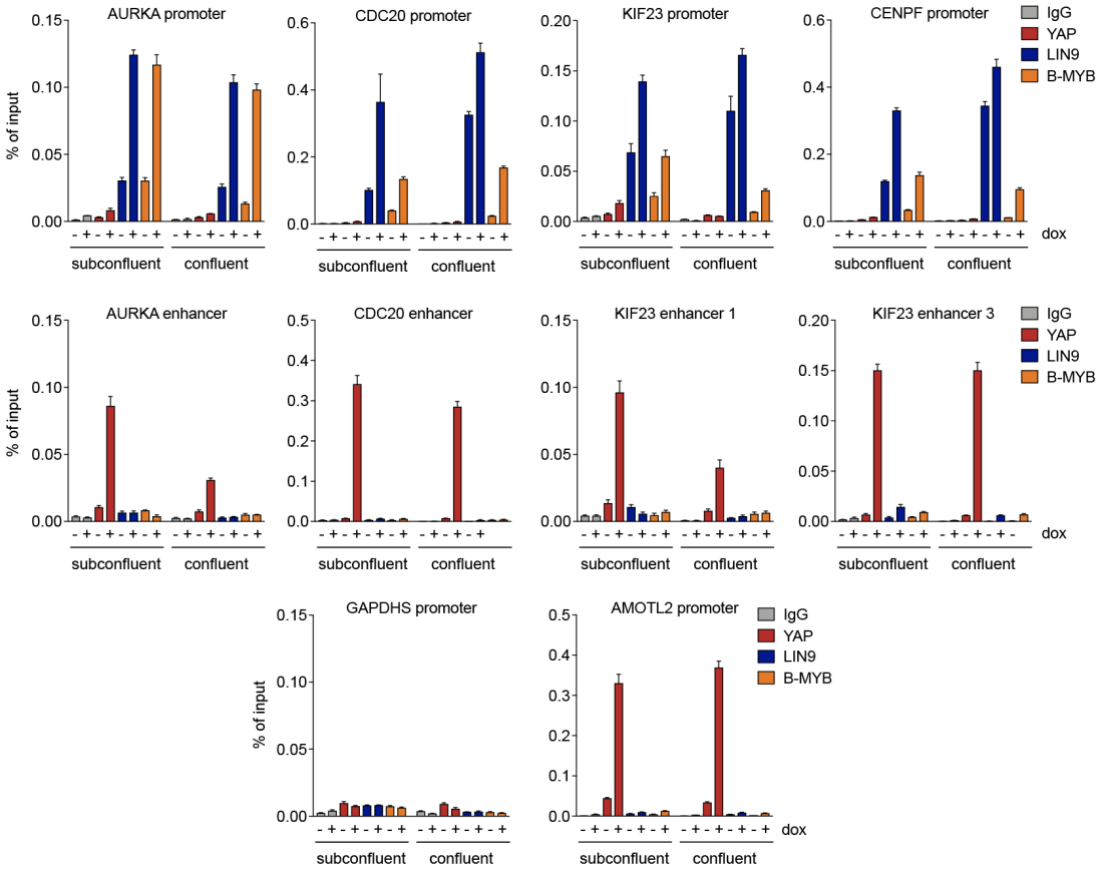

Figure 22: YAP promotes promoter binding of LIN9 and B-MYB in subconfluent and confluent cells. Binding of YAP, LIN9, and B-MYB to the promoters and enhancers of common YAP and MMB target genes was analyzed by ChIP-qPCR. Chromatin was isolated from subconfluent and confluent MCF10A YAP5SA cells, which were left untreated or treated with 0.5 µg/ml doxycycline (dox) for 2 days to induce YAP5SA expression. Chromatin was immunoprecipitated with antibodies specific for YAP, LIN9, and B-MYB. Nonspecific IgG served as a control. 1% of chromatin amount used for the IP served as an input control. Immunoprecipitated chromatin and input chromatin were subjected to qPCR using primers specific for promoter and enhancer regions (identified by 4C-seq) of the indicated genes. *GAPDHS* promoter served as a negative control. The promoter of the well-known YAP target gene *AMOTL2* was used as a positive control. Enrichment was calculated as percent (%) of input. Error bars represent error margins calculated using the SD of three technical replicates from the ChIP and input sample as described in **2.2.2.9.2**.

These results indicate that YAP can promote chromatin-association of B-MYB and LIN9 independently from regulating their expression. In conclusion, these data suggest that YAP induces the expression of MMB target genes by at least two mechanisms: on the one hand, by regulating the expression of the MMB subunit B-MYB, either directly or indirectly, and on the on other hand, by stimulating the chromatin-association of B-MYB and LIN9 at LIN9-bound promoters.

3.10 YAP binds to a distal enhancer that interacts with the promoter of B-MYB through chromatin looping

To determine how YAP regulates the expression of B-MYB in MCF10A YAP5SA cells, ChIP data were analyzed for the binding of YAP to the human *MYBL2* gene locus. The genome browser track of the *MYBL2* gene shown in **Figure 23B** illustrates that before and after induction of YAP5SA expression no YAP binding could be detected at the promoter of *MYBL2*, which was verified in subconfluent and confluent MCF10A YAP5SA cells by conventional ChIP-qPCR assay (**Figure 23C, left**). This finding suggests that YAP regulates the expression of *MYBL2* via binding to a distal enhancer.

To test this hypothesis of long-range interaction, 4C-seq was performed with the human *MYBL2* promoter as a viewpoint. Analysis of the 4C-seq data revealed a significant interaction of the *MYBL2* promoter with a region 12 Mb upstream of the *MYBL2* TSS (**Figure 23A, 23B**). Indeed, this region turned out to be an enhancer due to the presence of H3K4me1 and the absence of H3K4me3 as determined by ChIP-seq. Importantly, YAP binding to this enhancer was strongly induced upon doxycycline treatment and correlated with increased levels of H3K27ac, indicating that YAP induced the activity of this enhancer (**Figure 23B**). Binding of YAP to the identified *MYBL2* enhancer could be validated in an independent ChIP-qPCR experiment (**Figure 23C**).

Taken together, these findings indicate that YAP activates the expression of B-MYB by binding to a distal enhancer, which interacts with the *MYBL2* promoter by forming a chromatin loop.

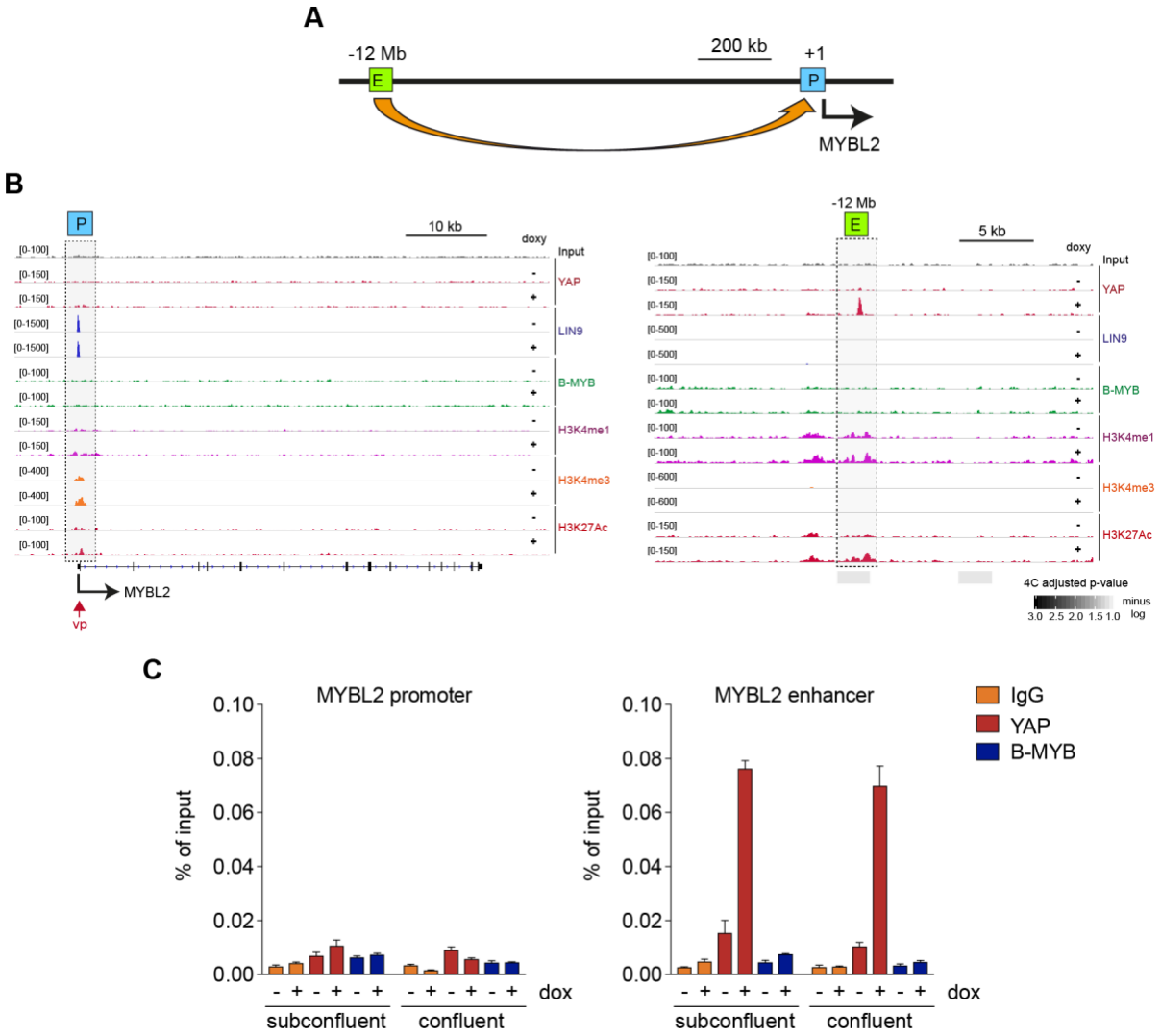

Figure 23: Identification of a YAP-bound enhancer that interacts with the promoter of *MYBL2*.
(**A-B**) MCF10A YAP5SA cells untreated or treated with doxycycline for 2 days to induce YAP5SA were used for ChIP-seq and 4C-seq. (**A**) Scheme illustrating the long-range interaction between the *MYBL2* promoter (labelled as P) and a -12 Mb from the TSS located enhancer (labelled as E) as identified by 4C-seq. (**B**) Genome browser tracks of the human *MYBL2* locus (left) and a genomic region -12 Mb away from the *MYBL2* TSS displaying a YAP-bound enhancer (right). Shown is the chromatin-binding of the indicated proteins and histone modifications as determined by ChIP-seq. The normalized and merged input is shown at the top. Adjusted *P*-values < 0.01 were used to identify distal regions that significantly interacted with the *MYBL2* promoter (viewpoint) in 4C-seq and are shown as boxes in grey shades below browser tracks. (**C**) ChIP-qPCR of subconfluent and confluent MCF10A YAP5SA cells treated with doxycycline for 2 days. ChIP was performed using YAP- and B-MYB-specific antibodies. 1% of chromatin was used as input control. IgG served as a nonspecific control. Immunoprecipitated chromatin and input chromatin were subjected to qPCR using primers specific for the promoter and the 4C-seq-identified enhancer of *MYBL2*. Binding of IgG, YAP, and B-MYB was calculated as percent (%) of input. Error bars represent error margins calculated using the SD of three technical replicates from the ChIP and input sample as described in **2.2.2.9.2.**

3.11 MMB and YAP physically interact

Binding of YAP to enhancers that interact with MMB-bound promoters and enhanced promoter-binding of B-MYB upon YAP5SA induction led to the assumption that YAP and MMB physically interact.

This idea was first investigated using *in situ* proximity ligation assay (PLA). Endogenous YAP was found to be in close proximity with endogenous LIN9 and B-MYB in the nuclei of human HeLa and murine KPL2 cells as represented by red fluorescent dots (**Figure 24A, 24B**). The specificity of the antibodies used for PLA was assessed in HeLa cells by incubation with only one of the two antibodies, which resulted in loss of the red signal (**Figure 24A**). The red signal in PLA seems to specifically result from the close proximity of the detected proteins, as it was lost when either *Yap/Taz* were depleted by siRNAs or when *Lin9* was deleted upon 4-OHT-induced $CreER^{T2}$ activation in KPL2 cells (**Figure 24B**). Notably, the deletion of *Lin9* did not only disrupt the interaction of YAP and LIN9 but also of YAP and B-MYB, which suggests that the MuvB core is needed for mediating the YAP-B-MYB interaction (**Figure 24B**).

Next, co-immunoprecipitation assays were performed to confirm the protein-protein interaction between YAP and B-MYB. Whole cell lysates of HeLa cells transiently expressing FLAG-tagged YAP and HA-tagged B-MYB were used for immunoprecipitation of YAP with a FLAG-specific antibody. Subsequent immunoblotting revealed the presence of the immunoprecipitated FLAG-tagged YAP but also of co-immunoprecipitated HA-tagged B-MYB, indicating the interaction between YAP and B-MYB (**Figure 24C**). Considerably, HA-tagged B-MYB could not be detected in immunoprecipitated lysates of HeLa cells expressing only HA-tagged B-MYB but no FLAG-tagged YAP.

To verify the YAP-B-MYB interaction, immunoprecipitation experiments of endogenous YAP and B-MYB from nuclear extracts of murine KPL2 cells were performed. In these experiments, endogenous YAP was co-precipitated with endogenous B-MYB and vice versa (**Figure 24D**). Importantly, neither YAP nor B-MYB were detected in immunoprecipitates of nonspecific IgG.

Together, the results from PLA and co-immunoprecipitation assays revealed that YAP physically interacts with LIN9 and B-MYB of the MMB complex.

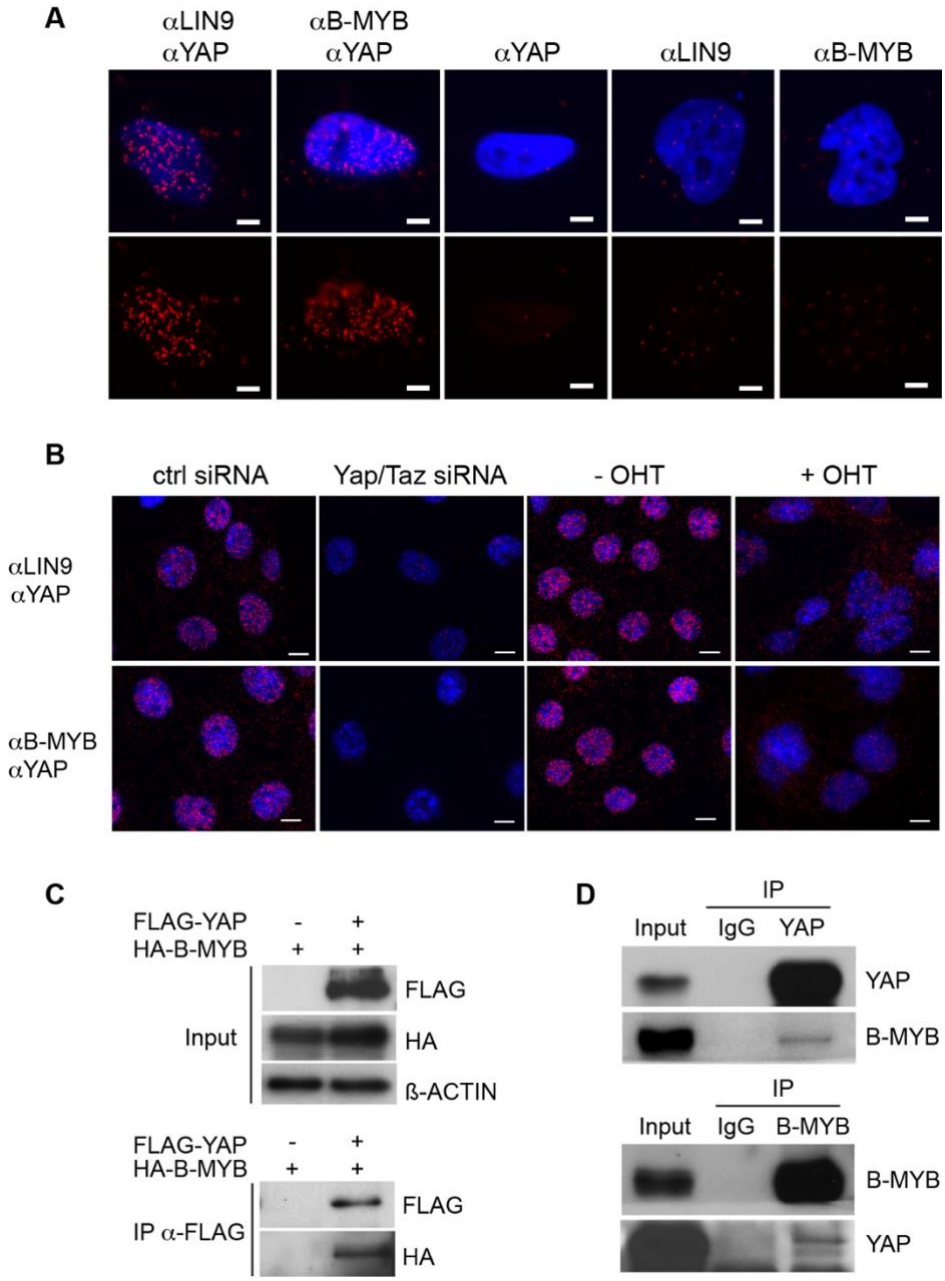

Figure 24: YAP physically interacts with LIN9 and B-MYB of the MMB complex.
(**A**) Proximity ligation assays (PLA) in HeLa cells using YAP, LIN9, and B-MYB specific antibodies. Detected dimers are represented by red fluorescent dots. Nuclei were counterstained using Hoechst (blue). Incubation with either YAP, LIN9, or B-MYB antibody alone was used as a negative control. Scale bars: 5 µm. (**B**) PLA of LIN9 and YAP or B-MYB and YAP was performed in KPL2 cells transfected with control (ctrl) or *Yap/Taz*-specific siRNAs or in untreated (- OHT) or 4-OHT-treated (+ OHT) KPL2 cells to delete *Lin9*. Nuclei were counterstained with Hoechst (blue). Specificity of the interactions was confirmed by the reduced number of red fluorescent dots upon depletion of *Yap/Taz* (left) or 4-OHT-induced deletion of *Lin9* (right). Scale bars: 10 µm. (**C**) Whole cell lysates of HeLa cells transiently expressing FLAG-tagged YAP and HA-tagged B-MYB were used for immunoprecipitation (IP) with FLAG-specific antibodies and subsequent immunoblotting with FLAG- and HA-specific antibodies. 2% of the amount used for the IP was loaded onto the gel as an input control. ß-ACTIN levels were determined as a loading control. (**D**) Nuclear extracts of KPL2 cells were used for immunoprecipitation of endogenous YAP and B-MYB followed by immunoblotting of both B-MYB and YAP to analyze co-immunoprecipitation. Immunoprecipitation with nonspecific IgG was used as a control. 6.25% of the amount used for the IP was used as input material to verify the presence of endogenous proteins and to detect ß-ACTIN levels as loading controls. (**A-B**) PLA and microscopy were performed by Stefan Gaubatz.

3.12 MMB is required for YAP-induced mitotic gene expression and entry into mitosis

To address whether LIN9 and B-MYB are important for the biological function of YAP, asynchronous MCF10A YAP5SA cells were transfected with siRNAs against *LIN9* or *MYBL2* and subsequently, treated with doxycycline to induce YAP5SA expression. Immunofluorescent staining of phosphorylated histone H3, a marker of mitotic cells, showed that YAP is able to promote mitosis, since the induction of YAP5SA significantly increased the number of pH3-positive cells from 3.5% in untreated siCtrl-transfected cells to approx. 8% in doxycycline-treated siCtrl-transfected cell (**Figure 25A, 25B**). The percentage of pH3-positive cells in doxycycline-treated cells was almost equal to that in untreated cells when cells were transfected with siLIN9 or siMYBL2, indicating that YAP5SA was unable to induce mitosis when *LIN9* or *MYBL2* were depleted (**Figure 25A, 25B**).

Moreover, doxycycline-treatment of quiescent serum-starved MCF10A cells transfected with a control siRNA dramatically increased the percentage of pH3-positive cells from 0% to approx. 30%, indicating that YAP is capable of stimulating quiescent cells to re-enter mitosis (**Figure 25C, 25D**). This increase in the number of mitotic cells correlated with a strong induction of several YAP and MMB co-regulated genes such as *KIF23*, *AURKA*, and *TOP2A* but also with a strong increase of *MYBL2* expression (**Figure 25E**). Depletion of both *LIN9* and *MYBL2* strongly impaired the ability of YAP5SA to induce both mitotic gene expression and re-entry into mitosis in serum-starved cells (**Figure 25C-E**). In summary, these findings indicate that YAP needs the MMB complex to fully activate mitotic gene expression and to promote entry into mitosis.

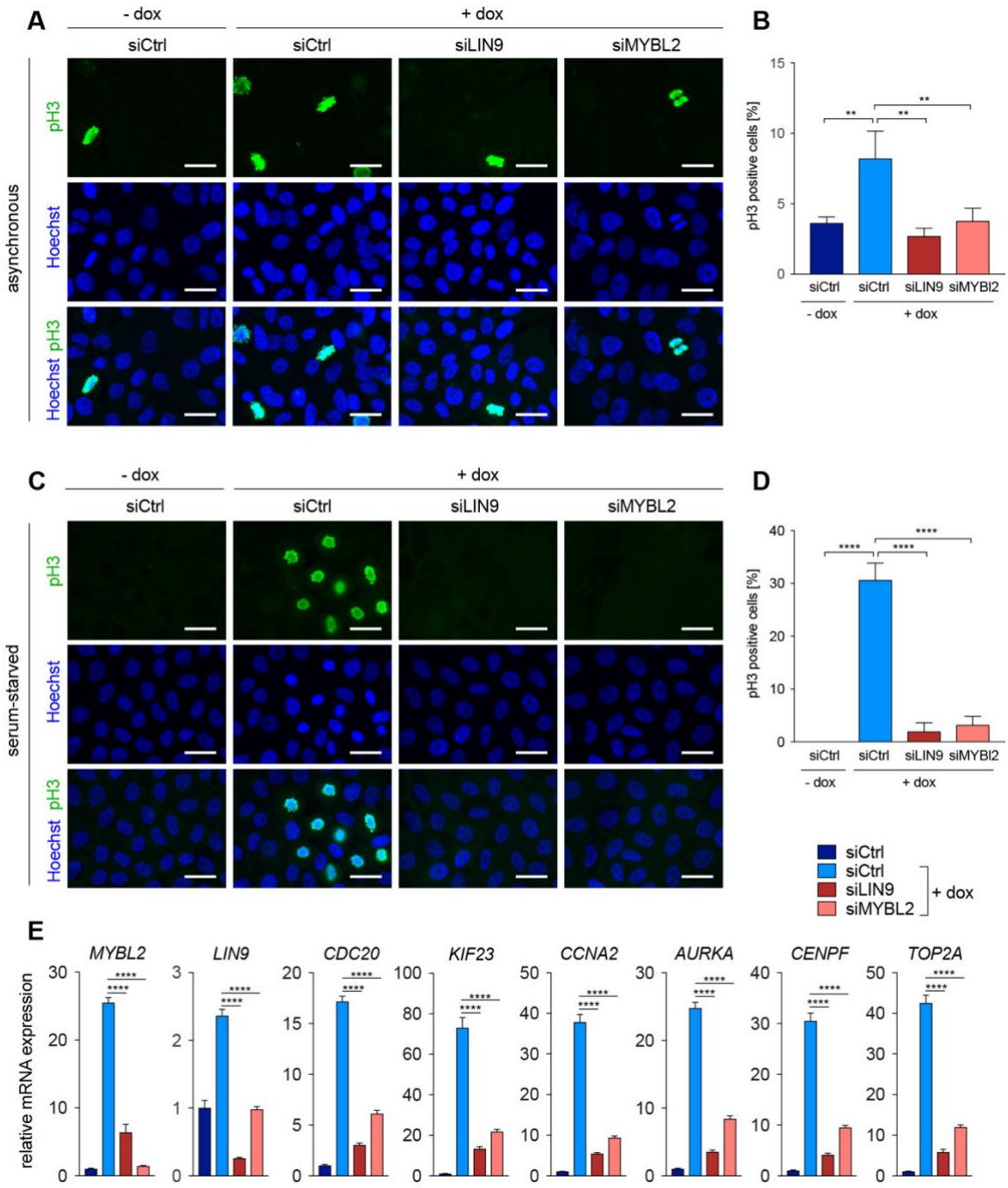

Figure 25: MMB is required for YAP-induced expression of mitotic genes and entry into mitosis.
(**A**) MCF10A YAP5SA cells were transfected with control siRNA or siRNA specifically targeting human *LIN9* or *MYBL2*. YAP5SA expression was induced by adding 0.5 µg/ml doxycycline 24 h after siRNA transfection. 24 h later, cells were fixed and immunostained with a phosphorylated histone H3 (pH3) specific antibody. Nuclei were counterstained with Hoechst (blue). Shown are microscopic examples. Scale bars: 25 µm. (**B**) Quantification of pH3-positive cells shown in (**A**). Depicted are the means and SD of three independent experiments. Per condition and experiment at least 500 cells were counted. Statistical significance was analyzed using one-way ANOVA and Tukey's post-test. (**C**) MCF10A YAP5SA cells were starved with serum- and EGF-free medium for 48 h and transfected with control siRNA or siRNA specifically targeting human *LIN9* or *MYBL2*. YAP5SA expression was induced with 0.5 µg/ml doxycycline 24 h after siRNA transfection. 14 h after adding dox, cells were treated with 50 ng/ml nocodazole for 24 h to arrest cells in G2/M phase of the cell cycle. Cells were fixed and immunostained with a pH3-specific antibody. Nuclei were counterstained with Hoechst (blue). Shown are microscopic examples. Scale bars: 25 µm. →

3.13 Genes co-regulated by MMB and YAP are clinically relevant for cancer patients

In order to determine whether genes co-regulated by YAP and MMB are clinically relevant for cancer, cDNA microarray data sets of human lung tumor samples published by Garber et al. (2001) were analyzed for genes co-expressed with *MYBL2*. Of the top 20 genes co-expressed with *MYBL2* in large-cell lung cancer (LCLC), lung adenocarcinoma, small-cell lung cancer (SCLC), and squamous cell lung cancer (SqCLC), 11 genes are known YAP target genes (**Figure 26A**). The expression of YAP target genes correlated with the expression of *MYBL2* in these lung cancer samples as can be seen from the correlation coefficients depicted in **Figure 26B**.

Lung tumors isolated from *K-Ras*$^{LSL\text{-}G12D/+}$*; p53*$^{fl/fl}$ mice 16 weeks after tumor initiation by infection with Cre-expressing lentivirus were immunohistochemically stained with antibodies specific for activated B-MYB and YAP. Microscopic examination revealed that both B-MYB and YAP are co-expressed at high levels in murine lung adenocarcinoma tissue (**Figure 26C**). Notably, the expression of common YAP/MMB target genes correlated with the overall survival of lung adenocarcinoma patients as shown in the Kaplan-Meier plots in **Figure 26D**. Lung cancer patients with tumors expressing high levels of genes co-regulated by YAP and MMB, such as *CDC20* and *TOP2A*, had a significantly shorter overall survival than patients with lung tumors expressing low levels of these genes (**Figure 26D, top**). By contrast, high expression of genes only regulated by YAP but not by MMB (*AMOTL2*, *CYR61*, and *SDPR*) correlates with a better and longer survival of patients (**Figure 26D, bottom**). Together, these data indicate that YAP and B-MYB themselves but also their co-regulated target genes are expressed at elevated levels in lung tumors and are associated with a poor prognosis and a shorter overall survival of lung cancer patients.

(**D**) Quantification of pH3-positive cells shown in (**C**). Depicted are the means and SD of three independent experiments. Per condition and experiment at least 700 cells were counted. Statistical significance was analyzed using one-way ANOVA and Tukey's post-test. (**E**) RNA was isolated of serum-starved MCF10A YAP5SA cells treated as described in (**C**). mRNA expression of the indicated genes measured by qPCR is depicted relative to the mRNA expression in siCtrl untreated (-dox) cells. *GAPDH* was used for normalization. The experiment was performed three times independently. Shown are the means and SD of one representative example. Statistics of technical replicates was done using one-way ANOVA followed by Tukey's post-test. (**B,D,E**) Asterisks are as follows: $^{**}P \leq 0.01$; $^{****}P \leq 0.0001$

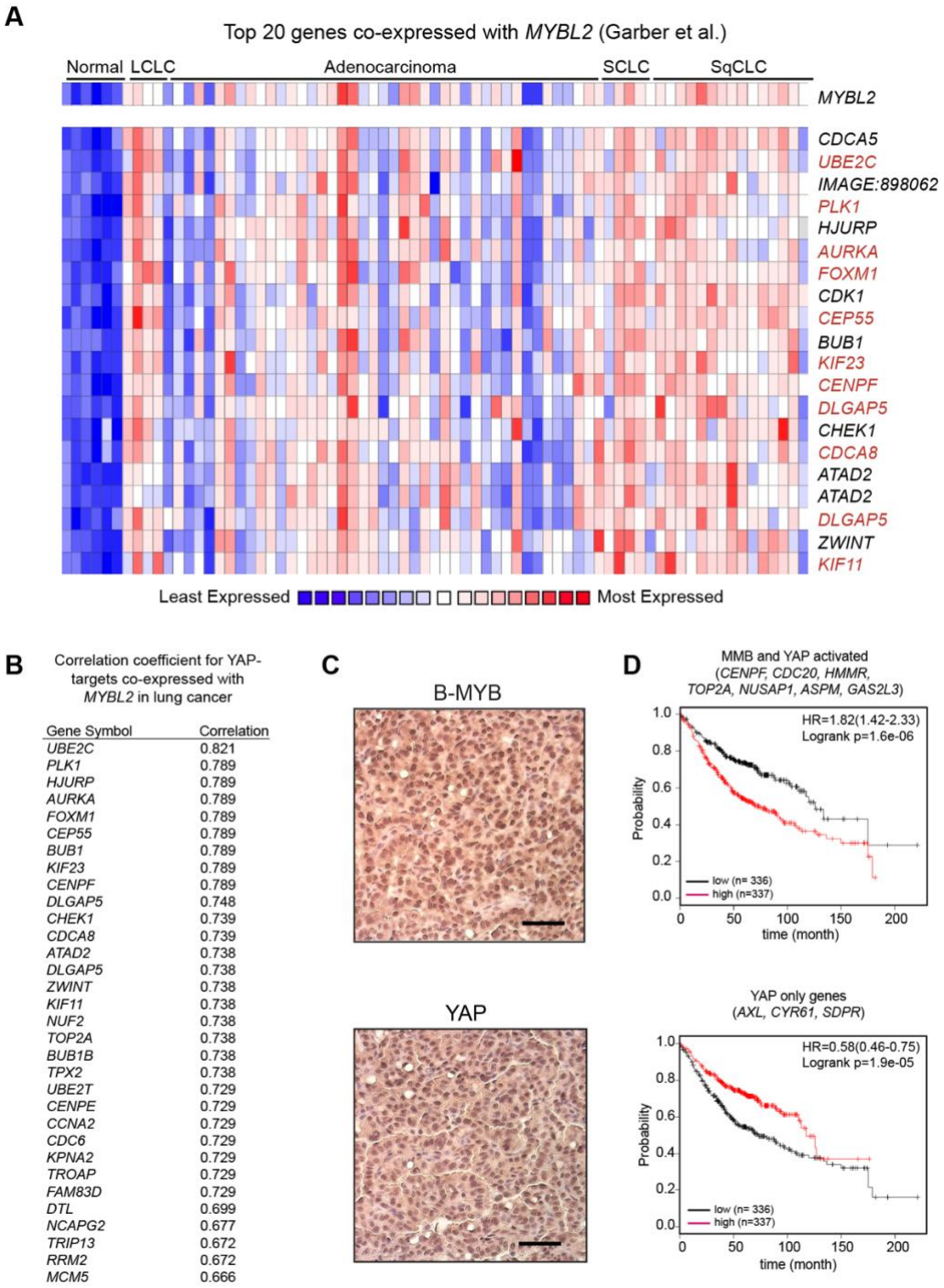

Figure 26: Genes co-regulated by MMB and YAP are relevant for cancer.
(**A**) Heat map from Oncomine analysis of genes co-expressed with *MYBL2* in different types of lung cancer described by Garber et al. (2001). Shown are the top 20 *MYBL2* co-expressed genes with known YAP target genes depicted in red. Blue represents least and red most expressed genes in the heat map. (**B**) Correlation coefficients of YAP target genes co-expressed with *MYBL2* in lung cancer (Garber et al. 2001). (**C**) *K-Ras*$^{LSL-G12D/+}$*; p53*$^{fl/fl}$ mice were infected with Cre-expressing lentivirus to induce tumorigenesis by activation of oncogenic K-RAS G12D and loss of p53. 16 weeks after tumor initiation, lungs were dissected. Expression of B-MYB (phospho-T487) and YAP in paraffin embedded lung adenocarcinoma tissue was analyzed by immunohistochemistry. Nuclei were counterstained with hematoxylin. Scale bars: 50 µm. (**D**) Kaplan-Meier plots showing the overall survival of lung cancer patients with low (black) or high (red) expression of the indicated common MMB and YAP regulated genes (top) or YAP-only target genes (bottom). HR, hazard ratio

4 Discussion

4.1 MMB – a potential target for the treatment of cancer

The first part of this thesis dealt with the analysis of gene and cell cycle regulation by MMB in cancer cells. MMB directly regulates the expression of a large panel of late cell cycle genes. Strikingly, B-MYB, FOXM1, and several MMB target genes are frequently overexpressed in human cancers and are part of a gene signature that is associated with a poor clinical outcome in cancer patients, suggesting a role for MMB in tumorigenesis (Carter et al. 2006; Sadasivam and DeCaprio 2013). Although this complex has been widely characterized biochemically, the exact mechanisms how increased expression of MMB target genes promotes tumor growth *in vivo* have not been investigated so far. Recently, our laboratory could show that the loss of LIN9 or B-MYB leads to reduced tumor formation in a mouse model for NSCLC driven by oncogenic K-RAS and loss of p53, indicating that MMB indeed plays a role in tumorigenesis *in vivo* (Iltzsche et al. 2017).

In first experiment of this thesis, it was shown that the complete loss of LIN9 in primary lung adenocarcinoma cells established from lung tumors of *K-Ras*$^{LSL\text{-}G12D/+}$*; p53*$^{fl/fl}$*; Lin9*$^{fl/fl}$ mice of the aforementioned study strongly impairs the ability of tumor cells to proliferate and to progress properly through mitosis and cytokinesis. Furthermore, genome-wide expression analysis revealed that the loss of LIN9 leads to decreased expression of genes mainly associated with mitotic and cytokinetic processes such as microtubule binding, mitotic spindle assembly, and chromosome segregation.
Thus, proliferation defects and mitotic abnormalities upon *Lin9* deletion are most likely a result from the restricted expression of late cell cycle genes. These findings from cell culture experiments provide a mechanistic explanation why tumor cells are dependent on functional LIN9 and how the loss of LIN9 restrains lung tumorigenesis *in vivo* (Iltzsche et al. 2017). Based on these results, MMB could be considered as a therapeutic target for cancer. Targeting MMB could be especially relevant for *K-RAS*-mutated tumors, such as non-small cell lung cancer (NSCLC), as it was shown recently that *K-RAS* mutant cells undergo mitotic stress and are thus selectively sensitive to the loss of mitotic genes (Sarthy et al. 2007; Luo et al. 2009; Weng et al. 2012). However, direct targeting of MMB might be difficult because MMB does not contain any enzymatic activity. As MMB is a multiprotein complex whose structural composition is based on the interaction between the distinct proteins, one challenging but not impossible strategy to target MMB might be by disrupting protein-protein interactions of certain MMB subunits.

To approach this, one might consider the use of structure-based drug design. However, to design drugs based on the structure of MMB, further structural characterization of MMB and the interaction between the distinct subunits is required (Modell et al. 2016). So far, only parts of the crystal structure of DREAM but not of MMB have been published (Guiley et al. 2015).

The use of the recently developed strategy of phthalimide conjugation for protein degradation by the laboratory of James E. Bradner might provide another mechanism to specifically target MMB subunits for degradation (Winter et al. 2015). In this strategy, the target protein is marked for proteasomal degradation using a bifunctional ligand in which one part is specific for binding to the target protein and the other part is conjugated to phthalimide, which has been shown to bind cereblon, a member of a cullin-RING ubiquitin ligase (CRL) complex.

However, the disruption of the interaction between specific MMB subunits or the degradation of certain MMB subunits would lead to the complete loss of MMB. This might be lethal for both normal non-transformed and transformed cancer cells because it was shown that deletion of *Lin9* in adult mice rapidly leads to lethality (Reichert et al. 2010).

As mentioned before mitotic and cytokinetic MMB target genes are part of gene signatures that are associated with a poor clinical outcome of cancer, e.g., of lung and breast cancer (Paik et al. 2004; Carter et al. 2006; Tian et al. 2010). Studies of our laboratory showed that the shRNA-mediated depletion of the MMB target genes *Kif23* or *Prc1* inhibits lung tumor formation in a mouse model for NSCLC (Iltzsche et al. 2017; Hanselmann et al. 2018). Notably, it was shown that *in vitro*, non-tumorigenic BJ cells are much less sensitive to *PRC1* inhibition than several tumor cell lines, indicating an increased sensitivity of tumor cells towards the depletion of *PRC1* (Hanselmann et al. 2018). MMB targets include several mitotic kinesins, which are microtubule-based motor proteins and contain enzymatic activity. Mitotic kinesis are considered as useful druggable targets for cancer therapy (Huszar et al. 2009). In contrast to the commonly used anti-mitotic agents, such as microtubule-targeted drugs, mitotic kinesin inhibitors are thought to be more selective and to have less side effects due to the specific mitotic function of each kinesin (Huszar et al. 2009). Currently, promising substances targeting the two mitotic kinesins EG5 (also known as KSP or KIF11) and CENPE have entered phase I and II clinical trials (Rath and Kozielski 2012; Song et al. 2013).

Besides targeting downstream targets of MMB or complete inhibition of the MMB complex, disrupting the interaction of MMB with YAP, which was identified in this thesis, might lead to reduced MMB target gene expression and thus provide another potential strategy for the development of cancer therapeutics.

4.2 YAP activates the transcription of mitotic and cytokinetic MMB target genes

The characterization of the MMB-dependent transcriptome in murine *Lin9*-deleted lung cancer cells revealed that LIN9-dependent genes include several genes known to be regulated by YAP. YAP together with its paralog TAZ are effector proteins of the Hippo pathway (Ehmer and Sage 2016).

The second and major part of this thesis dealt with the characterization of the newly identified crosstalk between YAP and the MMB complex. The results showed that YAP and MMB co-regulate a same set of late cell cycle genes with important functions during mitosis and cytokinesis but also revealed a mechanism for the interaction between YAP and MMB and the co-regulation of common genes.

YAP has been well-known for being an important regulator of cell proliferation (Ehmer and Sage 2016). Several studies have shown that YAP cooperates with the two transcription factors E2F and Myc to regulate the expression of early cell cycle genes and thus to mediate G1-to-S transition (Mizuno et al. 2012; Ehmer et al. 2014; Kapoor et al. 2014; Shen and Stanger 2015; Croci et al. 2017). DePinho and colleagues, for instance, could show that elevated expression of YAP due to amplification of the *Yap* gene locus mediates tumor relapse of KRAS bypassed pancreatic ductal adenocarcinoma (PDAC) (Kapoor et al. 2014). These findings are in line with those of Shao et al. (2014b) showing that YAP promotes cell survival in KRAS-dependent tumor cells upon suppression of KRAS. Enrichment of E2F binding sites at the promoter of YAP targets suggested that YAP/TEAD act cooperatively with E2F to rescue G1/S genes that control cell proliferation, DNA synthesis, and replication in KRAS bypassed tumors (Kapoor et al. 2014). All of these findings support a role and show a mechanism of YAP for the regulation of G1/S genes and thereby for mediating cell cycle entry.

However, the YAP/TEAD-regulated genes found by Kapoor et al. (2014) in murine pancreatic tumors also included several late cell cycle G2/M genes such as *Aurka*, *Aurkb*, *Ccna2*, *Ccnb1*, *Ccnb2*, and *Cdc20*. These findings are similar to that of Zanconato et al. (2015) showing that YAP regulates genes important for both S-phase and mitosis. The authors further showed that promoters of YAP-regulated genes are enriched for E2F motifs and thus hypothesized that YAP cooperates from enhancers with E2F bound to promoters to regulate cell cycle gene expression (Zanconato et al. 2015). The activation of G2/M genes by YAP was confirmed in several cancer types such as in hepatocellular carcinoma, embryonal rhabdomyosarcoma, and breast cancer but also in non-transformed lung epithelial cells (Bai et al. 2012; Tremblay et al. 2014; Lange et al. 2015; Zanconato et al. 2015).

In contrast to early cell cycle genes, however, the promoters of G2/M genes do not contain E2F binding sites. Instead, G2/M gene promoters are enriched for CHR-binding motifs, which are known to be bound by LIN54 of the MMB complex (Elkon et al. 2003; Linhart et al. 2005; Zhu et al. 2005; Schmit et al. 2009; Muller et al. 2014). It is thus unlikely that YAP co-regulates G2/M genes together with E2F and so far, no suitable mechanism has been shown how YAP induces the expression of late cell cycle genes.
Consistent with the aforementioned findings of other laboratories, expression analyses in this thesis revealed that YAP regulates the expression of G2/M genes in both murine and human lung cancer cells but also in non-transformed breast epithelial cells. However, the results of this work extend previously published data by showing that a large panel of G2/M genes are co-regulated by YAP and MMB and by indicating that MMB is required for YAP-dependent activation of G2/M gene expression (**Figure 25**).

4.3 YAP induces the expression of B-MYB and enhances chromatin-association of LIN9 and B-MYB

The findings of this thesis go beyond previously published data by revealing that YAP regulates G2/M gene expression in at least two ways: first, by inducing the expression of the MMB subunit B-MYB and second, by promoting chromatin-association of LIN9 and B-MYB at the promoters of several mitotic and cytokinetic genes. Mechanistically, analyses from ChIP-seq and 4C-seq experiments indicate that YAP binds to distal enhancers that interact with MMB-bound promoters via chromatin looping. The results of PLA and Co-IP assays support a model of long-range interaction between enhancers bound by YAP and promoters bound by MMB by showing that YAP physically interacts with LIN9 and B-MYB. It was shown before that YAP interacts with FOXM1 - a transcription factor that is known to associate with MMB to form the FoxM1-MMB complex (Eisinger-Mathason et al. 2015; Fischer and Muller 2017; Weiler et al. 2017). However, interactions of YAP with B-MYB or with LIN9 have been unknown so far.
Comparing the Hi-C promoter-enhancer interaction map published by Jin et al. (2013) with ChIP-seq data of YAP and LIN9 showed that genes bound by LIN9 but not those without LIN9 binding are significantly regulated by YAP in RNA-seq. This suggests that LIN9 binds to a subset of cell cycle genes, which are activated by YAP from distant enhancers. The observation from this work that the vast majority of YAP binding sites are located in enhancers or super-enhancers in both murine and human cells is consistent with data from several other publications showing that YAP modulates transcription from distant enhancers (Galli et al. 2015; Stein et al. 2015; Zanconato et al. 2015).

Using ChIP-seq and a published Hi-C promoter-enhancer interaction map by Jin et al. (2013), Zanconato et al. (2015) could previously show that YAP/TAZ/TEAD form a complex with AP-1 (JUN/FOS). This complex binds almost exclusively to distal enhancer sites that interact with promoters of cell cycle genes through chromatin looping.

Experiments from inhibiting endogenous YAP and from activating YAP5SA in this thesis clearly showed that YAP regulates the expression of the B-MYB encoding gene *MYBL2*. In contrast, *LIN9* expression was neither influenced by inhibition nor by activation of YAP. This indicates that YAP regulates *MYBL2* but not *LIN9* expression. Interestingly, FOXM1 has been identified as a YAP target gene before (Mizuno et al. 2012; Eisinger-Mathason et al. 2015; Fan et al. 2015; Weiler et al. 2017). In addition, previous studies identified the two MYB family members A-MYB and c-MYB to be regulated by YAP (Mizuno et al. 2012; Mohseni et al. 2014; Zanconato et al. 2015). The findings of this thesis show for the first time that also B-MYB is a YAP target gene.

Previously it was shown that YAP induces the expression of the long noncoding RNA (lncRNA) metastasis-associated lung adenocarcinoma transcript 1 (MALAT1), which in turn was shown in another publication to activate the expression of B-MYB (Tripathi et al. 2013; Wang et al. 2014). These data suggest one possible way in which YAP might regulate the expression of B-MYB. In addition, ChIP- and 4C-seq from this study provide another mechanism by revealing that YAP does not directly bind to the promoter of *MYBL2*, but instead binds to a -12 Mb away from the TSS located enhancer that interacts with the *MYBL2* promoter through chromatin looping.

However, this result from 4C-seq only provides topological information and the functional relevance for this region has yet to be investigated. This could be done, e.g., by analyzing whether deletion of the identified *MYBL2* enhancer using CRISPR-Cas9 results in reduced B-MYB expression or affects formation of the chromatin loop. Furthermore, the promoter-associated interaction partners of YAP for regulating *MYBL2* expression from the distal enhancer remain unknown. One possibility might be that YAP cooperates from the *MYBL2* enhancer with E2F transcription factors, which are known to regulate cell-cycle dependent expression of *MYBL2* by direct binding to the *MYBL2* promoter (Liu et al. 1996; Zwicker et al. 1996).

Interestingly, YAP induced the expression of B-MYB at mRNA and protein level only in confluent but not in subconfluent cultures, whereas it strongly induced the chromatin-association of B-MYB in both conditions. One explanation for this could emerge from routine cell culturing conditions. Cells plated on plastic cell culture dishes are growing on a very stiff substrate with a spread cell shape, which has been shown to favor nuclear localization and activity of YAP in response to ECM stiffness (Dupont et al. 2011).

Seeding cells at a very high density leads to contact inhibition due to enhanced cell-cell contacts, thereby inducing cytoplasm translocation and inactivation of YAP (Meng et al. 2016). This allows to analyze the effects of YAP5SA overexpression without background activity of endogenous YAP in confluent cells. Thus, the effects of YAP5SA induction on the expression of B-MYB in subconfluent cells might be blunted by a higher basal background activity of endogenous YAP. What argues against this, however, is that the basal DNA binding of endogenous YAP in non-induced (-doxy) MCF10A YAP5SA cells seeded at subconfluent conditions was overall very weak and only slightly stronger than in cells seeded at confluent conditions (**Figure 22** and **Figure 23**). For further experiments, it could be considered to grow cells at high confluence on soft substrates such as fibronectin-coated acrylamide hydrogels with a stiffness of 0.7 kPa as it was shown by Dupont et al. (2011) to completely exclude blunting effects due to basal activity of endogenous YAP.

That the enhanced binding of MMB to promoters of G2/M genes upon YAP5SA induction is a secondary effect arising from increased cell proliferation and an enhanced number of cells in G2/M is unlikely given that *MYBL2* mRNA expression, which is cell cycle regulated, was unchanged in subconfluent cells (Liu et al. 1996; Zwicker et al. 1996). However, to completely exclude this possibility, future experiments could aim at having a closer look at cell cycle profiles upon YAP induction. Specifically, MCF10A YAP5SA cells could be induced for YAP5SA expression for different periods of time as it was done in **Figure 21A** followed by analyses of cell cycle profiles by flow cytometry, MMB target gene expression, and chromatin binding of MMB to G2/M gene promoters.

Overall, YAP5SA induction did not increase the expression of *LIN9*, instead it even led to slightly decreased *LIN9* mRNA levels in subconfluent cells although it simultaneously strongly promoted binding of LIN9 to promoters of MMB target genes. These results together with the physical interaction of YAP with B-MYB or with LIN9 indicate that the enrichment of B-MYB and LIN9 at promoters of G2/M genes upon YAP5SA induction does not only occur due to increased B-MYB and LIN9 expression levels but rather due to so far unknown mechanisms.

Notably, the basal binding of LIN9 in untreated non-induced cells was much stronger in confluent than in subconfluent cells, at least for three out of four promoters (**Figure 22**). For the binding of B-MYB it was exactly the other way around: At all four analyzed promoters, basal B-MYB binding in non-induced cells was weaker in confluent than in subconfluent cells, which is likely to result from the reduced expression of B-MYB in confluent cells. As a mixture of asynchronously growing cells was used for this assay, the different distribution of cells in the distinct phases of the cell cycle might explain the different basal LIN9 levels in confluent and subconfluent cells.

The high occupancy of LIN9 at promoters in confluent cells might reflect LIN9 as a part of the repressor DREAM complex and occur due to an increased number of arresting cells in G0/G1 as a result of contact inhibition. However, there are reasons to doubt this hypothesis. Although promoters in subconfluent cells might be less occupied by LIN9 as a part of DREAM, they should conversely be more occupied by LIN9 as a part of MMB. This idea is supported by previous data from our laboratory showing that, unlike B-MYB binding, there is no difference in LIN9 binding at promoters of G2/M genes between quiescent and S-phase cells (Osterloh et al. 2007).

Overall, results from ChIP assays raise the question whether YAP promotes binding of B-MYB to promoters already pre-bound by the MuvB core or whether YAP recruits the complete MMB complex to G2/M gene promoters. It is not possible to answer this question on the basis of the results of this thesis. However, in order to approach this issue, future studies could initially focus on determining how induction of YAP influences the binding of B-MYB and LIN9 in distinct cell cycle phases by carrying out ChIP experiments with chromatin isolated from synchronized cells. Future research should further investigate the enhanced chromatin-association of B-MYB upon YAP induction, for instance by using cells stably expressing either doxycycline-inducible B-MYB alone or both doxycycline-inducible B-MYB and YAP5SA. Using ChIP-assays and PI-flow cytometry, one could first analyze whether induction of B-MYB alone is able to promote replacement of DREAM by MMB and to induce cell cycle progression in serum-starved cells. Second, one could analyze whether overexpression of YAP5SA next to overexpressed B-MYB further increases cell cycle progression and binding of MMB to promoters of G2/M genes .

Currently, it remains unclear how the interaction between MMB and YAP is mediated and whether other proteins or protein complexes are involved (**Figure 24**). Recently, Dong and colleagues have shown that, next to the known inhibitory phosphorylation of YAP by LATS kinases, YAP is phosphorylated at several residues by CDK1 during G2/M. CDK1-mediated phosphorylation of YAP was sufficient to promote cell migration and invasion (Yang et al. 2013). However, the biological role of the CDK1-mediated phosphorylation of YAP during G2/M is largely unknown. As this phosphorylation specifically occurs during G2/M and promotes the mitotic function of YAP, it might be necessary for mediating the interaction between MMB and YAP. To address this question, it would be initially important to see whether the interaction between YAP and MMB is restricted to specific phases of the cell cycle. This could be done by synchronizing cells at specific stages of the cell cycle and analyze the interaction of YAP with B-MYB or with LIN9 for example by PLA or by Co-IP experiments.

To analyze whether CDK1-mediated phosphorylation is needed for the MMB-YAP interaction, future experiments could use the phosphorylation-deficient YAP3A or 4A mutants generated by Yang et al. (2013). In the YAP3A mutant, the CDK1 phosphorylation sites at threonine-119, serine-289, and serine-367 are mutated to the non-phosphorylatable alanine. The YAP4A mutant additionally contains the S127A mutation that prevents inhibition of YAP by LATS kinases (Yang et al. 2013).
Moreover, future work could aim to identify the specific domain of the YAP protein that is needed for the interaction with MMB by performing co-immunoprecipitation studies with truncated YAP deletion mutants. Finding a YAP deletion mutant that fails to interact with MMB but is still capable to interact with TEAD could give further information about the importance of the MMB-YAP interaction for the ability of YAP to induce the expression of G2/M genes and mitosis. Despite mapping the interaction domain of YAP, one could perform affinity purifications using differentially tagged constructs of YAP and B-MYB followed by mass spectrometry to identify other proteins that might be involved in the interaction between YAP and MMB.

4.4 MMB is required for YAP-induced cell cycle progression

The ability of YAP to induce mitotic gene expression and cell cycle re-entry in serum-starved, quiescent cells was strongly dependent on MMB as demonstrated by RNAi-mediated depletion of *MYBL2* and *LIN9* and subsequent induction of YAP5SA (**Figure 25**).
It was shown recently that a Cre-mediated triple knockout of all three pocket proteins pRb, p130, and p107 (TKO) is not sufficient for prolonged proliferation of mature hepatocytes, which instead further arrest in G0/G1 (Ehmer et al. 2014). Arrested TKO hepatocytes were found to have reduced YAP/TEAD expression levels and increased inhibitory YAP phosphorylation, explaining the decreased expression of E2F target genes even after the loss of all three pocket proteins. The ectopic expression of YAP5SA triggered re-entry of TKO hepatocytes into the cell cycle, indicating that the proliferation of TKO hepatocytes was limited because of reduced YAP activity. Based on these findings and on the here presented results showing that YAP regulates G2/M gene expression together with MMB, one could speculate now that the proliferation of TKO hepatocytes is limited because of reduced YAP-dependent G2/M gene expression.
Interestingly, Piccolo and colleagues showed that in MDA-MB-231 breast cancer cells YAP activates the expression of the oncogene *MYC* by binding to a distal enhancer that interacts with the *MYC*-promoter through chromatin-looping (Zanconato et al. 2015).

Later on, data from Campaner and colleagues went beyond the aforementioned results by revealing that MYC is able to globally shift the genomic distribution of YAP and favoring the recruitment of YAP to MYC- and TEAD-bound promoter sites to activate genes required for cell cycle entry (Croci et al. 2017). They further showed that the cooperation between YAP and MYC is needed to induce gene expression and cell cycle entry in serum-starved 3T9 cells. As indicated by EdU- and BrdU-incorporation and RNA-seq experiments, YAP and MYC cooperate to specifically induce entry into S-phase by activating genes required for DNA replication, nucleotide metabolism, and pyrimidine synthesis (Croci et al. 2017).

Data of this work extend these findings by showing that YAP is able to induce cell cycle progression beyond S phase into mitosis and that this is strongly dependent on the presence of the MMB subunits LIN9 and B-MYB (**Figure 25**). The present study further indicated that overexpression of either wild-type or constitutively active YAP5SA in *Lin9*-deleted murine lung adenocarcinoma cells can partially rescue the phenotype of LIN9 loss (**Figure 10**). In another experiment, it was shown that LIN9 protein expression is completely lost after a 3-day long treatment with 4-OHT. However, transfection of YAP-overexpressing constructs in the rescue experiment was done 24 h after initiating the Cre-mediated deletion of *Lin9* by adding 4-OHT. At this time point, some LIN9 protein might still be present and YAP might be able to stabilize MMB, which would at least partly explain the reduced mitotic defects seen in YAP-overexpressing cells. This would also suggest that the phenotype of LIN9 loss in YAP-overexpressing cells only occurred time-delayed and was not yet visible at the time of cell harvest. This assumption might be addressed in future studies.

4.5 Clinical relevance for the crosstalk between MMB and YAP

Finally, co-expression of YAP targets with *MYBL2* in human lung cancer tissue and the correlation of the expression of YAP/MMB co-regulated genes with a shorter survival of lung cancer patients suggested that common MMB and YAP target genes are of clinical relevance. Whereas a high expression of genes co-regulated by YAP and MMB was associated with a poor prognosis in lung cancer patients, a high expression of well-described genes regulated only by YAP but not by MMB rather correlated with a longer survival of patients. This is consistent with what has been found by Hiemer et al. (2015) who showed that the expression of the canonical YAP/TAZ target genes *CTGF* and *CYR61* did not significantly change with regard to tumor onset, grade, and stage of oral squamous cell carcinoma (OSCC).

In contrast, a high expression of *AURKA* and *BIRC5*, which were found in this thesis to be co-regulated by MMB and YAP, correlated with a higher tumor grade and a more advanced stage of OSCC (Hiemer et al. 2015). It is noteworthy that YAP has been found to be active and nuclear in several cancer types including late-stage ovarian, colon, gastric, liver, esophageal, and non-small cell lung cancers (Piccolo et al. 2014). Moreover, several previously published studies have shown that the activation of YAP is associated with progression, a poor prognosis, and more frequent relapse of non-small cell lung cancer (Wang et al. 2010; Kim et al. 2015; Guo et al. 2017).

Recently the kinase and tumor suppressor LKB1 was identified to regulate YAP activity in a negative manner (Mohseni et al. 2014). *LKB1*, also known as *STK11*, is somatically mutated in 15% to 30% of NSCLC and is thus, next to *TP53*, one of the most frequently mutated tumor suppressors in human lung cancer (Ding et al. 2008; Zhang et al. 2015b). Interestingly, deletion of *Yap* significantly inhibited lung adenocarcinoma (ADC) progression in $Kras^{G12D}$-activated, *Lkb1*-deficient mice (Zhang et al. 2015b). Additionally, Survivin, also known as BIRC5, was identified to act as a downstream mediator of YAP in promoting malignant progression of $Kras^{G12D}$-activated, *Lkb1*-deficient lung ADC. Although Survivin was demonstrated to be regulated by YAP, no exact mechanism for this regulation was shown. In the present study, *Survivin/BIRC5* was one of the genes found to be co-regulated by MMB and YAP, suggesting that it is regulated by YAP from a distal enhancer that interacts with the MMB-bound promoter in a similar way as it was shown here for other common MMB/YAP targets.

An important question that arises from this study and that should be addressed in future work is whether the oncogenic property of YAP to promote tumor growth *in vivo* is mediated through the interaction with MMB. This could be addressed using a recently described lung cancer mouse model of *LSL-*$Kras^{G12D}$*; LSL-rtTA; tetO-YAPS127A* mice in which activation of YAP promotes KRAS G12D-initiated lung tumor progression (Lau et al. 2014). In this model, mice harbor a doxycycline-inducible constitutively active allele of *Yap1* (*tetO-YapS127A*) in addition to Cre-inducible conditional alleles of oncogenic *LSL-*$Kras^{G12D}$ and of the reverse-tetracycline transactivator (*LSL-rtTA*). Lung tumorigenesis is initiated by intranasal infection of mice with Adeno-Cre, which activates KRAS G12D and rtTA. This is followed by treatment with doxycycline to activate YAP along with tumor initiation. On the assumption that future work will uncover the specific motif in the YAP protein that mediates the interaction with MMB, one could consider generating mice with the aforementioned genetic background expressing a dox-inducible mutant of YAP, which is unable to interact with MMB. Analyzing the tumor progression in those mice compared to mice expressing YAP that is still able to interact with MMB might reveal whether the interaction with MMB contributes to the tumor promoting characteristics of YAP.

4.6 Working model and conclusion

MuvB has been linked to the Hippo pathway in previously published studies. The Hippo kinase LATS2 has been shown to enhance the ability of DYRK1A to phosphorylate the MuvB subunit LIN52, thereby promoting the assembly of the repressor DREAM complex (Litovchick et al. 2011; Tschop et al. 2011) (**Figure 27, left**). DYRK1A-mediated phosphorylation of LIN52 was important to enter quiescence or senescence.

The results reported here substantially extend the knowledge of the connection between Hippo and MuvB by showing that Hippo signaling acts through the downstream effector YAP independently from DYRK1A by regulating the activator Myb-MuvB/MMB subunit B-MYB. More specifically, the results support a model in which YAP regulates the expression of G2/M genes in at least two ways (**Figure 27**, **right**). First, YAP induces the expression of B-MYB by binding to a -12 Mbp from the TSS located distal enhancer that interacts with the promoter of *MYBL2* through chromatin-looping. Second, YAP interacts with B-MYB and promotes binding of B-MYB to the promoters of mitotic and cytokinetic genes through binding to distal enhancers that interact with MMB-regulated promoters through chromatin looping.

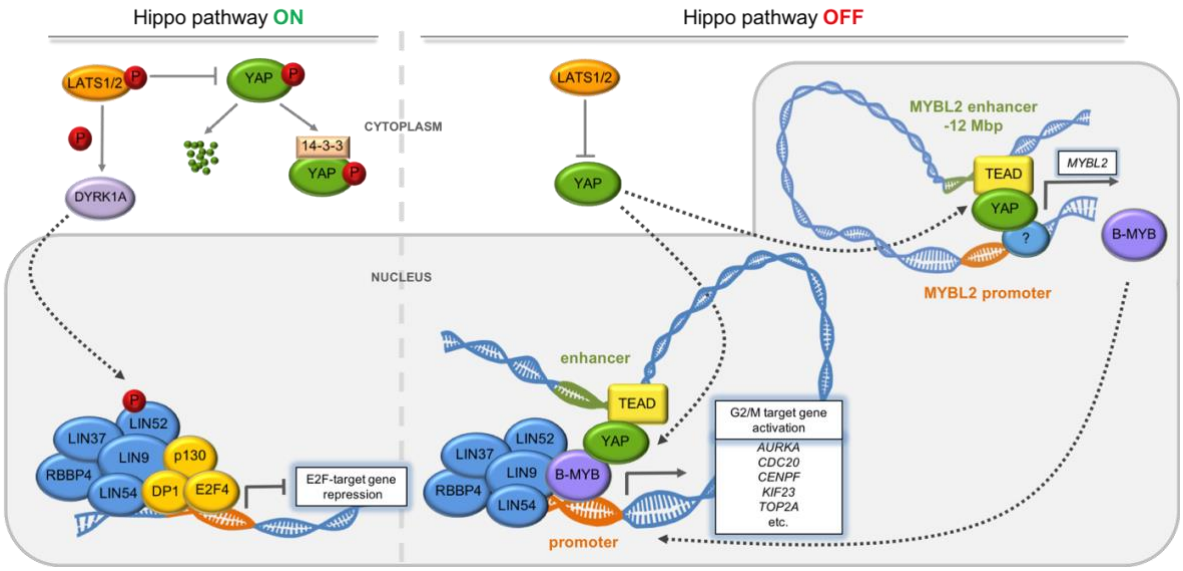

Figure 27: Model for the crosstalk between MMB and YAP.
Model for the crosstalk between DREAM/MMB and Hippo signaling based on published data and data from this thesis. **Left:** When Hippo signaling is ON, LATS1/2 kinases phosphorylate YAP leading to its cytoplasmic retention and degradation. LATS2 phosphorylates and activates DYRK1A, which in turn phosphorylates LIN52 of the MuvB core, thereby promoting the assembly of the repressor DREAM complex (Litovchick et al. 2011; Tschop et al. 2011). **Right:** When Hippo signaling is OFF, YAP can translocate into the nucleus and binds with TEAD proteins to distal enhancer regions of G2/M genes. One of the YAP target genes is *MYBL2*, the gene encoding for B-MYB, which is regulated through binding of YAP to a distal enhancer located 12 Mbp upstream of the TSS. YAP promotes binding of B-MYB to promoters and communicates from distal enhancers with MMB-bound promoters of G2/M genes via chromatin looping.

Collectively, these results provide for the first time a mechanism for the transcriptional regulation of G2/M genes by YAP through its association with the MMB complex. Thus, inactive Hippo signaling in cancer cells leads to unrestricted cell proliferation due to enhanced expression of G1/S and G2/M genes required for cell cycle entry and progression. On the one hand, loss of DYRK1A activation by LATS prevents the assembly of DREAM, thereby causing de-repression and thus increased expression of E2F-regulated G1/S genes important for cell cycle entry. On the other hand, elevated levels of active YAP due to the loss of upstream Hippo signaling induce the expression of B-MYB and enhance B-MYB promoter-binding, thereby contributing to an increased expression of G2/M genes. As MMB and YAP co-regulated genes are generally associated with a poor prognosis in cancer patients, disrupting the interaction between MMB and YAP might provide a novel therapeutic strategy for the treatment of cancer.

5 References

Azzolin L, Panciera T, Soligo S, Enzo E, Bicciato S, Dupont S, Bresolin S, Frasson C, Basso G, Guzzardo V et al. 2014. YAP/TAZ incorporation in the beta-catenin destruction complex orchestrates the Wnt response. *Cell* **158**: 157-170.

Bai H, Gayyed MF, Lam-Himlin DM, Klein AP, Nayar SK, Xu Y, Khan M, Argani P, Pan D, Anders RA. 2012. Expression of Yes-associated protein modulates Survivin expression in primary liver malignancies. *Human pathology* **43**: 1376-1385.

Barbacid M, Ortega S, Sotillo R, Odajima J, Martin A, Santamaria D, Dubus P, Malumbres M. 2005. Cell cycle and cancer: genetic analysis of the role of cyclin-dependent kinases. *Cold Spring Harbor symposia on quantitative biology* **70**: 233-240.

Barnum KJ, O'Connell MJ. 2014. Cell cycle regulation by checkpoints. *Methods in molecular biology (Clifton, NJ)* **1170**: 29-40.

Beall EL, Manak JR, Zhou S, Bell M, Lipsick JS, Botchan MR. 2002. Role for a Drosophila Myb-containing protein complex in site-specific DNA replication. *Nature* **420**: 833-837.

Blagosklonny MV, Pardee AB. 2000-2013. The Restriction Point of the Cell Cycle. Madame Curie Bioscience Database [Internet], Austin (TX): Landes Bioscience.

Bracken AP, Ciro M, Cocito A, Helin K. 2004. E2F target genes: unraveling the biology. *Trends in biochemical sciences* **29**: 409-417.

Bradford MM. 1976. A rapid and sensitive method for the quantitation of microgram quantities of protein utilizing the principle of protein-dye binding. *Analytical biochemistry* **72**: 248-254.

Bulger M, Groudine M. 2011. Functional and mechanistic diversity of distal transcription enhancers. *Cell* **144**: 327-339.

Cai M, Gao F, Lu W, Wang K. 2016. w4CSeq: software and web application to analyze 4C-seq data. *Bioinformatics (Oxford, England)* **32**: 3333-3335.

Calo E, Wysocka J. 2013. Modification of enhancer chromatin: what, how, and why? *Molecular cell* **49**: 825-837.

Carter SL, Eklund AC, Kohane IS, Harris LN, Szallasi Z. 2006. A signature of chromosomal instability inferred from gene expression profiles predicts clinical outcome in multiple human cancers. *Nature genetics* **38**: 1043-1048.

Classon M, Dyson N. 2001. p107 and p130: versatile proteins with interesting pockets. *Experimental cell research* **264**: 135-147.

Cordenonsi M, Zanconato F, Azzolin L, Forcato M, Rosato A, Frasson C, Inui M, Montagner M, Parenti AR, Poletti A et al. 2011. The Hippo transducer TAZ confers cancer stem cell-related traits on breast cancer cells. *Cell* **147**: 759-772.

Creyghton MP, Cheng AW, Welstead GG, Kooistra T, Carey BW, Steine EJ, Hanna J, Lodato MA, Frampton GM, Sharp PA et al. 2010. Histone H3K27ac separates active from poised enhancers and predicts developmental state. *Proceedings of the National Academy of Sciences of the United States of America* **107**: 21931-21936.

Croci O, De Fazio S, Biagioni F, Donato E, Caganova M, Curti L, Doni M, Sberna S, Aldeghi D, Biancotto C et al. 2017. Transcriptional integration of mitogenic and mechanical signals by Myc and YAP. *Genes & development* **31**: 2017-2022.

Davidson CJ, Guthrie EE, Lipsick JS. 2013. Duplication and maintenance of the Myb genes of vertebrate animals. *Biology open* **2**: 101-110.

DeBruhl H, Wen H, Lipsick JS. 2013. The complex containing Drosophila Myb and RB/E2F2 regulates cytokinesis in a histone H2Av-dependent manner. *Molecular and cellular biology* **33**: 1809-1818.

Dekker J, Rippe K, Dekker M, Kleckner N. 2002. Capturing chromosome conformation. *Science (New York, NY)* **295**: 1306-1311.

DeRan M, Yang J, Shen CH, Peters EC, Fitamant J, Chan P, Hsieh M, Zhu S, Asara JM, Zheng B et al. 2014. Energy stress regulates hippo-YAP signaling involving AMPK-mediated regulation of angiomotin-like 1 protein. *Cell reports* **9**: 495-503.

Ding L, Getz G, Wheeler DA, Mardis ER, McLellan MD, Cibulskis K, Sougnez C, Greulich H, Muzny DM, Morgan MB et al. 2008. Somatic mutations affect key pathways in lung adenocarcinoma. *Nature* **455**: 1069-1075.

Down CF, Millour J, Lam EW, Watson RJ. 2012. Binding of FoxM1 to G2/M gene promoters is dependent upon B-Myb. *Biochimica et biophysica acta* **1819**: 855-862.

DuPage M, Dooley AL, Jacks T. 2009. Conditional mouse lung cancer models using adenoviral or lentiviral delivery of Cre recombinase. *Nature protocols* **4**: 1064-1072.

Dupont S, Morsut L, Aragona M, Enzo E, Giulitti S, Cordenonsi M, Zanconato F, Le Digabel J, Forcato M, Bicciato S et al. 2011. Role of YAP/TAZ in mechanotransduction. *Nature* **474**: 179-183.

Edgar R, Domrachev M, Lash AE. 2002. Gene Expression Omnibus: NCBI gene expression and hybridization array data repository. *Nucleic acids research* **30**: 207-210.

Ehmer U, Sage J. 2016. Control of Proliferation and Cancer Growth by the Hippo Signaling Pathway. *Molecular cancer research : MCR* **14**: 127-140.

Ehmer U, Zmoos AF, Auerbach RK, Vaka D, Butte AJ, Kay MA, Sage J. 2014. Organ size control is dominant over Rb family inactivation to restrict proliferation in vivo. *Cell reports* **8**: 371-381.

Eisinger-Mathason TS, Mucaj V, Biju KM, Nakazawa MS, Gohil M, Cash TP, Yoon SS, Skuli N, Park KM, Gerecht S et al. 2015. Deregulation of the Hippo pathway in soft-tissue sarcoma promotes FOXM1 expression and tumorigenesis. *Proceedings of the National Academy of Sciences of the United States of America* **112**: E3402-3411.

Elkon R, Linhart C, Sharan R, Shamir R, Shiloh Y. 2003. Genome-wide in silico identification of transcriptional regulators controlling the cell cycle in human cells. *Genome research* **13**: 773-780.

Fan Q, Cai Q, Xu Y. 2015. FOXM1 is a downstream target of LPA and YAP oncogenic signaling pathways in high grade serous ovarian cancer. *Oncotarget* **6**: 27688-27699.

Fan R, Kim NG, Gumbiner BM. 2013. Regulation of Hippo pathway by mitogenic growth factors via phosphoinositide 3-kinase and phosphoinositide-dependent kinase-1. *Proceedings of the National Academy of Sciences of the United States of America* **110**: 2569-2574.

Feil R, Wagner J, Metzger D, Chambon P. 1997. Regulation of Cre recombinase activity by mutated estrogen receptor ligand-binding domains. *Biochemical and biophysical research communications* **237**: 752-757.

Fine DA, Rozenblatt-Rosen O, Padi M, Korkhin A, James RL, Adelmant G, Yoon R, Guo L, Berrios C, Zhang Y et al. 2012. Identification of FAM111A as an SV40 host range restriction and adenovirus helper factor. *PLoS pathogens* **8**: e1002949.

Fischer M, Muller GA. 2017. Cell cycle transcription control: DREAM/MuvB and RB-E2F complexes. *Critical reviews in biochemistry and molecular biology* **52**: 638-662.

Fredriksson S, Gullberg M, Jarvius J, Olsson C, Pietras K, Gustafsdottir SM, Ostman A, Landegren U. 2002. Protein detection using proximity-dependent DNA ligation assays. *Nature biotechnology* **20**: 473-477.

Frolov MV, Dyson NJ. 2004. Molecular mechanisms of E2F-dependent activation and pRB-mediated repression. *Journal of cell science* **117**: 2173-2181.

Fuhrmann-Benzakein E, Garcia-Gabay I, Pepper MS, Vassalli JD, Herrera PL. 2000. Inducible and irreversible control of gene expression using a single transgene. *Nucleic acids research* **28**: E99.

Gagrica S, Hauser S, Kolfschoten I, Osterloh L, Agami R, Gaubatz S. 2004. Inhibition of oncogenic transformation by mammalian Lin-9, a pRB-associated protein. *The EMBO journal* **23**: 4627-4638.

Galli GG, Carrara M, Yuan WC, Valdes-Quezada C, Gurung B, Pepe-Mooney B, Zhang T, Geeven G, Gray NS, de Laat W et al. 2015. YAP Drives Growth by Controlling Transcriptional Pause Release from Dynamic Enhancers. *Molecular cell* **60**: 328-337.

Garber ME, Troyanskaya OG, Schluens K, Petersen S, Thaesler Z, Pacyna-Gengelbach M, van de Rijn M, Rosen GD, Perou CM, Whyte RI et al. 2001. Diversity of gene expression in adenocarcinoma of the lung. *Proceedings of the National Academy of Sciences of the United States of America* **98**: 13784-13789.

Guiley KZ, Liban TJ, Felthousen JG, Ramanan P, Litovchick L, Rubin SM. 2015. Structural mechanisms of DREAM complex assembly and regulation. *Genes & development* **29**: 961-974.

Gullberg M, Andersson A-C. 2010. Visualization and quantification of protein-protein interactions in cells and tissues. *Nature methods* **7**.

Guo J, Wu Y, Yang L, Du J, Gong K, Chen W, Dai J, Li X, Xi S. 2017. Repression of YAP by NCTD disrupts NSCLC progression. *Oncotarget* **8**: 2307-2319.

Guo X, Zhao B. 2013. Integration of mechanical and chemical signals by YAP and TAZ transcription coactivators. *Cell & bioscience* **3**: 33.

Gyorffy B, Surowiak P, Budczies J, Lanczky A. 2013. Online survival analysis software to assess the prognostic value of biomarkers using transcriptomic data in non-small-cell lung cancer. *PloS one* **8**: e82241.

Hagege H, Klous P, Braem C, Splinter E, Dekker J, Cathala G, de Laat W, Forne T. 2007. Quantitative analysis of chromosome conformation capture assays (3C-qPCR). *Nature protocols* **2**: 1722-1733.

Hanselmann S, Wolter P, Malkmus J, Gaubatz S. 2018. The microtubule-associated protein PRC1 is a potential therapeutic target for lung cancer. *Oncotarget* **9**: 4985-4997.

Harashima H, Dissmeyer N, Schnittger A. 2013. Cell cycle control across the eukaryotic kingdom. *Trends in cell biology* **23**: 345-356.

Harper JW, Adami GR, Wei N, Keyomarsi K, Elledge SJ. 1993. The p21 Cdk-interacting protein Cip1 is a potent inhibitor of G1 cyclin-dependent kinases. *Cell* **75**: 805-816.

Harrison MM, Ceol CJ, Lu X, Horvitz HR. 2006. Some C. elegans class B synthetic multivulva proteins encode a conserved LIN-35 Rb-containing complex distinct from a NuRD-like complex. *Proceedings of the National Academy of Sciences of the United States of America* **103**: 16782-16787.

Harvey KF, Pfleger CM, Hariharan IK. 2003. The Drosophila Mst ortholog, hippo, restricts growth and cell proliferation and promotes apoptosis. *Cell* **114**: 457-467.

Harvey KF, Zhang X, Thomas DM. 2013. The Hippo pathway and human cancer. *Nature reviews Cancer* **13**: 246-257.

Hauser S, Ulrich T, Wurster S, Schmitt K, Reichert N, Gaubatz S. 2012. Loss of LIN9, a member of the DREAM complex, cooperates with SV40 large T antigen to induce genomic instability and anchorage-independent growth. *Oncogene* **31**: 1859-1868.

Heintzman ND, Stuart RK, Hon G, Fu Y, Ching CW, Hawkins RD, Barrera LO, Van Calcar S, Qu C, Ching KA et al. 2007. Distinct and predictive chromatin signatures of transcriptional promoters and enhancers in the human genome. *Nature genetics* **39**: 311-318.

Hiemer SE, Zhang L, Kartha VK, Packer TS, Almershed M, Noonan V, Kukuruzinska M, Bais MV, Monti S, Varelas X. 2015. A YAP/TAZ-Regulated Molecular Signature Is Associated with Oral Squamous Cell Carcinoma. *Molecular cancer research : MCR* **13**: 957-968.

Hnisz D, Abraham BJ, Lee TI, Lau A, Saint-Andre V, Sigova AA, Hoke HA, Young RA. 2013. Super-enhancers in the control of cell identity and disease. *Cell* **155**: 934-947.

Hossain Z, Ali SM, Ko HL, Xu J, Ng CP, Guo K, Qi Z, Ponniah S, Hong W, Hunziker W. 2007. Glomerulocystic kidney disease in mice with a targeted inactivation of Wwtr1. *Proceedings of the National Academy of Sciences of the United States of America* **104**: 1631-1636.

Huang da W, Sherman BT, Lempicki RA. 2009. Systematic and integrative analysis of large gene lists using DAVID bioinformatics resources. *Nature protocols* **4**: 44-57.

Huang W, Lv X, Liu C, Zha Z, Zhang H, Jiang Y, Xiong Y, Lei QY, Guan KL. 2012. The N-terminal phosphodegron targets TAZ/WWTR1 protein for SCFbeta-TrCP-dependent degradation in response to phosphatidylinositol 3-kinase inhibition. *The Journal of biological chemistry* **287**: 26245-26253.

Huszar D, Theoclitou ME, Skolnik J, Herbst R. 2009. Kinesin motor proteins as targets for cancer therapy. *Cancer metastasis reviews* **28**: 197-208.

Iaquinta PJ, Lees JA. 2007. Life and death decisions by the E2F transcription factors. *Current opinion in cell biology* **19**: 649-657.

Iltzsche F, Simon K, Stopp S, Pattschull G, Francke S, Wolter P, Hauser S, Murphy DJ, Garcia P, Rosenwald A et al. 2017. An important role for Myb-MuvB and its target gene KIF23 in a mouse model of lung adenocarcinoma. *Oncogene* **36**: 110-121.

Jackson EL, Olive KP, Tuveson DA, Bronson R, Crowley D, Brown M, Jacks T. 2005. The differential effects of mutant p53 alleles on advanced murine lung cancer. *Cancer research* **65**: 10280-10288.

Jackson EL, Willis N, Mercer K, Bronson RT, Crowley D, Montoya R, Jacks T, Tuveson DA. 2001. Analysis of lung tumor initiation and progression using conditional expression of oncogenic K-ras. *Genes & development* **15**: 3243-3248.

Jin F, Li Y, Dixon JR, Selvaraj S, Ye Z, Lee AY, Yen CA, Schmitt AD, Espinoza CA, Ren B. 2013. A high-resolution map of the three-dimensional chromatin interactome in human cells. *Nature* **503**: 290-294.

Johnson DG, Walker CL. 1999. Cyclins and cell cycle checkpoints. *Annual review of pharmacology and toxicology* **39**: 295-312.

Johnson L, Greenbaum D, Cichowski K, Mercer K, Murphy E, Schmitt E, Bronson RT, Umanoff H, Edelmann W, Kucherlapati R et al. 1997. K-ras is an essential gene in the mouse with partial functional overlap with N-ras. *Genes & development* **11**: 2468-2481.

Johnson TK, Schweppe RE, Septer J, Lewis RE. 1999. Phosphorylation of B-Myb regulates its transactivation potential and DNA binding. *The Journal of biological chemistry* **274**: 36741-36749.

Kadoch C, Crabtree GR. 2015. Mammalian SWI/SNF chromatin remodeling complexes and cancer: Mechanistic insights gained from human genomics. *Science advances* **1**: e1500447.

Kango-Singh M, Nolo R, Tao C, Verstreken P, Hiesinger PR, Bellen HJ, Halder G. 2002. Shar-pei mediates cell proliferation arrest during imaginal disc growth in Drosophila. *Development (Cambridge, England)* **129**: 5719-5730.

Kapoor A, Yao W, Ying H, Hua S, Liewen A, Wang Q, Zhong Y, Wu CJ, Sadanandam A, Hu B et al. 2014. Yap1 activation enables bypass of oncogenic Kras addiction in pancreatic cancer. *Cell* **158**: 185-197.

Kim D, Pertea G, Trapnell C, Pimentel H, Kelley R, Salzberg SL. 2013. TopHat2: accurate alignment of transcriptomes in the presence of insertions, deletions and gene fusions. *Genome biology* **14**: R36.

Kim MH, Kim YK, Shin DH, Lee HJ, Shin N, Kim A, Lee JH, Choi KU, Kim JY, Lee CH et al. 2015. Yes associated protein is a poor prognostic factor in well-differentiated lung adenocarcinoma. *International journal of clinical and experimental pathology* **8**: 15933-15939.

Kolupaeva V, Janssens V. 2013. PP1 and PP2A phosphatases--cooperating partners in modulating retinoblastoma protein activation. *The FEBS journal* **280**: 627-643.

Korenjak M, Taylor-Harding B, Binne UK, Satterlee JS, Stevaux O, Aasland R, White-Cooper H, Dyson N, Brehm A. 2004. Native E2F/RBF complexes contain Myb-

interacting proteins and repress transcription of developmentally controlled E2F target genes. *Cell* **119**: 181-193.

Krupczak-Hollis K, Wang X, Kalinichenko VV, Gusarova GA, Wang IC, Dennewitz MB, Yoder HM, Kiyokawa H, Kaestner KH, Costa RH. 2004. The mouse Forkhead Box m1 transcription factor is essential for hepatoblast mitosis and development of intrahepatic bile ducts and vessels during liver morphogenesis. *Developmental biology* **276**: 74-88.

Kutner RH, Zhang XY, Reiser J. 2009. Production, concentration and titration of pseudotyped HIV-1-based lentiviral vectors. *Nature protocols* **4**: 495-505.

Lakso M, Sauer B, Mosinger B, Jr., Lee EJ, Manning RW, Yu SH, Mulder KL, Westphal H. 1992. Targeted oncogene activation by site-specific recombination in transgenic mice. *Proceedings of the National Academy of Sciences of the United States of America* **89**: 6232-6236.

Lange AW, Sridharan A, Xu Y, Stripp BR, Perl AK, Whitsett JA. 2015. Hippo/Yap signaling controls epithelial progenitor cell proliferation and differentiation in the embryonic and adult lung. *Journal of molecular cell biology* **7**: 35-47.

Langmead B, Salzberg SL. 2012. Fast gapped-read alignment with Bowtie 2. *Nature methods* **9**: 357-359.

Langmead B, Trapnell C, Pop M, Salzberg SL. 2009. Ultrafast and memory-efficient alignment of short DNA sequences to the human genome. *Genome biology* **10**: R25.

Latorre I, Chesney MA, Garrigues JM, Stempor P, Appert A, Francesconi M, Strome S, Ahringer J. 2015. The DREAM complex promotes gene body H2A.Z for target repression. *Genes & development* **29**: 495-500.

Lau AN, Curtis SJ, Fillmore CM, Rowbotham SP, Mohseni M, Wagner DE, Beede AM, Montoro DT, Sinkevicius KW, Walton ZE et al. 2014. Tumor-propagating cells and Yap/Taz activity contribute to lung tumor progression and metastasis. *The EMBO journal* **33**: 468-481.

Lee MJ, Byun MR, Furutani-Seiki M, Hong JH, Jung HS. 2014. YAP and TAZ regulate skin wound healing. *The Journal of investigative dermatology* **134**: 518-525.

Lehtinen MK, Yuan Z, Boag PR, Yang Y, Villen J, Becker EB, DiBacco S, de la Iglesia N, Gygi S, Blackwell TK et al. 2006. A conserved MST-FOXO signaling pathway mediates oxidative-stress responses and extends life span. *Cell* **125**: 987-1001.

Lewis PW, Beall EL, Fleischer TC, Georlette D, Link AJ, Botchan MR. 2004. Identification of a Drosophila Myb-E2F2/RBF transcriptional repressor complex. *Genes & development* **18**: 2929-2940.

Li W, Cooper J, Zhou L, Yang C, Erdjument-Bromage H, Zagzag D, Snuderl M, Ladanyi M, Hanemann CO, Zhou P et al. 2014. Merlin/NF2 loss-driven tumorigenesis linked to CRL4(DCAF1)-mediated inhibition of the hippo pathway kinases Lats1 and 2 in the nucleus. *Cancer cell* **26**: 48-60.

Liang J, Lacroix L, Gamot A, Cuddapah S, Queille S, Lhoumaud P, Lepetit P, Martin PG, Vogelmann J, Court F et al. 2014. Chromatin immunoprecipitation indirect peaks highlight long-range interactions of insulator proteins and Pol II pausing. *Molecular cell* **53**: 672-681.

Liberzon A, Subramanian A, Pinchback R, Thorvaldsdottir H, Tamayo P, Mesirov JP. 2011. Molecular signatures database (MSigDB) 3.0. *Bioinformatics (Oxford, England)* **27**: 1739-1740.

Linhart C, Elkon R, Shiloh Y, Shamir R. 2005. Deciphering transcriptional regulatory elements that encode specific cell cycle phasing by comparative genomics analysis. *Cell cycle (Georgetown, Tex)* **4**: 1788-1797.

Litovchick L, Florens LA, Swanson SK, Washburn MP, DeCaprio JA. 2011. DYRK1A protein kinase promotes quiescence and senescence through DREAM complex assembly. *Genes & development* **25**: 801-813.

Litovchick L, Sadasivam S, Florens L, Zhu X, Swanson SK, Velmurugan S, Chen R, Washburn MP, Liu XS, DeCaprio JA. 2007. Evolutionarily conserved multisubunit

RBL2/p130 and E2F4 protein complex represses human cell cycle-dependent genes in quiescence. *Molecular cell* **26**: 539-551.

Liu N, Lucibello FC, Zwicker J, Engeland K, Muller R. 1996. Cell cycle-regulated repression of B-myb transcription: cooperation of an E2F site with a contiguous corepressor element. *Nucleic acids research* **24**: 2905-2910.

Liu-Chittenden Y, Huang B, Shim JS, Chen Q, Lee SJ, Anders RA, Liu JO, Pan D. 2012. Genetic and pharmacological disruption of the TEAD-YAP complex suppresses the oncogenic activity of YAP. *Genes & development* **26**: 1300-1305.

Loven J, Hoke HA, Lin CY, Lau A, Orlando DA, Vakoc CR, Bradner JE, Lee TI, Young RA. 2013. Selective inhibition of tumor oncogenes by disruption of super-enhancers. *Cell* **153**: 320-334.

Low BC, Pan CQ, Shivashankar GV, Bershadsky A, Sudol M, Sheetz M. 2014. YAP/TAZ as mechanosensors and mechanotransducers in regulating organ size and tumor growth. *FEBS letters* **588**: 2663-2670.

Luo J, Emanuele MJ, Li D, Creighton CJ, Schlabach MR, Westbrook TF, Wong KK, Elledge SJ. 2009. A genome-wide RNAi screen identifies multiple synthetic lethal interactions with the Ras oncogene. *Cell* **137**: 835-848.

Ma B, Chen Y, Chen L, Cheng H, Mu C, Li J, Gao R, Zhou C, Cao L, Liu J et al. 2015. Hypoxia regulates Hippo signalling through the SIAH2 ubiquitin E3 ligase. *Nature cell biology* **17**: 95-103.

Makita R, Uchijima Y, Nishiyama K, Amano T, Chen Q, Takeuchi T, Mitani A, Nagase T, Yatomi Y, Aburatani H et al. 2008. Multiple renal cysts, urinary concentration defects, and pulmonary emphysematous changes in mice lacking TAZ. *American journal of physiology Renal physiology* **294**: F542-553.

Malumbres M, Barbacid M. 2001. To cycle or not to cycle: a critical decision in cancer. *Nature reviews Cancer* **1**: 222-231.

Mannefeld M, Klassen E, Gaubatz S. 2009. B-MYB is required for recovery from the DNA damage-induced G2 checkpoint in p53 mutant cells. *Cancer research* **69**: 4073-4080.

Marino S, Vooijs M, van Der Gulden H, Jonkers J, Berns A. 2000. Induction of medulloblastomas in p53-null mutant mice by somatic inactivation of Rb in the external granular layer cells of the cerebellum. *Genes & development* **14**: 994-1004.

Meng Z, Moroishi T, Guan KL. 2016. Mechanisms of Hippo pathway regulation. *Genes & development* **30**: 1-17.

Mizuno T, Murakami H, Fujii M, Ishiguro F, Tanaka I, Kondo Y, Akatsuka S, Toyokuni S, Yokoi K, Osada H et al. 2012. YAP induces malignant mesothelioma cell proliferation by upregulating transcription of cell cycle-promoting genes. *Oncogene* **31**: 5117-5122.

Mo JS, Meng Z, Kim YC, Park HW, Hansen CG, Kim S, Lim DS, Guan KL. 2015. Cellular energy stress induces AMPK-mediated regulation of YAP and the Hippo pathway. *Nature cell biology* **17**: 500-510.

Modell AE, Blosser SL, Arora PS. 2016. Systematic Targeting of Protein-Protein Interactions. *Trends in pharmacological sciences* **37**: 702-713.

Mohseni M, Sun J, Lau A, Curtis S, Goldsmith J, Fox VL, Wei C, Frazier M, Samson O, Wong KK et al. 2014. A genetic screen identifies an LKB1-MARK signalling axis controlling the Hippo-YAP pathway. *Nature cell biology* **16**: 108-117.

Morgan DO. 2007. *The Cell Cycle - Principles of Control*. New Science Press Ltd, London.

Morita S, Kojima T, Kitamura T. 2000. Plat-E: an efficient and stable system for transient packaging of retroviruses. *Gene therapy* **7**: 1063-1066.

Muller GA, Quaas M, Schumann M, Krause E, Padi M, Fischer M, Litovchick L, DeCaprio JA, Engeland K. 2012. The CHR promoter element controls cell cycle-dependent gene transcription and binds the DREAM and MMB complexes. *Nucleic acids research* **40**: 1561-1578.

Muller GA, Stangner K, Schmitt T, Wintsche A, Engeland K. 2017. Timing of transcription during the cell cycle: Protein complexes binding to E2F, E2F/CLE, CDE/CHR, or CHR promoter elements define early and late cell cycle gene expression. *Oncotarget* **8**: 97736-97748.

Muller GA, Wintsche A, Stangner K, Prohaska SJ, Stadler PF, Engeland K. 2014. The CHR site: definition and genome-wide identification of a cell cycle transcriptional element. *Nucleic acids research* **42**: 10331-10350.

Nie Y, Liu H, Sun X. 2013. The patterns of histone modifications in the vicinity of transcription factor binding sites in human lymphoblastoid cell lines. *PloS one* **8**: e60002.

Nor Rashid N, Yusof R, Watson RJ. 2011. Disruption of repressive p130-DREAM complexes by human papillomavirus 16 E6/E7 oncoproteins is required for cell-cycle progression in cervical cancer cells. *The Journal of general virology* **92**: 2620-2627.

Novak A, Guo C, Yang W, Nagy A, Lobe CG. 2000. Z/EG, a double reporter mouse line that expresses enhanced green fluorescent protein upon Cre-mediated excision. *Genesis (New York, NY : 2000)* **28**: 147-155.

Osterloh L, von Eyss B, Schmit F, Rein L, Hubner D, Samans B, Hauser S, Gaubatz S. 2007. The human synMuv-like protein LIN-9 is required for transcription of G2/M genes and for entry into mitosis. *The EMBO journal* **26**: 144-157.

Overholtzer M, Zhang J, Smolen GA, Muir B, Li W, Sgroi DC, Deng CX, Brugge JS, Haber DA. 2006. Transforming properties of YAP, a candidate oncogene on the chromosome 11q22 amplicon. *Proceedings of the National Academy of Sciences of the United States of America* **103**: 12405-12410.

Paik S, Shak S, Tang G, Kim C, Baker J, Cronin M, Baehner FL, Walker MG, Watson D, Park T et al. 2004. A multigene assay to predict recurrence of tamoxifen-treated, node-negative breast cancer. *The New England journal of medicine* **351**: 2817-2826.

Park HJ, Costa RH, Lau LF, Tyner AL, Raychaudhuri P. 2008. Anaphase-promoting complex/cyclosome-CDH1-mediated proteolysis of the forkhead box M1 transcription factor is critical for regulated entry into S phase. *Molecular and cellular biology* **28**: 5162-5171.

Park HW, Kim YC, Yu B, Moroishi T, Mo JS, Plouffe SW, Meng Z, Lin KC, Yu FX, Alexander CM et al. 2015. Alternative Wnt Signaling Activates YAP/TAZ. *Cell* **162**: 780-794.

Piccolo S, Dupont S, Cordenonsi M. 2014. The biology of YAP/TAZ: hippo signaling and beyond. *Physiological reviews* **94**: 1287-1312.

Pilkinton M, Sandoval R, Colamonici OR. 2007. Mammalian Mip/LIN-9 interacts with either the p107, p130/E2F4 repressor complex or B-Myb in a cell cycle-phase-dependent context distinct from the Drosophila dREAM complex. *Oncogene* **26**: 7535-7543.

Polyak K, Kato JY, Solomon MJ, Sherr CJ, Massague J, Roberts JM, Koff A. 1994. p27Kip1, a cyclin-Cdk inhibitor, links transforming growth factor-beta and contact inhibition to cell cycle arrest. *Genes & development* **8**: 9-22.

Pott S, Lieb JD. 2015. What are super-enhancers? *Nature genetics* **47**: 8-12.

Quaas M, Muller GA, Engeland K. 2012. p53 can repress transcription of cell cycle genes through a p21(WAF1/CIP1)-dependent switch from MMB to DREAM protein complex binding at CHR promoter elements. *Cell cycle (Georgetown, Tex)* **11**: 4661-4672.

Quinlan AR, Hall IM. 2010. BEDTools: a flexible suite of utilities for comparing genomic features. *Bioinformatics (Oxford, England)* **26**: 841-842.

Ramirez F, Ryan DP, Gruning B, Bhardwaj V, Kilpert F, Richter AS, Heyne S, Dundar F, Manke T. 2016. deepTools2: a next generation web server for deep-sequencing data analysis. *Nucleic acids research* **44**: W160-165.

Rao SS, Huntley MH, Durand NC, Stamenova EK, Bochkov ID, Robinson JT, Sanborn AL, Machol I, Omer AD, Lander ES et al. 2014. A 3D map of the human genome at kilobase resolution reveals principles of chromatin looping. *Cell* **159**: 1665-1680.

Rath O, Kozielski F. 2012. Kinesins and cancer. *Nature reviews Cancer* **12**: 527-539.

Rebhan M, Chalifa-Caspi V, Prilusky J, Lancet D. 1997. GeneCards: integrating information about genes, proteins and diseases. *Trends in genetics : TIG* **13**: 163.

Reichert N, Wurster S, Ulrich T, Schmitt K, Hauser S, Probst L, Gotz R, Ceteci F, Moll R, Rapp U et al. 2010. Lin9, a subunit of the mammalian DREAM complex, is essential for embryonic development, for survival of adult mice, and for tumor suppression. *Molecular and cellular biology* **30**: 2896-2908.

Rhodes DR, Yu J, Shanker K, Deshpande N, Varambally R, Ghosh D, Barrette T, Pandey A, Chinnaiyan AM. 2004. ONCOMINE: a cancer microarray database and integrated data-mining platform. *Neoplasia (New York, NY)* **6**: 1-6.

Robinson JT, Thorvaldsdottir H, Winckler W, Guttman M, Lander ES, Getz G, Mesirov JP. 2011. Integrative genomics viewer. *Nature biotechnology* **29**: 24-26.

Robinson MD, McCarthy DJ, Smyth GK. 2010. edgeR: a Bioconductor package for differential expression analysis of digital gene expression data. *Bioinformatics (Oxford, England)* **26**: 139-140.

Roussel MF. 1999. The INK4 family of cell cycle inhibitors in cancer. *Oncogene* **18**: 5311-5317.

Sadasivam S, DeCaprio JA. 2013. The DREAM complex: master coordinator of cell cycle-dependent gene expression. *Nature reviews Cancer* **13**: 585-595.

Sadasivam S, Duan S, DeCaprio JA. 2012. The MuvB complex sequentially recruits B-Myb and FoxM1 to promote mitotic gene expression. *Genes & development* **26**: 474-489.

Sarthy AV, Morgan-Lappe SE, Zakula D, Vernetti L, Schurdak M, Packer JC, Anderson MG, Shirasawa S, Sasazuki T, Fesik SW. 2007. Survivin depletion preferentially reduces the survival of activated K-Ras-transformed cells. *Molecular cancer therapeutics* **6**: 269-276.

Schindelin J, Arganda-Carreras I, Frise E, Kaynig V, Longair M, Pietzsch T, Preibisch S, Rueden C, Saalfeld S, Schmid B et al. 2012. Fiji: an open-source platform for biological-image analysis. *Nature methods* **9**: 676-682.

Schmit F, Cremer S, Gaubatz S. 2009. LIN54 is an essential core subunit of the DREAM/LINC complex that binds to the cdc2 promoter in a sequence-specific manner. *The FEBS journal* **276**: 5703-5716.

Schmit F, Korenjak M, Mannefeld M, Schmitt K, Franke C, von Eyss B, Gagrica S, Hanel F, Brehm A, Gaubatz S. 2007. LINC, a human complex that is related to pRB-containing complexes in invertebrates regulates the expression of G2/M genes. *Cell cycle (Georgetown, Tex)* **6**: 1903-1913.

Seidel C, Schagdarsurengin U, Blumke K, Wurl P, Pfeifer GP, Hauptmann S, Taubert H, Dammann R. 2007. Frequent hypermethylation of MST1 and MST2 in soft tissue sarcoma. *Molecular carcinogenesis* **46**: 865-871.

Shao D, Zhai P, Del Re DP, Sciarretta S, Yabuta N, Nojima H, Lim DS, Pan D, Sadoshima J. 2014a. A functional interaction between Hippo-YAP signalling and FoxO1 mediates the oxidative stress response. *Nature communications* **5**: 3315.

Shao DD, Xue W, Krall EB, Bhutkar A, Piccioni F, Wang X, Schinzel AC, Sood S, Rosenbluh J, Kim JW et al. 2014b. KRAS and YAP1 converge to regulate EMT and tumor survival. *Cell* **158**: 171-184.

Shen Z, Stanger BZ. 2015. YAP regulates S-phase entry in endothelial cells. *PloS one* **10**: e0117522.

Sherr CJ, Roberts JM. 1999. CDK inhibitors: positive and negative regulators of G1-phase progression. *Genes & development* **13**: 1501-1512.

Soderberg O, Gullberg M, Jarvius M, Ridderstrale K, Leuchowius KJ, Jarvius J, Wester K, Hydbring P, Bahram F, Larsson LG et al. 2006. Direct observation of individual

endogenous protein complexes in situ by proximity ligation. *Nature methods* **3**: 995-1000.

Song H, Zhou S, Wang R, Li S. 2013. Kinesin spindle protein (KSP) inhibitors in combination with chemotherapeutic agents for cancer therapy. *ChemMedChem* **8**: 1736-1749.

Splinter E, de Wit E, van de Werken HJ, Klous P, de Laat W. 2012. Determining long-range chromatin interactions for selected genomic sites using 4C-seq technology: from fixation to computation. *Methods (San Diego, Calif)* **58**: 221-230.

Stadhouders R, Kolovos P, Brouwer R, Zuin J, van den Heuvel A, Kockx C, Palstra RJ, Wendt KS, Grosveld F, van Ijcken W et al. 2013. Multiplexed chromosome conformation capture sequencing for rapid genome-scale high-resolution detection of long-range chromatin interactions. *Nature protocols* **8**: 509-524.

Stadhouders R, van den Heuvel A, Kolovos P, Jorna R, Leslie K, Grosveld F, Soler E. 2012. Transcription regulation by distal enhancers: who's in the loop? *Transcription* **3**: 181-186.

Stein C, Bardet AF, Roma G, Bergling S, Clay I, Ruchti A, Agarinis C, Schmelzle T, Bouwmeester T, Schubeler D et al. 2015. YAP1 Exerts Its Transcriptional Control via TEAD-Mediated Activation of Enhancers. *PLoS genetics* **11**: e1005465.

Subramanian A, Tamayo P, Mootha VK, Mukherjee S, Ebert BL, Gillette MA, Paulovich A, Pomeroy SL, Golub TR, Lander ES et al. 2005. Gene set enrichment analysis: a knowledge-based approach for interpreting genome-wide expression profiles. *Proceedings of the National Academy of Sciences of the United States of America* **102**: 15545-15550.

Sun A, Bagella L, Tutton S, Romano G, Giordano A. 2007. From G0 to S phase: a view of the roles played by the retinoblastoma (Rb) family members in the Rb-E2F pathway. *Journal of cellular biochemistry* **102**: 1400-1404.

Takahashi Y, Miyoshi Y, Takahata C, Irahara N, Taguchi T, Tamaki Y, Noguchi S. 2005. Down-regulation of LATS1 and LATS2 mRNA expression by promoter hypermethylation and its association with biologically aggressive phenotype in human breast cancers. *Clinical cancer research : an official journal of the American Association for Cancer Research* **11**: 1380-1385.

Tanaka Y, Patestos NP, Maekawa T, Ishii S. 1999. B-myb is required for inner cell mass formation at an early stage of development. *The Journal of biological chemistry* **274**: 28067-28070.

Tapon N, Harvey KF, Bell DW, Wahrer DC, Schiripo TA, Haber D, Hariharan IK. 2002. salvador Promotes both cell cycle exit and apoptosis in Drosophila and is mutated in human cancer cell lines. *Cell* **110**: 467-478.

Tavner F, Frampton J, Watson RJ. 2007. Targeting an E2F site in the mouse genome prevents promoter silencing in quiescent and post-mitotic cells. *Oncogene* **26**: 2727-2735.

The Cancer Genome Atlas Network. 2015. Comprehensive genomic characterization of head and neck squamous cell carcinomas. *Nature* **517**: 576-582.

The UniProt Consortium. 2017. UniProt: the universal protein knowledgebase. *Nucleic acids research* **45**: D158-D169.

Tian S, Roepman P, Van't Veer LJ, Bernards R, de Snoo F, Glas AM. 2010. Biological functions of the genes in the mammaprint breast cancer profile reflect the hallmarks of cancer. *Biomarker insights* **5**: 129-138.

Tian Y, Kolb R, Hong JH, Carroll J, Li D, You J, Bronson R, Yaffe MB, Zhou J, Benjamin T. 2007. TAZ promotes PC2 degradation through a SCFbeta-Trcp E3 ligase complex. *Molecular and cellular biology* **27**: 6383-6395.

Tremblay AM, Missiaglia E, Galli GG, Hettmer S, Urcia R, Carrara M, Judson RN, Thway K, Nadal G, Selfe JL et al. 2014. The Hippo transducer YAP1 transforms activated satellite cells and is a potent effector of embryonal rhabdomyosarcoma formation. *Cancer cell* **26**: 273-287.

Tripathi V, Shen Z, Chakraborty A, Giri S, Freier SM, Wu X, Zhang Y, Gorospe M, Prasanth SG, Lal A et al. 2013. Long noncoding RNA MALAT1 controls cell cycle progression by regulating the expression of oncogenic transcription factor B-MYB. *PLoS genetics* **9**: e1003368.

Tschop K, Conery AR, Litovchick L, Decaprio JA, Settleman J, Harlow E, Dyson N. 2011. A kinase shRNA screen links LATS2 and the pRB tumor suppressor. *Genes & development* **25**: 814-830.

von Eyss B, Jaenicke LA, Kortlever RM, Royla N, Wiese KE, Letschert S, McDuffus LA, Sauer M, Rosenwald A, Evan GI et al. 2015. A MYC-Driven Change in Mitochondrial Dynamics Limits YAP/TAZ Function in Mammary Epithelial Cells and Breast Cancer. *Cancer cell* **28**: 743-757.

Wang J, Wang H, Zhang Y, Zhen N, Zhang L, Qiao Y, Weng W, Liu X, Ma L, Xiao W et al. 2014. Mutual inhibition between YAP and SRSF1 maintains long non-coding RNA, Malat1-induced tumourigenesis in liver cancer. *Cellular signalling* **26**: 1048-1059.

Wang W, Xiao ZD, Li X, Aziz KE, Gan B, Johnson RL, Chen J. 2015. AMPK modulates Hippo pathway activity to regulate energy homeostasis. *Nature cell biology* **17**: 490-499.

Wang Y, Dong Q, Zhang Q, Li Z, Wang E, Qiu X. 2010. Overexpression of yes-associated protein contributes to progression and poor prognosis of non-small-cell lung cancer. *Cancer science* **101**: 1279-1285.

Weiler SME, Pinna F, Wolf T, Lutz T, Geldiyev A, Sticht C, Knaub M, Thomann S, Bissinger M, Wan S et al. 2017. Induction of Chromosome Instability by Activation of Yes-Associated Protein and Forkhead Box M1 in Liver Cancer. *Gastroenterology* **152**: 2037-2051.e2022.

Weinberg RA. 2014. *The Biology of Cancer*. Garland Science, Taylor & Francis Group, LLC, New York City.

Weng MT, Lee JH, Wei SC, Li Q, Shahamatdar S, Hsu D, Schetter AJ, Swatkoski S, Mannan P, Garfield S et al. 2012. Evolutionarily conserved protein ERH controls CENP-E mRNA splicing and is required for the survival of KRAS mutant cancer cells. *Proceedings of the National Academy of Sciences of the United States of America* **109**: E3659-3667.

Whyte WA, Orlando DA, Hnisz D, Abraham BJ, Lin CY, Kagey MH, Rahl PB, Lee TI, Young RA. 2013. Master transcription factors and mediator establish super-enhancers at key cell identity genes. *Cell* **153**: 307-319.

Winter GE, Buckley DL, Paulk J, Roberts JM, Souza A, Dhe-Paganon S, Bradner JE. 2015. DRUG DEVELOPMENT. Phthalimide conjugation as a strategy for in vivo target protein degradation. *Science (New York, NY)* **348**: 1376-1381.

Wiseman EF, Chen X, Han N, Webber A, Ji Z, Sharrocks AD, Ang YS. 2015. Deregulation of the FOXM1 target gene network and its coregulatory partners in oesophageal adenocarcinoma. *Molecular cancer* **14**: 69.

Wolter P, Hanselmann S, Pattschull G, Schruf E, Gaubatz S. 2017. Central spindle proteins and mitotic kinesins are direct transcriptional targets of MuvB, B-MYB and FOXM1 in breast cancer cell lines and are potential targets for therapy. *Oncotarget* **8**: 11160-11172.

Wu S, Huang J, Dong J, Pan D. 2003. hippo encodes a Ste-20 family protein kinase that restricts cell proliferation and promotes apoptosis in conjunction with salvador and warts. *Cell* **114**: 445-456.

Xiang L, Gilkes DM, Hu H, Takano N, Luo W, Lu H, Bullen JW, Samanta D, Liang H, Semenza GL. 2014. Hypoxia-inducible factor 1 mediates TAZ expression and nuclear localization to induce the breast cancer stem cell phenotype. *Oncotarget* **5**: 12509-12527.

Xu S, Grullon S, Ge K, Peng W. 2014. Spatial clustering for identification of ChIP-enriched regions (SICER) to map regions of histone methylation patterns in embryonic stem cells. *Methods in molecular biology (Clifton, NJ)* **1150**: 97-111.

Yang S, Zhang L, Liu M, Chong R, Ding SJ, Chen Y, Dong J. 2013. CDK1 phosphorylation of YAP promotes mitotic defects and cell motility and is essential for neoplastic transformation. *Cancer research* **73**: 6722-6733.

Yin F, Yu J, Zheng Y, Chen Q, Zhang N, Pan D. 2013. Spatial organization of Hippo signaling at the plasma membrane mediated by the tumor suppressor Merlin/NF2. *Cell* **154**: 1342-1355.

Yu FX, Zhao B, Guan KL. 2015. Hippo Pathway in Organ Size Control, Tissue Homeostasis, and Cancer. *Cell* **163**: 811-828.

Yu FX, Zhao B, Panupinthu N, Jewell JL, Lian I, Wang LH, Zhao J, Yuan H, Tumaneng K, Li H et al. 2012. Regulation of the Hippo-YAP pathway by G-protein-coupled receptor signaling. *Cell* **150**: 780-791.

Zanconato F, Forcato M, Battilana G, Azzolin L, Quaranta E, Bodega B, Rosato A, Bicciato S, Cordenonsi M, Piccolo S. 2015. Genome-wide association between YAP/TAZ/TEAD and AP-1 at enhancers drives oncogenic growth. *Nature cell biology* **17**: 1218-1227.

Zender L, Spector MS, Xue W, Flemming P, Cordon-Cardo C, Silke J, Fan ST, Luk JM, Wigler M, Hannon GJ et al. 2006. Identification and validation of oncogenes in liver cancer using an integrative oncogenomic approach. *Cell* **125**: 1253-1267.

Zhang H, Liu CY, Zha ZY, Zhao B, Yao J, Zhao S, Xiong Y, Lei QY, Guan KL. 2009. TEAD transcription factors mediate the function of TAZ in cell growth and epithelial-mesenchymal transition. *The Journal of biological chemistry* **284**: 13355-13362.

Zhang H, Ramakrishnan SK, Triner D, Centofanti B, Maitra D, Gyorffy B, Sebolt-Leopold JS, Dame MK, Varani J, Brenner DE et al. 2015a. Tumor-selective proteotoxicity of verteporfin inhibits colon cancer progression independently of YAP1. *Science signaling* **8**: ra98.

Zhang W, Gao Y, Li F, Tong X, Ren Y, Han X, Yao S, Long F, Yang Z, Fan H et al. 2015b. YAP promotes malignant progression of Lkb1-deficient lung adenocarcinoma through downstream regulation of survivin. *Cancer research* **75**: 4450-4457.

Zhang Y, Liu T, Meyer CA, Eeckhoute J, Johnson DS, Bernstein BE, Nusbaum C, Myers RM, Brown M, Li W et al. 2008. Model-based analysis of ChIP-Seq (MACS). *Genome biology* **9**: R137.

Zhao B, Li L, Lei Q, Guan KL. 2010. The Hippo-YAP pathway in organ size control and tumorigenesis: an updated version. *Genes & development* **24**: 862-874.

Zhao B, Wei X, Li W, Udan RS, Yang Q, Kim J, Xie J, Ikenoue T, Yu J, Li L et al. 2007. Inactivation of YAP oncoprotein by the Hippo pathway is involved in cell contact inhibition and tissue growth control. *Genes & development* **21**: 2747-2761.

Zhao B, Ye X, Yu J, Li L, Li W, Li S, Yu J, Lin JD, Wang CY, Chinnaiyan AM et al. 2008. TEAD mediates YAP-dependent gene induction and growth control. *Genes & development* **22**: 1962-1971.

Zhu Z, Shendure J, Church GM. 2005. Discovering functional transcription-factor combinations in the human cell cycle. *Genome research* **15**: 848-855.

Zwicker J, Liu N, Engeland K, Lucibello FC, Muller R. 1996. Cell cycle regulation of E2F site occupation in vivo. *Science (New York, NY)* **271**: 1595-1597.

6 Appendix

6.1 List of Figures

6.2 List of Tables

6.3 Abbreviations

3C	Chromosome conformation capture
4-OHT	4-Hydroxytamoxifen
4C	Circular chromosome conformation capture
4C-seq	Circular chromosome conformation capture followed by high-throughput sequencing
ADC	Adenocarcinoma
APS	Ammonium persulfate
bp	Base pairs
BSA	Bovine serum albumin
$CaCl_2$	Calcium chloride
cDNA	Complementary deoxyribonucleic acid
ChIP	Chromatin immunoprecipitation
ChIP-seq	Chromatin immunoprecipitation followed by high-throughput sequencing
CIN	Chromosomal instability
Co-IP	Co-immunoprecipitation
DAB	Diaminobenzidine (tetrahydrochloride)
ddH_2O	Double-distilled/purified water
DEPC	Diethyl pyrocarbonate
DMEM	Dulbecco's modified eagle medium
DMSO	Dimethyl sulfoxide
DNA	Deoxyribonucleic acid
dNTP	Deoxyribonucleotide triphosphate
dox/doxy	Doxycycline
DREAM	DP, RB-like, E2F and multi-vulval class B complex
DTT	Dithiothreitol
EB	Elution buffer
ECL	Enhanced chemiluminescence solution
EDTA	Ethylenediaminetetraacetic acid
EGF	Epidermal growth factor
ESB	Electrophoresis sample buffer
ev	Empty vector
FBS	Fetal bovine serum
G0/G0 phase	Quiescent/resting phase

G1/G1 phase	Gap1 phase
G2/G2 phase	Gap2 phase
gDNA	Genomic deoxyribonucleic acid
GFP	Green fluorescent protein
H_2O	Water
HBS	HEPES buffered saline
HCl	Hydrochloric acid
HEPES	Hydroxyethyl-piperazineethane-sulfonic acid
HRP	Horseradish peroxidase
IF	Immunofluorescence
IHC	Immunohistochemistry
IP	Immunoprecipitation
kb	Kilobase/kilo base pairs
KP	*K-Ras$^{LSL\text{-}G12D/+}$; p53$^{fl/fl}$; Lin9$^{+/+}$*
KPL	*K-Ras$^{LSL\text{-}G12D/+}$; p53$^{fl/fl}$; Lin9$^{fl/fl}$*
LB	Luria Bertani
M/M phase	Mitosis/Mitotic phase
MMB	Myb-MuvB complex
MuvB	Multi-vulval class B core
NaCl	Sodium Chloride
NEB	New England Biolabs
NGS	Next-generation sequencing
Opti-MEM	Opti-Minimum essential media (reduced serum media)
OSCC	Oral squamous cell carcinoma
PBS	Phosphate buffered saline
PBS-T	Phosphate buffered saline with 0.1% Tween 20
PCR	Polymerase chain reaction
PEG	Polyethylene glycol
Pen-Strep	Penicillin-Streptomycin
PI	Propidium iodide
PIC	Protease inhibitor cocktail
PLA	Proximity ligation assay
PMSF	Phenylmethylsulfonyl fluoride
PSP	3% paraformaldehyde, 2% sucrose in phosphate buffered saline
PVDF	Polyvinylidene fluoride
qPCR	quantitative real-time PCR

RNA	Ribonucleic acid
RNA-seq	Ribonucleic acid sequencing
RNAi	Ribonucleic acid interference
RPMI	Roswell Park Memorial Institute medium
RT	Room temperature
S/S phase	Synthesis phase
SDS	Sodium dodecyl sulfate
SDS-PAGE	Sodium dodecyl sulfate-polyacrylamide gel electrophoresis
siRNA	Small interfering ribonucleic acid
TAE	Tris-acetate-ethylenediaminetetraacetic acid buffer
TBS	Tris-buffered saline
TBS-T	Tris-buffered saline with 0.1% Tween 20
TE	Tris- Ethylenediaminetetraacetic acid (EDTA)
TEMED	Tetramethylethylenediamine
TU	Transducing units
UV	Ultraviolet
VP	Verteporfin
WB	Western Blot
wt	Wild-type

6.4 Curriculum vitae

6.5 Publication list and conference contributions

6.5.1 Publications

Iltzsche F.*, Simon K.*, Stopp S.*, **Pattschull G.***, Francke S., Wolter P., Hauser S., Murphy DJ., Garcia P., Rosenwald A., and Gaubatz S. (2016): **An important role for Myb-MuvB and its target gene KIF23 in a mouse model of lung adenocarcinoma.** *Oncogene* **36**, 110–121; https://doi.org/10.1038/onc.2016.181
(Iltzsche et al. 2017)

Wolter P.*, Hanselmann S.*, **Pattschull G**., Schruf E., and Gaubatz S. (2017): **Central spindle proteins and mitotic kinesins are direct transcriptional targets of MuvB, B-MYB and FOXM1 in breast cancer cell lines and are potential targets for therapy.** Oncotarget. 2017; 8:11160-11172; https://doi.org/10.18632/oncotarget.14466
(Wolter et al. 2017)

* These authors contributed equally to this work.

6.5.2 Conference contributions

06/2018	Poster at the 10th Cell Cycle Meeting at the Salk Institute for Biological Studies, La Jolla, CA, USA; Poster: “The Myb-MuvB complex and YAP interact to co-regulate cancer-relevant genes involved in mitosis and cytokinesis” by Grit Pattschull, Susanne Walz, Björn von Eyss, and Stefan Gaubatz
10/2017	Talk at the 12th International GSLS Students’ Symposium Eureka! at the RVZ, Würzburg, Germany; Talk: “The Myb-MuvB complex and YAP1 interact to co-regulate cancer-relevant genes involved in mitosis and cytokinesis” by Grit Pattschull, Susanne Walz, Björn von Eyss, and Stefan Gaubatz

07/2017	Talk at the Gordon Research Conference (GRC) "Cell Growth and Proliferation" in West Dover, VT, USA; Talk: "The Myb-MuvB complex and YAP1 interact to co-regulate cancer-relevant genes involved in mitosis and cytokinesis" by Grit Pattschull, Susanne Walz, Björn von Eyss, and Stefan Gaubatz
10/2016	Poster at the 11th International GSLS Students' Symposium Eureka! at the RVZ, Würzburg, Germany; Poster "Loss of the Myb-MuvB core component Lin9 results in major cellular abnormalities, proliferation defects, and downregulation of mitotic genes" by Grit Pattschull, Fabian Iltzsche, Carsten Ade, and Stefan Gaubatz
10/2015	Poster at the 10th International GSLS Students' Symposium Eureka! at the RVZ, Würzburg, Germany; Poster: "Role of the DREAM complex in mitotic fidelity and aneuploidy" by Grit Pattschull, Fabian Iltzsche, and Stefan Gaubatz

6.6 Acknowledgements

An erster Stelle gilt mein Dank Prof. Dr. Stefan Gaubatz, welcher mir ein spannendes Projekt gab und mir ermöglichte an diesem in einem sehr angenehmen Umfeld zu arbeiten. Ich danke ihm insbesondere für die vielen stundenlangen wissenschaftlichen Diskussionen und die mit dem Projekt einhergehenden Herausforderungen, an denen ich maßgeblich als Wissenschaftlerin gewachsen bin. Sein positives Denken und seine wissenschaftliche Neugier daran Neues zu erforschen haben mich sehr stark inspiriert und motiviert.

Für eine gute Zusammenarbeit und tatkräftige Unterstützung sowohl in experimentellen Angelegenheiten als auch in der bioinformatischen Auswertung der Ergebnisse danke ich: Dr. Björn von Eyss, Dr. Susanne Walz, Dr. Carsten Ade, Dr. Elmar Wolf, Eva Rühl und Ashley Curran. Außerdem möchte ich meinem *Thesis Committee* bestehend aus Prof. Dr. Almut Schulze und Prof. Dr. Alexander Buchberger für Ratschläge und Hilfe bezüglich meines Projektes danken. Ich danke auch allen Mitarbeitern der *Graduate School of Life Sciences* insbesondere Dr. Gabriele Blum-Oehler. Durch die GSLS konnte ich mich auch neben meinen wissenschaftlichen Fähigkeiten weiterentwickeln und habe nebenbei noch viele liebe Menschen kennen gelernt. Ein ganz besonderes Dankeschön geht an meine lieben Arbeitskollegen für die schöne und unvergessliche Zeit im Labor: Susanne Spahr, Adelgunde Wolpert, Marco Gründl, Steffen Hanselmann und Camila Fetiva. An dieser Stelle möchte ich auch unseren Bachelor- und Masterstudenten danken, die immer neues Leben ins Labor gebracht haben: Sven, Jonas, Laura, Marcela, Melissa und Woojin.

Auch wenn man den überwiegenden Teil seines Lebens als Doktorand/in im Labor verbringt, so ist es doch umso wichtiger Halt und Kraft außerhalb vom Labor zu erhalten. Ich danke meinen lieben Eltern und meiner Schwester für ihre Unterstützung und ihren Glauben an mich. Danke an meinen Freund Patrick für seine Ausdauer und Geduld während einer herausfordernden Phase meines Lebens. Mit seiner Liebe, Kraft und Stärke hat er mich während der gesamten Zeit meiner Promotion begleitet. Zu guter Letzt danke ich all meinen lieben Freunden für die vielen schönen Momente hauptsächlich in aber auch außerhalb von Würzburg.

6.7 Affidavit

6.7.1 Affidavit

I hereby confirm that my thesis entitled “Crosstalk between the MMB complex and YAP in transcriptional regulation of cell cycle genes” is the result of my own work. I did not receive any help or support from commercial consultants. All sources and/or materials applied are listed and specified in the thesis.

Furthermore, I confirm that this thesis has not yet been submitted as part of another examination process neither in identical nor in similar form.

Place, Date Signature

6.7.2 Eidesstattliche Erklärung

Hiermit erkläre ich an Eides statt, die Dissertation „Interaktion zwischen dem MMB-Komplex und YAP bei der transkriptionellen Regulation von Zellzyklusgenen“ eigenständig, d.h. insbesondere selbstständig und ohne Hilfe eines kommerziellen Promotionsberaters, angefertigt und keine anderen als die von mir angegebenen Quellen und Hilfsmittel verwendet zu haben.

Ich erkläre außerdem, dass die Dissertation weder in gleicher noch in ähnlicher Form bereits in einem anderen Prüfungsverfahren vorgelegen hat.

Ort, Datum Unterschrift